Role of membrane cytoskeleton in fenestra biogenesis

Meihua Ju

鞠美华

Translational Vision Research Laboratory

Institute of Ophthalmology, UCL, London

A thesis submitted for the degree of

Doctor of Philosophy at the University College London

October 2012

I, Mehua Ju, confirm that the work presented in the thesis is my own. Where information has been derived from other sources, I confirm that this has been indicated in the thesis.

Abstract

Fenestrae are transcellular membrane pores that mediate blood-tissue exchange in highly specialized vascular endothelia such as in choroidal capillaries. Substances that traverse the pore never encounter the contents of the cytoplasm and are transported in a rapid and presumably energy-efficient manner. Fenestrae arise in attenuated regions of the endothelial cell periphery and are highly organized in clusters termed sieve plates. My PhD project was based on the identification of novel components of fenestrae and how these components contribute to mechanisms regulating fenestra formation.

Using an *in vitro* biogenesis model coupled with proteomic analysis, we identified several proteins enriched in fenestrated plasma membranes. Localisation of candidate proteins was accomplished by immunolabelling, confocal microscopy, and transmission electron microscopy. Functional roles for the candidate proteins in fenestra biogenesis were probed through gain and loss of function techniques. Coimmunoprecipitation was used to uncover protein-protein interactions, and biochemical reagents were applied to probe the signalling pathways involved in fenestra formation.

Through extensive investigation, we identified the ERM (ezrin/radixin/moesin) protein moesin as a component of fenestral sieve plates. Inhibition of moesin function by expression of a dominant negative mutant or siRNA resulted in inhibition of fenestra formation, whereas knockdown of another regulator of the actin cytoskeleton, annexin II, led to a robust increase in fenestra formation. Biochemical and structural analyses showed that these modulators control the formation of an actin-fodrin submembrane cytoskeleton that is essential for sieve plate and fenestra formation, and that this cytoskeleton is directly linked to the fenestra pore protein PV-1. The transmembrane protein Na,K-ATPase is also a structural component of the submembrane complex, and functions as a regulator of fenestra formation *in vitro* and *in vivo*.

These findings provide a conceptual framework linking the actin cytoskeleton to membrane remodeling during fenestra biogenesis and new molecular tools for probing fenestra structure and function.

Acknowledgements

I would like to thank my supervisor, Professor Dave Shima, for providing me with this great opportunity to advance in Cell Biology. His creative ideas, insightful advice and enthusiasm toward science had been the inspiration throughout the program. I also want to thank Dave for all his support and tolerance to my maladjustment in this country in the beginning of the program.

My deep appreciation goes to Dr. Eric Ng for his always support and stimulating discussions. I thank both Dave and Eric for providing me a platform in the laboratory to pursue both fascinating basic science and drug development, which I believe both are essential for discovering novel therapies for patients.

I want to thank Dr. Peter Munro and Dr. Eija Jakoloton for their tremendous help in electron microscopy. My thanks also goes to Dr. Patric Turowski, my secondary supervisor, for always being helpful; Dr. Anne Goodwin for her meticulous editing of the thesis; Dr. Dominik Krilleke for providing the recombinant rodent VEGF164; Dr. Richard Foxton for critically reading the thesis; Dr. Sofia Ioannidou for her pioneering work on moesin; Dr. Matt Hayes for advice on immunostaining of annexin II; Bhavika Patel and Yemscrach Tadesse for their involvement in the protein work; Dr.Victoria Coles for her immunostaining work in liver sinusoidal endothelial cells; Anwei Mbah for her immunostaining work on syntaxins; and Danny Daniel for his help on IT and thesis printing.

My appreciation goes toward all my dear colleagues in the TVR lab, Asma Aslam, Lucy Ensum, Laura Paneghetti, Eva Kubala, Owen Anderson, Shannon Bunker, Claire Robinson, Peter Lundh, Nori Nagai, Kanako Nagai, Brett Hosking, Daiju Iwata, Sentaro Kusuhara, Raul de la Flor, Arthur Finkelstein and Rupesh Agrawal. You made my five years in London a cherishable memory.

I also want to thank Dr. Greg Robinson, Dr. Carolina Mailhos and Dr. Lois Smith, for their faith in me and the encouragement all along. I thank my friends in Boston especially Nan and April for always being there for me.

Finally I owe my PhD to my family, the sacrifices they have made and the support they have been giving me all this time. My daughter, Phoebe, braved through the ordeal of moving and resettling. I am so proud of her as the young lady she grew into.

献给我亲爱的父母

和我亲爱的女儿

To my parents

and my daughter

Table of contents

Table of figures

Chapter 1

Introduction to Fenestrae

Abbreviations

AMD	age-related macular degeneration
FACR	fenestrae-associated cytoskeleton ring
GEnC	glomerular endothelial cell
GFR	glomerular filtration rate
HSPG	heparan sulfate proteoglycans
HuVEC	human umbilical vein endothelial cells
LSEC	liver sinusoidal endothelial cells
PMA	phorbolmyristate acetate
PV-1	plasmalemmal vesicle–associated protein–1
RA	retinoic acid
RPE	retinal pigment epithelium
TGF-β	transforming growth factor β
VEGF	vascular endothelial growth factor
VVOs	vesiculo-vacuolar organelles

Chapter 1 Introduction to Fenestrae

1.1 Heterogeneity of Endothelial cells

A major role of the circulatory system is to provide for nutrient supply and waste removal, a concept postulated by the English physician William Harvey (Harvey, 1908). The structures that allow these exchange processes are the blood vessels, an extended network of arteries, veins and capillaries. As the primary barrier to free blood-tissue exchange, vascular endothelial cells form the inner lining of all blood vessels in the body. For a long time, endothelial cells were considered to be a homogeneous population of cells, like a sheet of nucleated cellophane, separating the vascular space from the interstitium (Florey, 1966). However, since the 1980s, ground-breaking evidence has shown that the endothelium plays additional, critical roles in the cardiovascular system, including solute change – transport and exchange, haemostasis, regulation of vascular tone, coagulation, inflammatory response, vasculogenesis and angiogenesis (Moncada, 1977; Furchgott, 1980 and 1983; Furchgott, 1980; Palmer, 1987 and 1988).

Endothelia differ on the basis of morphology and can be accordingly classified as 'continuous', 'fenestrated' or 'discontinuous'. In continuous capillaries, luminal and abluminal plasma membranes only fuse at the cell junctions. Fenestrated capillaries are characterised by clusters of orderly transcellular pores with a diameter of approximately 60 nm, which most often contain a proteinaceous diaphragm (Bennett, 1959; Rhodin, 1962; Simionescu, 1974; Bearer, 1985; Robert and Palade, 2000). Discontinuous capillaries exhibit clustered holes without a diaphragm, and the pores are usually bigger with a diameter of 80-200 nm. They are also often referred to as sinusoids, or fenestrae without a diaphragm (Roberts and Palade, 2000).

These morphological differences in endothelium correlate with vascular permeability properties, which facilitate the function of the organ. For example, large vessels and

microvessels of the blood-brain- or blood-retinal barrier are made from continuous endothelium. In contrast, fenestrated capillaries are more likely present at sites of filtration, secretion and absorption because of their higher permeability to low molecular weight, hydrophilic molecules (Levick and Smaje, 1987). The organ distribution of these different endothelial phenotypes is summarised below (Table 1-1).

Table 1-1 Heterogeneity of Endothelium

	Tissue of organ	Properties	Function
Continuous			
	CNS	low number of vesicles and complex tight junctions	blood-brain barrier
	lymph nodes	high endothelial venules	lymphocyte homing
	Muscle	high number of vesicles	exchange/transport
Discontinuous			
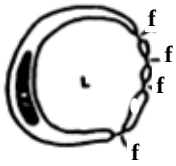	endocrine glands	fenestrae	secretion
	gastrointestinal tract	fenestrae	absorption
	choroid plexus	fenestrae	secretion
	choriocapillaries	fenestrae	secretion / absorption (?)
(diaphragmed fenestra)			
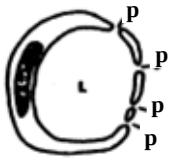	kidney glomeruli	pores	filtration
	liver	large gaps	exchange of particles
	bone marrow	marrow sinus	hemopoisis, delivery of blood cells
	spleen	splenic sinus of red pulp	blood cell processing
(fenestra without a diaphragm)			

L –lumen; f – fenestra; p- pore (adapted from Risau, 1995).

Heterogeneity of endothelial barrier phenotypes can also exist within the same organ. The kidney, for example, contains three different endothelial phenotypes: fenestrated diaphragmed endothelium in peritubular capillaries, discontinuous (also called fenestrated without-a- diaphragm) endothelium in glomerular capillaries, and continuous endothelium in other parts. Evidence suggests that endothelium is not predetermined to adopt organ-specific barrier phenotypes, but rather that it is the tissue microenvironment which influences the endothelium (Van Driel, 1988; Burns, 1992). Nevertheless, organ-specific differentiation is reversible. When endothelial cells are removed from an organ environment and cultured *in vitro*, fenestrations (Milici, 1985) and high electrical resistance characteristic of the blood-brain barrier (Risau, 1991; Rubin 1991) are lost.

1.2 Vascular permeability

In order to provide supply of nutrients and a mean of waste removal, the vascular system needs to be "permeable" to allow the ready exchange of small molecules, such as gases, ions, water, nutrients and wastes between blood and tissue. Small amount of plasma protein also need to cross the normal vascular barrier, and in some occasions, even whole cells (e.g., lymphocytes) need to across the semi-permeable vascular endothelial wall.

There are two general pathways across the endothelium for blood-tissue exchange: paracellular and transcellular. The paracellular route is through the minute space between contacting cells. Paracellular permeability is determined by the adhesive properties of proteins that comprise tight junctions and adherens junctions. The transcellular route is movement of substances through the cell, either by the shuttling of vesicles such as caveolae or vesiculo-vacuolar organelles (VVOs) or passive transport through transendothelial channels (TECs) or fenestrae. (Fig. 1-1).

Molecular exchange in normal tissues primarily takes place in capillaries. The fluid passing from the blood into normal tissues is a plasma filtrate – consisting largely of

water, small solutes and very little plasma protein. The basal permeability level of normal tissue varies considerably in different types of endothelium lining the capillaries, and is affected by changes in hydrostatic pressure, opening of the closed vessels, blood flow, etc (Nagy, 2008). Water and small solutes are able to diffuse through endothelial cells, or pass readily through the intercellular junction and through endothelial fenestrae. Large molecules cross the vascular barrier by shuttling through caveolae, VVOs or TECs (Dvorak, 2007).

Vascular permeability increases rapidly when the microvasculature is exposed acutely to vascular permeability factors, such as VEGF (vascular endothelial growth factor), histamine and serotonin. These vascular permeability factors cause disassociation of tight/adherens junctions (Deissler, 2008), and even induce endothelial cells to contract to form paracellular gaps (Majno, 1969). The vascular permeability factors also induce the diaphragms-interconnecting VVOs to open to allow plasma-protein extravasating transcellularly (Nagy, 2006). Macromolecules also extravasate through fenestrae in response to vasoactive mediators (Feng, 1997). The result is not only the quantity of extravasated fluid greatly increased, but also the quality of the extravsates changed - rich in plasma protein to levels close to plasma, referred as an “exudate”.

Although there’s a regulated increase in vascular permeability to both water and solutes as capillaries grow and form new vessels, angiogenesis, the generation of new blood vessels from preexisting vasculature, in physisological systems (Dejana, 2001), vascular hyperpermeability is more marked in disease states. Pathological angiogenesis associated with various diseases, such as cancer, stroke, diabetes and wet AMD (age-related macular degeneration), is characterised by vascular leakage. These novel vasculatures are inherently weak and leaky which results in tissue oedema and causes considerable damages in pathologies.

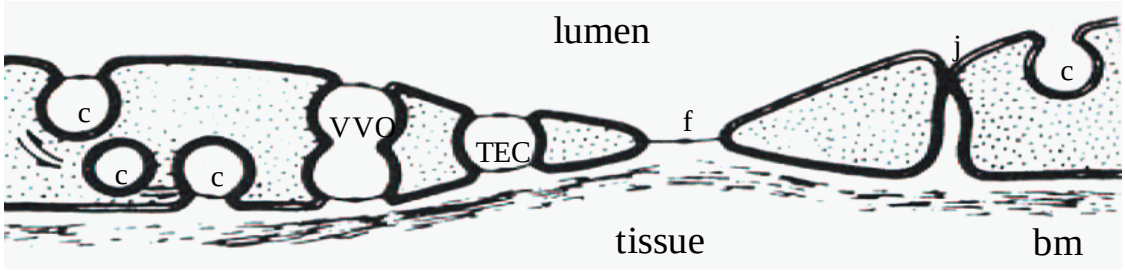

j- tight or adherens junctions;

c- caveolae;

VVO- vesiculovacular organelles;

TEC- transendothelial channels;

f- fenestra;

bm – base membrane.

(Adapted from Simionescu, 1983)

Fig. 1-1 Schematic of structures mediating paracellular and transcellular permeability

1.3 Properties and functions of fenestrae

Endothelial fenestrae were first observed in ultrastructural studies of glomerular capillaries by Gautier, Bernhard and Oberling (1950). In subsequent reports the endothelial structure was confirmed by Hall (1954), Yamada (1955), and Pease (1955) in the renal system, and later fenestrae were recognised in other organs, e.g., the thyroid (Trier, 1958) and liver (Wisse, 1970).

1.3.1 Structure of fenestrae

Fenestra, meaning window in Latin, describes a transcellular pore with a diameter of 60-70 nm (Bennett, 1959), though the pore diameter ranges from 100 to 200 nm in liver sinusoidal endothelial cells (LSEC) (Wisse, 1985). Fenestral pores span the entire thickness of the cell without disrupting the continuity of the cell membrane. Substances that traverse the pore never encounter the contents of the cytoplasm and are transported in a rapid and presumably energy-efficient manner (Rhodin, 1962). A quick-freeze, deep-etch ultrastructural study unveiled the structure of the fenestral diaphragm, which is composed of 8-12 radial fibrils interweaving to a central knob. The fibrils further divided the fenestrae into small pores with an average maximum arc length of 5.46 nm (Bearer, 1985). This agrees with tracer studies in which fenestral diaphragms are readily permeable to horseradish peroxidase (4.5 nm in diameter), but not to ferritin (11 nm in diameter) (Clementi, 1969) (Fig. 1-2A).

Fenestrae arise in attenuated regions of the endothelial cell periphery and are organised in clusters termed sieve plates (Braet, 1996). Within the sieve plate, fenestrae occur in ordered arrays with an average distance between neighboring fenestral centers of approximately 130 nm (Clementi, 1969; Simionescu, 1974). This highly ordered organisation implies involvement of an underlying cytoskeleton (Stan, 2004; Ioannidou, 2006) (Fig. 1-2B).

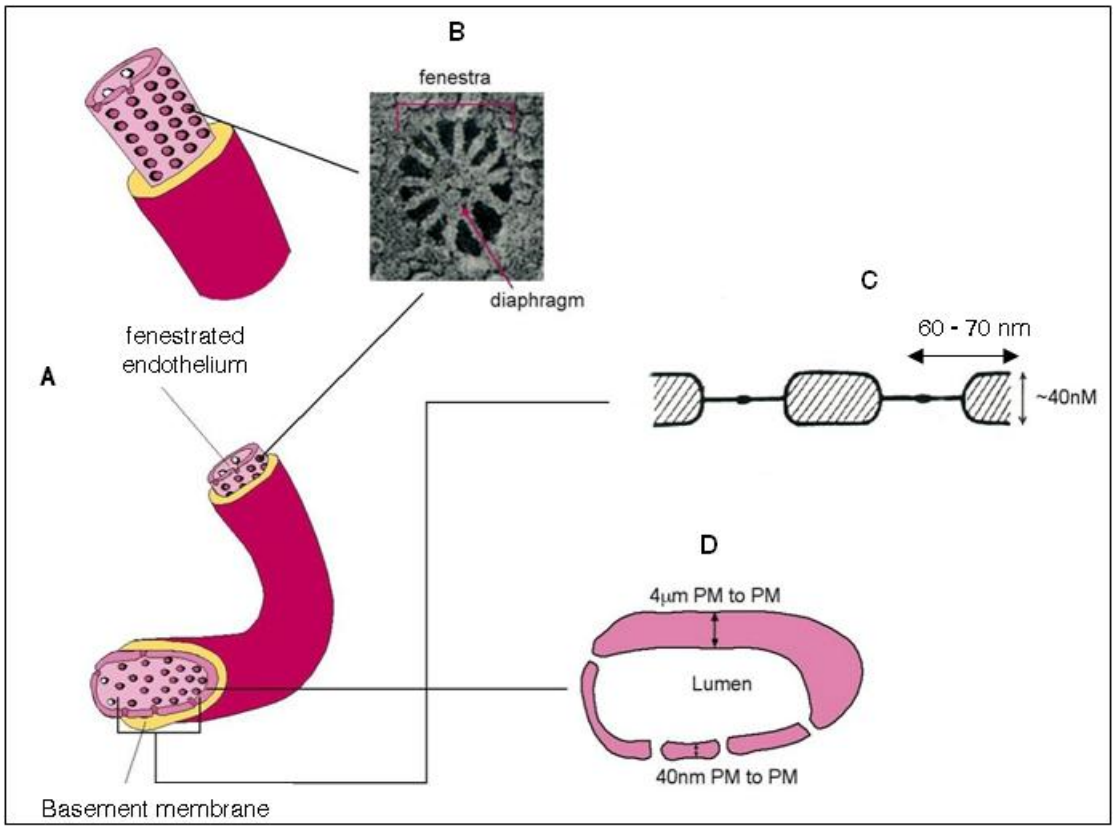

Fig. 1-2A Structure of fenestrae.

A. Schematic illustration of fenestrated endothelium.
B. A single fenestra and fenestral diaphragm.
C. Fenestral pores span the entire thickness of the cell without disrupting the continuity of the cell membrane.
D. A transverse profile of fenestrated endothelial cell membrane. PM, plasma membrane.

a)

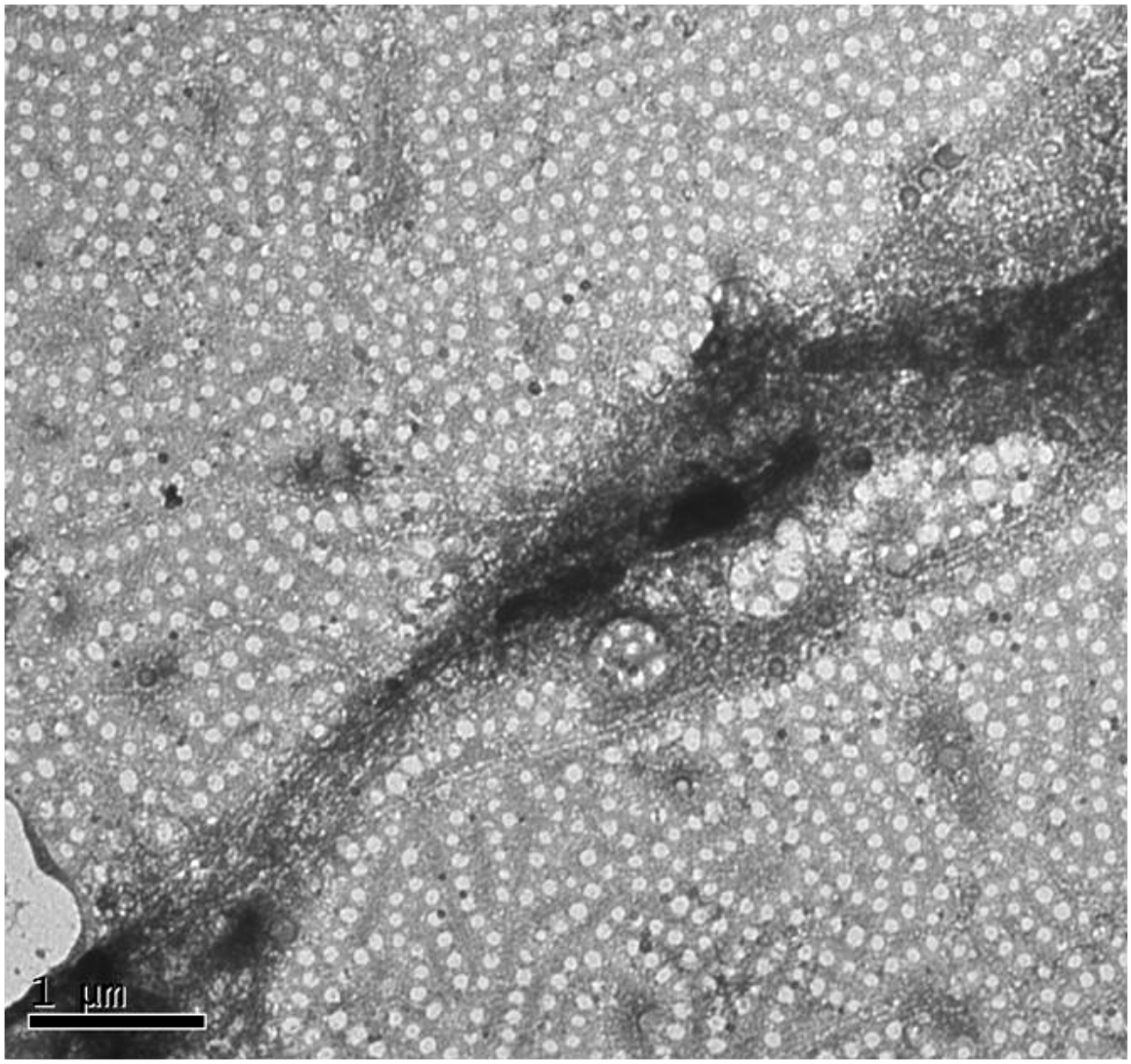

b)

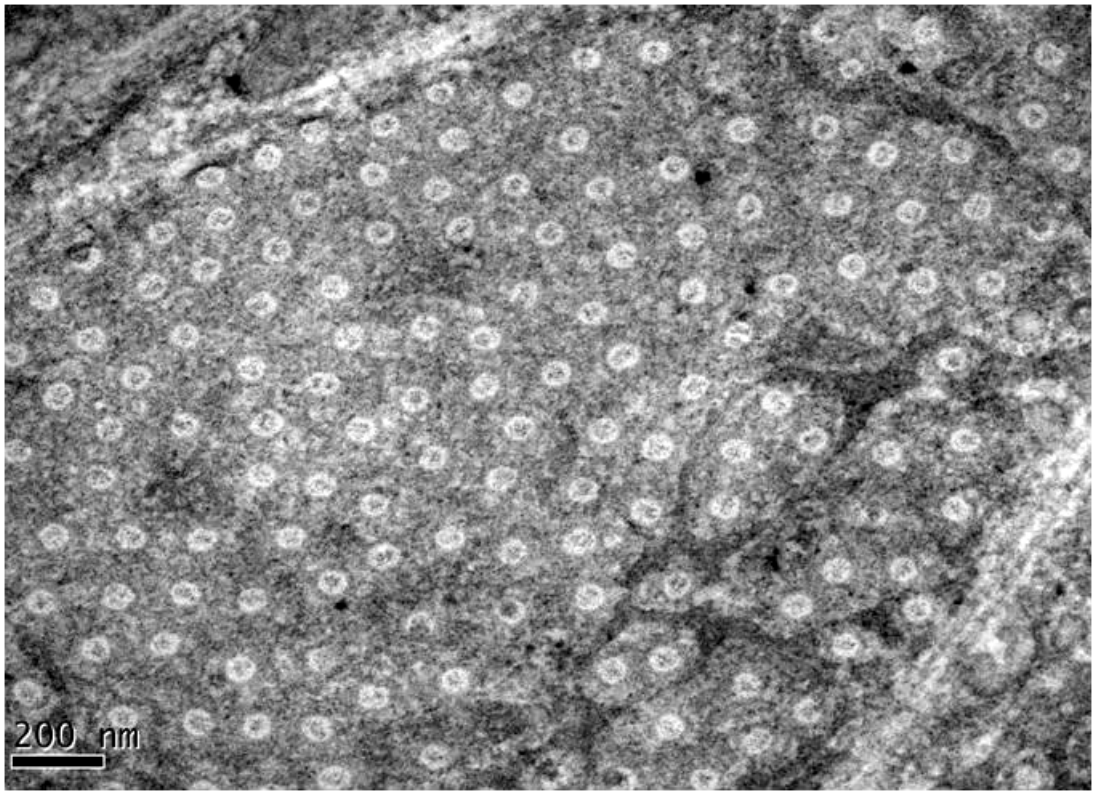

Fig. 1-2B Fenestral sieve plates

Fenestral sieve plates and linear organisation of fenestrae in bEND5 cells. Whole mount TEM image (a) and section TEM image (b) from fenestrated bEND5 cell. Scale bar: A, 1 μm; B, 200 nm.

1.3.2 Molecular composition of fenestrae

Little is known about the mechanism of fenestra formation nor of the components of the pore. One compositional feature is the clustering of anionic cell-surface molecules at fenestration sites (Simionescu, 1982). Filamentous tufts were revealed by perfusion-fixation in capillary fenestrae. These so-called fascinae fibers were postulated to be heparan sulfate proteoglycans (HSPG). Interestingly, they are only present on the luminal side of the fenestral diaphragm (Rostgaard, 1997). Fenestral diaphragms bind lectins poorly on their luminal side, which may represent interference from HSPG (Simionescu, 1982; Pino, 1986).

Cholesterol rings were discovered to surround the openings of fenestrae, plasmalemmal vesicles and transendothelial channels, but interestingly, not the fenestrae without a diaphragm, such as in the liver sinusoid and kidney glomeruli (Simionescu, 1983).

The cytoskeleton has long been postulated to be involved in fenestral structure. Actin filaments are found in close proximity to fenestrae (Braet, 2002; Nagai, 2004). However, only LSEC fenestrae were found to have a well-defined fenestra-associated cytoskeleton ring (FACR) (Braet, 1995 and 1996), which is postulated to regulate the diameter of LSEC fenestrae. The nature of the FARC still needs to be defined.

In 1999, Stan *et al*. identified plasmalemmal vesicle–associated protein–1 (PV-1) as a component protein of fenestral diaphragms, as well as stomatal diaphragms in caveolae and transendothelial channels (1999). The same group further demonstrated that multiple PV-1 homodimers reside in close proximity within the same diaphragm. They proposed a model in which PV1 dimers form the fibrils of the diaphragms, and the c-terminus of PV-1 proteins interweave to form the central knob (Stan, 2004) (Fig. 1-3). The known molecular components of fenestrae are summarised in Table 1-2.

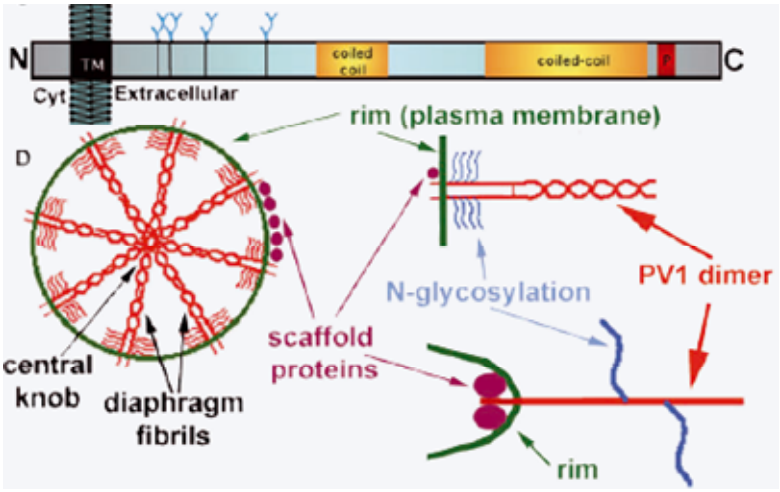

Fig. 1-3 Schematic illustration of a proposed model of the fenestral diaphragm. PV-1 dimers form diaphragm fibrils, and the fibrils interweave in the centre to form the central knob of the fenestral diaphragm. Glycosylation in the N-terminus of PV-1 keeps the diaphragm "floating".
(Adapted from Stan, 2004).

Table 1-2 Comparison of three types of endothelial cell fenestrations

Fenestrae type	Diaphragmed	Non-diaphragmed	Progressively non-diaphragmed (diaphragmed during embryonic development)
Type of endothelium in which fenestrations are expressed	Systemic capillaries, e.g., gastrointestinal, renal peritubular and Choriocapillaries	"Discontinuous" endothelium, e.g., hepatic sinusoidal	Glomerular capillaries
Diameter (nm)	60-70	100-175	60-80
PV-1 expression	Yes	No (only in development)	No (only in development)
Cytoskeletal ring	?	Yes	?
Cholesterol ring	Yes	No	?
Basal lamina	Yes	No	Yes
Glycocalyx	Yes	?	Yes

Adapted from Satchell and Braet, 2009

1.3.3 Function of Fenestrae

Fenestrated capillaries are highly permeable to low-molecular weight, hydrophilic molecules, consistent with their purported role in filtration, secretion and absorption (Levick, 1987). For larger, lipid-insoluble molecules, the permeability of fenestrated endothelium is similar to that of continuous endothelium (Johnson, 1966; Granger, 1979). By evaluating a series of published data, Levick and Smaje calculated the hydraulic conductance and permeability of small solutes through a fenestral pathway (1987). The fenestral diaphragm, the ~25 nm glycocalyx layer and 50-100 nm basement membrane make up the fenestral pathway. The analysis showed that a single diaphragmed fenestra with a diameter of 60 nm (area 0.003 μm^2) has a greater conductance than 1 μm^2 of continuous endothelium (skeletal muscle). Similarly, for small solutes such as B12 and inulin, the permeability across fenestrated endothelium in the submandibular gland is 15-28 times greater than in the continuous capillaries of skeletal muscle (Mann, 1979). Furthermore, endothelial hydraulic conductance and permeability to small lipophobic molecules increases with fenestral density in a variety of mammalian tissues (Levick,1987)

Fenestrae can be observed as individual structures lying in the cytoplasm. But most often, they appear as highly organised clusters – 'sieve plates'. Fraser and Wisse, decided to use the term sieve plate to indicate a possible sieving function of fenestrae (Fraser, 1978; Natio and Wisse, 1978). In the kidney, glomerular endothelial cell (GEnC) fenestrae are necessary for the high hydraulic conductivity of the glomerular capillary wall. They provide a primary sieving function for blood components that is refined by transit through the thick basement membrane and podocyte slit pore to produce primary urine (Ryan, 1975) (Fig. 1-4). In the liver, sinusoidal endothelial fenestrae filter fluids, solutes and particles that are exchanged between the sinusoidal lumen and the space of Disse, allowing only particles smaller than the fenestrae to

reach the parenchymal cells or to leave the space of Disse (De Zanger and Wisse, 1982). They are also believed to filter out potentially hazardous substances in the blood at the liver sinusoids (Braet and Wisse, 2002). A series of studies undertaken by Fraser's group demonstrated that fenestrae in LSEC play an important role in lipoprotein metabolism (Wight, 1983; Fraser, 1986 and 1988; Clark, 1988) (Fig. 1-5). In the choroid plexus, fenestrae are believed to function in the filtration of blood to give rise to cerebrospinal fluid (Engelhardt, 2001). The primary capillaries in the hypophyseal portal are extensively fenestrated, so hormones released by hypothalamic neurons can easily enter the blood stream (Marieb and Hoehn, 2007). In the retina there is a huge demand for nutrient delivery and waste removal from the outer retina by the underlying choriocapillaris, which is facilitated by fenestrae (Pino, 1980).

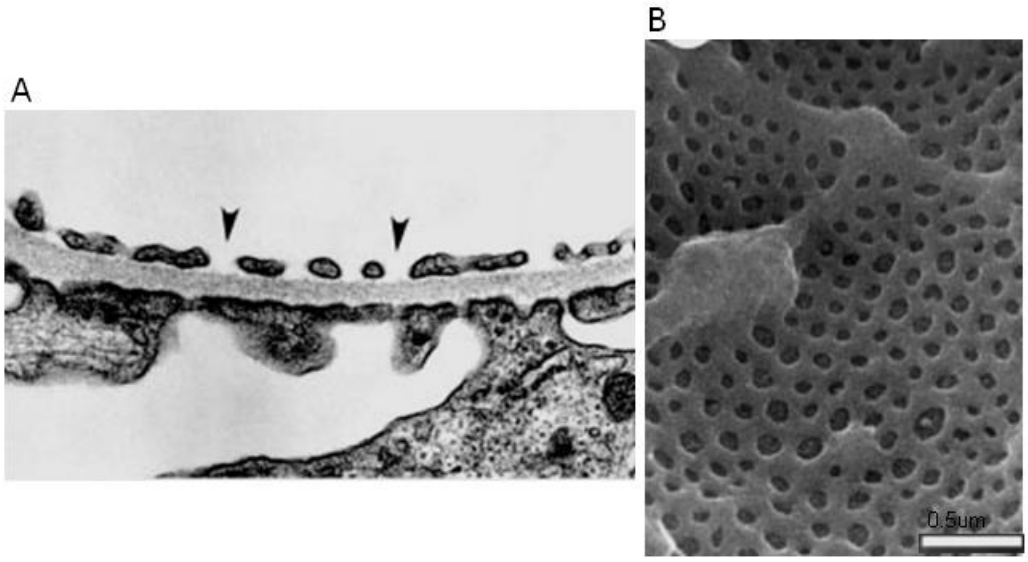

Fig. 1-4 Endothelial fenestrations in renal glomerular capillaries.

A. TEM image shows abundant fenestrations without diaphragms in GEnC.

B. SEM images of the luminal surface of glomerular capillaries with clusters of endothelial fenestrations

(Adapted from Kamba, 2006)

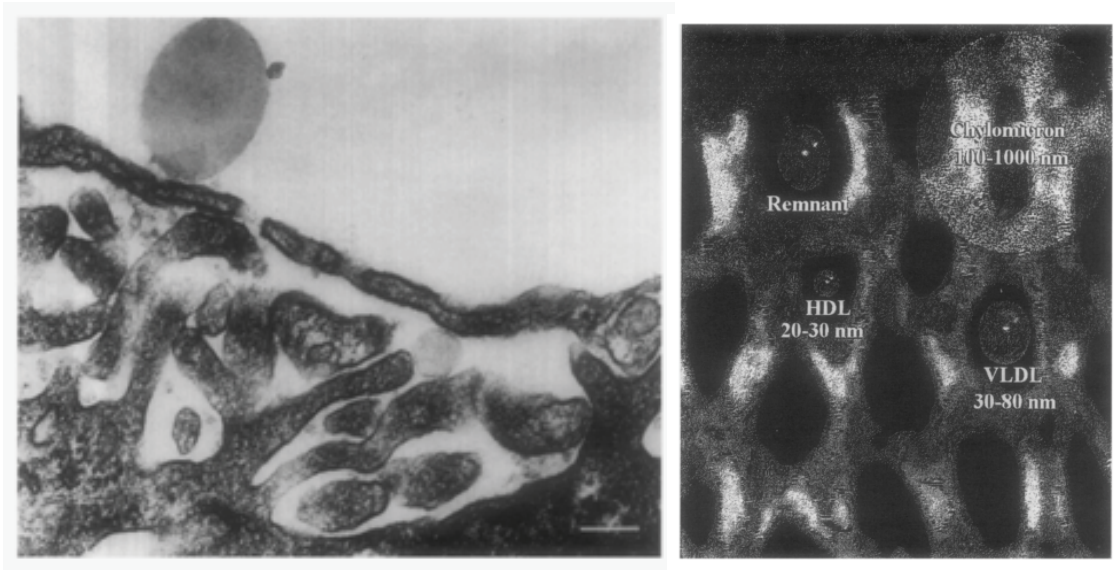

Fig. 1-5 Fenestrae sieve lipoproteins in the liver.

A. TEM image of a chylomicron within the lumen of the sinusoid and a chylomicron remnant trapped in the space of Disse.
B. Comparison of the relative size of LSEC fenestrae with the mean diameters of various lipoproteins.

(Adapted from Fraser, 1995)

1.3.4 Regulation of fenestrae

Organ-specific differentiation of endothelial cells is reversible. Fenestration is lost when fenestrated capillaries are taken out from their organ environment and cultured *in vitro* (Milici, 1985). This suggests that interactions of endothelium with a tissue environment via soluble factors or cell-cell interactions plays an important role in endothelial differentiation.

1.3.4.1 Tissue environment

It has long been observed that fenestrated endothelium occurs in close proximity to epithelium. It was postulated that the interaction between the two cell types may be important for the differentiation and maintenance of fenestrae. Cultivation of endothelial cells on extracellular matrix derived from epithelial cells results in endothelial fenestra formation (Milici, 1985). The results suggest that extracellular matrix and/or growth factors are needed for induction and maintenance of endothelial fenestrae. Indeed, fenestrated capillaries are in constant contact with the extracellular matrix, for example, the thick basement membrane of the kidney glomerulus, or the multi-lamellate Bruch's membrane. In addition to providing a structural scaffold, specific extracellular matrix components may play an active role in fenestra formation (Carley, 1988).

1.3.4.2 Signalling proteins

Among the signalling proteins that might have an influence on fenestration, vascular endothelial growth factor (VEGF) is the strongest candidate. This factor appears to be responsible for induction and/or maintainance of fenestrae (Rhurberg, 2003). In fact, epithelial cells adjacent to fenestrated endothelium, such as podocytes in the glomerulus (Bailey, 1999), epithelium in the choroid plexus (Josko, 2001), and retinal pigment epithelium (RPE) next to the choriocapillaris (Adamis, 1993), constitutively express VEGF, whereas fenestrated endothelial cells constitutively express VEGF

receptors (Breier, 1992). Roberts and Palade provided direct *in vivo* evidence of fenestrae induction by VEGF. In normally non-fenestrated venular and capillary endothelium, fenestration and increased microvascular permeability were observed after topical or intradermal administration of VEGF (Roberts and Palade, 1995). More recently, Sugimoto *et al.* observed rapid loss of endothelial cell fenestrae when neutralising VEGF antibodies or soluble VEGF receptor 1 (sFlt-1) were intravenously injected into mice and let them circulating for various time period up to 24 hours, which resulted in endothelial cell swelling and proteinuria (2003). *In vitro*, VEGF weakly induces fenestrae formation in cultured capillary endothelial cells (Esser, 1998). Treatment of cultured cells with phorbol myristate acetate (PMA) and retinoic acid (RA) also led to an increase, whereas transforming growth factor β (TGF-β) caused a decrease in the surface density of fenestrae (Lombardi, 1986, 1987 and 1988). Although the physical relevance of these signalling pathways remains to be established, PMA and RA are potent differentiation agents for many cell types, and TGF-β can prevent cell differentiation.

1.3.4.3 Cytoskeleton

The highly ordered arrangement of fenestrae in sieve plates implies the importance of the cytoskeleton for forming fenestrae and the maintaining their structural organisation. *In vitro* studies have established the involvement of the actin cytoskeleton in regulation of the number and size of LSEC fenestrae (Arias, 1990; Braet, 1995). Spector *et al.* used a variety of anti-actin drugs, including latrunculins, jasplakinolides, swinholide A, misakinolida A, halichondramides and pectennotoxin II, to target the actin cytoskeleton and disrupt its organisation. Although each class of drugs alters the distribution patterns of actin in a unique way, they all induce a rapid, 2-3 fold increase in the number of fenestrae in LSEC (Spector, 1999). These results suggest that the induction of fenestrae by microfilament disruption is a direct result of actin reorganisation rather than a side effect of the anti-actin drugs. In a study using the mouse brain endothelial cell line bEND5, microfilament disruption by cytochalasin B

or latrunculin A induced *do novo* formation of a vast number of fenestrae, which confirmed the importance of actin rearrangement and in particular depolymerisation of stress fibers for fenestrae formation (Ioannidou, 2006). This model system produces the most abundant formation of fenestrae to date. In *ex vivo* glomerular culture, cytochalasins prevent the loss of endothelial fenestrations that normally occur after 48 hours (Andrews, 1981). This indicates that fenestrae are inducible structures and the organisation of actin plays an essential role in their dynamics. The precise role of actin dynamics in fenestra formation remains elusive, however.

1.3.4.4 Diaphragm protein PV-1

PV-1 is a single span, type II membrane glycoprotein that forms homodimers *in situ* (Stan, 1997 and 1999). The size of the PV-1 monomer before post-translational modifications is 50 kD, and 60 kD in its N-glycosylated mature form (Ghitescu, 1997). PV-1 binds avidly to heparin at physiological pH (Lupas. 1996). Besides being the key component for diaphragms in fenestrae, caveolae and transendothelial channels, PV-1 is important for the formation of systemic endothelial fenestrations.

PV-1 was upregulated in response to VEGF in a murine tumor angiogenesis model and in human umbilical vein endothelial cells (HuVEC) in culture (Strickland, 2005). PV-1 is highly expressed, along with VEGF, in tumor vessels, which have abundant fenestrations (Roberts, 1997). Treatment of cultured endothelial cells with PMA causes upregulation of PV-1 and fenestrations (Stan, 2004). Inhibition of PV-1 upregulation using siRNA prevents diaphragmmed fenestra formation in HuVEC cells (Stan, 2004). In bEND5 cells, PV-1 is important for regulation of the size of fenestrae and their organisation into sieve plates: knockdown of PV-1 did not reduce the density of fenestrations formed in response to latrunculin A but resulted in the disorganisation of sieve plates with more variable distance between fenestrae and greater variation in fenestral pore size (20–400 nm) (Ioannidou, 2006). Therefore both PV-1 and actin dynamics are important, but exactly how they interact in fenestra formation is yet to be established.

1.3.5 Formation of fenestrae

Although fenestrae were discovered over half a century ago, their means of formation remains elusive. Several models have been proposed.

1.3.5.1 Formed from preexisting plasmalemmal vesicles

It has long been believed that fenestrae arise from preexisting structures such as caveolae and VVOs. In this model, fenestrae are suggested to be formed by fusion of caveolae or VVOs with the apical and basal membranes of an endothelial cell (Furuya, 1990; Dvorak, 1996). This hypothesis seems plausible given that fenestrae and caveolae share structural features - both have PV-1 as key component in their diaphragms, similar tissue distribution, common putative roles in the regulation of vascular permeability, and a relationship to the VEGF signalling cascade. However, caveolin-1 is found neither in adrenal cortical microvascular endothelial cell in culture (Esser, 1998), nor in glomerular endothelial cell fenestrae *in vivo* (Sorensson, 2002). Furthermore, glomerular endothelial fenestrae appear normal in caveolin-1 knockout mice that are completely lacking caveolae (Sorensson 2002).

1.3.5.2 *De novo* formation

By using the specific actin inhibitor misakinolide, Braet *et al.* revealed that LSEC fenestrae arise from a supposed fenestrae-forming center (1998). Although the exact mechanism of the fusion of two opposing cell membranes to form fenestrae has not been investigated, it likely requires the presence of unique compositional membrane microdomains and/or cell membrane-attached cytoskeletal structures (Simionescu 1982 and 1983). However, this needs further study to show whether the model applies to the formation of fenestrae in tissues other than LSEC.

1.4 Fenestrae and disease

Aberrant endothelial permeability leads to abnormal extravasation of blood components and accumulation of fluid in the extravascular space, resulting in tissue

dysfunction. Any alteration in fenestral size or density will affect the bidirectional exchange of macromolecules and can alter the balance between health and disease.

In the liver, sinusoidal endothelial fenestrae function as a selective sieve between the sinusoidal blood and the parenchymal cells. LSEC fenestrae and their biological relevance in various diseases such as fibrosis, cirrhosis, steatosis, hepatitis, inflammation, and metastasis have been described in detail (reviews of Braet 2002 and 2005). It has been widely acknowledged that changes in endothelial filtration directly influence the transport of chylomicron remnants and other lipoproteins, metabolism, and the occurrence of atherosclerosis (Fraser, 1995). In comparison to rats, rabbits have significantly smaller fenestrae and chickens have fewer fenestrae. Rabbits and chickens that are fed cholesterol rapidly develop high serum cholesterol levels which lead to the development of atherosclerosis (Wright, 1983; Fraser, 1986). The lower porosity of the liver sieve correlates well with the susceptibility and vulnerability of both species to dietary cholesterol. The smaller size of rabbit LSEC fenestrae hinders the egress of large chylomicron remnants from the sinusoidal blood, leading to the subsequent development of hypercholesterolaemia and atherosclerosis. Conversely, the hypolipidemic agent pantethine increased the rabbit liver sieve porosity by 80% and halved the resultant hypercholesterolemia (Fraser, 1988 and 1989). Nicotine induces a decline in liver sieve porosity in rats and a concomitant increase in serum cholesterol levels (Fraser, 1988 and 1989). Alcoholic defenestration, a result of chronic alcohol abuse, involves a decrease in both number and porosity of LSEC fenestrae. This effect is believed to be a factor in pathogenesis of the hyperlipoproteinemia associated with alcoholism (Clark, 1988). In liver cirrhosis, defenestrated sinusoidal endothelium and the presence of a subendothelial membrane were found in all forms of hepatic cirrhosis. Rogers *et al*. demonstrated that these structural alterations block the hepatic uptake of dietary retinol within the chylomicron remnants. The resulting retinol deficiency transforms fat-sorting cells into myofibroblasts with enhanced extracellular matrix products, resulting in perisinusoidal fibrosis and ultimately in cirrhosis (1992).

Furthermore, since retinol is known to be important in cell differentiation (Lupulescu, 1994), the blocked retinol metabolism in fat-sorting cells resulting from LSEC defenestration may promote the development of certain cancers.

GEnC fenestrae are integral components of the glomerular filtration barrier. These fenestrae make up 30-50% of the lumen surface area. The high hydraulic conductivity of the glomerular capillary wall requires an adequate density and size of glomerular endothelial cell fenestrae (Deen, 2001). Glomerular filtration rate (GFR) is dependent on the fractional area of the fenestrations and on the fenestral glycocalyx. GEnC fenestrations are important in the restriction of protein passage. For patients with preeclampsia, a condition in which significant amounts of urinary protein are associated with pregnancy-induced hypertension, the density of GEnC fenestrae is reduced and accounts for the decreased GFR. Changes in GEnC fenestral density and size also correlate with changes in the GFR brought about by gentamicin administration (Avasthi, 1980).

Although the endothelium and its fenestrations have not been studied in the majority of human glomerular diseases, GEnC fenestrae appear to contribute to GFR reduction in a variety of diseases, including cyclosporine nephropathy (Kobayashi, 1991), serum sickness nephritis (Chowdhury, 1996), Thy-1 nephritis (Ichimura. 2008) and animal diabetic models (Davila, 2005; Evan,1980). In human diabetic nephropathy and transplant glomerulopathy, fenestration loss correlates with albuminuria (Toyoda, 2007; Yamamoto, 2007). All of the above conditions are associated with proteinuria despite the reduction in GFR. Taken together, these observations suggest that dysfunction or loss of GEnC fenestrations, as well as alterations in the endothelial glycocalyx, may contribute to the increased passage of albumin across the glomerular filtration barrier.

There are also pathological conditions in which the continuous endothelium becomes fenestrated. The tumour promoter phorbol ester can induce diaphragmed fenestrae in large endothelium *in vitro* (Lombardi, 1987). Furthermore, the neovasculature of many solid tumours is highly fenestrated (Capo, 1985; Shibata, 1986; Feng, 1999 and 2002).

Electron microscopy studies revealed the appearance or upregulation of vessel fenestrations in chronic allergic encephalomyelitis (Llena, 1976), rheumatoid arthritis (Spenger, 1983; Pappas, 1988) and diabetic retinopathy (Wallow, 1980).

Our lab has focused most attention on fenestration in choroidal vessels in the setting of the eye, particularly in relation to the development of age-related macular degeneration (AMD). Oxygen consumption of the mammalian retina (per gram of tissue) is the highest of all organs, including the kidney, cerebral cortex and cardiac muscle (Whikehart, 1994). Moreover, the photoreceptor layer has one of the highest metabolic rates of any known tissue, given that the amplication process requires vast quantities of metabolic energy (Futterman, 1975). The oxygen and nutrients for the 'greedy' photoreceptors are provided by the choriocapillaris, a unique, flattened capillary bed situated immediately external to the photoreceptors (Henkind, 1979), separated only by a single layer of retinal epithelial cells and Bruch's membrane. The lining of the capillaries on the side closest to the photoreceptor cells is attenuated and highly fenestrated to ensure the rapid and efficient delivery of nutrients and disposal of abundant waste products from the photoreceptor layer (Fig. 1-6). We hypothesise that fenestral dysfunction may lead to accumulation of wastes and/or deprivation of nutrients, and that this contributes to the progression of AMD.

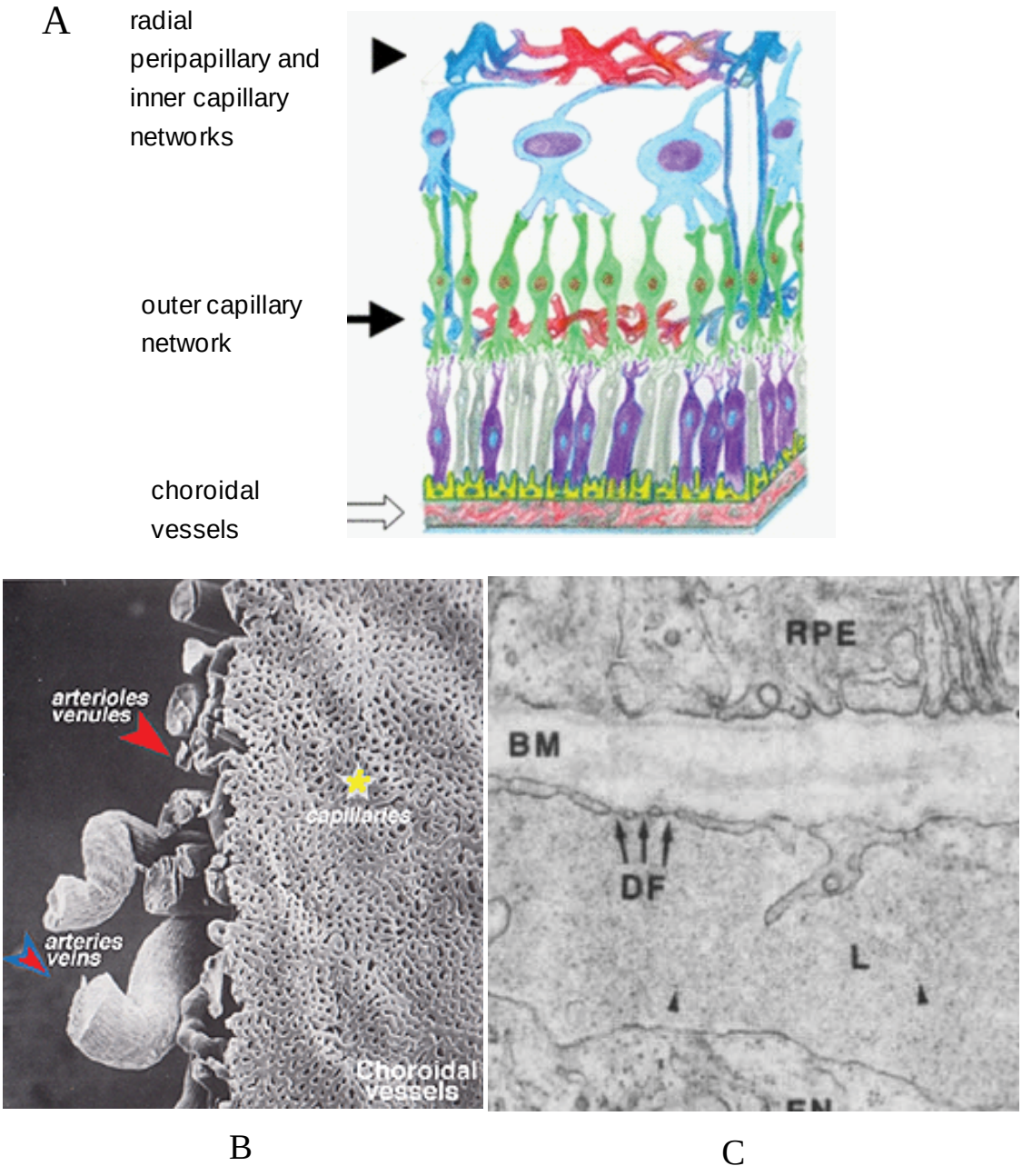

Fig. 1-6 Morphology and topology of the choriocapillaris.
A, The avascular photoreceptor-RPE layer relies on choroidal vessels for nutrient supply and waste removal; B, SEM image of a corrosion cast of the choriocapillaris bed under Bruch's membrane (adapted from Zhang, 1994); C, Fenestration in choriocapillaris endothelial cells. DF, diaphragmed fenestrae; BM, bruch's membrane; RPE, retinal pigment epithelium (adapted from Pino, 1987).

There is limited evidence to indicate a possible correlation between choriocapillary defenestration and retinal diseases such as AMD. In retinal degeneration (rd)-mice, loss of fenestration is the initial change observed in the choriocapillaris adjacent to degenerating RPE (Neuhardt, 1999). In a low-dose, D-galactose-induced aging model in mice, loss of choriocapillaris endothelial cell fenestration was observed adjacent to the largest outer collagenous layer deposits, whereas normal choriocapillaris fenestration overlaid areas of non-thickened Bruch's membrane (Ida, 2004). More recently, in a murine model of graded Bruch's membrane lipoidal degeneration, endothelial fenestration numbers were reduced where the choriocapillary endothelium basement membrane was thickened (Schmidt-Erfurth, 2008). Drusen, focal deposits that accumulate between the RPE basal membrane and the inner collagenous layer of Bruch's membrane, are significant risk factors for the development of AMD (Pauleikhoff, 1990). By carefully examining drusen distribution in aged human eyes, drusen depositions were found colocalising with the intercapillary pillars of the choroidal capillaries (Lengyel, 2004). A plausible explanation is that drusen formation is related to the clearance of cellular debris from the retina.

A greater understanding of the relevance of endothelial fenestrae in physiology and disease may one day allow one to manipulate fenestrae therapeutically. For example, VEGF has been used to restore fenestrations in LSEC and reduce portal hypertension in an animal model of cirrhosis (Xu, 2008). The restoration of endothelial health in diabetic glomerular disease holds promise for increasing GFR through increased fenestral density and decreasing proteinuria through restored glycocalyx structure. Similarly, the restoration of choriocapillary fenestration may slow drusen formation and RPE atrophy, thereby hindering the progression of AMD.

Since little is known about the mechanisms by which fenestrae are formed, nor of the components of the fenestral pore, it is virtually impossible to explore the role of fenestrae in diseases such as AMD. Taking advantage of an *in vitro* assay developed in

our lab, in which abundant fenestrae can be induced rapidly, we embarked on a detailed study of fenestral composition and biogenesis. In previous studies, we began to characterise novel components of the fenestrae using proteomics. We found the ERM (ezrin, radixin and moesin) protein moesin to be a component of fenestral sieve plates. The research described in this thesis involves identification of novel fenestral components, assessment of their potential roles in fenestrae formation and/or function, and use of this information to explore fenestral function *in vivo*.

Chapter 2

Material and Methods

Abbreviations

AMD	age-related macular degeneration
BSA	bovine serum albumin
DMEM	Dulbecco's modified Eagle medium
FACR	fenestrae-associated cytoskeleton ring
GEnC	glomerular endothelial cell
GFP	green fluorescent protein
GFR	glomerular filtration rate
HSPG	heparan sulfate proteoglycans
HuVEC	human umbilical vein endothelial cells
LSEC	liver sinusoidal endothelial cells
PBS	phosphate-buffered saline
PFA	paraformaldehyde
PMA	phorbol myristate acetate
PV-1	plasmalemmal vesicle–associated protein–1
RA	retinoic acid
RPE	retinal pigment epithelium
TGF-β	transforming growth factor β
VEGF	vascular endothelial growth factor
VVOs	vesiculo-vacuolar organelles

Chapter 2 Material and Methods

2.1 Reagents

All chemicals were purchased from Sigma-Aldrich (Dorset, UK), unless otherwise indicated. All culture media and related products were obtained from Invitrogen (Paisley, UK), unless otherwise stated. All restriction endonucleases were purchased from New England Biolabs. Oligonucleotides were provided by Ambion (Invitrogen, Paisley, UK). The water used for all the procedures described was MilliQ grade and autoclaved.

Mouse full length moesin with GFP tag was purchased from Invitrogen (EST clone 5044557). The N-terminal portion of mouse moesin (1-1143) was amplified from EST clone 5044557 by PCR using oligonucleotides 5'-GACGCTTCCGTTCCTGCTC-3' and 5'-GCCACCATGCCGAAGACG-3' and ligated into pcDNA3.1/CT-GFP-TOPO (Invitrogen). Mouse full length moesin with HA tag was purchased from GeneCopoeia (EX-Mm03944-M07).

2.2 Bacterial culture

2.2.1 Preparation of electrocompetent cells

Five milliliters of XL-1 blue bacteria (Stratagene) from an overnight culture were added to 800 ml of LB medium and grown at 37ºC with shaking to an OD595 of 0.6. The culture was incubated for 30 minutes on ice and centrifuged at 5,000 rpm for 20 minutes at 4ºC using a JA-10 rotor in an Avanti J-E centrifuge (Beckman Coulter). The pellet was washed twice with 800 ml ice-cold water, once with 400 ml ice-cold 10% glycerol, and was finally resuspended in 1 volume ice-cold 10% glycerol. Aliquots of the preparation were stored at -80ºC.

2.2.2 Transformation

DNA (50-500 pg) was added to 80 µl of electrocompetent cells in a 1 mm electroporation cuvette (Bio-Rad). Mixtures were incubated on ice for 10 minutes and transformations were performed at 200 Ω, 25 µF, and 1.8 kV. Bacteria were incubated with 400 µl SOC medium at 37ºC for 1 hour, and then centrifuged at full speed in a microcentrifuge. Pellets were resuspended in 100 µl LB medium, plated on agar plates containing ampicillin (75 µg/ml) and incubated overnight at 37ºC.

2.2.3 Cryopreservation

Bacterial cultures were stored as 50% glycerol stocks at -80ºC

2.3 DNA techniques

2.3.1 Preparation of plasmid DNA

Plasmid DNA was purified from overnight cultures grown at 37ºC in LB containing ampicillin (75 µg/ml), using Qiagen plasmid mini kits, Endo-free plasmid midi, or maxi kits according to the manufacturer's instructions.

2.3.2 Quantitation of DNA

DNA solutions were placed in a quartz cuvette (1 cm path length) and the absorbance of the mixture was read at 260 nm and 280 nm using a Spectrophotometer. The OD260 of 1, corresponding to 50 µg/ml double stranded or 33 µg/ml single stranded DNA, was used as a reference for DNA concentration calculations. The OD260/280 ratio was used as an estimate for purity of the preparation. A ratio of 1.6-1.9 was considered acceptable.

2.3.3 Restriction enzyme digestion

For small scale diagnostic digests, 0.5 µg of DNA was incubated in the appropriate buffer with 5-10 U of restriction endonuclease in a total volume of 20 µl. The reaction was incubated at the appropriate temperature (25ºC or 37ºC) for 1-2 hours. For large scale digests, 5 µg of DNA was incubated in the appropriate buffer with 20-30 U of restriction endonuclease in a total volume of 70 µl. The reaction was incubated for 2-3 hours at 25ºC or 37ºC. Following digestion, enzymes were inactivated by incubating at 80ºC for 20 minutes.

Restriction enzymes Kpn I and Xho I were used in moesin constructs with GFP tag or HA tag.

2.3.4 PCR

Primers were 20-22 nucleotides in length, usually with two GC-basepairs at the 3'-end, and annealing temperatures of approximately 55ºC. The annealing temperature specific to each primer was calculated using the following formula: Tm = 3 x (sum of GC-basepairs) + 2 x (sum of AT-basepairs). Reactions were carried out in a Peltier thermal cycler (MJ Research).

2.3.5 DNA sequencing

Primers of approx. 18 nucleotides were designed to amplify a region within the gene of interest or the vector sequence surrounding the gene. Reactions were carried out using 500 ng of a given plasmid, 3-4 pmol of primer, and 8 µl of fluorochrome labelling mix, in a total volume of 20 µl. PCR conditions were as follows:

denaturation at 96ºC for 10 seconds;

annealing at 50ºC for 5 seconds;

extension at 60ºC for 4 minutes;

25 cycles.

Following amplification, DNA was ethanol-precipitated, electrophoresed then visualised. Sequencing was performed by the UCL Institute of Ophthalmology Sequencing Service. Sequence analysis and alignment was performed using the software programs MacVector (Accelrys) and Sequencher (Gene Codes Corporation).

For plasmids with GFP tag, the following primer set was used in sequencing:

T7: 5'- TAA TAC GAC TCA CTA TAG GG -3'

GFP Reverse: 5'- GGG TAA GCT TTC CGT ATG TAG C -3'

For plasmids with HA tag, the following primer set was used in sequencing:

Forward: 5'- GCG GTA GGC GTG TAC GGG T -3'

Reverse: 5' – GTG GCA CCT TCC AGG GTC -3'

2.3.6 DNA gel electrophoresis

Agarose gels were prepared by dissolving 0.6-2% agarose in TAE buffer (40 mM Tris Base pH8.0, 20 mM glacial acetic acid, 1 mM EDTA). Ethidium bromide was added to a final concentration of 0.5 µg/ml. DNA was mixed with 10x BlueJuice^{TM} gel loading buffer (Invitrogen) and electrophoresed at 5-20 V/cm in TAE buffer. A 100 bp or 1 kb DNA ladder (Invitrogen) was loaded in an adjacent well for comparison.

2.3.7 Gel purification of DNA fragments

Gel slices containing relevant DNA fragments were excised and stripped of agarose and contaminants using a gel extraction and nucleotide removal kit (Qiagen).

2.3.8 Cloning

2.3.8.1 Cohesive-end ligation

Restriction digests for the insert and vector were performed. The vector fragment was also dephosphorylated with 0.5 U/µg DNA of alkaline phosphatase (CIP, New England Biolabs), for 1 hour at 37ºC, to prevent recircularisation in the case of compatible ends. Following purification, vector and insert were ligated using 200-300 ng total DNA with a 2-4 fold molar excess of insert, and 400 U T4 DNA ligase (New England Biolabs) in 15 µl total volume. The reaction was carried out overnight at 15ºC. One µl of the ligation reaction was used to transform *Escherichia coli* as described above.

2.3.8.2 Blunt-end ligation

Restriction digests of vector and insert were performed as above. Fragments were incubated with T4 DNA polymerase (New England Biolabs) at 1-2 U/µg DNA, 200 µM dNTP mix (Ultrapure, Pharmacia), and 0.1 mg/ml bovine serum albumin (BSA), at 12ºC for 20 minutes so as to form blunt ends. The polymerase was inactivated by incubating at 75ºC for 10 minutes, and the vector was dephosphorylated with alkaline phosphatase as above. Following purification, vector and insert were ligated as described above, except using 2-fold molar excess of vector.

2.4 RNA techniques

2.4.1 RNA isolation

Total RNA was isolated from cells or tissues using the RNeasy mini kit (Qiagen). Three to five million bEND5 cells were lysed in 350 µl RLT buffer (Qiagen) by pipetting, and the contents loaded onto an RNeasy mini column. The lysate was passed through a QIAshredder spin column (Qiagen). RNA

purification was carried out according to the manufacturer's instructions. RNA was snap-frozen and stored at -80ºC.

2.4.2 RNA quantitation

RNA solutions were placed in a quartz cuvette (1 cm path length) and the absorbance of the mixture was read at 260 nm and 280 nm using a Spectrophotometer. An OD260 of 1, corresponding to 40 µg/ml RNA, was used as a reference for calculations. To obtain an accurate OD260/280 ratio, RNA was diluted in 10 mM TrisHCl pH 7.5. A ratio of 1.9-2.1 was expected for a pure preparation.

2.4.3 RT-PCR (Taqman)

Reverse transcription of RNA was performed using 300 ng RNA and the following reaction mix (ABI): 1 x RT buffer, 5.5 mM $MgCl_2$, 500 µM each dNTP, 2.5 µM random primers, 0.4 U/µl RNase Inhibitor, 1.25 U/µl Multiscribe Reverse Transcriptase, supplemented with Nuclease-Free water (Ambion) to a total volume of 60 µl. cDNA synthesis was carried out in a thermal cycler according to the following scheme:

Segment 1	1 cycle	25ºC for 10 minutes
Segment 2	1 cycle	42ºC for 60 minutes
Segment 3	1 cycle	95ºC for 5 minutes

Taqman cocktails were prepared using 1x PCR master mix (ABI), 5 µl cDNA, 250 nM of each primer, and 500 nM of probe, in a total volume of 25 µl.

Moesin, radixin, annxin II and fodrin were amplified with mouse primers and probe provided by TaqMan Gene Expression Assay from ABI with the following ID numbers:

Moeisn, Mm00447889_m1

Radixin, Mm00501337_m1

Annexin II, Mm00500307_m1

Fodrin, Mm01326617_m1

GAPDH served as the internal control in all reactions, and was amplified with rodent GAPDH primers and probe (ABI, Mm00484668_m1).

Reactions were loaded on Prism Optical tubes (ABI) and run in the ABI Prism 7700 Sequence Detection System using the following cycling conditions:

Segment 1	1 cycle	50ºC for 2 minutes
Segment 2	1 cycle	95ºC for 10 minutes
Segment 3	40 cycles	95ºC for 15 seconds
		60ºC for 1 minute

Results were analysed using SDS 7900HT Software 2.2 (ABI)

2.5 Protein techniques

2.5.1 Protein concentration determination

Protein concentrations were determined using a BCA kit (Thermo Scientific). BSA standards diluted in water and sample diluents were incubated with BCA reagent for 30 minutes at 37˚C and the absorbance was measured in a spectrophotometer at OD562. Standard curves were created based on the absorbance of BSA standards and were used to assign protein concentrations to samples

2.5.2 SDS-PAGE (sodium dodecyl sulfate polyacrylamide gel electrophoresis)

Gels were poured at a thickness of 1.5 mm using the Bio-Rad Mini gel assembly kit and acrylamide solutions from Bio-Rad. The separating gel and stacking gel were prepared as in Table 2-1.

Table 2-1A Separating gel

Gel	DDI (Distilled De-Ionised) water	29:1 Acrylamide : Bisacrylamide	1.5 M Tris-HCl (pH 8.8)	10% SDS (sodium dodecyl sulphate)
7.5%	4.9 ml	2.5 ml	2.5 ml	0.1 ml
10%	4.1 ml	3.3 ml	2.5 ml	0.1 ml
12%	3.4 ml	4.0 ml	2.5 ml	0.1 ml

Just before the gel was poured, 50 µl of freshly made 10% APS (ammonium persulfate) and 5 µl of TEMED (N, N, N', N'-tetramethylethylenediamine) were added.

Table 2-1B Stacking gel

Gel	DDI water	29:1 Acrylamide : Bisacrylamide	0.5 M Tris-HCl (pH 6.8)	10% SDS
Stacking gel	4.1 ml	3.3 ml	2.5 ml	0.1 ml

Just before the gel was poured, 50 µl of freshly made 10% APS and 10 µl of TEMED were added.

Samples were boiled with 5x sample buffer (Thermo Scientific) at 95ºC for 5 minutes prior to loading on the gel. Gels were run in Tris-glycine buffer (25 mM Tris, 250 mM glycine pH 8.3, 0.1% SDS) at 70-120 V.

2.5.3 Western-blot

Following electrophoretic separation, proteins were blotted onto Hybond-P PVDF (Amersham Biosciences) membranes using a semi-dry blotter (Bio-Rad). Membranes and pieces of Whatman paper were pre-soaked in transfer buffer (150 ml methanol, 100 ml tris-glycine buffer, in a total volume of 1000 ml) for 30 minutes. After a brief incubation of the gel in transfer buffer, gel and membrane were sandwiched between six pieces of Whatman paper, with the membrane facing the anode of the electroblotting apparatus. Transfer was carried out at 120 mA per gel for 1 hour (1.5mm thick gels). Blots were incubated with blocking buffer (5% non-fat dry milk in TBST -0.1% tween 20 in 0.1 M Tris buffer) for 2 hours at room temperature or overnight at 4ºC. The primary antibody was diluted in blocking buffer and applied for 2 hours at room temperature or overnight at 4ºC. After 3 ten-minute washes in TBST, horseradish peroxidise (HRP)-conjugated secondary antibodies were diluted in a similar fashion and applied for 1 hour at room temperature. Blots were washed 3 times in TBST. The product of the horseradish peroxidase reaction was detected by chemiluminescence (Amersham Biosciences). The primary and secondary antibodies used in experiments are listed in Table 2-2.

2.5.4 Coimmunoprecipitation

Medium stringency lysis buffer (0.025 M Tris, 0.15 M NaCl, 0.001 M EDTA, 1% NP-40, 5% glycerol, pH 7.4) and freshly added protease and phosphatise inhibitor cocktail (Thermo Scientific, Cat# 1861280)) were used for immunoprecipitation. Total protein (500 µg) was diluted to approximately 1 µg/ul with lysis buffer, then was pre-cleared with washed Pierce Protein A/G Agarose (Thermo Scientific, Cat# 20423). Two micrograms of antibody was added and incubated with antigen sample at 4ºC overnight with gentle mixing. Immune complexes were captured by adding 25 µl of washed Protein A/G

agarose bead slurry. Agarose beads were collected by centrifuge (1500 *g*, 30 minutes) and washed with ice-cold TBS (0.025 M Tris, 0.15 M NaCl, pH 7.2). Immune complexes were released by incubating with 30 µl of Elution Buffer (0.15 M glycine-HCl buffer, pH 2.8) for 10 minutes. This step was repeated twice and the two supernatant fractions were combined and neutralised by adding 10% total volume of 1 M Tris, pH 9. The immunoprecipitation products were frozen at -20ºC or used directly for SDS-PAGE. Horseradish peroxidase-conjugated secondary antibodies from Amersham Biosciences (as described in 2.8.3), or Clean-Blot IP HRP reagent (Thermo Scientific, Cat# 21230) was used in the following western immune analysis.

Table 2-2 Antibodies and conditions used in western blot

Primary antibodies		
Antibody	**Dilution**	**Company and Catalog#**
Ms anti-β-actin	1:2000	Sigma, #A228
Rb anti-actin	1:2000	Sigma, #A2066
Rt anti-PV-1	1:2000	Covalab, custom-made, 1 mg/ml
Rb anti-PV-1	1:4000	Covalab,custom-made, 2 mg/ml
Rb anti-moesin	1:2000	Cell signalling, #3150
Ms anti-moesin	1:2000	BD Transduction, #610401
Rb anti-phospho-ERM	1:2000	Cell signalling, #3141
Rb anti-radixin	1:2000	Sigma, #R3653
Rb anti-ezrin	1:2000	Cell signalling, #3145
Ms anti-HA	1:2000	Abcam, #ab18181
Rb anti-caveolin	1:2000	BD Transduction, #610059
Ms anti-Na/K-α-1	1:2000	Milllipore, #05-369
Rb anti-Na/K-β-2	1:2000	Abcam, # ab110730
Ms anti-α-fodrin	1:2000	Abcam, #ab11755
Rb anti-ankrin B	1:2000	Santa Cruz, #sc-12718
Ms anti-annexin II	1:2000	Santa Cruz, #sc-28385
Rb anti-src	1:2000	Cell signalling, #2108
Rb anti-phospho-src	1:2000	Cell signalling, #6943
Rb anti-PI3K p85	1:2000	Cell signalling, #4257
Rb anti-phospho-PI3K p85/p55	1:2000	Cell signalling, #4228
Rb anti-PI3K p110α	1:2000	Cell signalling, #4249
Rb anti-PI3K p110β	1:2000	Cell signalling, #3011
Rb anti-PI3K p110γ	1:2000	Cell signalling, #5405
Rb anti-PI3K Class III	1:2000	Cell signalling, #3358

To be coninued

Ms anti-raf-1	1:2000	Santa Cruz, #sc-7267
Ms anti-p-raf-1	1:2000	Santa Cruz, #sc-271929
Rb anti-Akt (pan)	1:2000	Cell signalling, #4691
Rb anti-phospho-Akt (Ser473)	1:2000	Cell signalling, #4060
Rb anti-phospho-Akt (Thr308)	1:2000	Cell signalling, #2965
Rb anti-phospho-GSK-3β	1:2000	Cell signalling, #9323
Rb anti-phospho-PTEN	1:2000	Cell signalling, #9551
Rb anti-phospho-PDK-1(Ser241)	1:2000	Cell signalling, #3438
Rb anti-p38 MAPK	1:4000	Cell signalling, #8690
Rb anti-phospho-p38 MAPK	1:4000	Cell signalling, #4511
Rb anti-p44/42 MAPK	1:4000	Cell signalling, # 4695
Rb anti-phospho-p44/42 MAPK	1:4000	Cell signalling, #4370
Secondary antibodies		
Antibody	**Dilution**	**Company and Catalog#**
Sheep anti-ms IgG (HRP)	1:1000	GE Healthcare, NA-931-1ML
Gt anti-rt IgG (HRP)	1:1000	GE Healthcare, NA-935-1ML
Donkey anti-rb IgG (HRP)	1:1000	GE Healthcare, NA-934-1ML
Clean-Blot IP Detection Reagent	1:400	Thermo Scientific, #21230

Ms – mouse; Rt - rat; Rb – rabbit; Gt – goat.

2.6 Tissue culture

2.6.1 Cell line maintenance

bEND5 and Py4.1 are two mouse endothelial cell lines used for induction of fenestrae *in vitro*. The bEND5 cell line was a gift from Dr. Britta Englehardt (University of Bern, Switzerland). It was derived from mouse brain endothelium transformed with polyoma middle T virus. These cells were maintained in Dulbecco's modified Eagle medium (DMEM) with high-glucose (4.5 g/l), sodium pyruvate (1%), 4 mM L-glutamine, 10% fetal bovine serum, penicillin/streptomycin, non-essential amino acids and 5 μM β-mercaptoethanol, at 37˚C with 5% CO_2. Cells used for induction of fenestrae were at a passage number between 15 and 35.

Py4.1 cells were a gift from Dr.Vicky Bautch (University of North Carolina). The Py4.1 cell line was derived from mouse ear and tail hemangiomas. It was maintained in DMEM with high-glucose (4.5 g/l), 2% fetal bovine serum and penicillin/streptomycin, at 37˚C with 10% CO_2.

The bEND5 cells were trypsinised using 5x trypsin EDTA solution for 5 minutes at 37˚C, and Py4.1 cells were trypsinised using 1x trypsin EDTA solution for 2 minutes at 37˚C. Culture medium was added to neutralize the trypsin, then the cells were isolated by centrifugation at 1000 rpm. Cells were frozen in 10% DMSO (dimethyl sulphoxide), 20% fetal bovine serum, and 70% complete medium, and were stored in liquid nitrogen.

2.6.2 Fenestra induction in endothelial cells

Coverslips were coated with 1% bovine gelatin (type B, Sigma) for 30 minutes at room temperature, and then rinsed quickly with phosphate-buffered saline (PBS). Cells were seeded at a density of 30,000/well in a 24-well plate. The

next day, when at 50-60% confluence, cells were induced by using latrunculin A (Sigma) at 1.25 µM for 3 hours. The cells were processed for biochemistry or morphology immediately after the end of the induction.

2.6.3 Transient transfection of endothelial cells

2.6.3.1 Plasmid transfection by Nucleofection

The bEND5 cells used for nucleofection were in the exponential growth phase (~65-80% confluence). In all experiments, an expression plasmid encoding green fluorescent protein (GFP) was transfected in parallel as a control for transfection efficiency. The required plasmid (5 µg in 1-5 µl) was mixed with 100 µl of Amaxa's Nucleofector^{TM} Solution V. Cells were trypsinised, then 2 ml of cells were pelleted for each nucleofection. The cells were resuspended in 100 µl of Amaxa's Nucleofector^{TM} Solution V with plasmid. The resuspended cells were immediately transferred into Amaxa certified cuvettes and were then nucleofected using program U13 of the Nucleofector Device (Amaxa, Germany). Immediately the cells were resuspended in 4 ml of pre-warmed bEND5 media and were plated into 2 wells of a 6-well plate. The transfected cells were incubated at 37˚C/5% CO_2 for 20-24 hours prior to experimental analysis.

2.6.3.2 siRNA transfection using Oligofectamine

On the day prior to transfection, bEND5 cells were seeded at a density equivalent to 25,000 cells per well of a 24-well plate, in antibiotic-free media. The next day, the cells were transfected in serum free DMEM without antibiotics. Transfection was carried out according to the Oligofectamine protocol (Invitrogen). Briefly, siRNA and Oligofectamine were separately mixed with Opti-MEM reduced serum medium (Invitrogen, Cat# 31985062). Then the siRNA-Opti-MEM and Oligofectamine-Opti-MEM solutions were combined and pre-incubated for 15-20 minutes before they were incubated with

cells for at least 4 hours. Cells were analysed at 24, 48 and 72 hours after transfection. To knock down moesin, radixin, annexin II or fodrin, we optimised a double transfection regimen (Diagram 2-1).

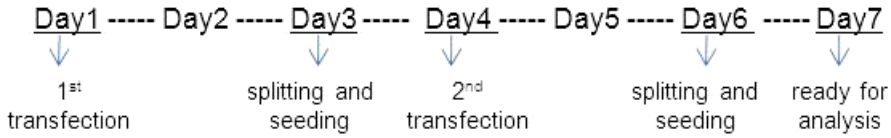

Diagram 2-1 Double siRNA transfection to knockdown moesin, radixin, annexin II or fodrin

Silencer Select siRNA was used to knock down moesin, radixin, annexin II and fodrin. Of the 3 siRNAs, the one with the best reduction efficiency was used for the experiment. The corresponding sequences are as follows:

Moesin siRNA sequence (5'->3'):

sense: GGCUGAAACUCAAUAAGAAtt

antisense: UUCUUAUUGAGUUUCAGCCaa

Radixin siRNA sequence (5'->3'):

sense: GGAAAGCUCUAGAACUGGAtt

antisense: UCCAGUUCUAGAGCUUUCCga

Annexin II siRNA sequence (5'->3'):

sense: GGGAUGCUCUGAACAUUGAtt

antisense: UCAAUGUUCAGAGCAUCCCtc

Fodrin siRNA sequence (5'->3'):

sense: GAAGUACAGAGGUUUCACAtt

antisense: UGUGAAACCUCUGUACUUCgt

2.7 Immunolabelling on coverslips and cryosections

Cells on coverslips were fixed either in -20ºC methanol for 7 minutes or in room temperature 4% paraformaldehyde (PFA) (Electron Microscopy Sciences) for 10 minutes. For PFA-fixed cells, fixation was followed by 5 washes in PBS and a 3 minute permeabilisation step in 0.1% Triton X-100 in PBS. Cells on coverslips were blocked for 15 minutes in blocking solution (5% goat or donkey serum, 0.2% fish skin gelatin in PBS). Coverslips were then inverted over 50 µl of primary antibody solution on a piece of parafilm, incubated for 30 minutes at room temperature, and washed 3 times, for 5 minutes each time, in blocking solution lacking serum. The antibodies used for immunolabelling are listed in the table below (Table 2-3). To visualise F-actin, Alexa 546-conjugated phalloidin (1:200; Molecular Probes) was included in secondary antibody preparations of methanol or PFA-fixed cells. Alexa 488-conjugated DNase I (1:200; Molecular Probes) was employed to detect G-actin on PFA-fixed cells. As negative controls, primary antibodies were omitted with secondary antibody incubations performed in the usual way. After three 5-minute washes in blocking solution lacking serum, coverslips were mounted on slides using gold antifade mounting medium (Invitrogen).

For immunolabelling of ocular cryosections, eyeballs from just-sacrificed C57BL/6 mice were enucleated, immediately embedded in OCT, then stored at -80˚C until use. Cryosections of 8-10 µm were cut, air-dried for 5 minutes at room temperature, then fixed in cold methanol for 10 minutes. After 3 washes in PBS, cryosection samples were immunolabelled with a procedure similar to that described above, except the incubation time for blocking was extended to 30 minutes and the incubation with primary or secondary antibody to 1 hour.

Table 2-3A Mouse primary antibodies used in immunofluorescence staining

1° Antibody	Function	Dilution	Company and Catalog#
β-Actin	Cytoskeletal protein	1:200	Sigma (A228)
Ankyrin B	Membrane skeleton	1:100	Santa Cruz (sc-12718)
Ankyrin G	Membrane skeleton	1:100	Santa Cruz (sc-137105)
Annexin II	Ca^{2+}/phospholipids binding	1:200	Santa Cruz (sc-28385)
Arp3	Actin-binding protein	1:100	BD Biosciences (612134)
Aquaporin 1	Integral protein, forms water-specific channel permitting water to move in the direction of an osmotic gradient.	1:100	Abcam (ab9566)
Aquaporin 4	Water-specific channel protein, osmoreceptor regulating body water balance.	1:100	Abcam (ab46182)
DP1	Interactin protein of Reticulon 4a, shapes tubular ER	1: 100	Abcam (ab17807)
FAK	Focal Adhesion Kinase, colocalizes with integrins in focal adhesion	1:100	BD Biosciences (610087)
Filamin 1	Crosslinks Actin to filaments	1: 100	Santa Cruz (sc-58763)
Fodrin	Component of membrane skeleton	1: 100	Abcam (ab11755)
HA	Epitope tag from influenza protein hemagglutinin used in fusion proteins	1:200	Abcam (ab18181)
Integrins	Transmembrane proteins linking extracellular matrix to cytoskeleton	1:100	BD Transduction (611435)
IRS p58/p53	ER marker, essential for ER retention	1:100	BD Transduction (612674)

KDEL	ER marker, essential for ER retention	1:200	Abcam (ab12223)
Lamp1	Lysosome associated membrane protein	1:100	Abcam (ab25630)
Myosin IIa	Motor proteins responsible for actin-based cell motility	1:100	Santa Cruz (sc-53095)
Na^+/K^+ ATPase	Electrogenic transmembrane ATPase	1:100	Millipore (05-369)
NPC	Nuclear pore complex proteins	1:200	Abcam (ab24609)
Rab4	Small GTP-binding proteins important for vesicular trafficking	1:100	BD Transduction (610888)
Rab5	GTP-binding protein, regulates the fusion of plasma membrane-derived clathrin-coated vesicles with early endosomes	1:100	Abcam (ab50253)
STX5A	Mediates endoplasmic reticulum to Golgi transport	1:100	Sigma (WH0006811M1)
Talin	Actin-binding protein found in focal adhesion complex	1:100	Santa Cruz (sc-81805)
β-Tubulin	Major building block of microtubules	1:5000	Sigma (T 4026)
Vinculin	Focal adhesion proteins	1:100	Santa Cruz (sc-73614)
Vimentin	Intermediate filament protein	1:100	BD Pharmingen (550513)

Table 2-3B Rabbit primary antibodies used in immunofluorescence staining

1° Antibody	Function	Dilution	Company and Catalog#
Actin	Actin	1:50	Sigma (A2066)
Calreticulin	ER marker	1:200	Abcam (ab4)
Calnexin	ER marker	1:200	Abcam (ab10286)
Caveolin	Caveolae coat protein	1:200	BD Transduction (610059)
CD44	Transmembrane glycoprotein	1:100	Abcam (ab24504)
Desmin	Class III intermediate filaments	1:100	Abcam (ab8592)
EEA1	Early endosome marker	1:150	Abcam (ab2900)
Ezrin	Linker protein between plasma membrane and cytoskeleton	1:200	Cell Signalling (3145)
ERGIC-53/P58	Type I membrane protein associated with the ER-Golgi intermediate compartment, mediates proteins transport from ER to Golgi	1:100	Sigma (E1031)
Moesin	Linker protein between plasma membrane and cytoskeleton	1:200	Cell Signalling (3150)
Phospho-ERM	Phosphorylated / active ERM(ezrin, radixin and moesin)	1:400	Cell Signalling (3141)
Nogo A+B	Located in membranes with high curvature, potent neurite outgrowth inhibitor	1:200	Abcam (ab47085)
PV-1	Diaphragm protein of fenestrae, caveolae and transendothelial channels	final: 5µg/ml	Covalab , custom-made
Radixin	Linker protein between plasma membrane and cytoskeleton	1:100	Sigma (R3653)
RTN3	Member of the Reticulon family, may be involved in membrane trafficking in early secretory pathway	1:100	Abcam (ab72814)

SAR1	Member of small GTPase, involved in transport from ER to Golgi apparatus	1:100	Abcam (74046)
Sec23	Components of the COPII (coat protein complex II) coat that covers ER-derived vesicles involved in transport from ER to Golgi apparatus.	1:100	Sigma (S7696)
Sec31A	Component protein of COPII coat	1:100	Sigma (HPA005457)
Tubulin	Building blocks of microtubules	1:100	Sigma (T3526)
VE Cadherin	Type I cell adhesion membrane proteins, associates with α-catenin, forming a link to cytoskeleton	1:100	Abcam (ab33168)
WASP	Member of Wiskott-Aldrich Syndrome Proteins, involved in transduction of cell surface receptors to the actin cytoskeleton	1:100	Calbiochem (ST1113)
WASL	Member of WASPs, regulates formation of actin filaments	1:100	Calbiochem (AP1049)

Table 2-3C Goat, rat and hamster primary antibodies used in immunofluorescence staining

1° Antibody	Function	Dilution	Company and Catalog#
Gt anti-Atlastin	Golgi-localized integral membrane protein; GTPase	1:100	Santa Cruz (sc-49158)
Gt anti- Cofilin	Actin-binding protein, promotes F-actin depolymerization	1:100	Santa Cruz (sc-8441)
Gt anti- Enolase	Glycolytic enzyme involved in differentiation	1:100	Santa Cruz (sc-7455)
Gt anti- EHM2	Member of NF2 (neurofibromin 2, merlin), connecting transmembrane proteins to cytoskeletal molecules	1:100	Santa Cruz (sc-14236)
Gt anti- hnRNP K	Heterogeneous nuclear ribonucleoprotein K, involved in nucleocytoplasmic shuttling	1:200	Abcam (ab12223)
Gt anti- NM-23	Potential suppressor of metastasis	1:100	Santa Cruz (sc-14789)
Gt anti-Paralemmin	Peripheral protein involved in cell structure and shape	1:100	Santa Cruz (sc-55972)
Gt anti- RTN2	Member of the Reticulon family, may be involved in membrane trafficking in early secretory pathway	1:100	Santa Cruz (sc-16682)
Gt anti-Transgelin	Binds actin, causing actin fibers to gel, may be an early indicator of the onset of transformation	1:100	Santa Cruz (sc-18153)
Rt anti- CD44	Transmembrane glycoprotein	1:100	BD Pharmingen (558739)
Rt anti- CD31	Integral membrane protein,	1:100	BD Pharmingen

			(550300)
Rt anti- PyMT	Poly virus middle T antigen, a major transforming protein	1:100	Santa Cruz (sc53481)
Rt anti- PV-1 (Meca-32)	Plasmalemma vesicle-associated protein (PLVAP, PV-1), diaphragm protein of fenestrae, caveolae and transendothelial channels	1:100	BD Pharmingen (550563)
Rt anti- PV-1 (Meca-32)	Diaphragm protein of fenestrae, caveolae and transendothelial channels	1:200 (final: 5µg/ml)	Covalab, custom-made (Cuk-0901)
Ht anti- CD31	Transmembrane glycoprotein	1:100	Chemicon (MAB1398Z)

Rt - rat; Gt – goat; Ht – Hamster

Table 2-3D Secondary antibodies used in immunofluorescence staining

2° Ab	Conjugation	Dilution	Company and Cat#
Gt anti-ms IgG (H+L)	AlexaFluor 488	1:500	Invitrogen (A11029)
Gt anti-ms IgG (H+L)	AlexaFluor 546	1:500	Invitrogen (A11030)
Gt anti-ms IgG (H+L)	AlexaFluor 633	1:500	Invitrogen (A21052)
Gt anti-ms IgG	TRITC	1:300	Sigma (T5393)
Gt anti-rt IgG (H+L)	AlexaFluor 488	1:500	Invitrogen (A11066)
Gt anti-rt IgG (H+L)	AlexaFluor 546	1:500	Invitrogen (A11081)
Gt anti-rt IgG (H+L)	AlexaFluor 594	1:500	Invitrogen (A11007)
Gt anti-rt IgG (H+L)	AlexaFluor 633	1:500	Invitrogen (A21094)
Dk anti-rt IgG (H+L)	Cy3	1:300	Jackson (712-165-150)
Gt anti-rb IgG (H+L)	AlexaFluor 488	1:500	Invitrogen (A11008)
Gt anti-rb IgG (H+L)	AlexaFluor 546	1:500	Invitrogen (A11010)
Gt anti-rb IgG (H+L)	AlexaFluor 633	1:500	Invitrogen (A21071)
Dk anti-Gt IgG (H+L)	AlexaFluor 488	1:500	Invitrogen (A11055)
Dk anti-Gt IgG (H+L)	AlexaFluor 594	1:500	Invitrogen (A11058)
Dk anti-Gt IgG (H+L)	Cy3	1:300	Jackson (705-165-003)
Gt anti-ht IgG (H+L)	AlexaFluor 488	1:500	Invitrogen (A21110)
Gt anti-ht IgG (H+L)	AlexaFluor 647	1:500	Invitrogen (A21451)

Ms – mouse; Rt - rat; Rb – rabbit; Gt – goat; Dk – donkey; Ht – hamster

2.8 *In vivo* vessel fenestration

2.8.1 Vascular fenestration in animal models

Male Sprague-Dawley (250-300 g) or C57BL/6 mice (25-30 g) were used throughout the *in vivo* study. All procedures were in accordance with Home Office standards and were reviewed by an institutional animal care committee.

Modified from the previously described methods (Roberts and Palade, 1995), rats were anesthetised with a mixture of ketamine (75 mg/kg body weight), Fort Dodge Animal Health, USA) and xylazine (25 mg/kg body weight) (IVX Animal Health, USA). The cremaster muscle was surgically exposed and 100 µl of saline, VEGF (75 ng in 100 µl) (kindly provided by Dr. Dominik Krilleke at UCL institute of Ophthalmology)ification) or ouabain (100 µl of 200 µM) (Sigma, O3125) was topically applied. To detect and localise vascular leakage, the femoral vein was exposed and used to inject 10 mg/kg body weight of lysine-fixable 3KD FITC-Dextran (Invitrogen, Cat# D3306). After 10 minutes, the cremaster was fixed in situ for 4 minutes with 4% PFA, then surgically removed, quickly immersed in 4% PFA, pinned flat on a piece of cork board and fixed overnight in 4% PFA.

For experiments using the skin model, abdomens of adult male C57BL/6 mice were shaved and injected intradermally with 30 µl of saline, VEGF (20 ng in 30 µl) or ouabain (30 µl of 200 µM). The elevated injection site was marked. Lysine-fixable 3 kD FITC-Dextran was injected in the tail vein. After 10 minutes, the skin at the injected sites was fixed *in situ* for 4 minutes then further processed as described above for the cremaster.

2.8.2 Imaging and processing for electron microscopy

Following overnight fixation in 4% PFA, specimens were trimmed and mounted with Vecta Shield (Vector Laboratory). Fluoresence leakage was checked and photographed using an epifluorescence microscope. Samples were dismounted and mounting medium was washed out in PBS. Under a fluorescence dissecting microscope, the tissue region with the most fluorescence intensity was cut and trimmed into small pieces to be processed for electron microscopy.

2.8.3 Quantification of vessel fenestration

To calculate the frequency of fenestrated vasculature, vessels in the most superficial layer of cremaster tissue were counted. Three well-preserved sections in close proximity were counted and the average frequency was calculated, and the final result was calculated from at least 3 rats from independent experiments. For each fenestrated vasculature, the vessel perimeter length, the fenestrated vessel length, and the number of fenestrae were determined. Fenestration prevalence and extent were calculated as follows:

Fenestration prevalence % = (Fenestrated vessel number in superfacial layer / Total vessel number in superfacial layer) X 100

Fenestration extent % = (Number of fenestrae / Number of fenestrated vessels) X 100

Or

Fenestration extent % = (Length of fenestraed part / Length of vessel perimeter) X 100

2.9 Morphology

2.9.1 Light microscopy

Images were captured using the following instruments and software packages:

1) LSM510 laser scanning confocal microscope (Zeiss); LSM 510 software (Zeiss).

2) LSM700 laser scanning confocal microscope (Zeiss); Zen2009 software (Zeiss).

3) Olympus Fluorescence microscope (Olympus); Image Pro-Plus 6.1 software (Olympus).

2.9.2 Electron microscopy

2.9.2.1 Transmission electron microscopy (TEM) of thin sections

All of the chemicals and consumables used to prepare specimens for electron microscopy were obtained from Agar Scientific, Stansted, UK unless otherwise stated. All steps were carried out at room temperature, and a rotator was used during alcohol dehydration and resin infiltration. Cell monolayers and animal tissue samples were fixed in a mixture of 3% (v/v) glutaraldehyde and 1% (w/v) PFA in 0.08 M sodium cacodylate buffer, pH 7.4 for 2 hours at room temperature and were either processed directly or after storage at 4°C for periods of up to 48 hours.

Following two brief rinses in cacodylate buffer, specimens were osmicated for 2 hours in 1% (w/v) aqueous osmium tetroxide (OsO_4), then dehydrated using 10 minute incubations in 50%,70%, 90% and 3 x 100% ethanol. Following the last change of absolute alcohol, specimens for TEM were passed through two 15 minute incubations of propylene oxide and placed in a 50:50 mixture of propylene oxide:araldite and left to infiltrate overnight. This solution was

replaced with 100% araldite and infiltration continued for a further 4 -8 hours prior to embedment in fresh araldite and overnight curing in a 60°C oven. Semi-thin sections (0.75 µm) for light microscopy and ultrathin sections (50-70 nm) for electron microscopy were cut with diamond knives (Diatome/Leica, Milton Keynes, UK). Semi-thin sections were stained with a 1% toluidine blue/borax mixture at 60˚C, and ultrathin sections were stained with Reynold's lead citrate. Stained ultrathin sections were examined in a JEOL 1010 TEM operating at 80 kV and images recorded using a Gatan Orius B digital camera and Digital Micrograph.

2.9.2.2 Wholemount TEM

Formvar grids for wholemount TEM were prepared by coating 400 mesh nickel grids (Gilder; Electron Microscopy Sciences) using 1% Formvar (Ted Pella, Inc.) in ethylene dichloride (Electron Microscopy Sciences). Grids were placed on coverslips, then carbon coated in a Cressington 208 Carbon Coater (Cressington) and UV-sterilised prior to their use in cell culture.

Cells were fixed in 1.25% glutaraldehyde (Electron Microscopy Sciences) and 2.5% PFA in 0.1 M PBS, for 1 hour at room temperature or overnight at 4ºC. Following three 5-minute washes in 0.1 M PBS, cells were post-fixed in 1% osmium tetroxide (Electron Microscopy Sciences) in distilled water for 30 minutes. After another 2 washes in distilled water, cells were dehydrated in an ascending ethanol series: 30%, 50%, 70%, 80%, 90%, 95%, 100%, and a repeat at 100%, for five minutes each. Then coverslips were quickly rinsed in hexamethyldisilizane, immersed in hexamethyldisilizane for 3 minutes and air-dried. Grids were examined in a JEOL 1010 TEM operating at 80 kV and images recorded using a Gatan Orius B digital camera and Digital Micrograph.

2.9.2.3 Immunolabelling for whole mount TEM

Prior to embedding, immuno-EM samples were prepared as previously described (Yu, 2003). Briefly, cells were fixed with PLP-fixative (2% formaldehyde in 0.01 M periodate, 0.075 M Lysine-HCl , 0.037 M sodium phosphate buffer, pH 7.4) at room temperature for 2 hours. Permeabilization was done with 0.01% saponin (Sigma) and cells were labelled with rabbit anti-moesin (Millipore) or mouse anti-Na,K-ATPase (Millipore, dilution, 1:50) followed by labelling with goat anti-rat or mouse Fab-fragment conjugated with 1.4 nm nanogold particles (Nanoprobes, 1:60 dilution). Nanogold particles were silver enhanced using the Nanoprobes Silver HQ kit and stabilized by consecutive incubations with 2% Na-acetate, 0.05 % gold chloride and 0.03% sodium thiosulfate. Finally the samples were treated with 1% reduced osmium tetroxide and processed for epon embedding as described (Seemann *et al.*, 2000).

2.9.2.4 Electron tomographic analysis

For electron tomographic analysis, bEnd5 cells were grown on 1.5-mm-sapphires discs coated with gelatin (Sigma G1890). After 1 hour treatment with 1.25 µM latrunculin A, the cells were covered with 20% BSA (Sigma-Aldrich) in DMEM (BioWhittaker) and high pressure frozen with Leica EM Pact device (Leica Microsystems). Substitution was carried out in 0.3% uranyl acetate (Ted Pella, Inc.), 2% OsO_4 and 10% water in ethanol using a freeze substitution device (AFS2, Leica Microsystems). Specimens were first kept at –90°C for 16 hours, after which the temperature was increased by 10°C/hour to 0°C. The specimens were then washed with cold ethanol and acetone, gradually infiltrated into Epon at room temperature (acetone:Epon at 1:1, 0:1, 0:1, 30 min each) and flat embedded. Sections 90 nm thick were cut parallel to the sapphire disc and imaged using Tecnai FEG 20 microscope (FEI Corp.) operated at 200 kV. Images were collected with a 4k × 4k Ultrascan 4000 CCD camera (Gatan Corp.) at 19,000×, providing a 2× binned pixel size of 1.2 nm. For a tilt series, the

specimen was tilted at 1-degree intervals using a high tilt specimen holder (model 2020; E.A. Fischione Instruments) between ±62°. The images were acquired by Serial EM software (Mastronarde, 2005) and dual-axis tomography was applied (Mastronarde, 1997). The alignment of tilt series and tomographic reconstruction were done with IMOD software package (Kremer, 1996) using 10-nm colloidal gold particles overlaid on the top of the section as fiducial markers. Modeling was done with Amira software (TGS Inc.).

2.9.3 Stereology for electron microscopy

To quantify fenestrated membrane area and fenestral density using wholemount TEM, images of 50-100 transfected cells from each treatment were captured at a magnification of 250x following confirmation of fenestration at 1000x magnification. Images at 250x magnification were opened in Image J, fenestral sieve plates were highlighted using threshold setting (Fig. 2-1), fenestrated membrane area was measured and the corresponding cell number was counted.

Average fenestrated membrane area per cell = total fenestrated membrane area / cell number

For fenestral density quantification using wholemount TEM, 3-5 images at 1000x magnification were taken for each identified cell. Images were opened in Image Pro-Plus 6.1 software. Total sieve plate area was measured and the number of fenestral pores was counted.

Fenestral density = number of fenestrae/ sieve plate area.

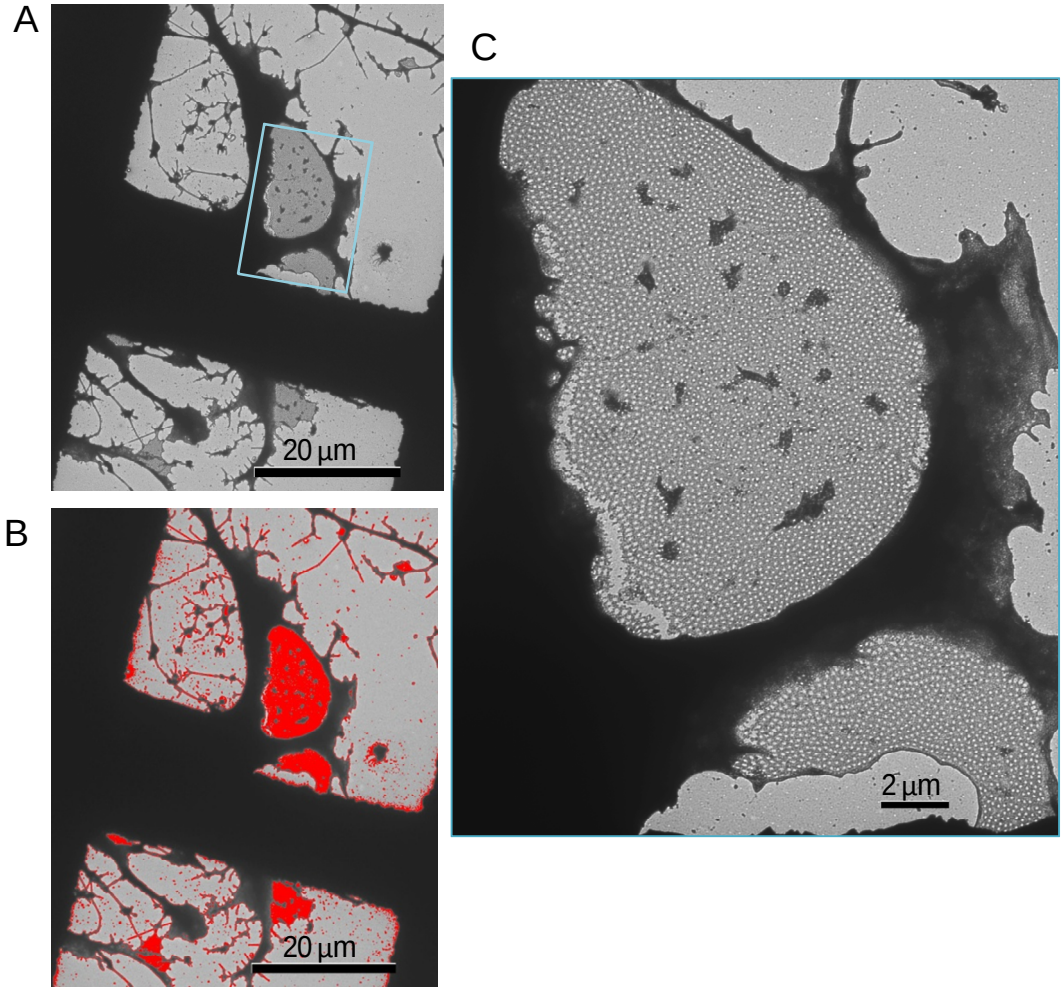

Fig. 2-1 Example of fenestraed membrane was highlighted by threshold holding using Image J software.

A. TEM image of part of a fenestrated bEND5 cell.
B. Fenestrated region was highlighted by threshold holding using Image J software.
C. Fenestration was confirmed by higher magnification.

2.9.4 Correlative LM-TEM (light microscopy-TEM) assay

Cells grown on glass coverslips containing grids were fixed with 4%PFA/0.1% glutaraldehyde for 15 minutes at room temperature, and then washed twice with PBS for 10 minutes. Cells were permeabilised with 0.1% Triton X-100 in PBS for 5 minutes and incubated in blocking buffer (5% donkey serum, 1% BSA, PBS) for 15 minutes. The immunolabelling procedure was the same as for cells on coverslips (section 2.7). After the last wash following secondary antibody incubation, coverslips with grids were mounted on slides with Vectashield mounting medium (Molecular Probes). Target cells were identified under a fluorescence microscope. The position of the target cells was recorded by marking on a drawing copy of the grid, assisted by images taken. The coverslip was carefully taken off the slide and the mounting media was rinsed off. Cells were fixed in 2.5% glutaraldehyde for 1hr at room temperature or overnight at 4°C. Cells were processed for visualisation by wholemount TEM (2.4.2.1), postfixed in 1% osmium tetroxide for 1 hour, then were dehydrated in an ascending ethanol series followed by HMDS (hexamethyldisilazane). The cells identified by fluorescence microscope were located in TEM and imaged (Diagram 2-2).

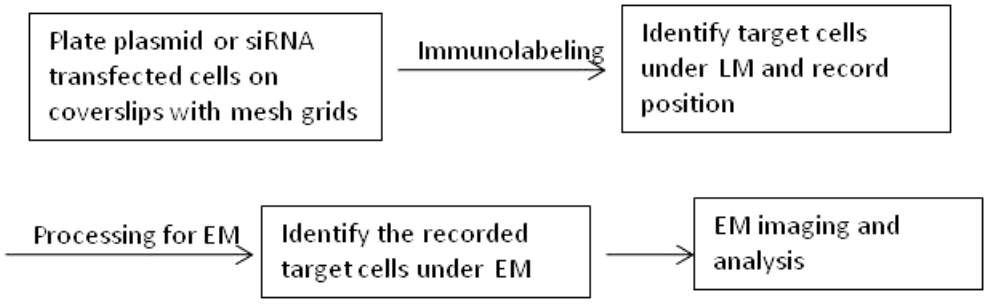

Diagram 2-2 Correlative LM-TEM assay

Chapter 3

In Vitro Induction of Fenestrae:

dynamics and search for novel components

Abbreviations

ABPs	actin binding proteins
AMD	age-related macular degeneration
BSA	bovine serum albumin
DMEM	Dulbecco's modified Eagle medium
ER	endoplasmic reticulum
ERGIC	ER-Golgi intermediate compartment
FAK	focal adhesion-associated kinase
FACR	fenestrae-associated cytoskeleton ring
GEnC	glomerular endothelial cell
GFP	green fluorescent protein
GFR	glomerular filtration rate
HSPG	heparan sulfate proteoglycans
HuVEC	human umbilical vein endothelial cells
LSEC	liver sinusoidal endothelial cells
MβCD	methyl-β-cyclodextrin
NPC	nuclear pore complex
PBS	phosphate-buffered saline
PFA	paraformaldehyde
PMA	phorbol myristate acetate
PV-1	plasmalemmal vesicle–associated protein–1
RA	retinoic acid
RPE	retinal pigment epithelium
SNARE	soluble N-ethylmaleimide sensitive fusion protein attachment protein receptor
TGF-β	transforming growth factor β
VEGF	vascular endothelial growth factor
VVOs	vesiculo-vacuolar organelles

Chapter 3 *In Vitro* Induction of Fenestrae: dynamics and search for novel components

3.1 *In vitro* cell assay for induction of fenestrae

Because of the small size of fenestrae, the fragility of the attenuated cytoplasm in the sieve plates, and the lack of specific markers, study of fenestrae is largely dependent on technically demanding ultrastructural methods. Furthermore, endothelial cells that have fenestrae *in vivo* become dedifferentiated and lose their fenestrated phenotype when cultured *in vitro* (Carley, 1988; Esser, 1998). Therefore, study of fenestrae has almost exclusively relied on *in vivo* and *ex vivo* morphological analysis. These techniques provide limited information, making dynamic interpretations difficult.

Attempts to induce and/or maintain endothelial fenestrations have led to use of PMA (Lombardi, 1986 and 1987), VEGF (Esser, 1998), RA (Lombardi, 1988), tumor-conditioned medium (Folkman, 1980), conditioned extracellular matrix (Milici, 1985; Carley, 1988; Esser 1998) and the F-actin disruption agents cytochalasin B and latrunculin A (Steffan, 1987; Braet, 1996 and 1998). Unfortunately, the induced number of fenestrae using these models is very low compared with the *in vivo* situation, and is insufficient for cell biological or biochemical studies. In primary culture of freshly isolated LSEC, the number of fenestrae can be upregulated 2-3 fold by using the F-actin filament disruption agents cytochalasin B and latrunculin A (Steffan, 1987; Breat, 1996). However, the fenestrated phenotype is lost in 2-3 days (Steffan, 1995; Braet, 2005; Elvevold, 2008).

By screening a large panel of endothelial cells for their response to factors previously reported to induce fenestrae *in vitro*, our laboratory developed a cell assay in which abundant fenestrae can be rapidly induced by treatment with the F-actin depolymerising agent latrunculin A in the bEND5 mouse endothelioma cell line (Fig.

3-1A) (Ioannidou, 2006). Using the known diaphragm protein PV-1 as an immunolabelling marker, our lab also established a correlative light microscopy-electron microscopy assay (correlative LM-EM assay) (Fig. 3-1B) (Ioannidou, 2006) which enables study of fenestrae by primarily using epifluorescence light microscopy, only using TEM for final confirmation. This assay greatly expedites the study of fenestrae and serves as a tool for gain- and loss-of function approaches.

3.2 Validation of *in vitro* assay of fenestra induction

I began my work with the *in vitro* assay of fenestra induction by treating bEND5 cells with 1.25 µM latrunculin A. The presence of fenestrae was confirmed by whole mount TEM, thin section TEM and freeze-fracture deep-etch techniques (Fig. 3-2A). In the induced bEND5 cells, most of the peripheral plasma membrane is perforated by numerous fenestrae. The fenestrae are organized in orderly patches of sieve plate, which excluded microtubules and most organelles. Freeze-fracture revealed that the sieve plates were extremely flat membrane sheets, which resembled the nuclear envelope with nuclear pores. From the sectioning TEM image of scraped, latrunculin A-treated bEND5 cells, dramatic attenuation in the fenestrated cell region and the side view of the fenestral sieve plates were clearly visible (Fig. 3-2B). The fenestral pores displayed remarkably consistent pore diameters of 60-70 nm. The fenestral diaphragm, especially the central knob part, was readily recognisable in many of the induced fenestrae (Fig. 3-2B).

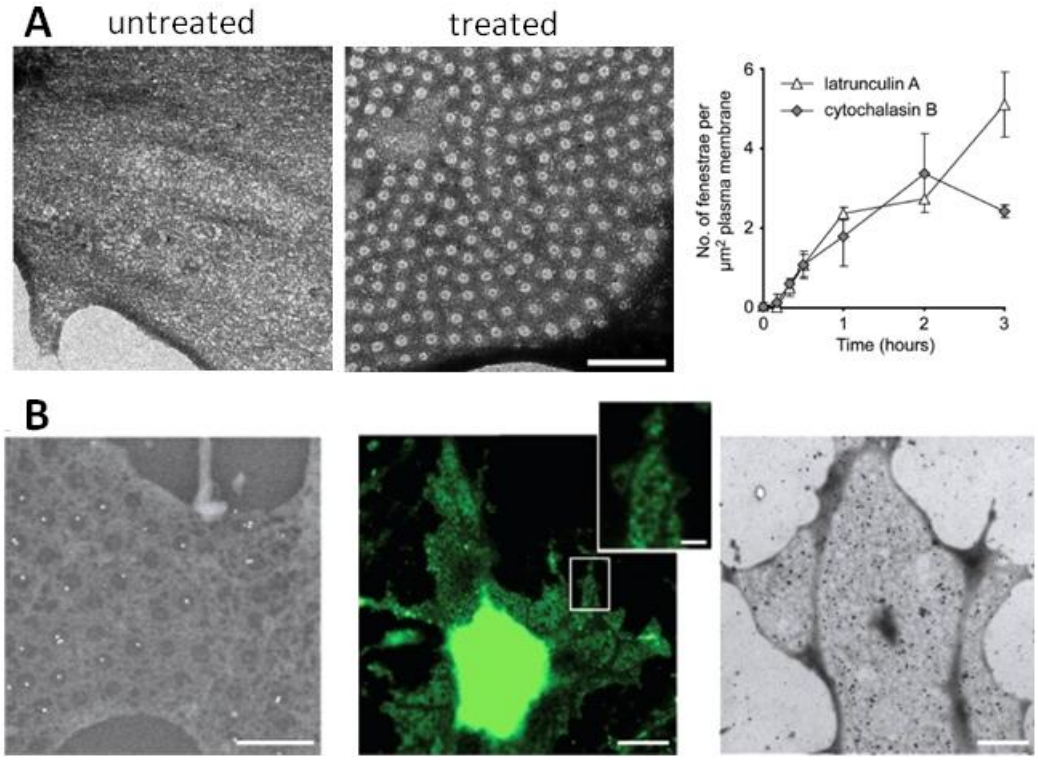

Fig. 3-1 Fenestra induction in bEND5 cells.

A. Numerous fenestrae were induced by treating bEND5 with latrunculin A (2.5 µM) for 3 hrs; Scale bar, 0.5 µm.
B. Correlative light microscopy-electron microscopy assay showing close correlation of PV-1 staining (green) with induced fenestrae. Scale bar, 0.5 µm. (Adapted from Ioannidou, 2006.)

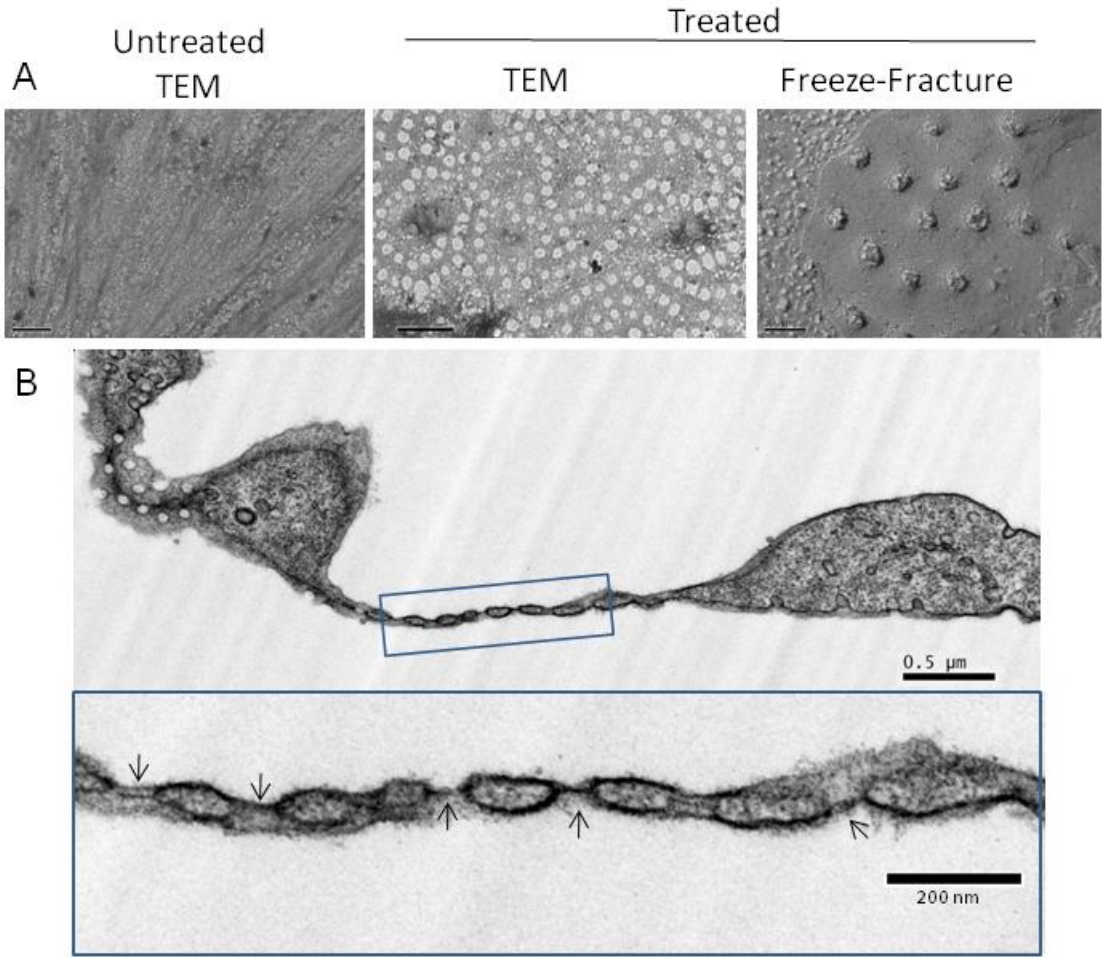

Fig. 3-2 Validation of fenestra induction in bEND5 cells.

A. Fenestra induction was confirmed by TEM and freeze-fracture electron microscopy. Scale bar: TEM, 0.5 μm; freeze-fracture, 200 nm.
B. Side view of fenestral sieve plates in a latrunculin A-treated bEND5 cell. Arrows, diaphragm of fenestral pore.

I further used immunofluorescence staining to identify the induced fenestral sieve plates in bEND5 cells. Using the optimised immunostaining method described in Chapter 2, non-specific binding from the second antibody or from generic IgG binding was controlled in minimum level (Supplemental Fig. 1-1). Before the addition of latrunculin A, F-actin fibres were vibrantly stained by fluorescence conjugated phalloidin, a marker specifically binds to F-actin filament. Most of the F-actin fibres were disassembled after 20 minutes of incubation with latrunculin A, and PV-1 underwent dynamic redistribution (Fig. 3-3A). By the end of 3 hours' incubation with latrunculin A, all of the F-actin filaments were disrupted and only short F-actin remnants or aggregates were present in bEND5 cell. Correspondingly, PV-1 marked the distinct sieve plates in the induced bEND5 cells (Fig. 3-3B). When co-stained with the microtubule marker – β-tubulin, the induced fenestral sieve plates are delineated by microtubules (Fig. 3-4, A and B). Because of the clear exclusion of microtubules and nucleus from the fenestral sieve plates, I tried to quantify the induced fenestral sieve plates by measuring the cell area where is stained by PV-1 but neither β-tubulin nor DAPI. The ratio of the PV-1^{+}/β-tubulin^{-}/DAPI^{-} cell area was significantly increased in latrunculin A treated bEND5 cells (Fig. 3-4C). However, the readily distinguishable sieve plates pattern is more easily to be recognised under the fluorescence microscope and serves a more useful mean for our study focused on fenestra formation in bEND5 cells.

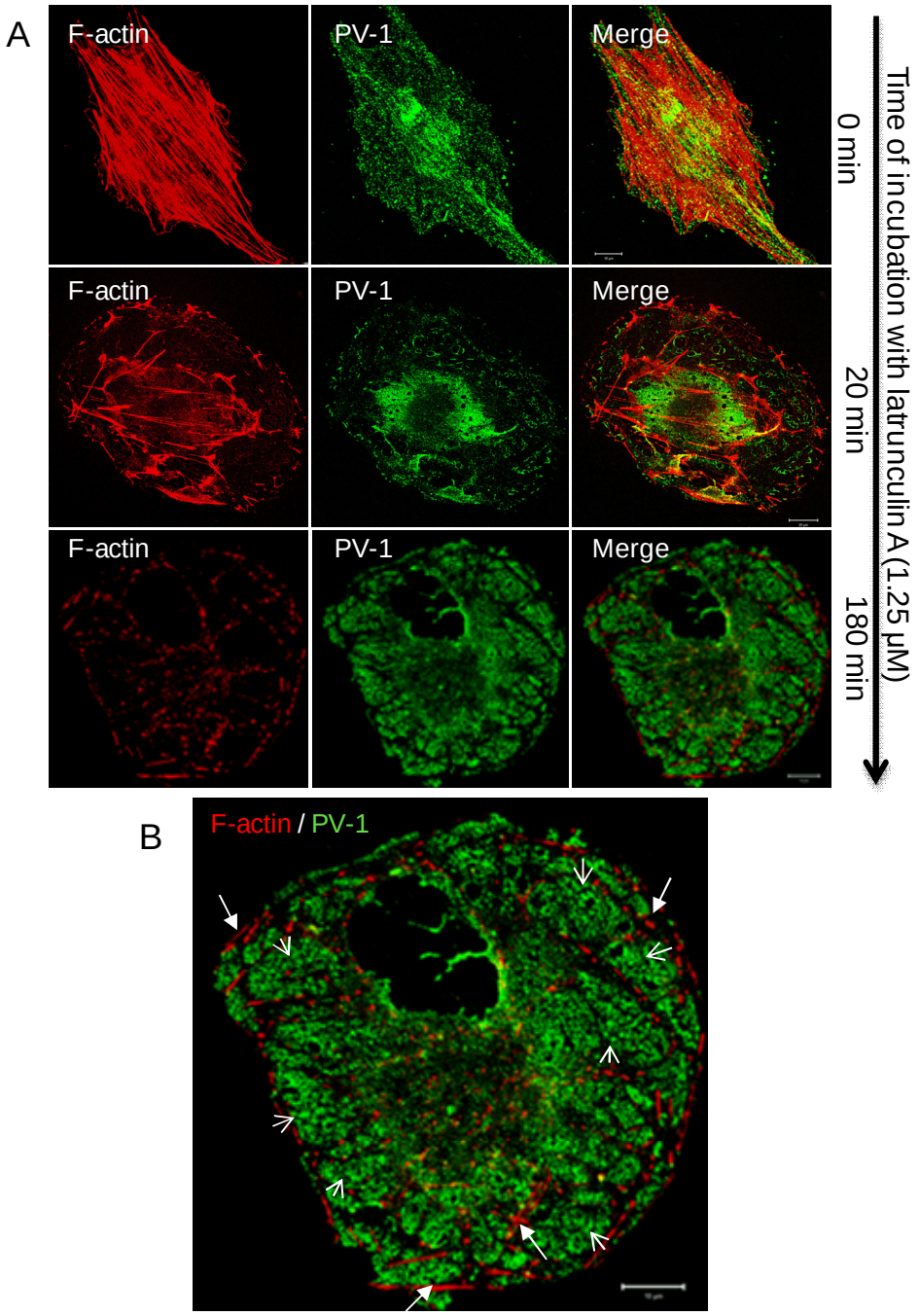

Fig. 3-3 Fenestra induction revealed by immunofluorescence analysis.

A. Alexa Fluor 594 conjugated phalloidin revealed F-actin disruption by latrunculin A. PV-1 went through a dynamic reorganisation, and marked the distinctive fenestral sieve plates in the end of incubation for 3 hours. Scale bar, 10 µm.

B. Maginified image of the fenestrae induced bEND5 cell. Long blocked arrows, F-actin remnants and aggregates; short open arrow s, fenestral sieve plates.

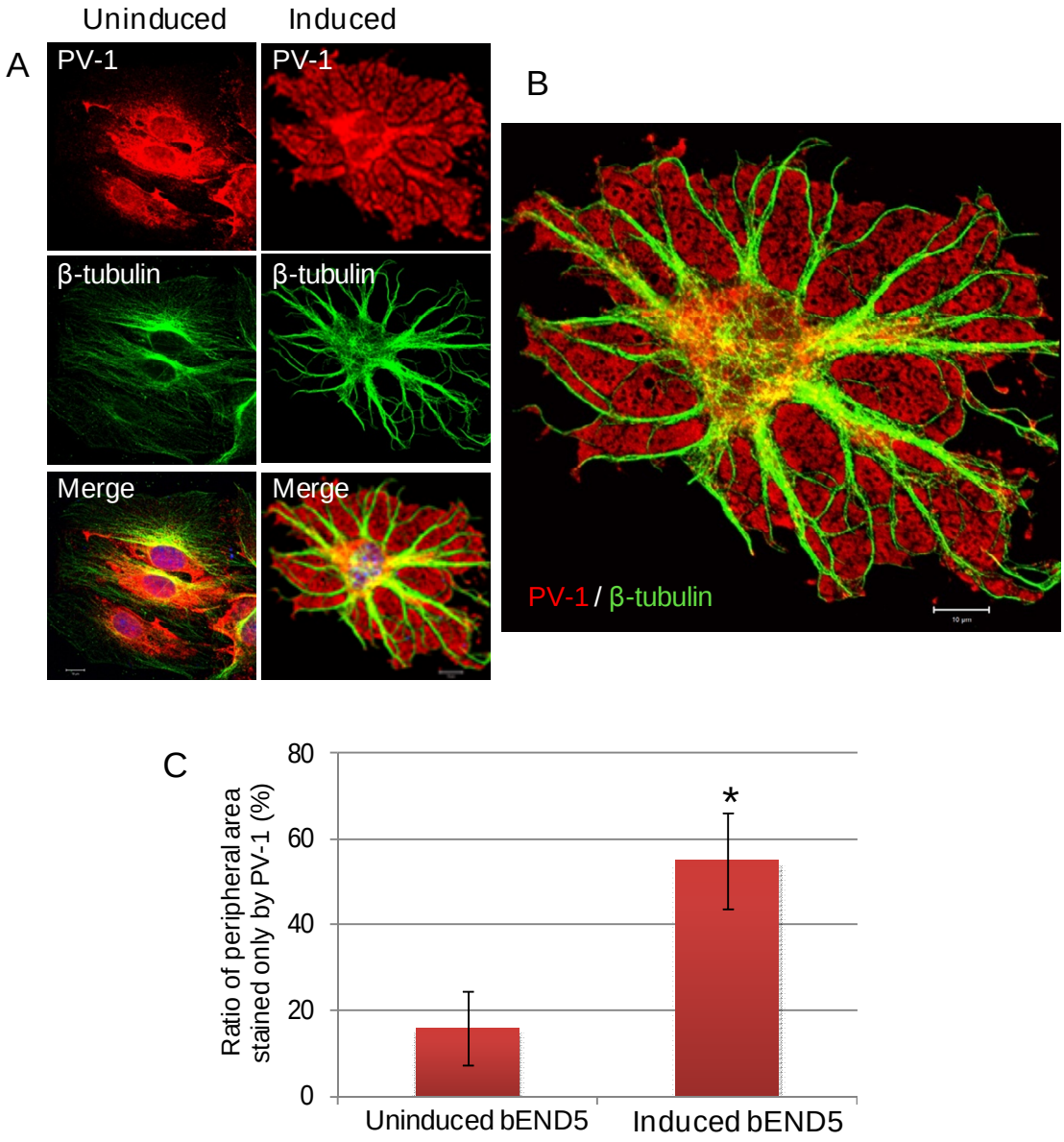

Fig. 3-4 Fenestral sieve plates are delineated by microtubules.

A. Fenestra formation was triggered by latrunculin A treatment (1.25 μm for 3 hours). The induced fenestral sieve plates were delineated by microtubules marked by β-tubulin. Scale bar, 10 μm
B. Magnified image of the induced bEND5 cell with fenestral sieve plates delineated by microtubules.
C. Quantification of ratio of the area where is immunostained by PV-1but not by β-tubulin or DAPI, which marks the nucleus. Ratio of peripheral PV-1 stained area = [Total area – (β-tubulin area + DAPI area)] / Total area X 100. N = 10 for each group, * $P < 0.0001$.

3.3 Characterisation of fenestra induction in bEND5 cells

3.3.1 Segregation of PV-1 and caveolin-1 during induction of fenestrae.

PV-1 is found not only in the diaphragm of fenestrae, but also in caveolae and transendothelial channels (Stan, 1999; Fig. 3-4A). PV-1 colocalised with caveolin-1, especially in membrane ruffles and at points of cell-cell contact in uninduced bEND5 cells, typical of caveolae distribution. However, after 3 hours of treatment with latrunculin A, PV-1 and caveolin-1 marked distinct regions – PV-1 marked the induced fenestral sieve plates whereas caveolin-1 was excluded (Fig. 3-5B).

3.3.2 Rapid kinetics during induction of fenestrae

A striking observation during fenestra induction is the rapid kinetics upon treatment with latrunculin A. The entire induction takes only 3 hours to complete. TEM images showed that fenestrae started to appear as early as 10 minutes after F-actin disruption, and disappeared 30 minutes after latrunculin A wash out (data not shown). Palade's group showed that VEGF can also induce fenestrae in normally non-fenestrated vessels within 10 minutes of topical or intradermal administration (Roberts, 1997). Since PV-1 is the diaphragm protein of both fenestrae and caveolae, we used it as a tracking marker to appreciate the rapid dynamics during fenestra induction.

To understand how PV-1 segregates from caveolae then shifted to fenestrae, we carried out a time course of fenestra induction to follow the movement of PV-1 and caveolae, as marked by caveolin-1. Mundy *et al*. showed that caveolar traffic in the membrane of CHO cells is controlled by both the actin cytoskeleton and microtubules. Disruption of actin filaments triggered rapid and massive movements of caveolin-1-positive structures toward the centrosomal region of the cell (Mundy, 2002). Consistent with Mundy's observation, we found that PV-1/caveolin-1-labelled caveolae moved toward the centre of the cell, presumably to a caveosome close to the microtubule organization centre, upon treatment with latraunculin A. From 60 minutes of induction, PV-1 was

observed to segregate from caveolae on the edge of the microtubule rich region. After 3 hours of induction, PV-1 shifted into fenestral sieve plates in the cell periphery, between the microtubule branches (Fig. 3-6). The time course clearly showed the need for membrane trafficking, membrane retraction, protein sorting followed by membrane spreading as PV-1 shifted into nascent fenestrae. We hypothesized that this was accomplished through mass internalisation of caveolae and their transport along microtubules to the perinuclear region.

3.3.3 Segregation of PV-1 and caveolin-1 was compromised by microtubule disruption

We further carried out experiments to investigate the potential role of microtubules during fenestra formation. bEND5 cells were treated with latrunculin A with or without pre-treatment of nocodazole, a microtubule depolymerisation reagent (Mundy, 2002). Consistent with Mundy's work, we observed increased accumulation of caveolae in a linear arrangement on the cell membrane with 1 hour of nocodazole treatment in uninduced bEND5 cells (Fig. 3-7, row ND). When the nocodazole pre-treated cells were incubated with latrunculin A, caveolin-1 and PV-1 were aggregated on the peripheral region of the cell without segregation, and distinct sieve plates were not observed. However, when bEND5 cells were treated with latrunculin A first, followed by nocodazole addition, the induced fenestral sieve plates were not much affected by the disruption of microtubules (Fig. 3-7). These results suggest that microtubules do not participate in the actual fenestral pore formation process, but more likely are involved in the vesicle/protein transportation required for fenestra formation.

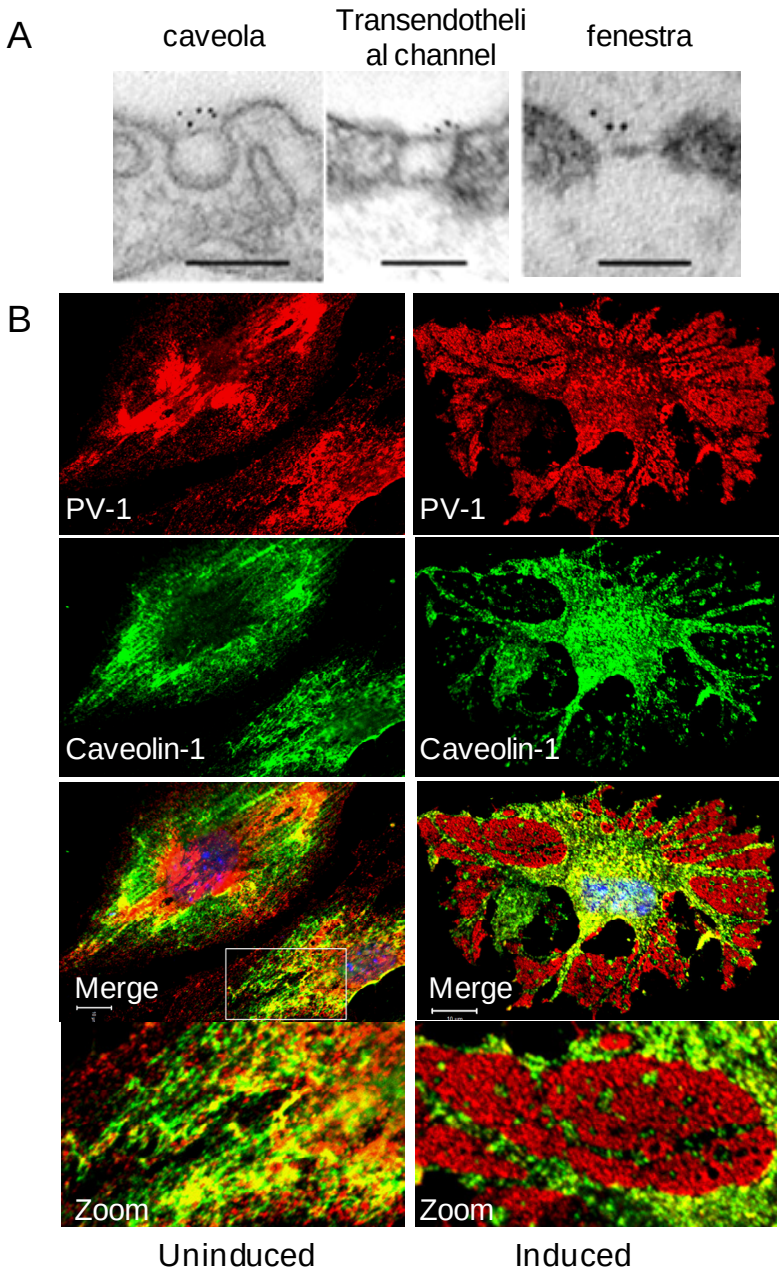

Fig. 3-5 Segregation of PV-1 from caveolin-1 during fenestra formation.

A. PV-1 is the common diaphragm protein in caveolae, transendothelial channels and fenestrae. Scale bar, 100 nm. (Adapted from Stan, 1999)

B. PV-1 and caveolin-1 colocalise in caveolae in uninduced bEND5 cells, but in latrunculin A induced bEND5 cells, PV-1 is separate from caveolin-1, marking the distinct fenestral sieve plates. Scale bar, 10 µm.

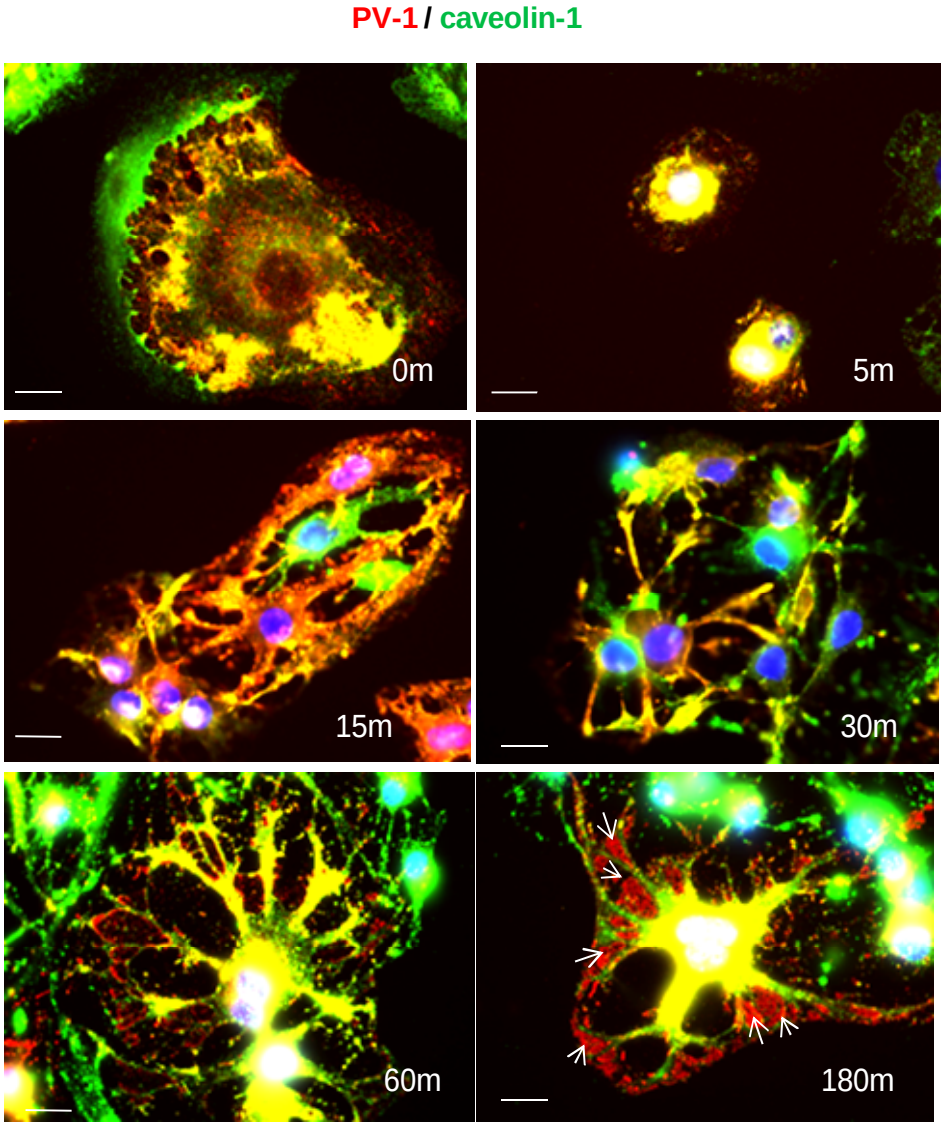

Fig. 3-6 Time course of PV-1 segregation from caveolae during the time course of fenestra induction. Scale bar, 10 μm; m, minutes

PV-1 co-localised with caveolin-1 marked caveolae in uninduced bEND5 cells (0 m). At 5 minuts, PV-1- and caveolin-1-positive intermediates (cavesomes?) were enriched in the perinuclear region and microtubule/organelle-rich region after 15 minutes of latrunculin A treatment; at 60 minutes, PV-1 segregation from caveolin-1 positive intermediates was visible. At the end of latrunculin A treatment (3 hours), fenestral sieve plates that were positive for PV-1 and negative for caveolin-1 were readily distinguishable (arrows).

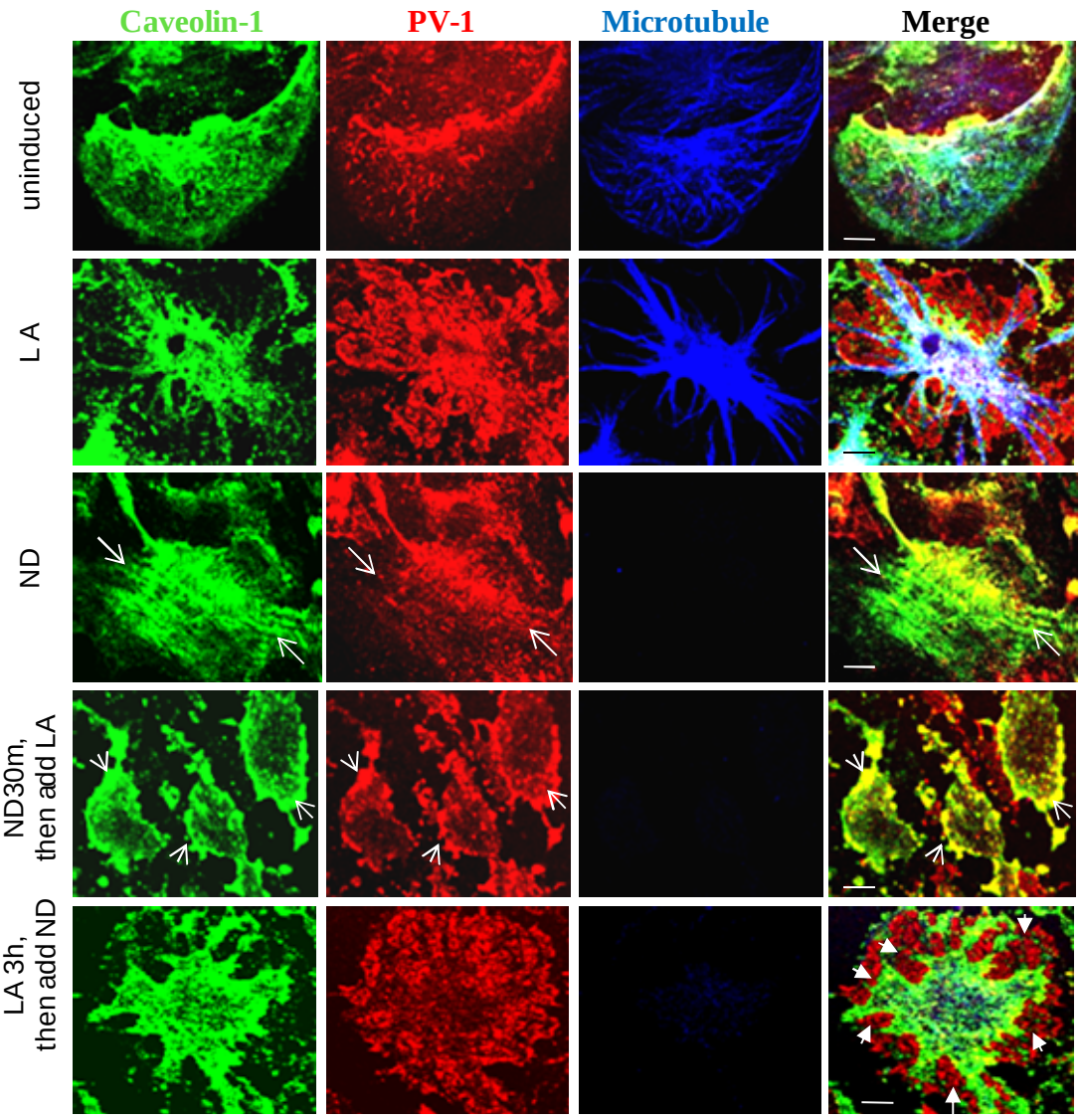

Fig. 3-7 Segregation of PV-1 from caveolae was compromised by microtubule disruption. Scale bar, 10 μm.

Nocodazole treatment (15 μM, 1 hour) resulted in linear accumulation of caveolae (long arrows in ND row). When nocodazole treatment was followed by latrunculin A-mediated actin disruption, PV-1 and caveolin-1 aggregated on the cell surface (short arrows). Nocodazole treatment after latrunculin A incubation didn't disrupt the already induced fenestral sieve plates (arrow heads).

ND, nocodazole, 15 μM; LA, latrunculin A, 1.25 μM.

3.3.4 Endocytosis is essential for fenestra formation

MβCD **(**Methyl-β-cyclodextrin) forms soluble inclusion complexes with cholesterol, thereby enhancing cholesterol solubility in an aqueous solution (Pitha, 1988; Irie, 1992). MβCD extracts cholesterol from the membrane and greatly inhibits both caveolae- and clathrin-dependent endocytosis (Rodal, 1999). Incubation of bEND5 cells with MβCD at a concentration of 10 μM induced accumulation of membrane-bound PV-1 into tubulo-vesicular structures, which became longer over incubation time with MβCD (Fig. 3-8). This observation is reminiscent of tethered vesicle shedding as reported for mesoangioblast stem cells (Candela, 2010). Combined treatment with MβCD and latrunculin A resulted in failure of sieve plate formation (Fig. 3-8).

To further substantiate the role of endocytosis in PV-1 dynamics and fenestra formation, we chose to inhibit the dynamin pathway. Dynamins are members of the GTPase superfamily. They function in membrane fission of budding vesiculo-tubular structures. Dynamin 1 and 2 are essential for clathrin-dependent and caveolae-dependent endocytosis from the plasma membrane, and for vesicle formation at the trans-Golgi network (Rappoport, 2008; Jones, 1998). Dynasore is a small molecule which specifically inhibits dynamin. It acts as a potent inhibitor of dynamin-dependent endocytic pathways by rapidly blocking coated vesicle formation (Macia, 2006). The reported concentration of dynasore to inhibit endocytic functions ranged from 15 μM to 80 μM (Macia, 2006), so I chose dynasore at 40 μM to incubate with bEND5 cells. Immunofluorescence staining showed that incubation of 1 hour resulted in decreased PV-1 immunostaining (Fig. 3-9). Further reduced PV-1 immunostaining and abnormal cell morphology were observed with a longer incubation of 3 hours. The combined treatment of bEND5 cells with latrunculin A and dynasore resulted in almost complete absence of detectable PV-1 and an abnormally reorganised actin cytoskeleton (Fig. 3-9). Based on these results, an assessment of fenestra formation is precluded, since PV-1 immunostaining is the primary marker of the sieve plates.

To summarise, fenestra formation is a highly dynamic biological process. F-actin depolymerises, PV-1 segregates from caveolin-1, and membrane and protein are busily trafficking through, at the least, endocytic pathway and microtubules. Fenestrae arise from the coordinating occurrences of these, and probably more, aspects in a given bEND5 cell.

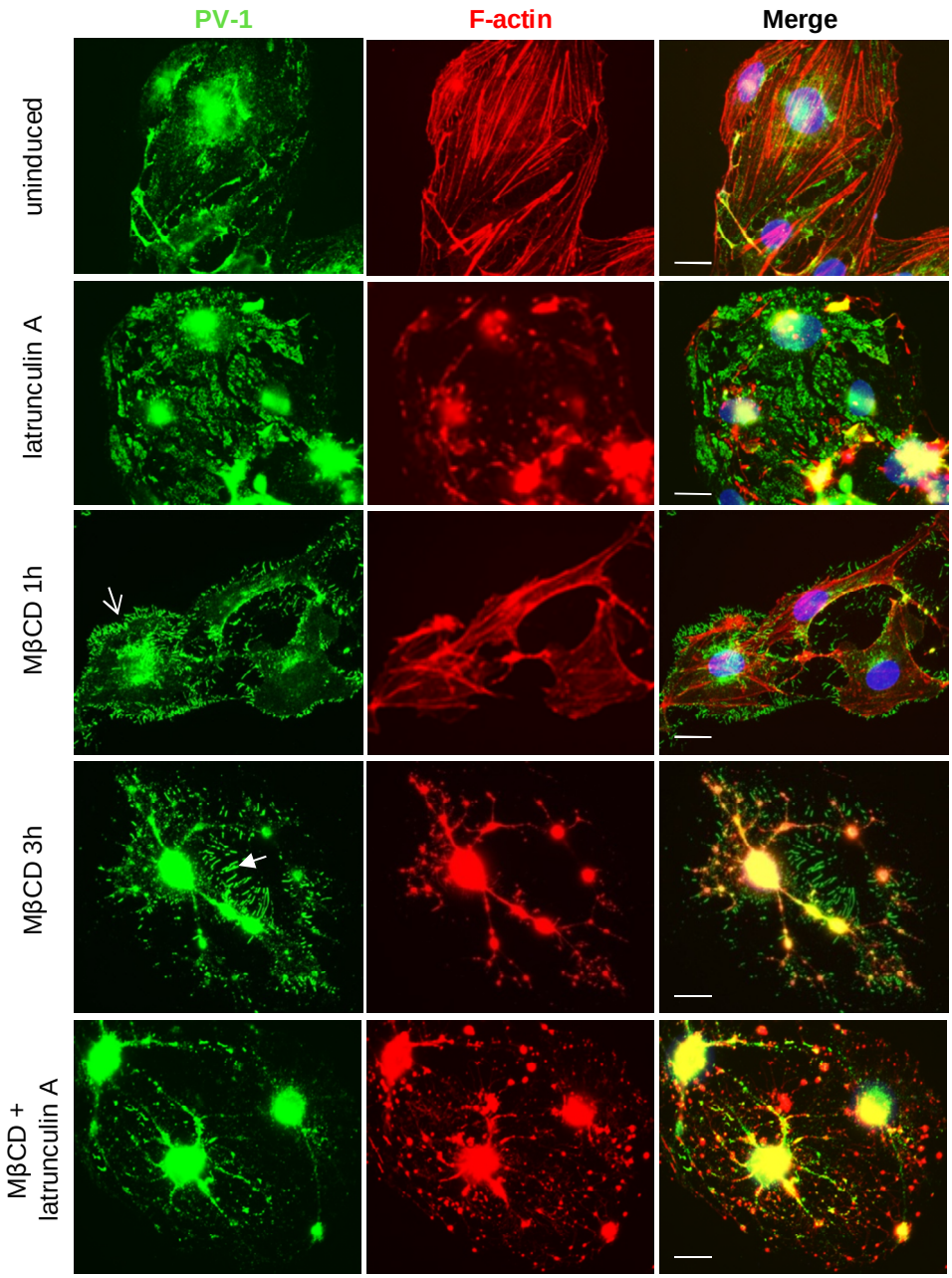

Fig. 3-8 Inhibition of latrunculin A-induced fenestra formation by MβCD treatment. Fenestrae in bEND5 cells were induced by latrunculin A (1.25 μM) for 3 hours. MβCD (10 μM) caused abnormal PV-1-positive structures on the cell surface (arrow) by 1 hour of treatment. Longer incubation resulted in tethered vesicle shedding (blocked arrow). Latrunculin A treatment in the presence of MβCD failed to induce fenestra formation in bEND5 cells. Scale bar, 10 μm.

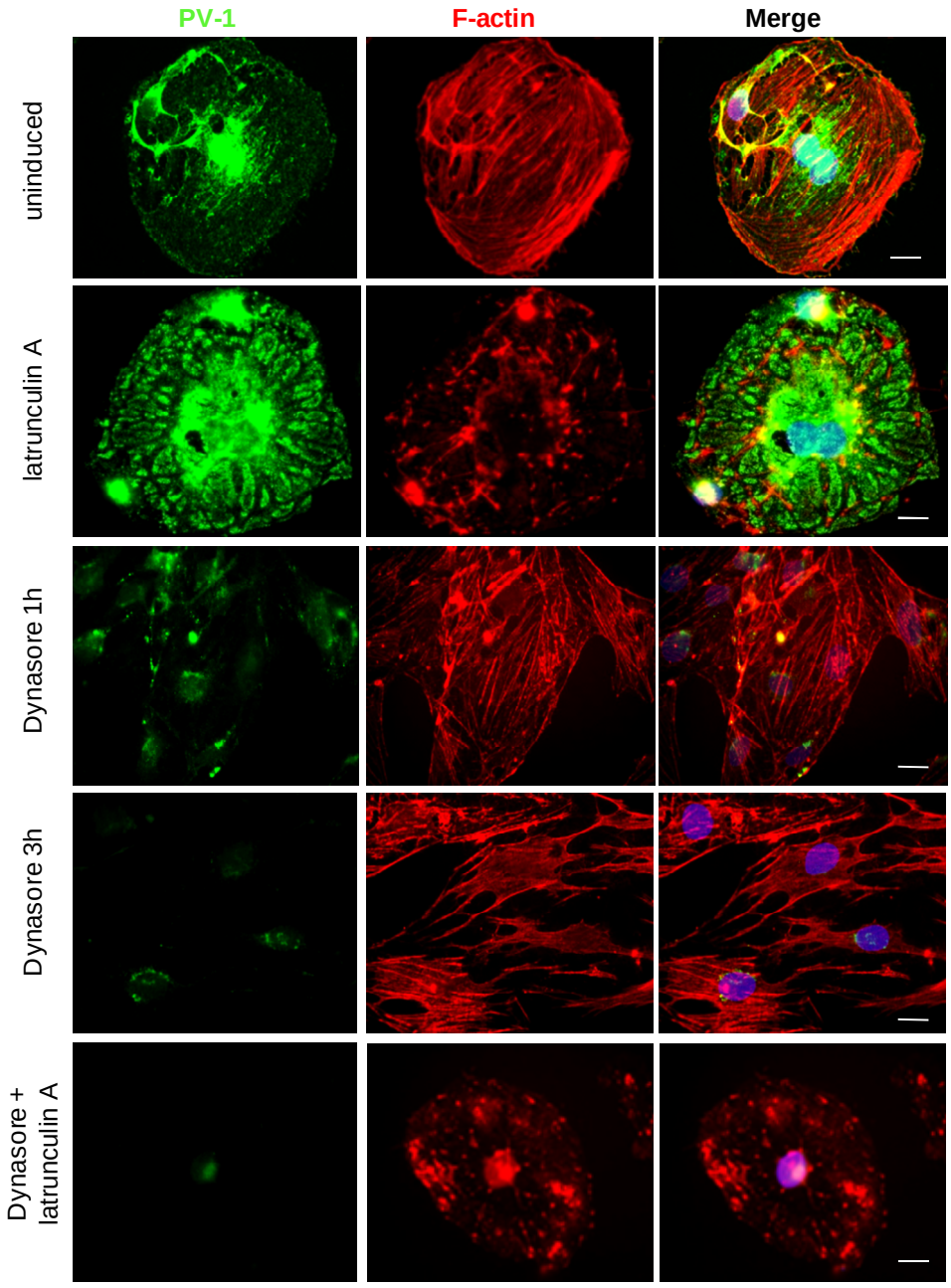

Fig. 3-9 Loss of detectable PV-1 caused by dynasore treatment

Fenestrae in bEND5 cells were induced by latrunculin A (1.25 μM) for 3 hours. Dynasore (40 μM) caused abnormal F-actin reorganisation and PV-1 loss. Scale bar. 10 μm.

3.4 Identification of novel components of fenestra

3.4.1 Involvement of actin binding proteins (ABPs) and F-actin microfilaments in fenestra formation

3.4.1.1 Candidate validation from proteomic analysis

The rapid kinetics of fenestra induction suggest that protein synthesis is unlikely to play a role; instead, fenestrae are more likely formed by rearrangement and recruitment of pre-exisiting components. However, little is known about the mechanism of fenestra formation or of the components of the pore. So far, the diaphragm protein PV-1 is the only known component of diaphragmed fenestrae. Cross-linking studies in cells rich in caveolae failed to identify any proteins associated with PV-1 (Stan, 2004). Therefore, our lab carried out a proteomic approach to identify novel component(s) of fenestrae. Briefly, taking advantage of the *in vitro* fenestra induction assay and using a cationic colloidal silica isolation method, cell membranes from uninduced cells and induced cells were captured, isolated and subjected to a biochemical analysis using two-dimensional gel electrophoresis and mass spectrometry. A subtractive analysis of non-fenestrated versus fenestrated plasma membrane proteomes identified 20 proteins (Supplemental Table 1) (Ioannidou, PhD Thesis, 2005). Surprisingly, many of the candidates were actin-binding proteins (Supplemental Fig. 1).

Using immunofluoresence analysis, I attempted define the localisation of all 20 proteins identified by proteomic analysis in fenestrated endothelial cells. Most of the candidates were either excluded from the sieve plates or displayed staining too weak to comment further. However, two of the candidates from the proteomic analysis, moesin and annexin II, showed distinct expression patterns in the induced bEND5 cells (Fig. 3-10 and11).

Moesin is a member of the ERM (ezrin, radixin and moesin) protein family. These proteins are well-documented crosslinkers between the plasma membrane and the

underlying F-actin cytoskeleton (Brestcher, 2002). Immunofluorescence analysis revealed that moesin was abundantly expressed in bEND5 cells and colocalised with PV-1 in fenestral sieve plates (Fig. 3-10).

Annexin II, another candidate fenestral protein from the proteomic study, was also highly expressed in bEND5 cells. Annexins are scaffolding proteins involved in regulation of membrane dynamics and organization (Gerke and Moss, 2002; Futter, 2007). Annexin II also participates in vesicle trafficking and cytoskeleton regulation (Hayes, 2004). In latrunculin A-treated bEND5 cells, annexin II was localised to large vesicular structures that were distributed within sieve plates (Fig. 3-12).

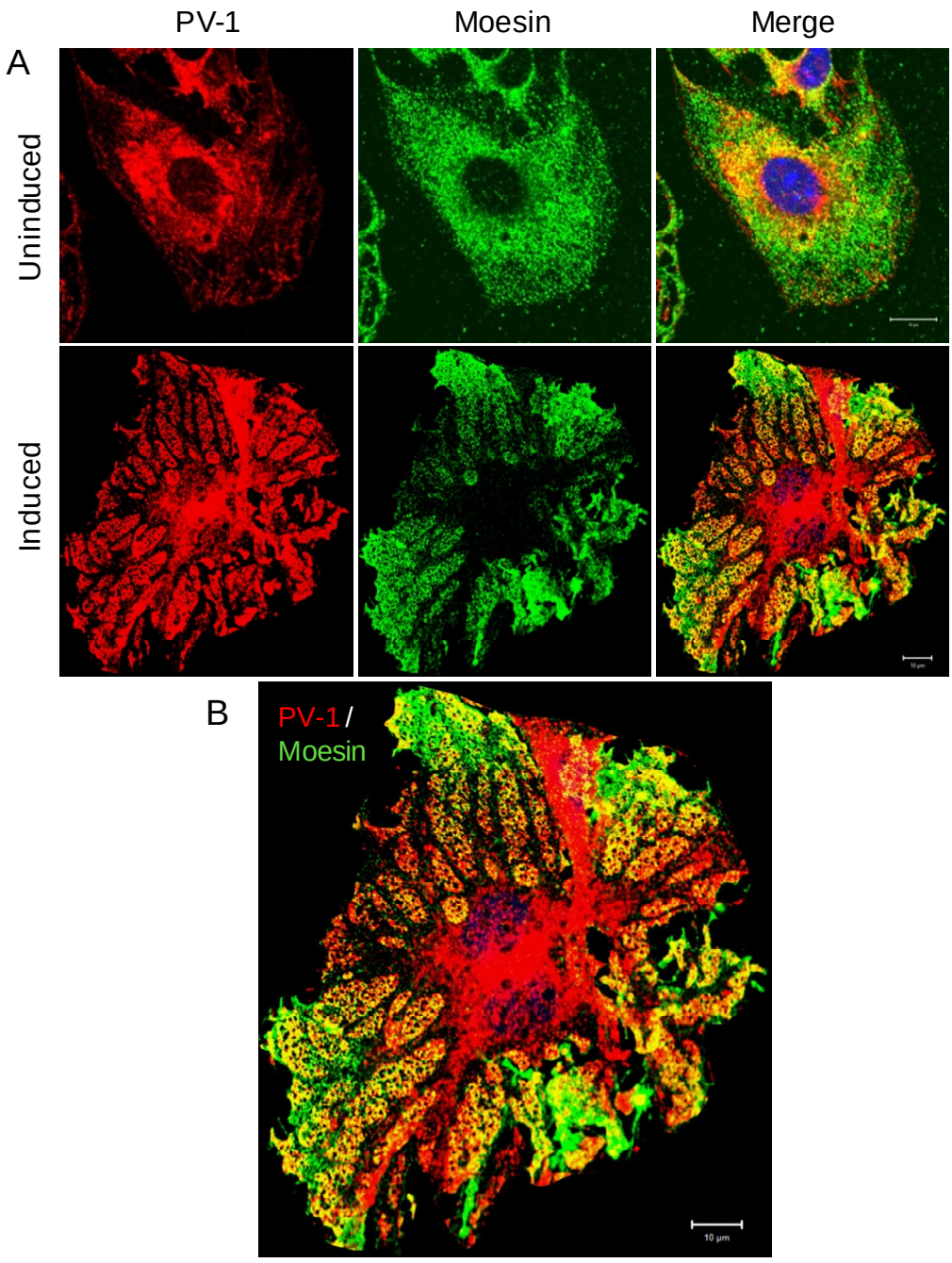

Fig. 3-10 Moesin is colocalised with PV-1 in fenestral sieve plates.

Moesin is abundantly expressed in bEND5 cells, it doesn't colocalise with PV-1 in uninduced bEND5 cells; however, moesin is reorganised into fenestral sieve plates and colocalised with PV-1 when fenestrae are induced by latrunculin A in bEND5 cells. Scale bar, 10 µm.

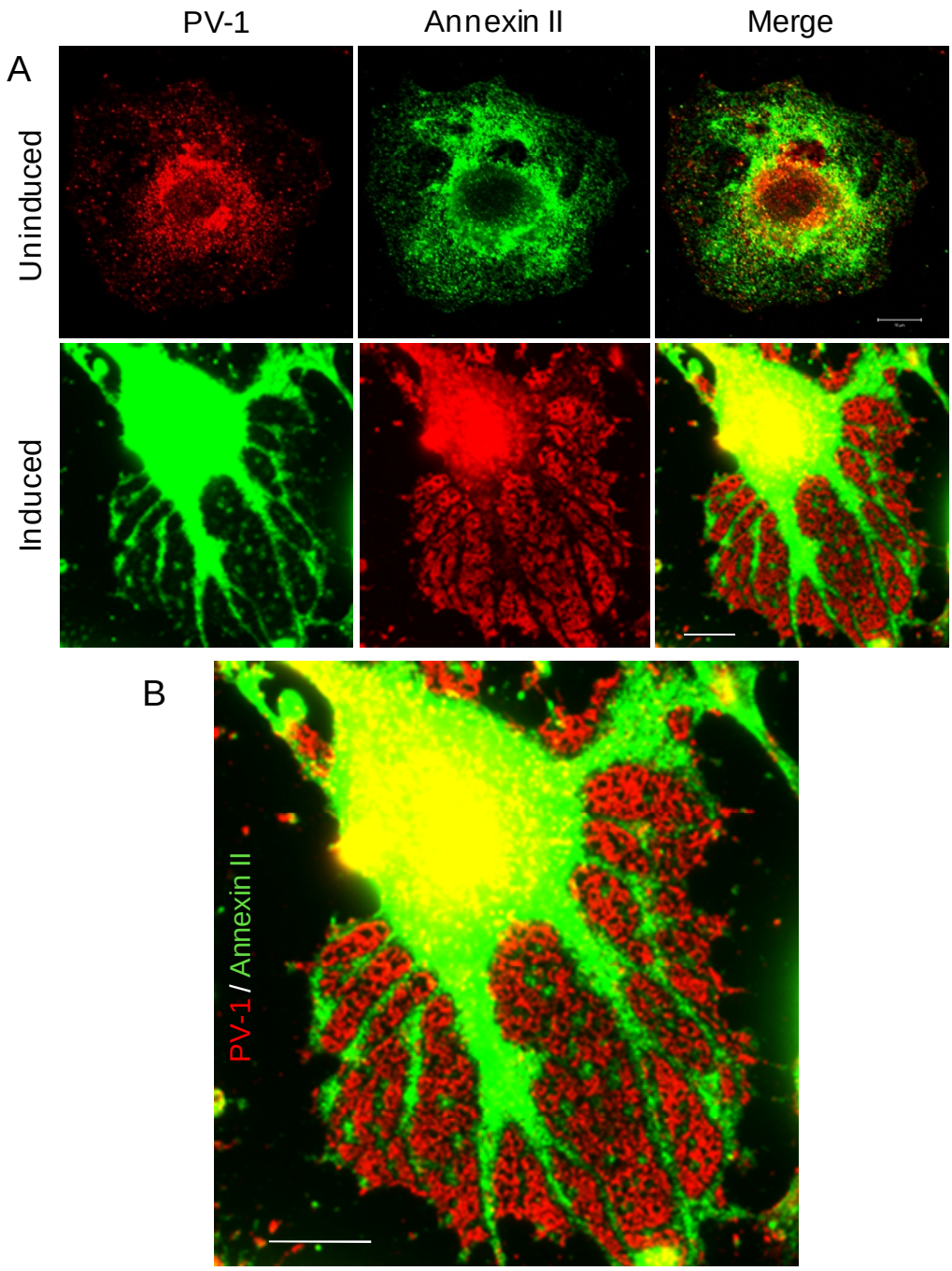

Fig. 3-11 The distribution of annexin II in fenestrated bEND5 cell.

Annexin II is present in fenestrated region of bEND5 cell, but unlike moesin, it is scattered like small islands among the sieve plates. Scale bar, 10 μm.

3.4.1.2 F-actin microfilaments are present in fenestral sieve plates

Actin is one of the most abundant and conserved structural proteins of eukaryotic cells. It is a major determinant of cell shape, division, motility and adhesion (Bershadsky, 1988; Bray, 1992). In nonmuscle cells, actin filaments are highly dynamic structures. They are constantly in the process of being assembled, disassembled and reorganised as the cell changes its shape, divides, crawls and adheres to a substratum or to neighbouring cells (Bershadsky, 1988; Bray, 1992; Mitchison, 1996; Small, 1999; Stossel, 1994; Theriot, 1994; Welch, 1997). The actin cytoskeleton also functions as a barrier to membrane fusion, such as exocytosis in secretory cells. Actin filament disruption by cytochalasin D significantly increases granule release in chromaffin cells (Aunis, 1988). In LSEC, fenestra number is increased by many different drugs that alter actin polymerisation (Steffan, 1987; Braet, 1996 (Hepatology); Braet, 1998), which suggests that the observed fenestra induction is a direct consequence of actin disruption rather than a side effect of anti-actin drugs.

In our *in vitro* cell model, the disruption of F-actin filaments is a prerequisite for fenestra induction, and we assumed that the post-latrunculin A remnants of actin were not important. However, the localisation of moesin and annexin II in sieve plates led us to re-examine the distribution of actin following fenestra induction. Upon treatment with latrunculin A, F-actin stress fibres and cortical actin began to disassemble as early as 5 minutes. By 3 hours of latraunculin A treatment, aggregates of comet actin and short F-actin filaments were scattered around the cell; fenestrae were formed in orderly sieve plates marked by PV-1; and, although the staining was faint, phalloidin-positive staining was reproducibly observed in all fenestral sieve plates, co-localising with PV-1 (Fig. 3-12). In contrast, no fluorescent signal was observed when probing the cells with the G-actin marker, DNAse I (data not shown), suggesting that the F-actin alone was in the sieve plates, but presumably too small to resolve into actin filaments.

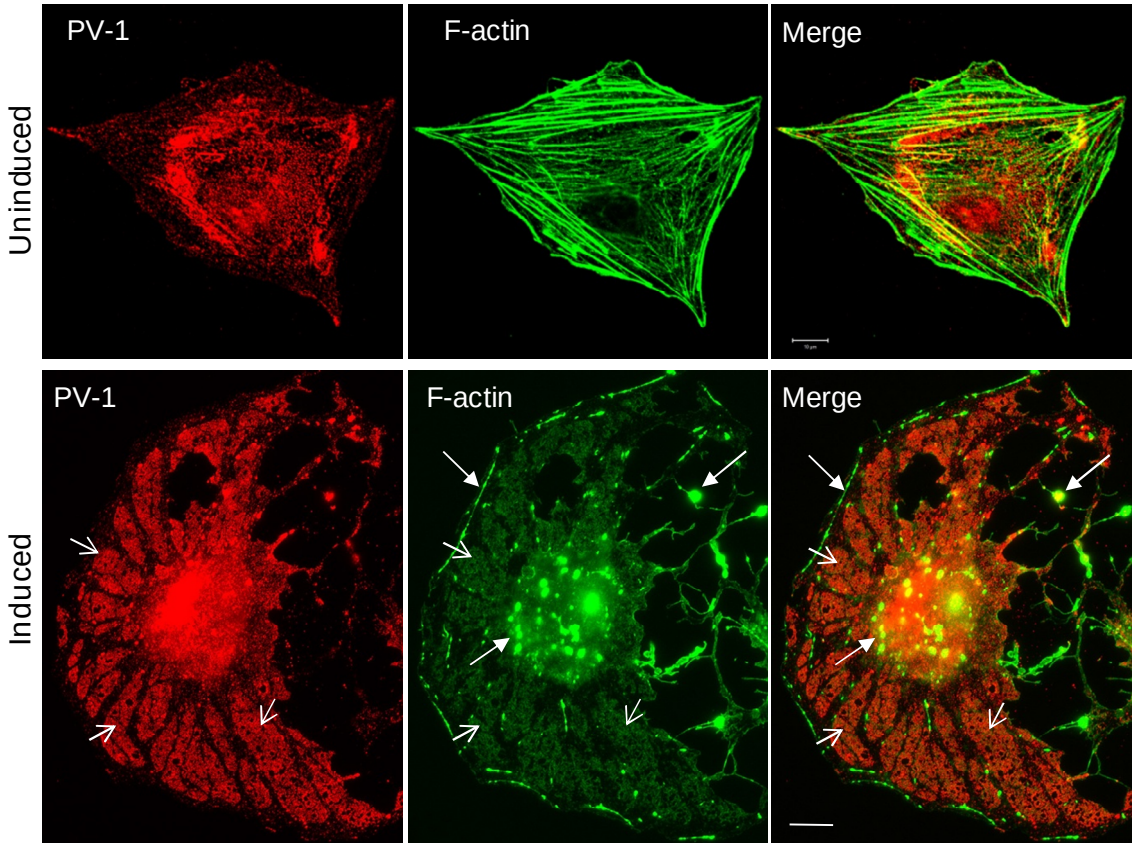

Fig. 3-12 F-actin microfilaments were present in fenestral sieve plates.
After incubating with latrunculin A (1.25 μM) for 3 hours, PV-1 marked distinct fenestral sieve plates were induced in bEND5 cells (arrows in bottom left). F-actin filaments disassembled to remnants and aggregates (arrowheads). However, rhodamine-conjugated phalloidin stained microfilaments were observed in places corresponding to fenestral sieve plates (arrows in bottom right)
Scale bar, 10 μm.

3.4.2 Exploration of other potential components involved in fenestra formation

3.4.2.1 Exclusion of other cytoskeletal structures from fenestral sieve plates

The dynamics of PV-1 described above, plus the potential involvement of the actin cytoskeleton in fenestra structure and/or formation, led us to perform a broader screen for cytoskeletal components such as intermediate filaments and other proposed membrane-cytoskeletal linker proteins. First, we carried out immunostaining on the induced bEND5 cells with β-tubulin and the intermediate filaments markers vimentin and desmin (Lazarides, 1976). β-tubulin marked microtubules were excluded from the fenestral sieve plates as expected, given the extremely thin profile in the sieve plate region. Similar to β-tubulin, vimentin was excluded from fenestral sieve plates, whereas desmin was weakly expressed and accumulated in the perinuclear area (Fig. 3-13). We also explored some other ABPs, such as cortactin, catenin, WASL and arp3, which promote actin polymerization. Immunofluorescence results revealed their exclusion from the fenestral sieve plates (representative images are shown in Fig. 3-14). The actin-filament-severing proteins cofilin and twifilin, the actin cross-linking protein transgelin, and the actin motor protein myosin IIa were also excluded from the sieve plates as well (data not shown). These findings suggest that the F-actin reorganisation during fenestra formation may be regulated by a subset of ABPs, such as moesin and annexin II.

3.4.2.2 Exclusion of focal adhesion proteins from fenestral sieve plates

The fenestrated bEND5 cell is characterised by its lamellipodium-like spread sheet, thus we explored candidates involved in cell spreading. Focal complexes and focal adhesion formed during cell spreading function as cytoskeletal organizing centers (Burridge, 1996). Focal adhesion describes where cells attach to the extracellular matrix. A focal adhesion complex is composed of proteins and lipids, with complicated connections between actin and the plasma membrane. Focal adhesion-associated kinase (FAK) is reportedly involved in cellular adhesion and spreading of cellular

processes (Hanks, 1992). Distinct focal adhesion sites marked by FAK were observed in uninduced bEND5 cells (Fig. 3-15). FAK staining completely vanished in induced bEND5 cells upon latrunculin A treatment, Furthermore, talin and vinculin, two membrane-cytoskeletal proteins enriched in focal adhesion complexes (Wolfgang, 1996), were also excluded from the induced fenestral sieve plates (Fig. 3-13). Therefore we conclude that cell membrane spreading during fenestra induction is not driven by forces produced by focal adhesions.

3.4.2.3 Possible involvement of intermediate compartments in fenestra formation

Our observations of fenestra formation, particularly the segregating of PV-1 from caveolae during fenestra induction, strongly suggest the involvement of protein sorting and membrane trafficking mediated by intermediate compartments, such as the caveosome, early endosome, recycling endosome, and/or vesicles generated from the endoplasmic reticulum (ER) or Golgi apparatus. By immuofluorescence staining, we found that the early endosome markers rab4 and rab5 were excluded from fenestral sieve plates. Similar staining results were observed for the COPII (coat proteins II) member sec23, sec31, and SAR1 (Fig. 3-16). The ER-Golgi intermediate compartment (ERGIC) mediates trafficking between the ER and the Golgi complex and facilitates the sorting of cargo (Appenzeller-Herzog, 2006). Dot-like staining of ERGIC-53 was scattered in and around fenestral sieve plates (Fig 3-16), suggesting the possible involvement of ERGIC in fenestra formation.

3.4.2.4 Involvement of membrane fusion proteins in fenestra formation

Despite the complexity of the process of fenestra formation, the end point is simple: to form transcellular pores. Immunostaining demonstrated that fusion-related proteins, such as the Rab proteins Rab4 and Rab5 (Fig. 3-16) and the exocyst component Exo70 (Fig. 3-17A), were mostly excluded from the induced fenestral sieve plates. SNARE (soluble N-ethylmaleimide sensitive fusion protein attachment protein receptor) superfamily proteins are essential for many intracellular membrane fusion events (Jahn,

2006). Syntaxin 5A was excluded from fenestral sieve plates (Fig. 3-17B); however, syntaxin 4 was present in the fenestrated cell region (Fig. 3-17C), implying a potential involvement in fenestra formation.

3.4.2.5 Potential involvement of high-curvature generating/stabilising proteins in fenestra formation

Fenestrae are transcellular pores with a sharp membrane curvature at the rim of the pore, where the two plasma membranes fuse. Membrane curvatures can be generated by special lipid composition, oligomerization of curvature scaffolding proteins, and/or reversible insertion of regions that act like wedges in the membrane (Harvey, 2005). It has been reported recently that positive membrane curvature can serve as a cue for localisation of a peripheral membrane protein (Ramamurthi, 2009).

Reticulons are a group of ubiquitous proteins which are primarily located on the ER. Reticulon 4, also called nogo A+B, has been implicated in inhibition of axon outgrowth (GrandPre, 2000). It has been reported that reticulon 4a/nogo A and its interacting protein, DP-1, are essential for shaping and stabilising highly curved ER membrane tubules (Voeltz, 2006). Recent evidence has shown that reticulon 4a/nogoA locates to regions of high membrane curvature in the ER and the assembling nuclear envelope (Kiseleva, 2007). Furthermore, the membrane-bending property of reticulon 4a/nogoA has been suggested to play a role in the formation of nuclear pore complex (NPC)-associated pores in the nuclear envelope (Antonin, 2009; Dawson, 2009).

We first investigated the distribution of ER in bEND5 cells with fenestra induction. Marked by calreticulin or calnexin, the ER was found redistributing to perinuclear and cytoplasmic branches between fenestral sieve plates, similar to the redistribution pattern of microtubules (Fig. 3-18). KDEL, a specific sequence that marks permanent retention of proteins in the ER, was also excluded from fenestral sieve plates (Fig. 3-18).

Reticulon 3 was located at the regions of regular ER and was excluded from fenestral sieve plates (Fig. 3-18). In contrast, reticulon 4/nogo A+B was found beyond the location of regular ER; it was observed on the edge of every single patch of fenestral sieve plates (Fig. 3-19A), similar to its reported location in the nuclear envelope (Kiseleva , 2007). DP-1 is the reported interacting protein for reticulon 4a/nogo A+B, but its localisation was not convincing due to the weak staining (Fig. 3-19B). Given the striking similarity in appearance between fenestral pores and nuclear pores, we also checked for possible inclusion of NPC proteins in fenestral sieve plates, but found that NPC proteins were excluded from these regions (Fig. 3-19C).

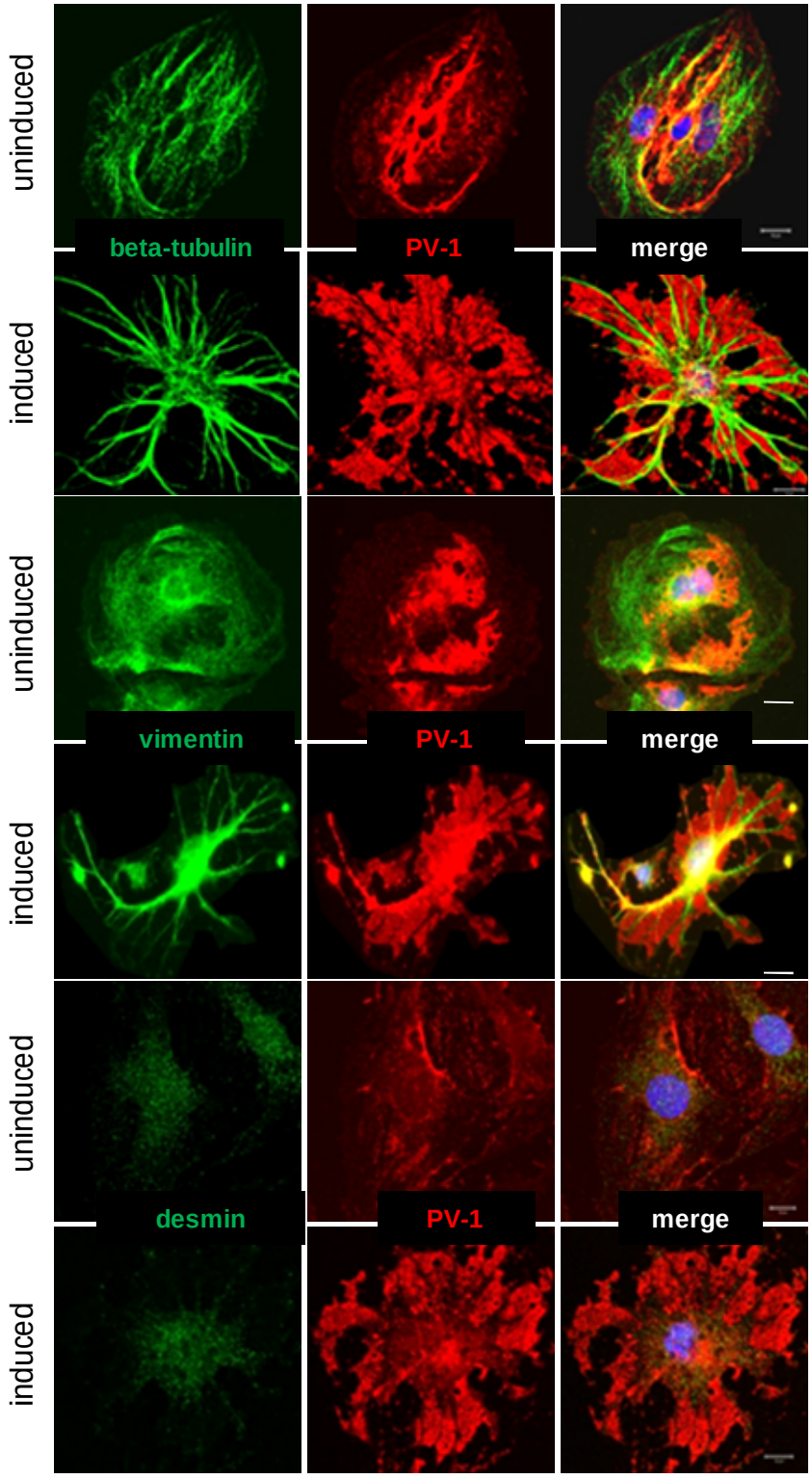

Fig. 3-13 Microtubules and intermediate filaments were excluded from fenestral sieve plates. PV-1 marked fenestral sieve plates in bEND5 cells were induced by latrunculin A of 1.25 μM for 3 hours. β-tubulin-labelled microtubules and vimentin-labeled intermediate filaments were excluded from the induced fenestral sieve plates. Another intermediate filament marker, desmin, was only weakly expressed in bEND5 cells. Scale bar, 10 μm.

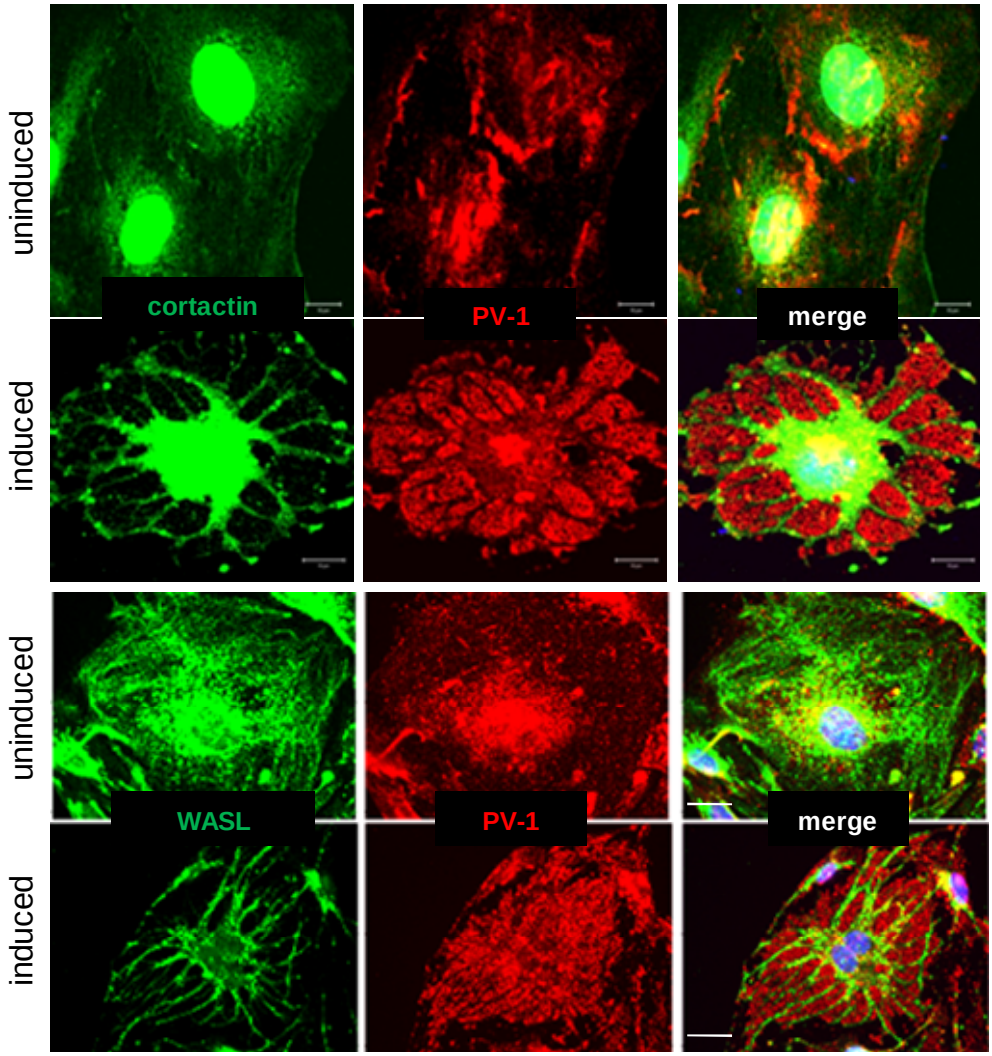

Fig. 3-14 Most of ABPs were excluded from fenestral sieve plates (representative images.) Fenestrae in bEND5 cells were induced by latrunculin A (1.25 μM) for 3 hours. Cortactin and WASL were highly expressed in bEND5 cells, but were excluded from the induced fenestral sieve plates. Scale bar, 10 μm.

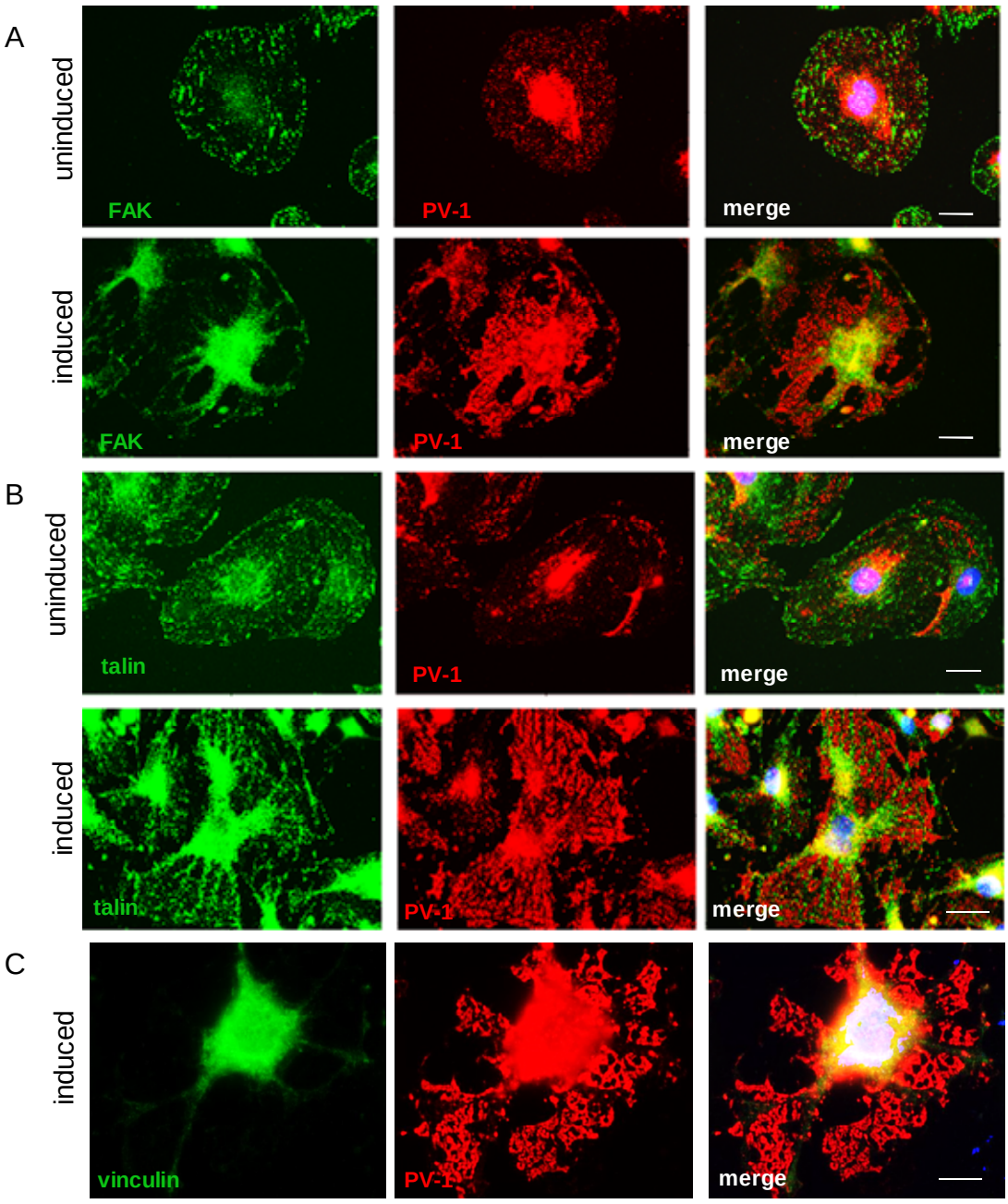

Fig. 3-15 Focal adhesion complex was disassociated during fenestra formation. Fenestrae in bEND5 cells were induced by latrunculin A (1.25 µM) for 3 hours. Focal adhesion points were marked by FAK in untreated bEND5 cells (A). Focal adhesion complexes were disassociated during fenestra formation, indicated by the exclusion of the focal adhesion proteins FAK (A), talin (B) and vinculin (C) from the induced fenestral sieve plates. Scale bar, 10 µm.

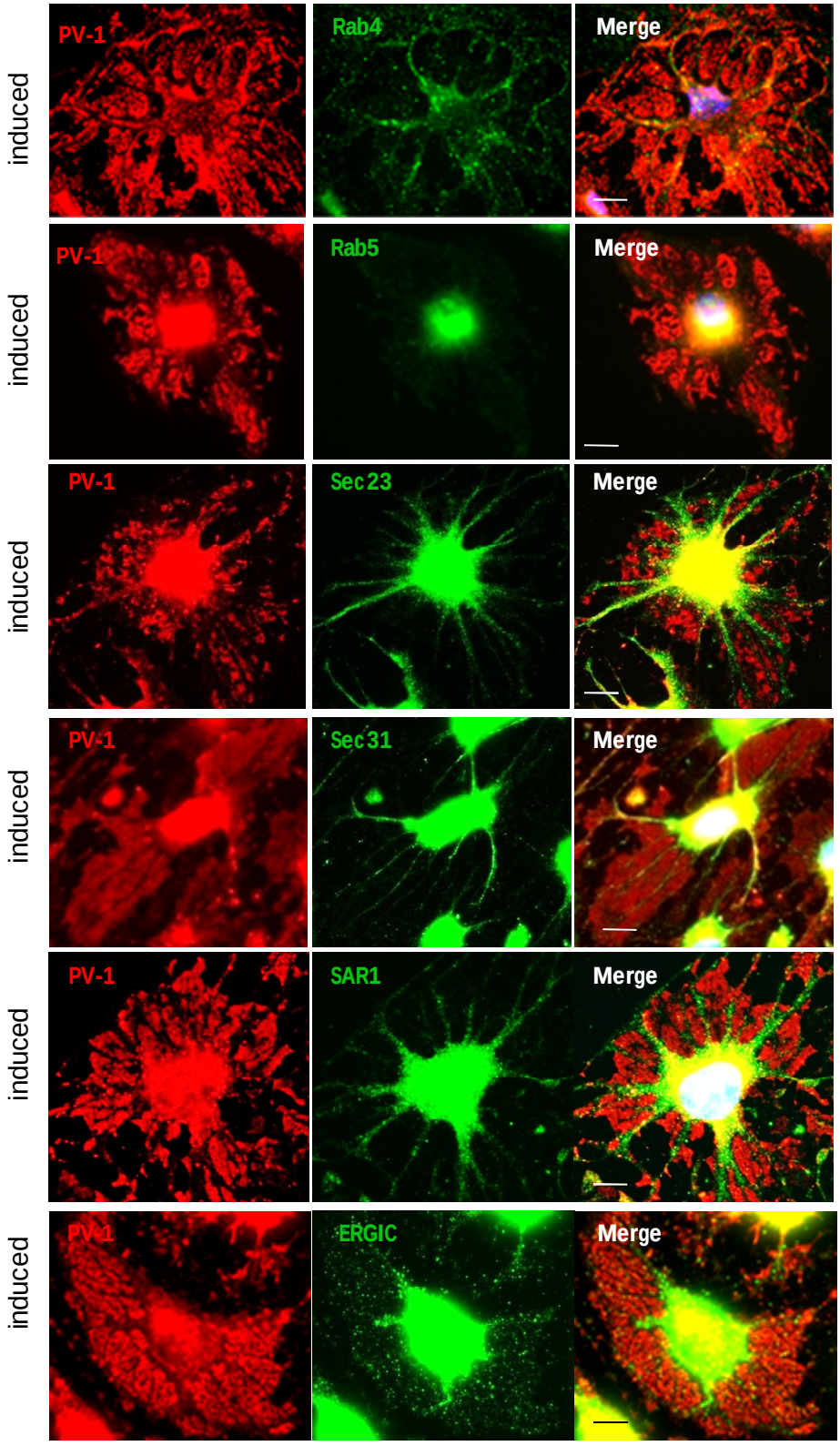

Fig. 3-16 Most of the proteins involved in protein/vesicle trafficking were excluded from fenestral sieve plates. Fenestrae in bEND5 cells were induced by latrunculin A (1.25 μM) for 3 hours. Rab4 and 5, sec23 and 31 and Sar1 were not present in the fenestral sieve plates; ERGIC showed weak staining in the sieve plates. Scale bar, 10 μm.

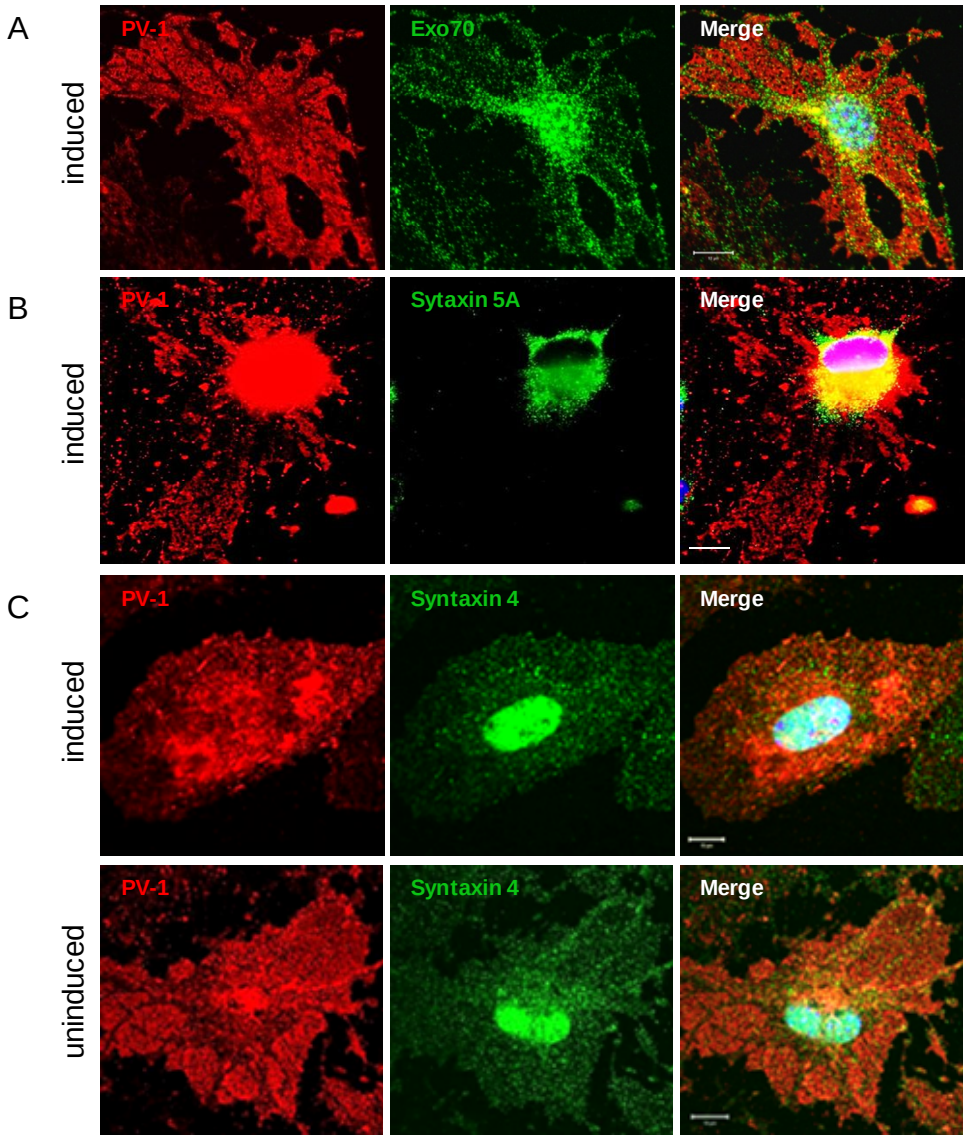

Fig. 3-17 Membrane fusion proteins in fenestral sieve plates. Fenestrae in bEND5 cells were induced by latrunculin A (1.25 μM) for 3 hours. Scale bar, 10 μm.

A. Exo70 was excluded from fenestral sieve plates

B. Syntaxin 5A was enriched in the perinuclear area in induced bEND5 cells.

C. Syntaxin 4 was present in fenestral sieve plates. (Courtesy of Anwei Mbah, UCL institute of Ophthalmology, London)).

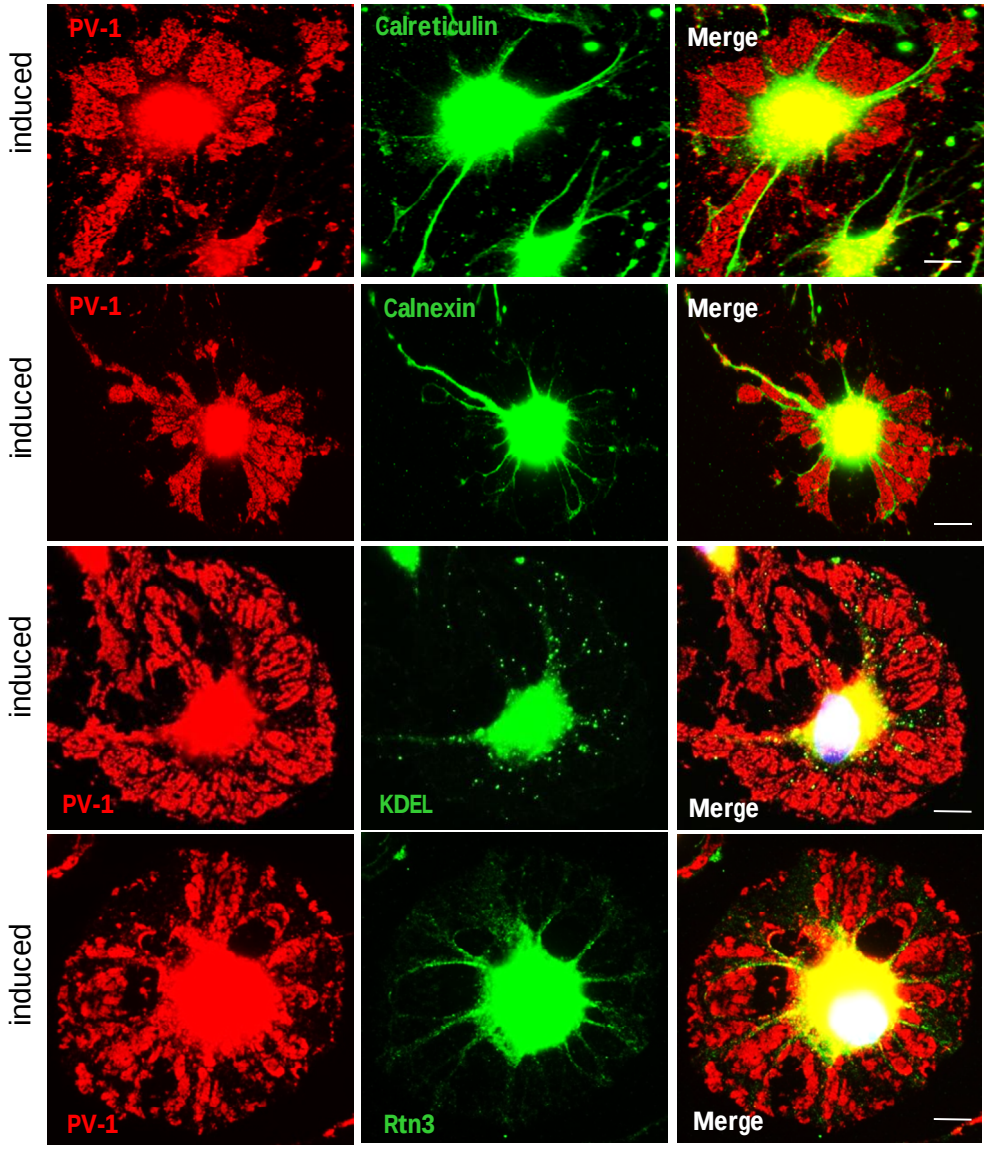

Fig. 3-18 ER protein markers were excluded from fenestral sieve plates. Fenestrae in bEND5 cells were induced by latrunculin A (1.25 μM) for 3 hours.
The ER markers calreticulin and calnexin, ER rentention protein KDEL, and ER marker reticulon 3 (Rtn 3) were all excluded from the induced fenestral sieve plates. Scale bar, 10 μm.

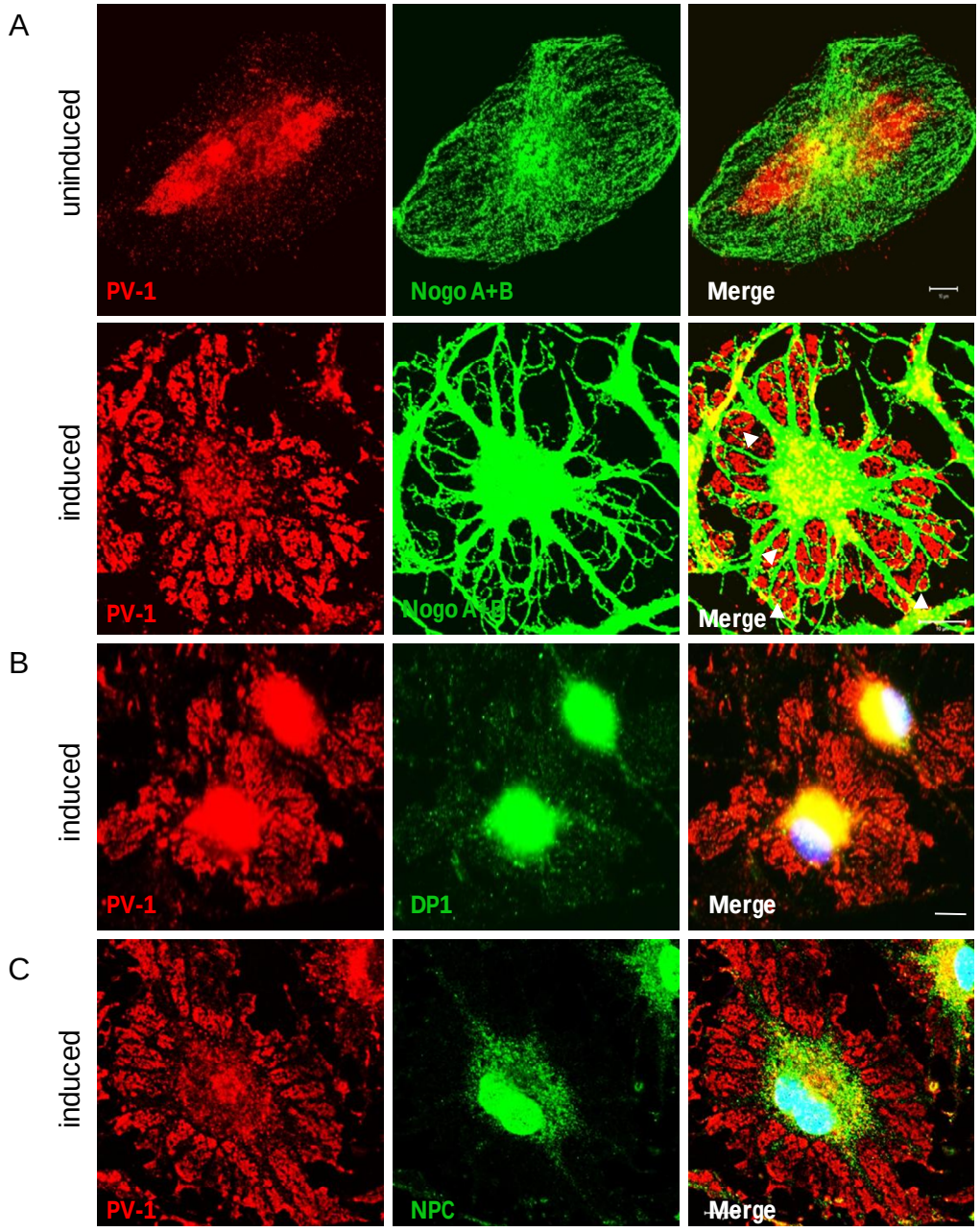

Fig. 3-19 High membrane curvature proteins were not present in fenestral sieve plates. Fenestrae in bEND5 cells were induced by latrunculin A (1.25 μM) for 3 hours. Nogo A+B was reorganised around small patches of the induced fenestral sieve plates, whilst DP-1 was faintly present in fenestral sieve plates, and NPC was enriched in perinuclear area. Scale bar, 10 μm.

3. 5 Summary and discussion

The *in vitro* assay of fenestra induction in which bEND5 cells are treated with latrunculin A is a valuable tool for study of fenestra biogenesis. The induction protocol is fast and easy, and the cell line can be maintained for tens of passages without losing the capability of fenestra induction. High levels of fenestrae, in the high hundreds to thousands per cell in number, an up to 100 fold increase compared to an uninduced cell, can be sustained. With distinguishable immunostaining of PV-1-positive sieve plates, it provides a convenient light microscopy assay.

The involvement of the actin cytoskeleton in regulation of fenestra number and size has been established for LSEC (Arias, 1990; Braet, 1995 and Braet 1996 (Hepatology); Spector, 1999) and isolated GEnC (Andrews, 1981). Although the exact role of actin reorganisation in fenestra biogenesis remains unclear, it has been implied that actin removal from membranes may be a general requirement for membrane fusion (Burgoyne, 1987; Orci, 1972; Muallem, 1995; Morales, 2000; Eitzen, 2002). The hypothesis, when applied to fenestrae, is that actin filaments act as a physical barrier, so that the apical and basal plasma membrane of the cell could only be brought in close apposition by cytoskeleton disruption. However, during yeast vacuole fusion, Eitzen *et al.* observed that an actin repolymerisation phase at the terminal stage of membrane fusion followed actin depolymerisation during docking (2002). In agreement with the above notions, we observed the presence of an F-actin microfilament network in the induced sieve plates, which could be stabilised by phalloidin for short periods of time (data not shown). Furthermore, just as high concentrations of actin-disrupting agents inhibited all phases of exocytosis (Orci, 1972; Muallem, 1995), high concentrations of latrunculin A inhibited fenestra induction (data not shown). Disruption of the F-actin cytoskeleton is a prerequisite for fenestra induction, but the F-actin reorganisation that follows may actually be a driving force for fenestra formation.

Using immunofluoresence staining, we screened protein candidates from proteomic analysis and proteins that are involved in cytoskeletal and membrane dynamics. Most

of the candidate proteins were excluded from fenestral sieve plates. However, the immunostaining results only reflect the steady state location of these proteins. Proteins excluded from fenestral sieve plates may still have played a role during fenestra formation. For example, microtubules, which are absolutely excluded from fenestral sieve plates, provide a means of transport for internalized caveolin/PV-1-positive vesicles during latrunculin A-induced fenestra formation. Interestingly, two ABPs, moesin and annexin II, were present in fenestrated cell regions. Moesin colocalises with PV-1 in fenestral sieve plates whilst annexin II is located in the sieve plate region but with a punctuate, vesicular pattern. The potential roles for moesin and annexin II in fenestra formation are further investigated in the following chapter.

Chapter 4

Moesin and annexin II differentially regulate fenestra formation

Abbreviations

ABPs	actin binding proteins
AMD	age-related macular degeneration
BSA	bovine serum albumin
DMEM	Dulbecco's modified Eagle medium
ER	endoplasmic reticulum
ERGIC	ER-Golgi intermediate compartment
ERM	ezrin, radixin, and moesin
FAK	focal adhesion-associated kinase
FACR	fenestrae-associated cytoskeleton ring
GEnC	glomerular endothelial cell
GFP	green fluorescent protein
GFR	glomerular filtration rate
HA	hemagglutinin
HSPG	heparan sulfate proteoglycans
HuVEC	human umbilical vein endothelial cells
LM-EM	light microscopy-electron microscopy
LSEC	liver sinusoidal endothelial cells
MβCD	methyl-β-cyclodextrin
NPC	nuclear pore complex
PBS	phosphate-buffered saline
PFA	paraformaldehyde
PIP2	phosphatidylinositol 4,5 biphosphate
PMA	phorbol myristate acetate
PV-1	plasmalemmal vesicle–associated protein–1
RA	retinoic acid
RPE	retinal pigment epithelium

SNARE	soluble N-ethylmaleimide sensitive fusion protein attachment protein receptor
TGF-β	transforming growth factor β
VEGF	vascular endothelial growth factor
VVOs	vesiculo-vacuolar organelles

Chapter 4 Moesin and annexin II differentially regulate fenestra formation

4.1 Background

Moesin, a membrane-organisation extension spike protein, is a member of the ERM protein family (ezrin, radixin, and moesin). The ERM proteins belong to a superfamily whose prototype is band 4.1 protein. All members in the band 4.1 superfamily share a highly conserved domain at their N-terminus, the FERM domain (4.1, ezrin, radixin and moesin) (Chishti, 1998; Bretscher, 2002). Although absent from plants and fungi, ERM proteins are highly conserved in the animal kingdom. Adult vertebrates express all three ERM proteins, whereas only moesin is expressed in *Drosphila* and ERM-1 protein in *C. elegans* (Bretscher, 2002).

ERM proteins are composed of a ~300 amino acid globular FERM domain at the N-terminus, followed by a ~200 amino acid central long helical rod domain, and they terminate with a ~100 amino acid C-terminal ERM-association domain (C-ERMAD) (Turunen, 1994; Hoeflich, 2003). The conserved FERM domain is suggested to bind directly or indirectly to the plasma membrane, and the C-ERMAD contains a major F-actin binding site (Fig. 4-1). Therefore, ERM proteins have been considered to be structural linkers between the plasma membrane and the actin cytoskeleton (Niggili, 2008).

An interesting aspect of ERM proteins is that they can exist in at least two conformational states: a head-to-tail, self-masking dormant form as monomers which are confined in the cytoplasm, and an active open form with the FERM and C-terminal tail domain dissociated (Bretscher, 2002). Li *et al*. further showed that the α-helical domain also plays a part in masking the FERM domain (2007). Data suggest that the conformational state of moesin is primarily regulated by binding to

phosphatidylinositol 4,5 biphosphate (PIP2) and by phosphorylation at the conserved threonine residue in the actin binding site. Upon activation, ERM proteins assume an open, active structure that allows them to connect the membrane to the underlying actin cytoskeleton (Bretscher, 1995) (Fig. 4-2). ERM proteins have been implicated as key organisers of specialised membrane domains, involved in microvillus formation, cell-cell adhesion, maintenance of cell shape, cell motility, membrane trafficking, signalling cascades, and other functions (Bretscher, 2002).

Annexins are a multi-gene superfamily with members expressed in all higher and some lower eukaryotes. The name annexin is derived from the Greek 'annex' meaning "bring/hold together", which describes the principal property of almost all annexins: the binding to and possibly holding together of certain biological structures, in particular membranes. The common property of all annexins is calcium-dependent binding to negatively charged phospholipids. Structurally, each annexin contains a conserved 'annexin repeat', a segment of some 70 amino acid residues repeated four or eight times within the protein (Gerke and Moss, 2002). Annexins are reported to have a wide variety of cellular functions including vesicle trafficking, cell division, apoptosis, calcium signalling and growth regulation (Gerke, 2002 and 2004; Hayes, 2004 and 2007; Rand, 2000; Rescher, 2007). They are found both in the cytoplasm and bound to membranes, suggesting their prominent role in membrane-related processes, in particular trafficking.

Among the members of the annexin family, annexin II is unique in two ways. One is that annexin II is found in most cells associated with dimeric S100 protein p11, forming the heterotetrameric complex anx22p112 (Johnsson, 1988). This complex is capable of linking membrane surfaces to one another, has been demonstrated to induce aggregation of artificial liposomes and chromaffin granules (Drust, 1991; Lambert, 1997). Another unique property of annexin II is that its association with early endosomes is Ca^{2+}-independent, but highly sensitive to cholesterol-sequestering agents (Babiychuk, 2000). Annexin II is also reported as a major component of purified

caveolae (Schnitzer, 1995), and a cytosolic caveolin-annexin II complex has been implicated in the transport of esterified cholesterol from the plasma membrane to internal membranes (Uittenbogaard, 2002). Both annexin II and moesin were identified as major components in microdomains that are resistant to detergent but sensitive to cholesterol-sequestering agents (Harder, 1997). In addition, annexin II, as an actin regulator like moesin, has been implicated in providing membrane-cytoskeleton linkage (Gerke and Moss, 2002). It has been reported that annexin II binds F-actin at certain sites on cell membranes (Filipenko, 2002; Hayes, 2006). During *de novo* actin assembly on phagosomal membranes, annexin II is recruited along with moesin/ezrin (Defacque, 2000).

Data from the proteomic analysis, and preliminary immunostaining data suggested these two proteins as potential candidates regulating fenestra formation, and were further explored in experiments described below.

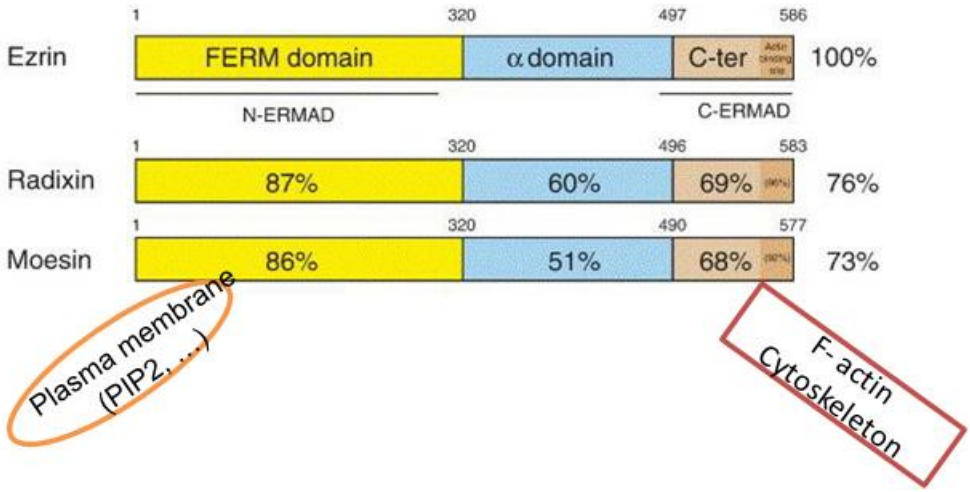

Fig. 4-1 Domain structure of ERM proteins..

ERM proteins possess a highly conservative FERM domain at the N-terminus, which binds to the plasma membrane, and a conserved F-actin-binding domain at the C-terminus. (Modified from Fievet, 2007).

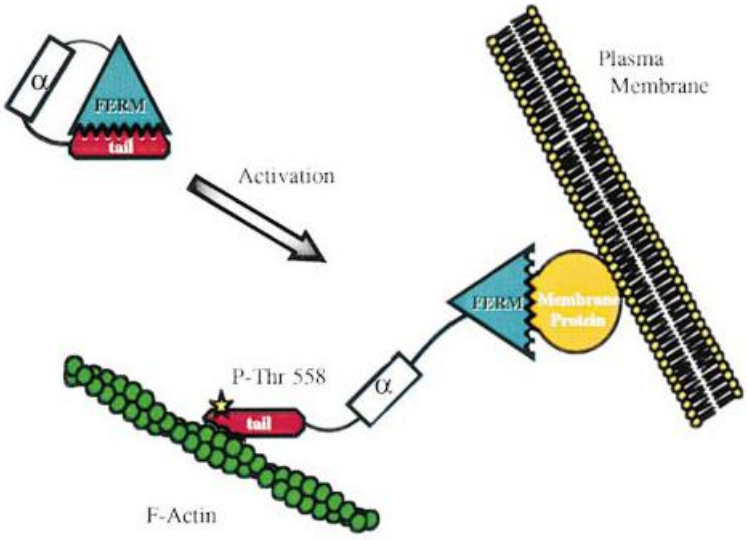

Fig. 4-2 Dormant and active forms of moesin.

Upon activation, the dormant form of moesin opens up to link the plasma membrane and the F-actin cytoskeleton. (Adapted from Pearson, 2000)

4.2 Localisation of moesin and annexin II

4.2.1 Moesin and annexin II were redistributed differently in fenestrated bEND5 cells

Immunostaining demonstrated that all three ERM proteins were present in bEND5 cells. However, upon treatment with latrunculin A for 3 hours, moesin was found highly enriched in the induced fenestral sieve plates, and colocalised with PV-1. The ERM member radixin was primarily present in the organelle- and microtubule-rich regions that surrounded sieve plates, whilst weakly expressed ezrin was located in the perinuclear area in induced bEND5 cells (Fig. 4-3). Annexin II was present in the organelle rich regions of the cell, but was also present in the fenestrated membrane region, though unlike moesin, it was distributed in scattered vesicular islands within the sieve plates (Fig. 4-3D).

4.2.2 Moesin was enriched in fenestral sieve plates and expressed in the choriocapillaris

Impressed by the striking colocalisation of moesin with PV-1 in fenestral sieve plates, further ultrastructural analysis was performed in collaboration with Eija Jokitalo at the University of Helsinki, in order to reveal moesin's exact localisation in fenestral sieve plates. Immunogold labeling followed by sectioning and TEM revealed enrichment of moesin in fenestral sieve plates, adjacent to but not present within the fenestral pore (Fig. 4-4). Moesin labeling in the sieve plates often appeared in association with electron-dense deposits (Fig. 4-4, arrowhead), suggestive of an underlying structure. A cross-section of the cell in non-fenestrated regions demonstrated that moesin immunolabelling was enriched under the plasma membrane (Fig. 4-4C), as previously reported (Edwards, 1997; Polesello, 2002).

I also examined the localisation of the ERM proteins at the choroid-retina interface, characterised by the highly fenestrated choriocapillaris. By staining whole eye cryosections from adult C57BL/6 mice, I found that moesin colocalised with PV-1 in the choriocapillaris, consistent with the proposed role for this protein in fenestral sieve plates. In contrast, ezrin was exclusively expressed in RPE cells whilst radixin was mainly found in the outer plexiform layer (Fig. 4-5).

4.2.3 Protein-protein interaction between moesin and PV-1

SDS-PAGE and western blot revealed that the expression of moesin and PV-1 did not change before and after fenestra induction by latrunculin A (Fig. 4-6A). The enrichment of moesin in fenestral sieve plates was due to rearrangement triggered by actin disruption. We further applied immunoprecipitation to investigate possible protein-protein interaction between moesin and PV-1 before and after fenestra induction. Our result showed that PV-1 coimmunoprecipitated with moesin, only in latrunculin A-treated, fenestrae-induced bEND5 cells, and similar results was obtained from moesin coimmunoprecipitation with PV-1 (Fig. 4-6, B and C). In contrast, there was no PV-1 coimmunoprecipitation with radixin, the close family member of moesin (data not shown). Our data indicate that during fenestra induction, moesin forms a specific link, directly or indirectly, with the fenestral diaphragm protein PV-1 in fenestral sieve plates.

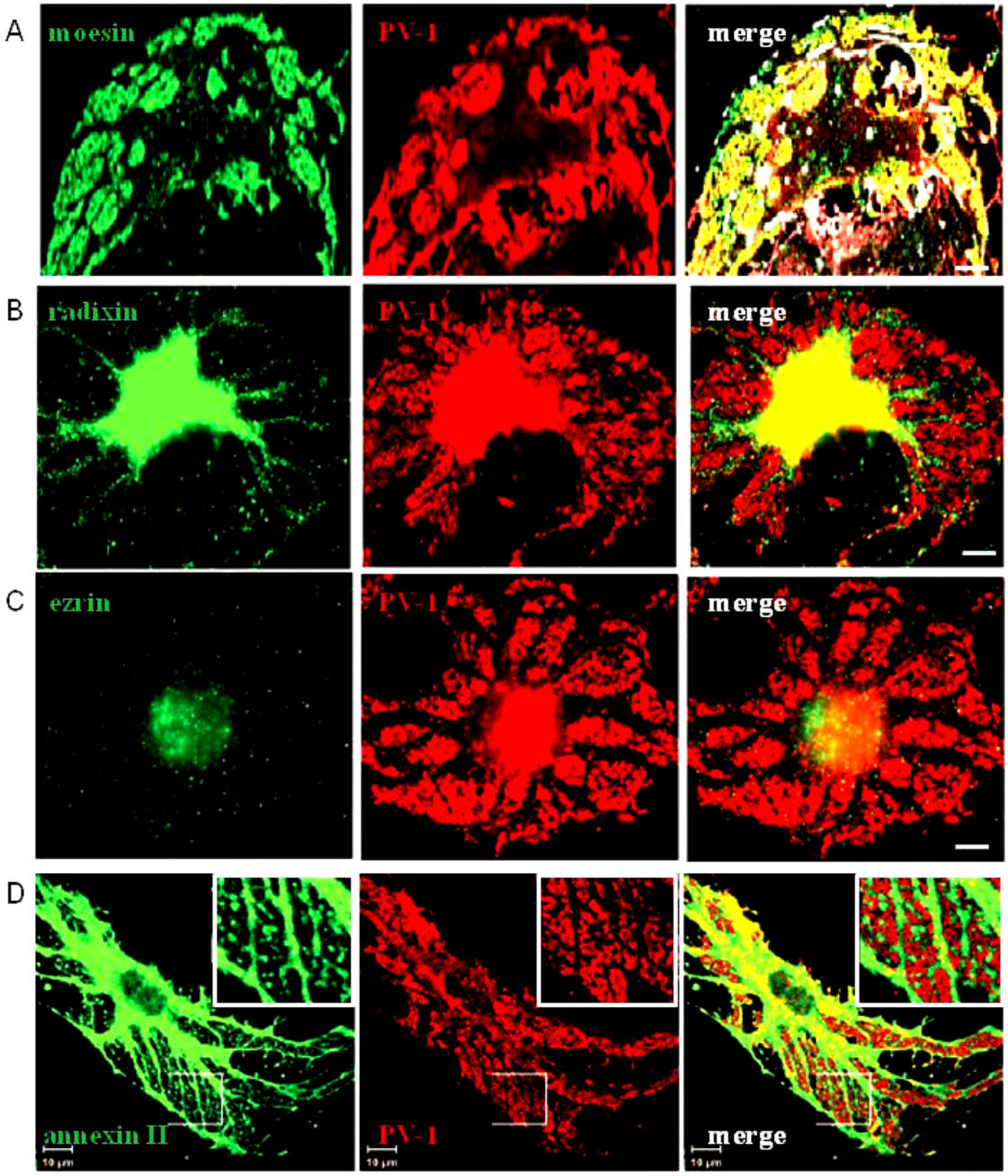

Fig. 4-3 Redistribution pattern of ERM proteins and annexin II in induced bEND5 cells. Fenestrae in bEND5 cells were induced by latrunculin A (1.25 μM) for 3 hours. Moesin colocalised with PV-1 in fenestral sieve plates (A); Radixin was excluded from the sieve plates (B), ezrin was weakly expressed and located in perinuclear regions; whilst annexin II scattered like islands in the gaps of fenestral sieve plates (D). Scale bar, 10 μm.

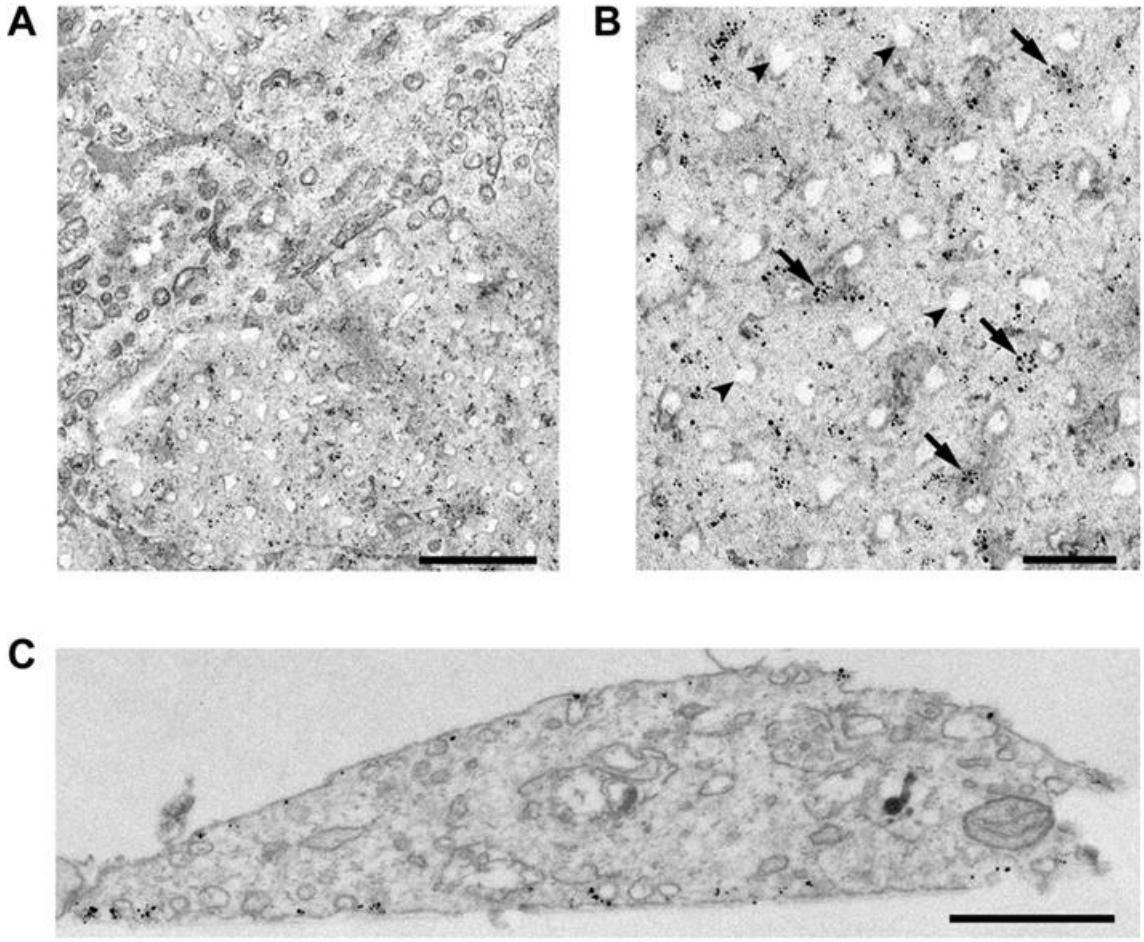

Fig. 4-4 Immunogold labelling confirmed the enrichment of moesin in fenestral sieve plates. Moesin is enriched in fenestral sieve plates (A), adjacent to fenestral pores (B). arrowheads, fenestral pores; arrows, silver-enhanced nanogold immunoconjugates. Typical plasma membrane localization of moesin in thicker, non-fenestrated cellular profiles (C). Scale bar: A, 1 μm; B, 0.5 μm ; C, 1μm.

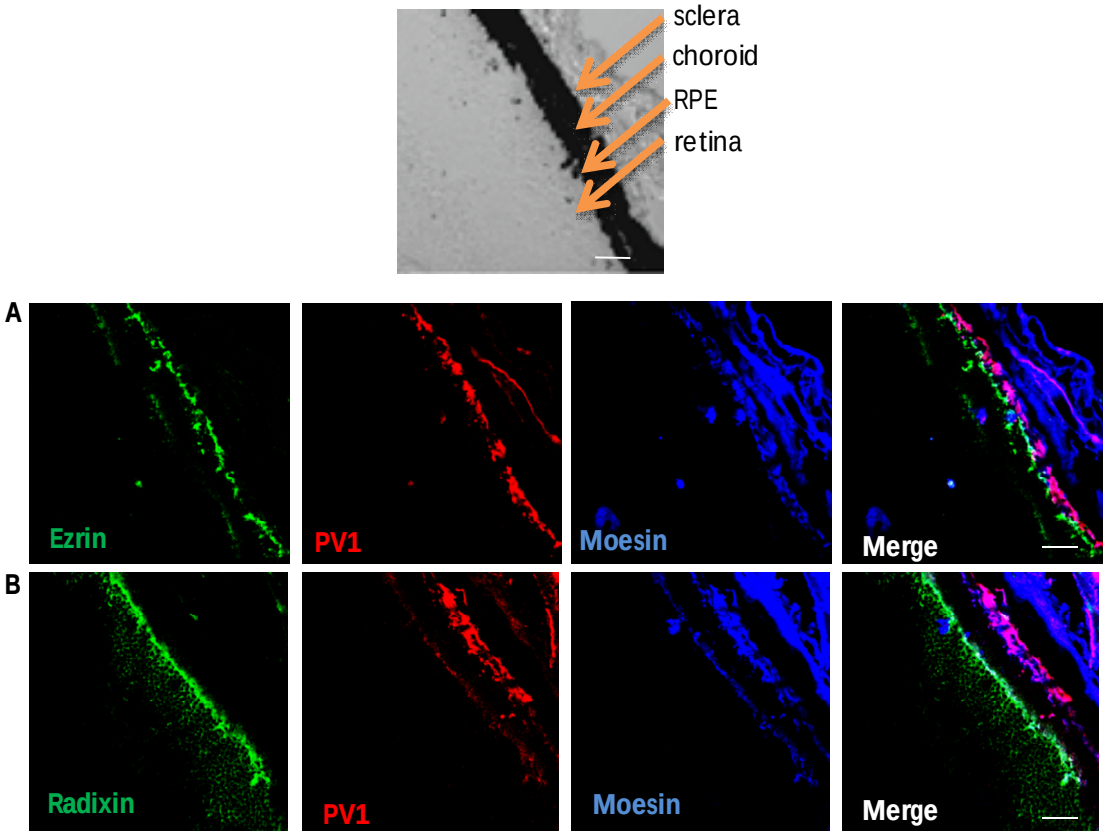

Fig. 4-5 Expression of ERM proteins in the RPE-Bruch's membrane-choriocapillaris complex. Moesin and PV-1 colocalised in the choriocapillaris, whereas ezrin was exclusively expressed in the RPE layer (A).Radixin was mainly expressed in the outer plexiform layer where the rods and cones connect (B).DIC, differential interference contrast microscopy.
Scale bar, 10 μm.

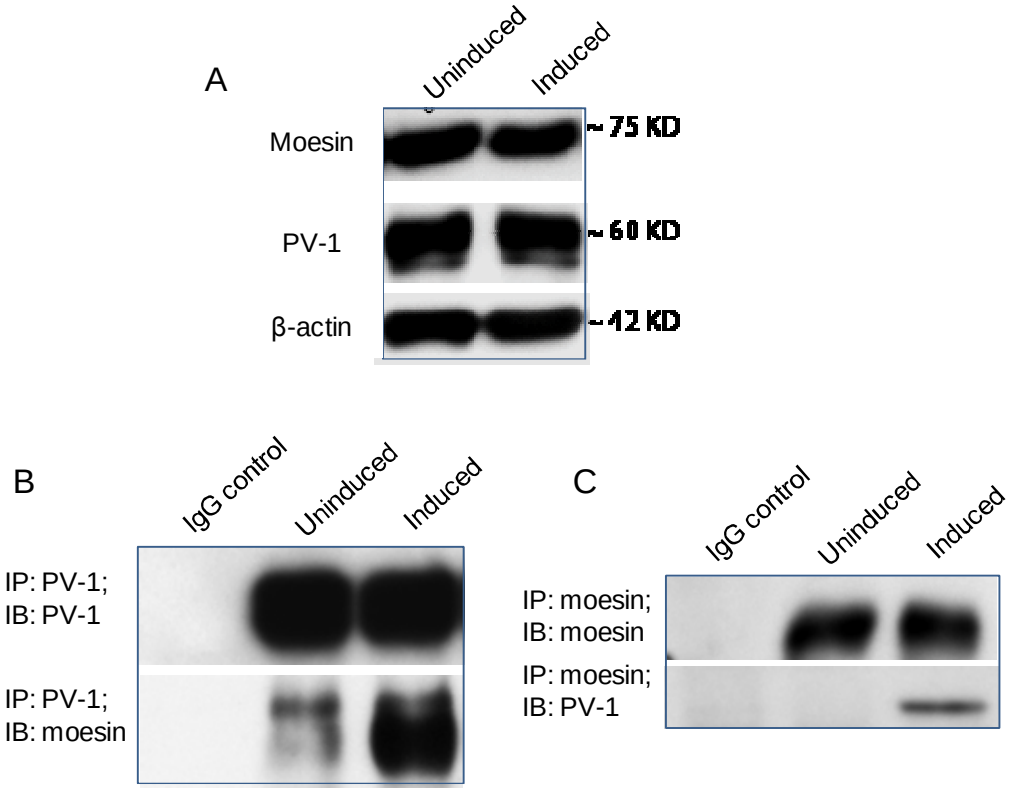

Fig. 4-6 Interaction between moesin and PV-1before and after fenestra induction.

A. Moesin and PV-1 expression were not affected by latrunculin A treatment for 3 hours.
B. Similar amount of PV-1 immunoprecipitated with PV-1 antibody in uninduced and induced bEND5 cells, however, moesin coimmunoprecipitated with PV-1 only in fenestra-induced bEND5 cells.
C. Similar amount of moesin immunoprecipitated with moesin antibody in uninduced and induced bEND5 cells, however,PV-1 coimmunoprecipitated with moesin exclusively in fenestra-induced bEND5 cells.

IP, immunoprecipitation antibody target; IB, immunoblot antibody target.

4.3 Functional role of moesin and annexin II in fenestra formation

4.3.1 Dominant-negative moesin prevented fenestra formation without affecting the formation of sieve-plate-like cell membrane microdomains

We first explored the functional role of moesin in fenestra formation by using dominant-negative constructs. As shown in the diagram in Fig. 4-7, we constructed plasmids encoding GFP- or hemagglutinin (HA) fusion proteins with full length moesin or truncated N-moesin and C-moesin, in which the C-terminal actin-binding domain or N-terminal FERM domain were removed, respectively. The N-moesin variant in particular has been shown to act as a dominant negative protein that displaces the endogenous protein and interferes with moesin function (Amieva, 1999).

Moesin is a prominent component of dynamic microextensions in many cell types. Its localisation matches the appearance and disappearance of filopodia and retraction fibres (Lankes, 1991; Franck, 1993; Amieva, 1995). By using the N-terminal membrane-binding domain of moesin fused with GFP (N-moesin-GFP), Amieva *et al*. demonstrated that N-moesin-GFP significantly affects cell surface architecture in NIH3T3 fibroblasts, causing formation of abnormally long and fragile filopodia that retract abnormally (1999). In contrast, expression of full-length moesin GFP (FL-moesinGFP) or its C-terminal domain (C-moesin-GFP) did not affect cell behavior (Amieva, 1999). In agreement with Amieva's observation, C-moesin-GFP overexpression did not displace endogenous moesin and did not affect fenestra formation (data not shown). Fluorescence microscopy analysis of cells expressing N-moesin-GFP confirmed that overexpression of the truncated variant displaced endogenous moesin from what appeared to be attenuated fenestral-sieve-plate-like microdomains (Fig. 4-8 A and B, top panel). PV-1 and filamentous actin were no longer present in the sieve-plate-like microdomains (Fig. 4-8A and-B, bottom panel). In contrast, FL-moesin-GFP expression did not displace endogenous moesin, PV-1 or F-actin from the sieve plates (Fig. 4-9A and B).

It was surprising to see sieve-plate-like microdomains in the N-moesin-GFP expressing cells. Confirmation of this finding and determination of the effects on fenestra formation required ultrastructural analysis. Therefore, we performed correlative LM-EM on transfected cells seeded onto TEM mesh grids covered with formvar film and coated with carbon and gelatin type-B. Following fenestra induction, cells were fixed for epifluorescence microscopy in the case of GFP fusion proteins, or for immunolabelling followed by epifluorescence microscopy in the case of HA fusion proteins. Overexpressing cells were identified, their positions on the grid were recorded and the grids processed and analyzed by wholemount TEM. As shown in Fig. 4-8C, the attenuated sieve-plate-like microdomains were readily identified in N-moesin-GFP-overexpressing cells; however, these membrane domains contained no fenestral pores. In contrast, the correlative LM-EM assay confirmed that sieve plates and fenestrae were abundant in FL-moesin-GFP overexpressing cells (Fig. 4-9C). Similar results were obtained with HA fusion protein variants (data not shown).

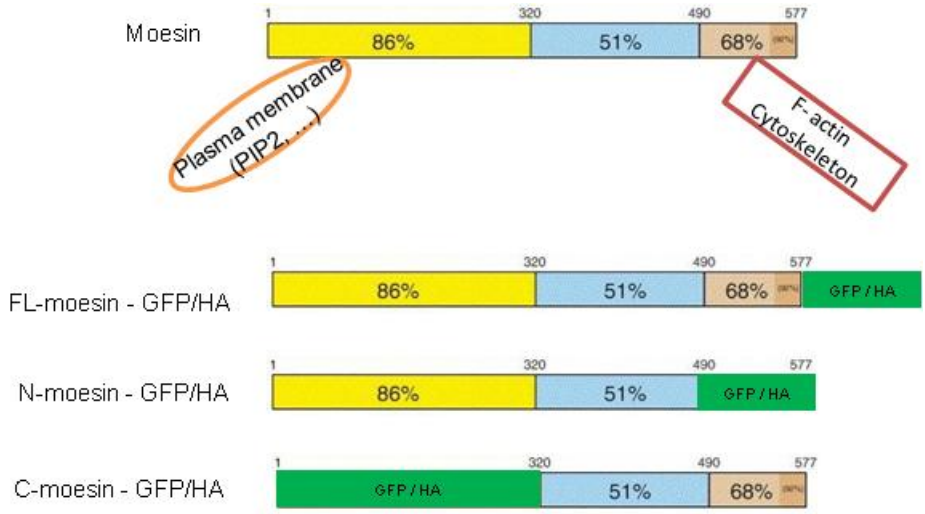

Fig. 4-7 Manipulation of moesin using different constructs.
The C-ERMD or FERM domain of moesin was replaced by GFP or HA to create truncated moesin fusion protein constructs. Full length moesin fusion protein was created by adding GFP or HA sequence to the end of the moesin C-terminus. (Recreated from Fievet, 2007).

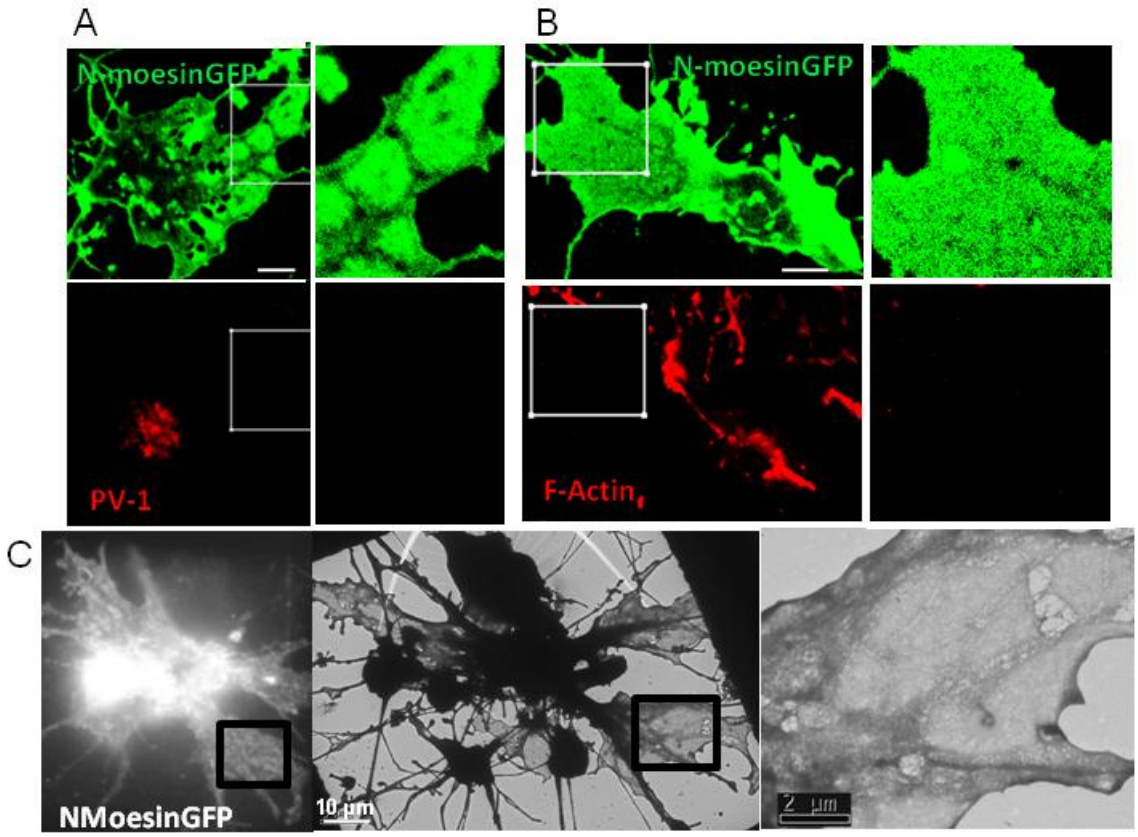

Fig. 4-8 N-moesin-GFP prevented fenestra formation without disrupting the organization of sieve plate-like microdomains.

bEND5 cells were transfected with N-moesin-GFP plasmid, and 24 hrs later they were treated with 1.25 µM latrunculin A for 3 hrs. Sieve-plate-like microdomains were formed in the plasma membrane of the treated cells (top panel of A and B), but neither PV-1 (A, bottom panel), nor reorganised microfilaments was observed in those microdomains (B, bottom panel). The correlative LM-EM assay showed that no fenestral pores were formed in the sieve-plate-like plasma membrane microdomains (C).

Scale bar in A and B: 10 µm.

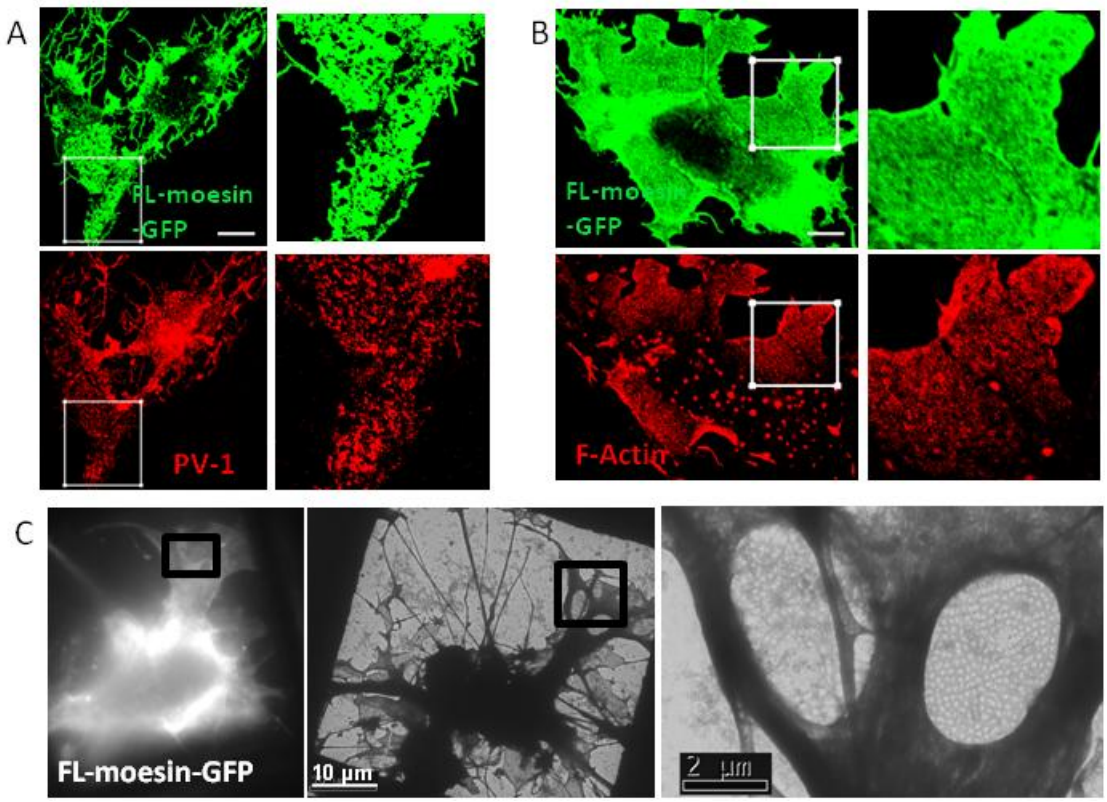

Fig. 4-9 FL-moesin-GFP had no effect on fenestra formation.
bEND5 cells were transfected with FL-moesin-GFP plasmid, and 24 hrs later they were treated with 1.25 µM latrunculin A for 3 hrs. Sieve-plate-like microdomains were formed in the plasma membrane of the treated cells (top panels of A and B). PV-1 recruitment and reorganised microfilaments were present in fenestral sieve plates (bottom panels of A and B). Correlative LM-EM confirmed that normal fenestra induction occurred in the treated cells (C).
Scale bar in A and B: 10 µm.

4.3.2 Down-regulating moesin or annexin II differentially affects fenestra formation

4.3.2.1 Knockdown of moesin or annexin II expression by siRNA transfection

To confirm and extend the findings with the dominant negative moesin, we created three siRNA oligonucleotides complementary to three distinct regions of mouse moesin mRNA. Using a double transfection method (Hayes, 2009) we identified one siRNA that efficiently reduced moesin mRNA and protein levels (Fig. 4-10, A and B). Radixin mRNA was not affected in moesin knockdown cells (data not shown) and a scrambled RNA oligonucleotide was used as a negative control.

In parallel, we also knocked down annexin II expression using a similar procedure. Three annexin II siRNAs were transfected into bEND5 cells and the one that showed the best down-regulating efficacy was identified and used for the following experiments. The reduced expression of moesin and annexin II was confirmed by real-time PCR, western blot and immunofluorescence staining (Fig. 4-10).

4.3.3.2 Moesin was required for fenestra formation, whereas annexin II negatively regulated fenestra formation

In the absence of latrunculin A treatment, moesin- or annexin II-knockdown bEND5 cells did not show any overt abnormality. However, upon latrunculin A treatment, immunofluorescence staining revealed a lack of PV-1 marked sieve plates in the induced bEND5 cells after moesin depletion. PV-1 accumulated in perinuclear and microtubule/organelle-rich thick regions of the cell (Fig. 4-11). On the contrary, annexin II depletion resulted in the formation of larger attenuated cell regions and more well-formed fenestral sieve plates (Fig. 4-12). Immunofluorescence analysis also revealed little PV-1 in the perinuclear region in annexin II-depleted cells compared to control siRNA transfected cells. Annexin II reduction therefore resulted in a more efficient and complete seregation of PV-1 from caveolae into fenestral sieve plates (Fig. 4-12, arrows).

To determine if there's any cellular structure existing between the tubular protrusions in the moesin knockdown cells, immunostaining with CD31 was carried out. The staining result revealed that moesin knockdown resulted in a failure to form and/or maintain attenuated cell regions when cells were treated with latrunculin A. Instead, cells formed numerous radial tubular protrusions, termed "arborisations". This arborization is a known result of actin cytoskeleton disruption in most cell lines (own observations; Ioannidou, 2006; Bar-Ziv, 1999) (Fig. 4-13).

To further elucidate the effects of moesin and annexin II down-regulation on fenestra formation, we applied the correlative LM-EM assay to study the phenotype caused by depletion of moesin or annexin II. Cells with low or absent immunostaining of moesin or annexin II were identified using epifluorescence microscopy, and their positions on the grids were recorded. The cells were subsequently identified under TEM and the phenotype was checked. Uninduced cells transfected with control siRNA, moesin siRNA or annexin siRNA looked indistinguishable at the light and ultrastructural levels (data not shown). However, cells chosen by LM for low or absent expression of moesin or annexin II had dramatically different phenotypes in fenestra formation. The attenuated cell region with fenestral pores was almost abolished by moesin knockdown (Fig. 4-14A). No effect was observed using control siRNA or radixin knockdown (data not shown), suggesting a specific effect of moesin knockdown on fenestra formation. Further speaking to this specificity, knockdown of annexin II had the opposite effect on fenestra formation, significantly increasing fenestrated plasma membrane area in latrunculin A-treated bEND5 cells (Fig. 4-14B).

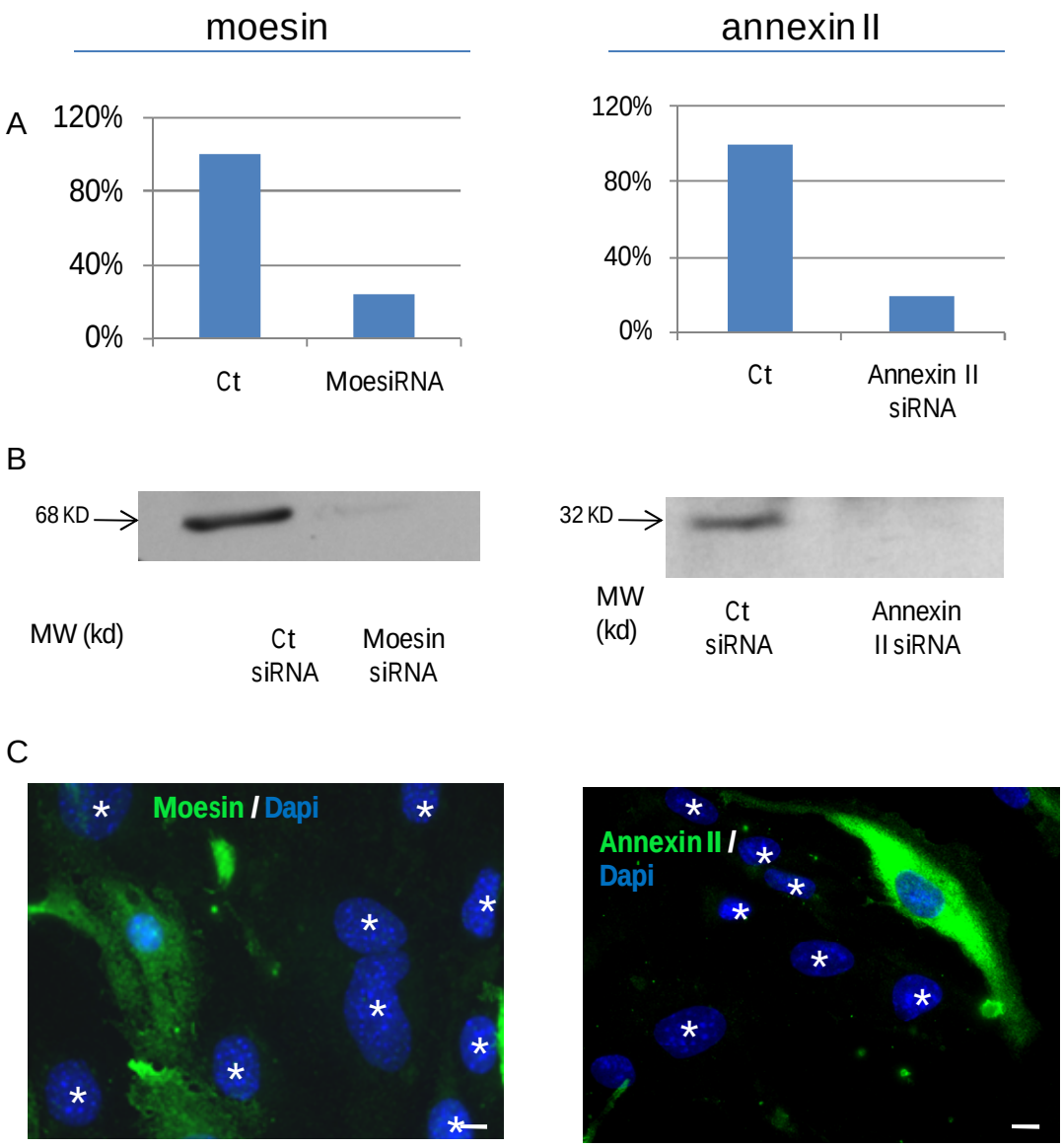

Fig. 4-10 Down-regulation of moesin and annexin II by siRNA transfection. Transfection with siRNA resulted in a reduction in the levels of mRNA (A) and protein (B) for moeisin and annexin II in bEND5 cells. Levels of mRNA were determined by real-time PCR(A), and protein expression was assessed using western blot (B) and immunofluorescence (C). The graphs shown in panel A depict the average of two independent experiments. * Moesin or annexin II depleted cells. Scale bar, 10 μm.

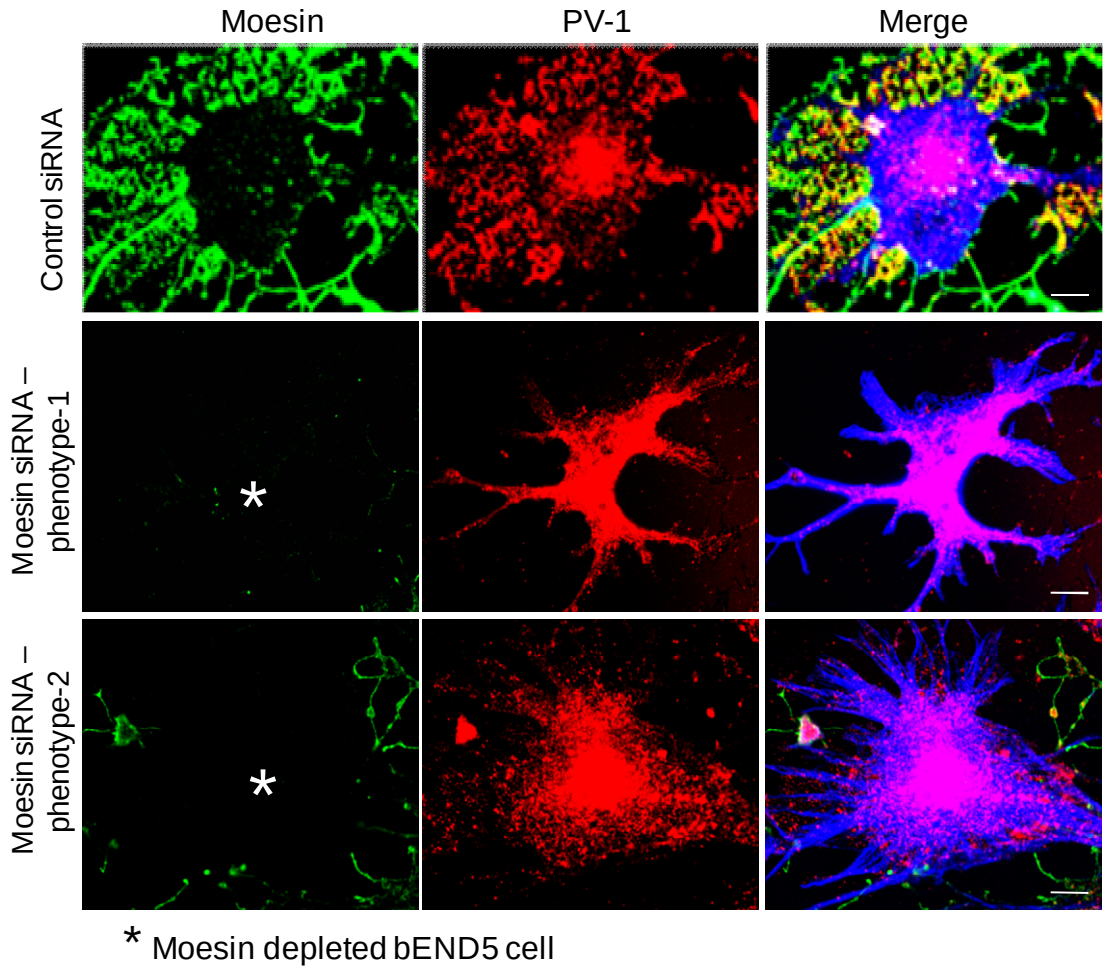

Fig. 4-11 Cell phenotypes resulted from moesin knockdown.
Fenestrae in bEND5 cells were induced by latrunculin A (1.25 μM) for 3 hours. Moesin knockdown resulted in an absence of distinct PV-1 marked sieve plates . Instead, PV-1 remained in the perinuclear and microtubule/organelle-rich regions. Two typical cell phenotypes were shown in the middle and bottom panels. Scale bar, 10 μm.

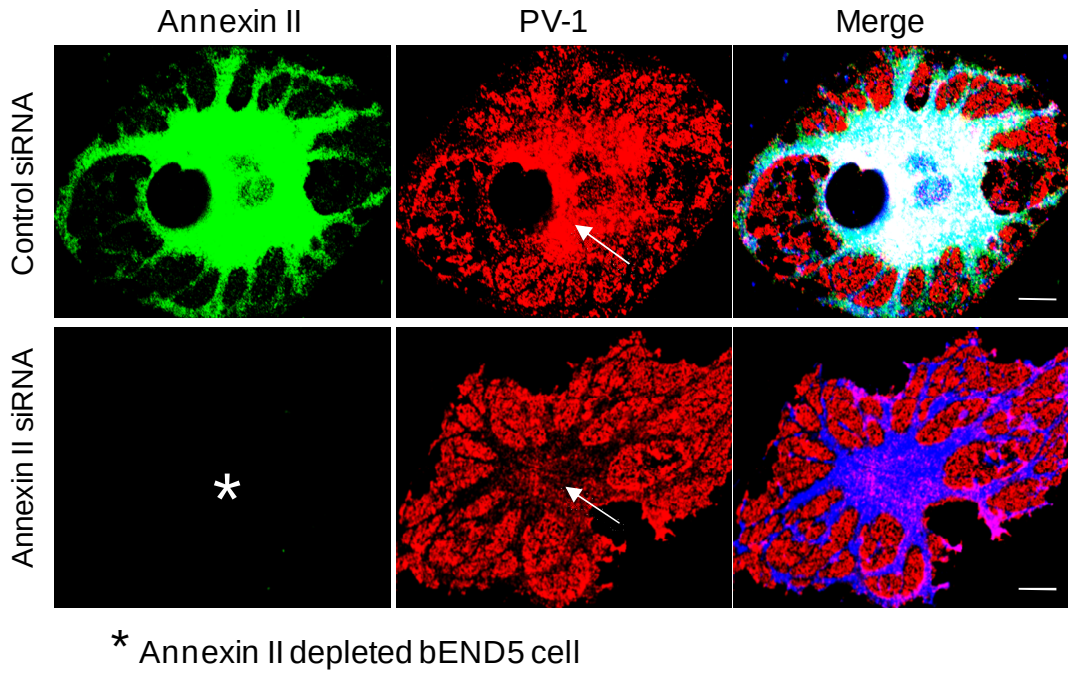

Fig. 4-12 Annexin II knockdown resulted in increased formation of PV-1-marked sieve plates.

Fenestrae in bEND5 cells were induced by latrunculin A (1.25 μM) for 3 hours. More PV-1 positive sieve plates were formed in annexin II knockdown bEND5 cells. In addition, there was less PV-1 accumulation in perinuclear cell region (arrow) when annexin II was depleted. Scale bar, 10 μm.

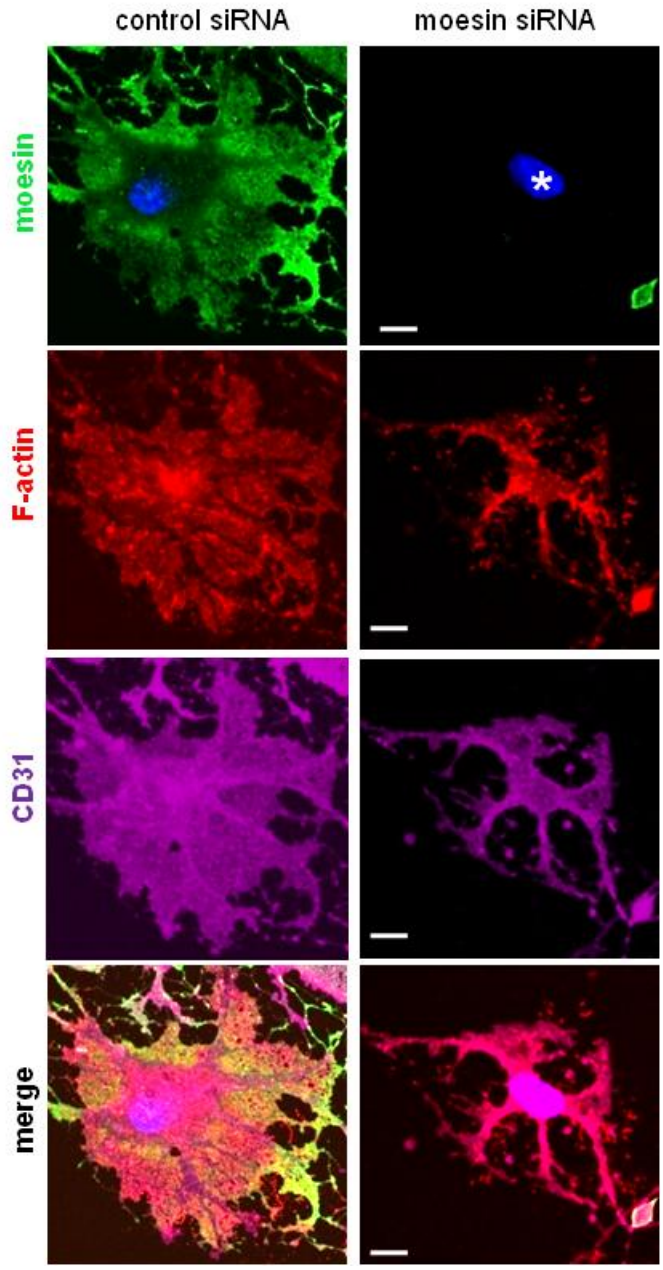

Fig. 4-13 Moesin knockdown compromises cell spreading in latrunculin A-treated bEND5 cells. Fenestrae in bEND5 cells were induced by latrunculin A (1.25 μM) for 3 hours.

In the absence of moesin, cell spreading (CD31-marked) and the reorganized F-actin microfilament network between microtubules were abolished when bEND5 cells were treated with latrunculin A to induce fenestrae. * Moesin depleted bEND5 cell.

Scale bar, 10 μm.

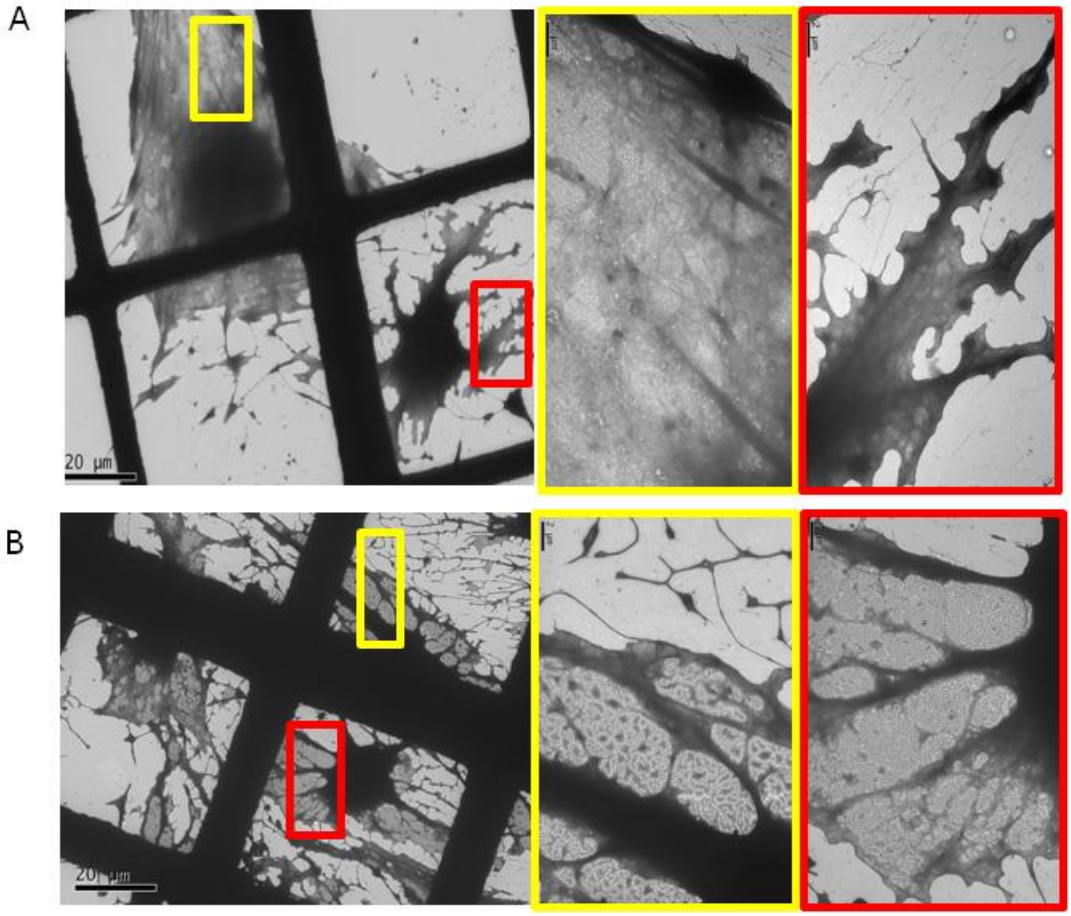

Fig. 4-14 Opposite effects on fenestra formation resulted from moesin or annexin II siRNA transfection, as confirmed by TEM. Scale bar, 20 μm.

A. Cell attenuation was not observed in moesin knockdown bEND5 cells; consequently, no fenestral pores were formed after latrunculin A induction .
B. Annexin II knockdown resulted in an increased area of fenestration .

4.3.3.3 Quantification of fenestra formation in moesin- or annexin II-depleted bEND5 cells

Since cell profile thickness differed between fenestrated and unfenestrated bEND5 cells, the TEM images enabled quantification of the fenestrated membrane area using Image J software. Using the correlative LM-EM assay, we identified 60-80 cells with reduced target protein expression after moesin siRNA, annexin II siRNA or control siRNA transfection. We quantified the fenestrated cell membrane area in all the identified cells. Moesin knockdown almost completely abolished membrane fenestration (> 90% reduction; 4-15B and C). In dramatic contrast, although bEND5 are very efficient in fenestrae induction, annexin II depletion significantly increased fenestrated cell membrane area by 25% (Fig. 4-15B and C).

In addition to the increased induction of fenestral sieve plates, annexin II reduction also significantly improved fenestra formation by increasing fenestral density (Fig. 4-16A). To quantify the density of fenestra, we took high-magnification TEM images of the fenestrated membrane in all identified cells. By using Pro-plus imaging software, the numbers of fenestrae were counted in two to four representative, well-fenestrated areas of every image, and the density of fenestrae was calculated and averaged for each image. The results showed that fenestral density was doubled in annexin II knockdown cells compared to control bEND5 cells (Fig. 4-16B). Annexin II depletion therefore increased fenestra formation by increasing both fenestral sieve plate area and fenestral density.

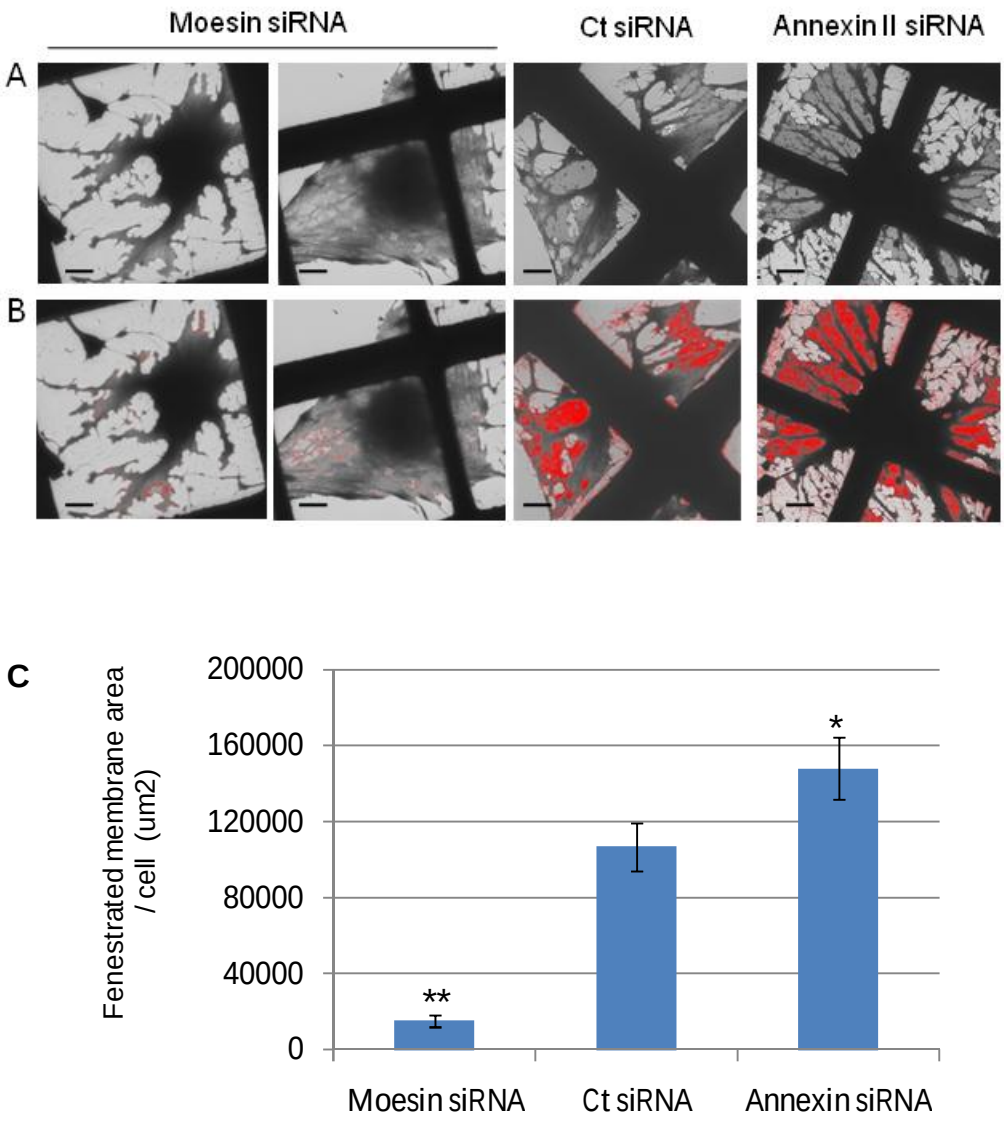

Fig. 4-15 Quantification of fenestration efficacy in moesin- or annexin II-depleted bEND5 cells.

A. Fenestration phenotype in moesin- or annexin II-depleted bEND5 cells treated with latrunculin A.
B. Selection of fenestrated cell area by threshold holding in Image J software.
C. Quantification of fenestrated cell area. $N \geq 20$; error bars denote ± SEM; * $P < 0.01$; ** $P < 0.001$.

Ct, control; scale bar in A and B, 10 μm.

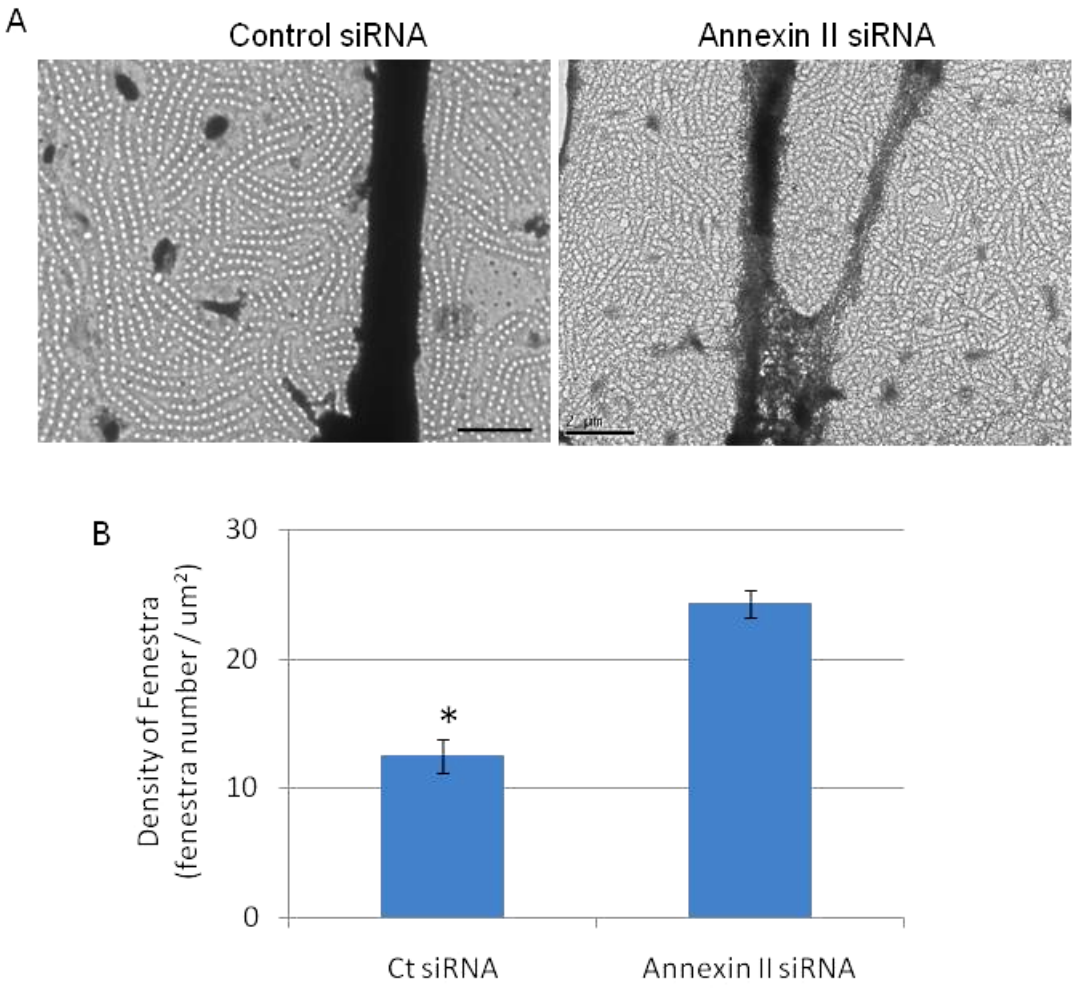

Fig. 4-16 Annexin II depletion doubled fenestral density.

A. Annexin II reduction resulted in increased fenestra number when bEND5 cells were treated with latrunculin A for fenestra induction. Scale bar, 2 μm.
B. Quantification of fenestra density in bEND5 cells treated with latrunculin A. N ≥ 20; error bars denote ± SEM; *, P < 0.001; Ct, control.

4.4 Discussion

Although ERM proteins are considered functionally redundant at the cell level, there is an almost exclusive distribution of ERM proteins in different tissues in adult vertebrates. Ezrin is mainly expressed in epithelial cells, where it is enriched at the apical surface (Berryman, 1993). Ezrin is the major component of the intestinal microvilli (Bretscher, 1983), and retinal pigment epithelial cells express only ezrin (Bonilha, 1999). Radixin is the dominant ERM protein in hepatocytes. It is also concentrated at bile canular membranes and cochlear stereocilia (Pataky, 2004; Katajiri, 2004). Moesin is found primarily in endothelial cells (Lankes, 1991). The distinct distribution of ERM proteins in separate tissues implies that they might have distinct roles.

Moesin, radixin and ezrin were all expressed in bEND5 cells, with ezrin expressed at the lowest abundance. There was no compensatory expression of radixin when moesin expression was reduced by siRNA transfection, and the striking colocalisation of moesin with PV-1 in the induced fenestral sieve plates suggested a unique role for moesin in fenestra biogenesis. Capable of binding to the plasma membrane through the FERM domain and anchoring actin microfilaments by the C-ERMD, moesin plays a crucial role in maintaining cell cortical integrity. Moesin is essential to establish and maintain cortical tension in interphase cells during mitosis (Kunda, 2008; Carreno, 2008). In moesin-deficient *Drosphila* eggs, the cortical actin network is severely disrupted (Jankovics, 2002), and Polesello *et al.* showed that moesin controls actin-based cell shape (2002). Indeed, reduction of moesin impaired F-actin remodeling triggered by latrunculin A and severely compromised the capability of bEND5 cells to extend an attenuated plasma membrane lamellapodia when the actin cytoskeleton was disturbed. Consequently, absence of moesin resulted in the failure of fenestra formation.

An interesting phenotype was observed in the moesin C-ERMD truncated cells. Despite inhibition of fenestra formation in N-moesin-GFP-overexpressing bEND5

cells, both light microscopy and electron microscopy data suggested that some aspects of the biogenesis program remained. For example, attenuated, organelle- and cytoskeleton-exclusion zones formed in the cell periphery following induction, and N-moesin-GFP was enriched in these domains, despite the absence of fenestrae. However, PV-1 and F-actin positive staining were absent from the N-moesin-GFP enriched, attenuated peripheral regions. Whether endogenous moesin displacement is directly responsible for the absence of PV-1 from the sieve-plate-like structures, or whether its absence is simply a consequence of the lack of fenestrae, is currently unknown. It is unlikely that the absence of PV-1 is directly responsible for the inhibition of fenestra formation, because PV-1 knockdown does not alter fenestral pore formation, but rather affects pore geometry and organization within the sieve plate (Ioannidou, 2006). On the other hand, active moesin is sufficient to induce cortical stiffening through F-actin rearrangement (Kunda, 2008), and FERM domain-truncated C-moesin-GFP has been used successfully to monitor dynamics of the actin cytoskeleton (Litman, 2000). Therefore a direct interaction of moesin and the F-actin resident in sieve plates seems more likely. These findings facilitate the dissection of fenestra biogenesis into distinct steps: first, an actin disruption-dependent process involving rearrangement of cytoplasmic organelles and the cytoskeleton together with cell attenuation, to enable close apposition of apical and basal plasma membranes; second, a moesin-dependent F-actin reassembly process leading to formation of fenestral pores.

Results from loss of function experiments revealed an unexpected effect of annexin II on fenestra formation. Depletion of annexin II in bEND5 cells not only increased the fenestrated area of the cell, but also increased fenestra density. Annexin II has been reported to regulate multivesicular endosome formation in the degradation pathway (Mayran, 2003). Transport from early endosomes to late endosomes after cholesterol accumulation depends on annexin II (Mayran, 2003). Annexin II may work to divert proteins required for fenestra formation, such as PV-1, to the degradation pathway. However, PV-1 levels are not significantly up-regulated by annexin II depletion (data

not shown). Thus, we reason that inhibition of degradation makes at most a minor contribution to the significantly increased potency of fenestra induction.

Biochemical studies showed that annexin II can bind to PIP2 with high specificity *in vivo* and has a role in organizing/stabilising lipid microdomains (Hayes, 2004; Rescher, 2004). The involvement of PIP2 in ERM activation is also well-documented (Niggili, 1995; Matsui, 1999). In fact, sequential binding to PIP2 and phosphorylation of a conserved threonine are necessary for the activation of ERM proteins (Fievet, 2004). Therefore, we speculate that the opposing effects of annexin II- and moesin depletion are due to competitive binding to PIP2-rich lipid microdomains in the process of cell membrane reorganization.

In conclusion, moesin and annexin II could differentially regulate fenestra formation via more than one mechanism, including actin reorganization, membrane remodeling, and vesicle trafficking. The results in this chapter depicted a dynamic picture of fenestra formation, a complex but well-coordinated process regulated by multiple factors.

Chapter 5

The fodrin membrane skeleton and Na,K-ATPase coordinately regulate fenestra formation

Abbreviations

ABPs	actin binding proteins
AMD	age-related macular degeneration
BSA	bovine serum albumin
DMEM	Dulbecco's modified Eagle medium
ER	endoplasmic reticulum
ERGIC	ER-Golgi intermediate compartment
ERM	ezrin, radixin, and moesin
FAK	focal adhesion-associated kinase
FACR	fenestrae-associated cytoskeleton ring
GEnC	glomerular endothelial cell
GFP	green fluorescent protein
GFR	glomerular filtration rate
HA	hemagglutinin
HSPG	heparan sulfate proteoglycans
HuVEC	human umbilical vein endothelial cells
LM-EM	light microscopy-electron microscopy
LSEC	liver sinusoidal endothelial cells
MβCD	methyl-β-cyclodextrin
MDCK	Madin-Darby canine kidney
NPC	nuclear pore complex
PBS	phosphate-buffered saline
PDK1	phosphoinositide-dependent protein kinase-1
PFA	paraformaldehyde
PI3K	phosphatidylinositol 3-kinase
PIP2	phosphatidylinositol 4,5 biphosphate
PMA	phorbol myristate acetate
PtdIns	phosphatidylinositol
PV-1	plasmalemmal vesicle–associated protein–1

RA	retinoic acid
RPE	retinal pigment epithelium
SNARE	soluble N-ethylmaleimide sensitive fusion protein attachment protein receptor
TGF-β	transforming growth factor β
VEGF	vascular endothelial growth factor
VVOs	vesiculo-vacuolar organelles

Chapter 5 The fodrin membrane skeleton and Na,K-ATPase coordinately regulate fenestra formation

5.1 Visualisation of cytoskeletal structure in fenestral sieve plates.

The fenestral sieve plate consists of a large, attenuated cell extension that is mostly devoid of organelles and many of the primary structural elements of the cytoskeleton such as microfilament bundles, microtubules and intermediate filaments (Fig. 3-11). However, formation of sieve plates and fenestrae starts within minutes of induction by latrunculin A, and the rapidly induced fenestral pores arise in highly organised linear arrays, implying the involvement of underlying cytoskeleton. Braet *et al.* suggested a fenestra-associated cytoskeleton ring around LSEC fenestrae (1995), and the presence of actin filaments around sinusoidal endothelial fenestrae was suggested by a heavy meromyosin decorated reaction (Nagai, 2004). To date, no obvious cytoskeletal architecture has been linked to fenestral organisation sieve plates.

Because of the data supporting a role for actin-binding proteins and F-actin in fenestra formation, we embarked on the task of describing the nature of the underlying cytoskeleton in fenestral sieve plates. Whole mount TEM, section TEM and SEM analysis all failed to reveal any obvious structure (Fig. 5-1). Our breakthrough came from the use of high-pressure freeze/freeze substitution and electron tomography. EM tomography is a sophisticated 3-D data collection and reconstruction method, which aims at a resolution high enough to allow the visualization of protein complexes (McDonald and Auer, 2006). Through our collaboration with the University of Helsinki in Finland, we tried tomographic techniques, but our initial efforts with tomography and chemical fixation yielded no progress. However, upon combining high-pressure freeze fixation with tomography, we consistently observed a cytoskeleton that runs proximal and parallel to the linear arrays of fenestral pores in sieve plates (Fig. 5-2).

Even the links between the cytoskeleton and the rim of the fenestral pore were sometimes distinguishable (Fig. 5-2, arrows). To date, this is the first clear visualisation of cytoskeletal structure in fenestral sieve plates.

The exclusion of microtubules and intermediate filaments from the fenestral sieve plates (Chapter 3, Fig. 3-11), the presence of short F-actin microfilaments and moesin, and now the cytoskeletal structure revealed by tomographic EM led us to explore the spectrin membrane cytoskeleton.

5.2 Introduction to the fodrin membrane skeleton

With few cytoplasmic elements or organelles and large areas of membrane that need fortification to withstand travel through the heart and vasculature, erythrocytes employ the use of a spectrin cytoskeleton. The membrane skeleton is immediately under the plasma membrane and enables membrane distensibility (De Matteis, 2000). The molecular basis of the spectrin membrane skeleton was first identified in erythrocytes (Singer, 1972; Lux, 1979; Goodman, 1981), and subsequently resolved in non-erythroid cells (Goodman, 1981 and 1999; Pratt, 1984; Heltianu, 1986; Bennett, 1993; Wu, 2001). The non-erythroid membrane skeleton is primarily composed of fodrin and its binding proteins ankyrin and protein 4.1 (Ungewickell, 1979; De Matteis, 2000; Pradhan, 2001). Fodrin is a rod-shaped protein that exists as an α- and β-heterotetramer, and end-to-end association of these tetramers with short actin filaments produces the hexagonal complexes (Brenner 1979 and 1980; Liu, 1987; Heimann, 1999) (Fig. 5-3). The existence of a short actin protofilament in the fodrin cytoskeleton is interesting, given our finding that F-actin labelling by phalloidin was reproducibly observed in the fenestra sieve plates. Moreover, in frog neuromuscular junctions, F-actin-fodrin complexes in non-release domains of the neuron terminal are not affected by actin depolymerising drugs (Job, 1998; Dunaevsky, 2000). We sought to test the hypothesis that a membrane skeleton composed of moesin, a member of the band 4.1 superfamily, actin and fodrin is the cytoskeletal structure in fenestral sieve plates.

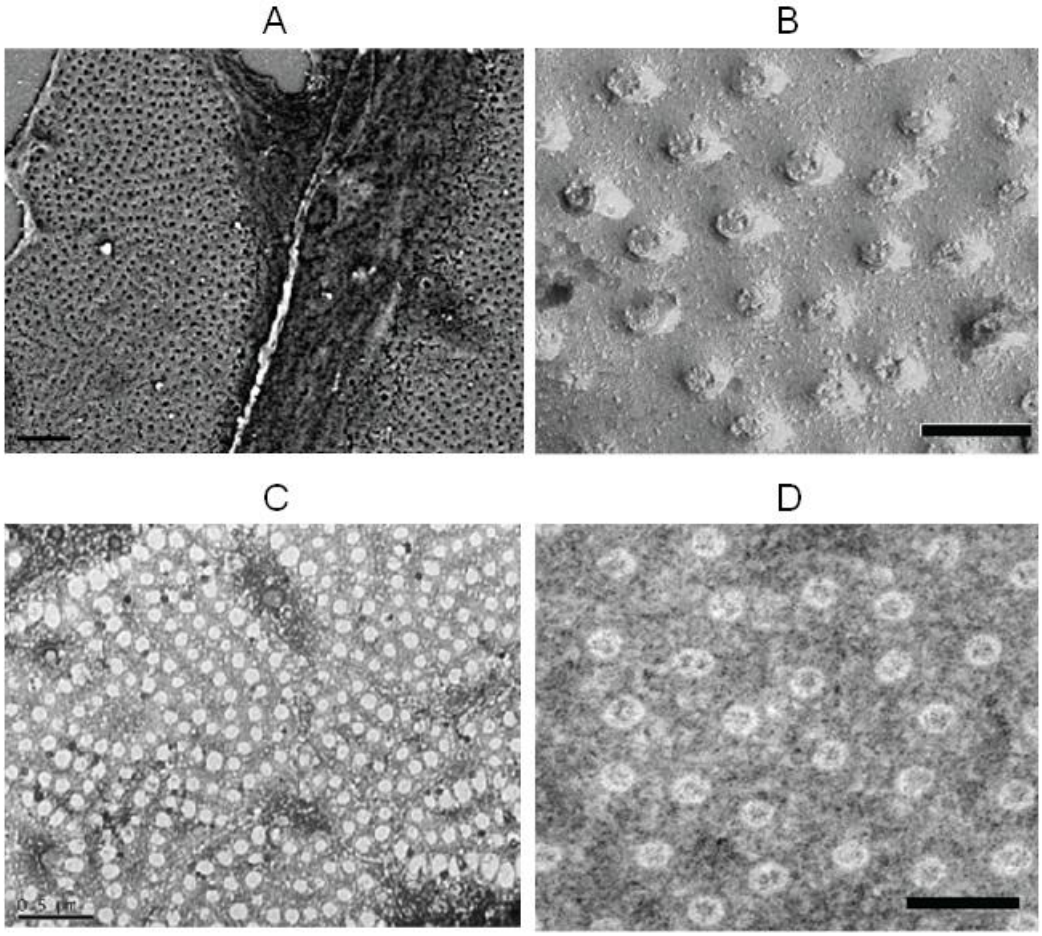

Fig. 5-1 Attemps pf visualising cytoskeletal structure in fenestral sieve plates.
Various ultrastructual analyses failed to reveal cytoskeletal structure in fenestral sieve plates.

A. SEM image of fenestral sieve plates. Scale bar, 2 µm
B. Freeze-fracture SEM image of fenestral sieve plates. Scale bar, 200 nm.
C. Wholemount TEM image of fenestral sieve plates. Scale bar, 0.5 µm.
D. Section TEM image of fenestral sieve plates. Scale bar, 200 nm.

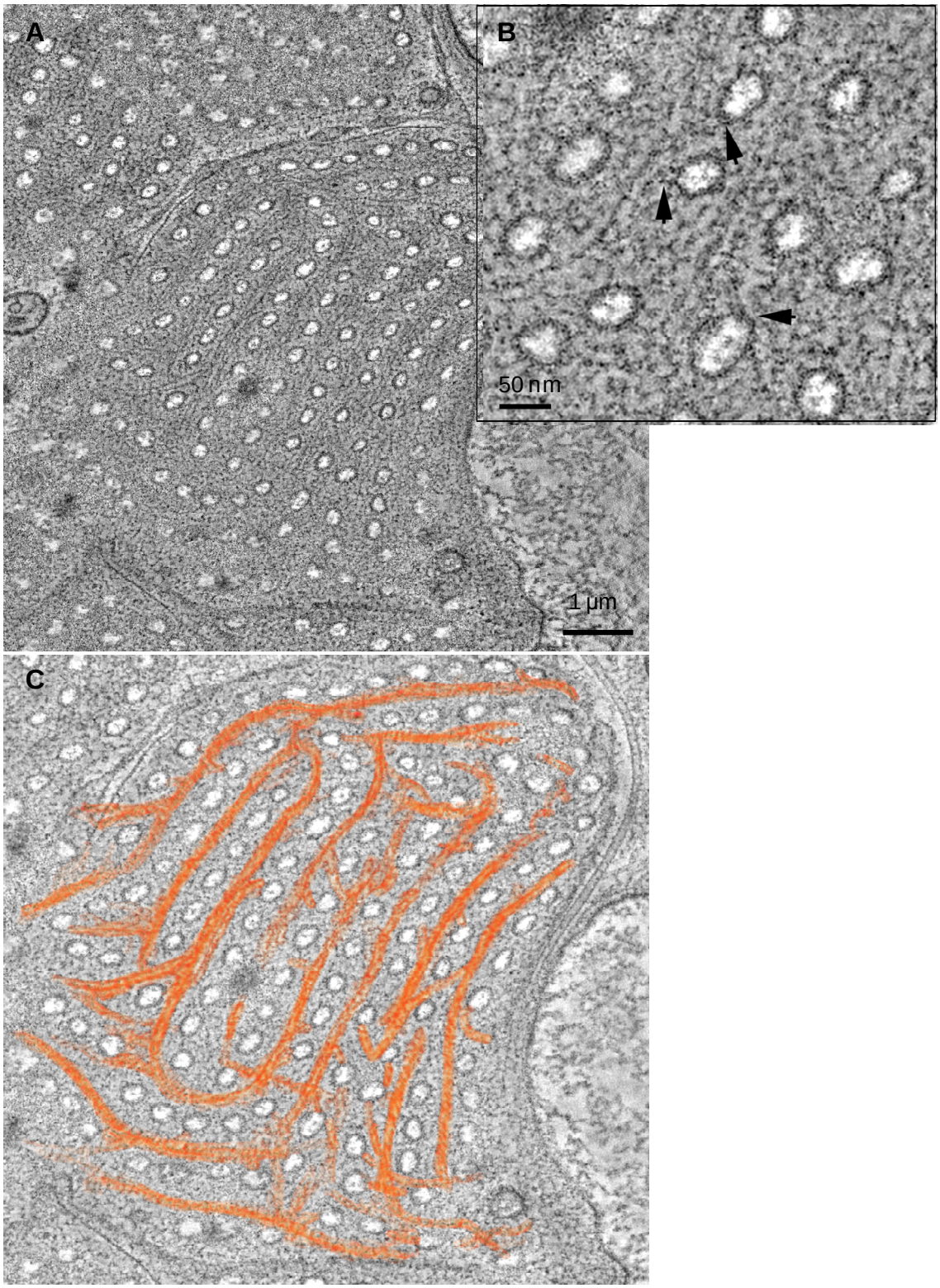

Fig. 5-2 Tomographic images revealed cytoskeletal structure in fenestral sieve plates. Tomographic image showed cytoskeletal structure running along fenestrae rows in the sieve plates (A); the proximal and parallel cytoskeleton was illustrated in C; B showed the magnified image of part of A, arrows in B pointed to the links between the cytoskeleton and the rim of fenestral pore.

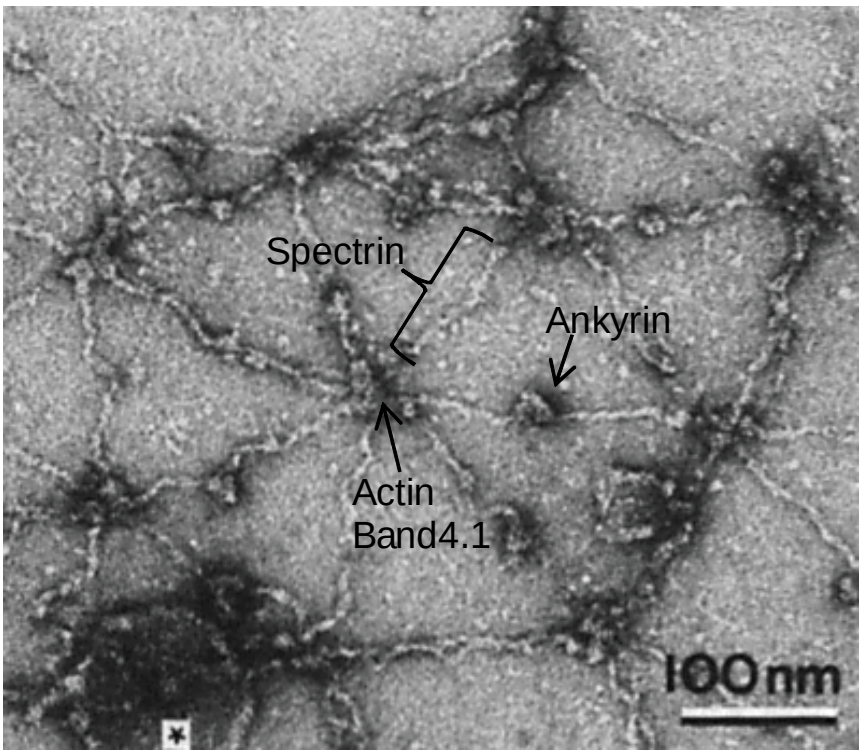

Fig. 5-3 Membrane skeleton in an erythrocyte.
Visualisation of the hexagonal lattice in the erythrocyte membrane skeleton.
(Adapted from Liu, 1987)

5.3 Fodrin colocalised with PV-1 in fenestral sieve plates

By immunostaining, we found that alpha fodrin was highly expressed in bEND5 cells, though its distribution was not much in accordance with PV-1 in uninduced cells (Fig. 5.4-A, upper panel). When the cells were treated with latrunculin A for fenestra induction, fodrin was redistributed throughout the whole cell, especially in perinuclear region. However, in the PV-1-marked fenestral sieve plates, fodrin was reorganized into a filamentous network colocalising with PV-1 (Fig. 5-4A, lower panel). Immunostaining with another well-documented cytoskeletal component, ankyrin, showed that ankyrin B was also present in fenestral sieve plates, though with a distinct dot-like pattern (Fig. 5-4B).

In the previous study, we found that moesin and PV-1 colocalised in the mouse choriocapillaris (fig. 4-5) Similarly we found that fodrin was strongly expressed and colocalised with PV-1 in choriocapillaries, though the expression of fodrin was not limited to the choriocapillaris (Fig. 5-5).

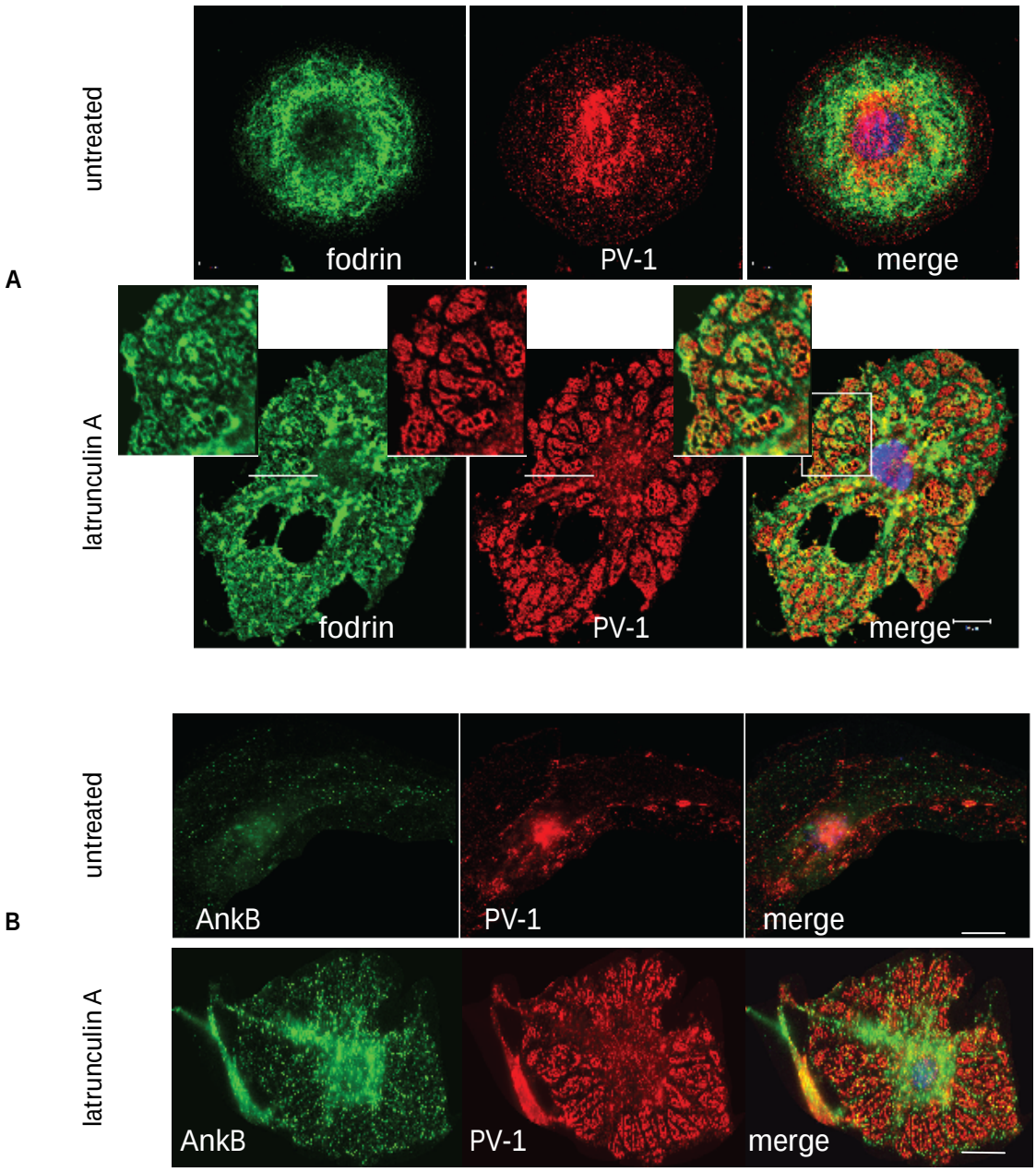

Fig. 5-4 Reorganisation of membrane skeleton components during fenestra formation.

A. Fodrin colocalised with PV-1 and reorganised into a filamentous network in the induced fenestral sieve plates.

B. Ankrin B appeared dot-like and was present in the fenestral sieve plates induced by latrunculin A.

Scale bar, 10 μm.

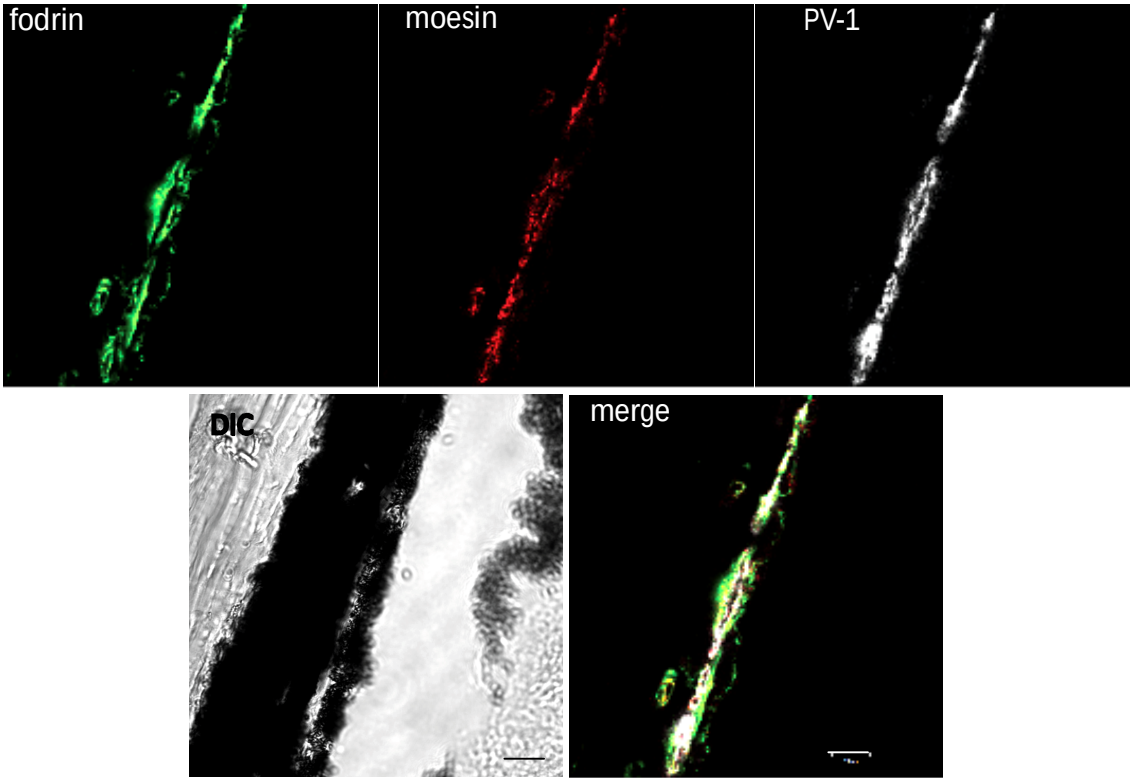

Fig. 5-5 Fodrin expression in choriocapillaries.

Fodrin with PV-1 and moesin were colocalised in choriocapillaries in mouse eye cross-section. DIC, differential interference contrast microscopy.

Scale bar: 10 μm

5.4 Fodrin knockdown inhibited fenestra formation

To determine whether fodrin was required for formation of fenestrae, we used siRNA to deplete fodrin in bEND5 cells. Three pre-selected siRNAs were transfected into bEND5 cells, and the one with the best efficacy was used for subsequent experiments. Both mRNA and protein levels indicated that fodrin expression was significantly reduced (~90%) after 48 hours of transfection (Fig.5-6).

In the uninduced, control siRNA-transfected bEND5 cells, PV-1 was mainly distributed in regions such as membrane ruffles, the perinuclear region and the cell membrane. Fodrin depletion resulted in the distribution of PV-1 throughout the cell (Fig. 5-7), implying its possible role in PV-1 immobilisation. Latrunculin A treatment induced abundant formation of PV-1-marked fenestral sieve plates in control siRNA-transfected cells. However, no PV-1 positive sieve plates formed at the cell periphery in fodrin-knockdown bEND5 cells; instead, PV-1 was mainly located in microtubule/organelle-rich thick arbors and the peri-nuclear region (Fig. 5-7) – a phenotype similar to that observed in moesin-depleted bEND5 cells (Fig. 4-11). Disruption of fenestra formation by fodrin depletion was further confirmed using TEM. In TEM micrographs, fodrin-deficient bEND5 cells typically appeared spiky, lacking an attenuated cell region between the microtubule/organelle-rich arbors (Fig. 5-8A). We identified more than 30 fodrin-depleted bEND5 cells under TEM using a correlative LM-EM assay. Fenestrated membrane area was quantified in those cells and in control siRNA-transfected cells. As demonstrated by the cell appearance in TEM images, fodrin knockdown abolished the attenuated cell region where fenestral sieve plates should have formed after treatment with latrunculin A (Fig. 5-8B). These results strongly indicate that fodrin plays a crucial role in the formation and/or maintenance of attenuated cell spreading following disruption of the actin cytoskeleton by latrunculin A.

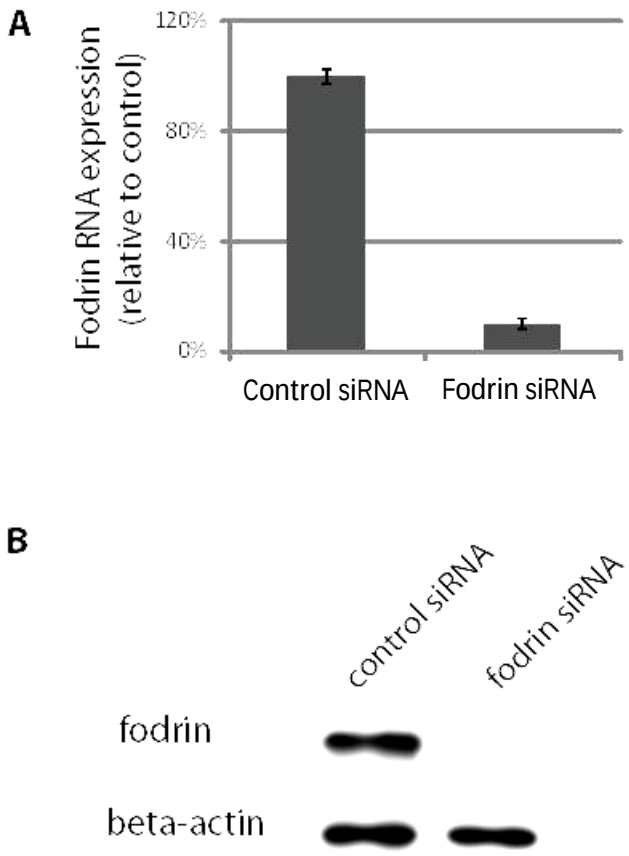

Fig. 5-6 Down-regulation of fodrin by siRNA transfection.
Fodrin expression was reduced by siRNA transfection both at the RNA level (A) and the protein level (B). Results in A was the average of 3 experiments (n = 3), error bars showed ±SEM.

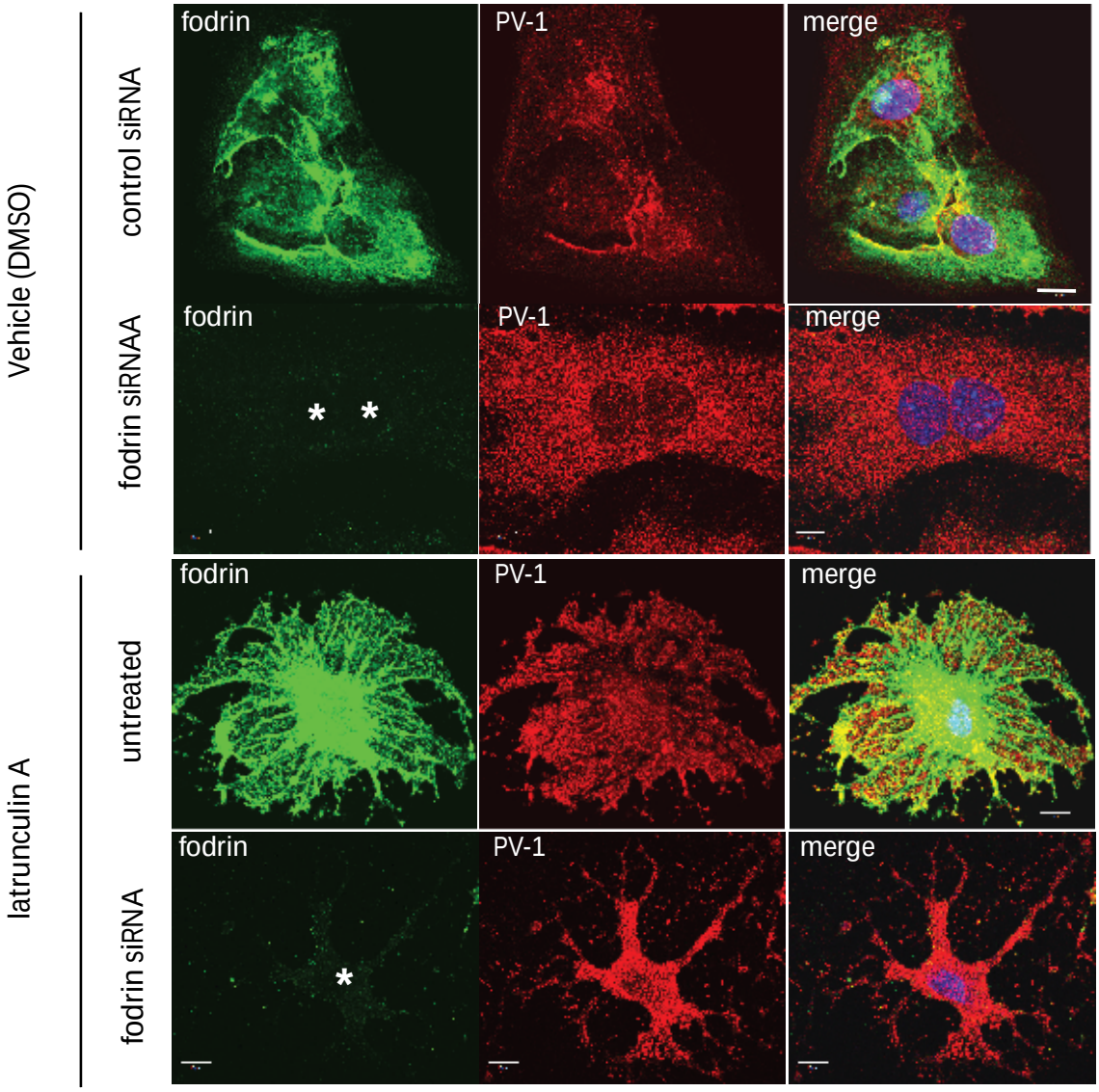

Fig. 5-7 Loss of fenestra formation in in fodrin-reduced bEND5 cells.
In vehicle treated, uninduced bEND cells, depletion of fodrin resulted in the loss of preferred localisation of PV-1, such as in the cell ruffles; instead, PV-1 was present homogeneously in the cell cytoplasm. Upon fenestrae induction triggered by latrunculin A, formation of PV-1 marked fenestral sieve plates was abolished in fodrin knockdown bEND5 cells.
* fodrin depleted bEND5cells; Scale bar, 10 μm.

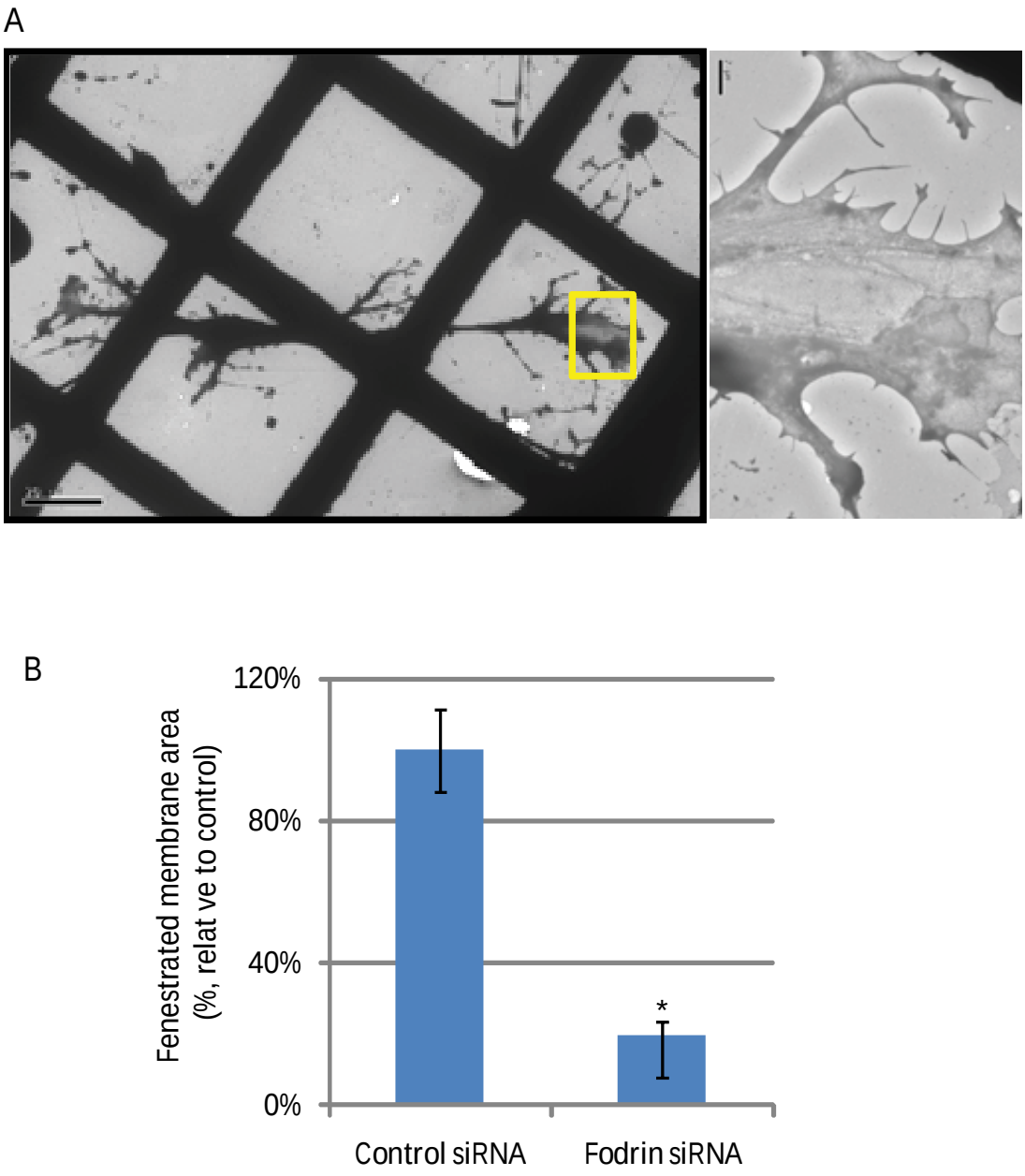

Fig. 5-8 Fodrin reduction abolished fenestra formation induced by latrunculin A.

A. Wholemount TEM confirmation of absent fenestra formation in a fodrin knockdown bEND5 cell. Scale bar, 20 μm.
B. Quantification of fenestration in fodrin siRNA-transfected, latrunculin A-treated bEND5 cells. $N \geq 20$; error bars denote ± SEM; * $P < 0.0001$.

5.5 Interaction between fodrin and other components in fenestral sieve plates

5.5.1 Interaction between fodrin and the fenestral diaphragm protein PV-1

The loss of localised PV-1 distribution in fodrin knockdown bEND5 cells and the colocalisation of fodrin and PV-1 in fenestral sieve plates suggested the involvement of fodrin in regulating PV-1 distribution in caveolae or fenestrae. I therefore designed experiments to test whether fodrin associates with PV-1. Immunoprecipitation analysis showed that PV-1 coimmunoprecipitated with fodrin in bEND5 cells – regardless of whether fenestrae had been induced (Fig. 5-9B). Since the distribution of fodrin and PV-1 is not limited to fenestral sieve plates in latrunculin A-treated bEND5 cells, fodrin might not bind solely to fenestral PV-1. Indeed, caveolin-1, like PV-1, also coimmunoprecipitated with fodrin (Fig. 5-9B). To exclude the possibility that the coimmunoprecipitation came from non-specific binding, VE Cadherin, which is not in the sieve plates (data not shown), was used as an negative control in the study (Fig. 5-9C).

5.5.2 Moesin is required for the interaction between fodrin and PV-1 in fenestral sieve plates

We demonstrated in the last chapter that moesin depletion diminishes fenestra formation whereas annexin II knockdown improves fenestrae induction. Reduction of moesin or annexin II did not affect fodrin expression, nor did the depletion of fodrin affect protein levels of moesin, annexin II or PV-1 (Fig. 5-10A). When moesin was depleted in bEND5 cells, the interaction between fodrin and PV-1 in caveolae was not affected in uninduced cells, but PV-1 failed to coimmuoprecipitate with fodrin in latrunculin A-induced cells. After annexin II knockdown, on the other hand, there was a slight increase of coimmunoprecipitated PV-1 with fodrin in latrunculin A-treated bEND5 cells (Fig. 5-10B). The association between fodrin and PV-1 was therefore specific to fenestrae in the induced bEND5 cells, and the interaction required moesin. Thus fodrin, PV-1 and moesin were reorganized into the same protein complex in fenestral sieve plates when latrunculin A was added to bEND5 cells.

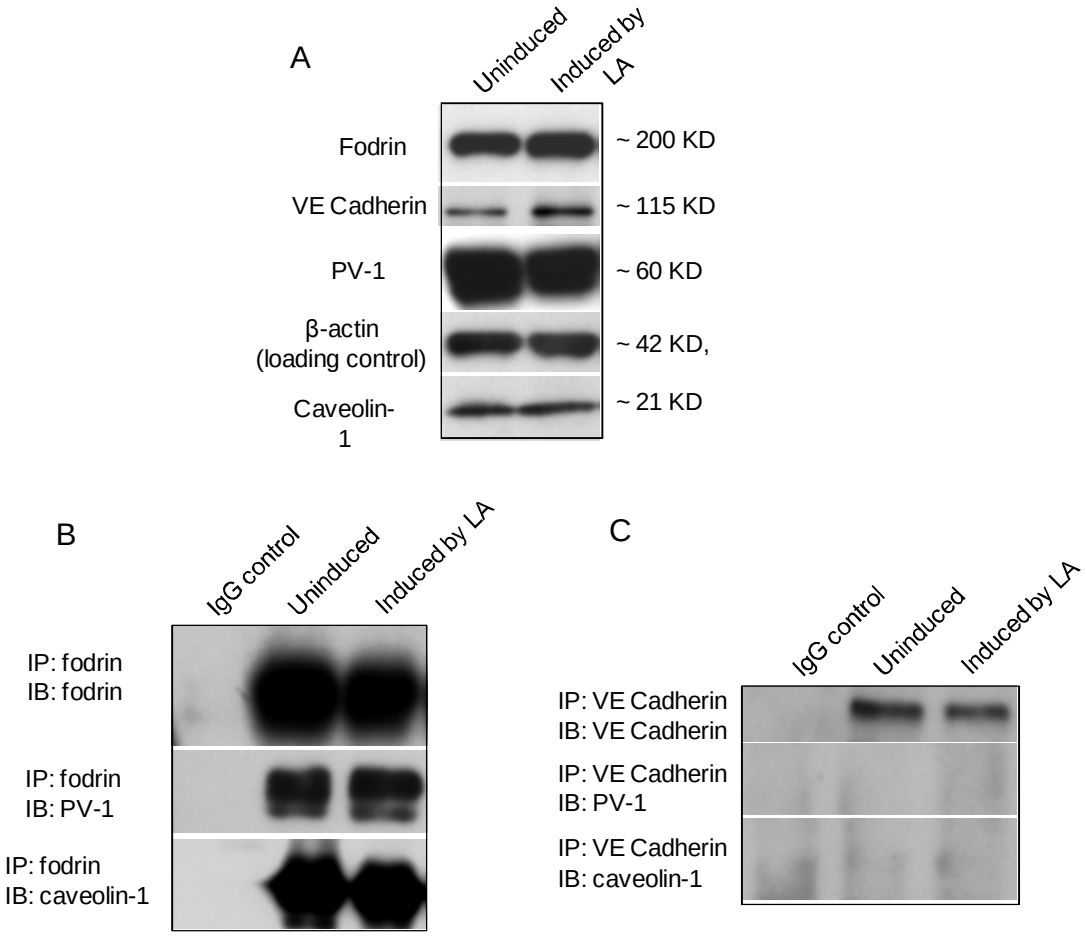

Fig. 5-9 Interaction between fodrin and PV-1 is specific.

A. Protein expression of fodrin, PV-1, caveolin-1and VE Cadharin was not affected by fenestra induction.
B. Both PV-1 and caveolin-1 coimmunoprecipitated with fodrin before and after fenestrae were induced by latrunculin A in bEND5 cells.
C. PV-1 and caveolin-1 didn't co-IP with VE Cadherin , which indicated that the co-IP of PV-1 or caveolin-1 with fodrin is specific.

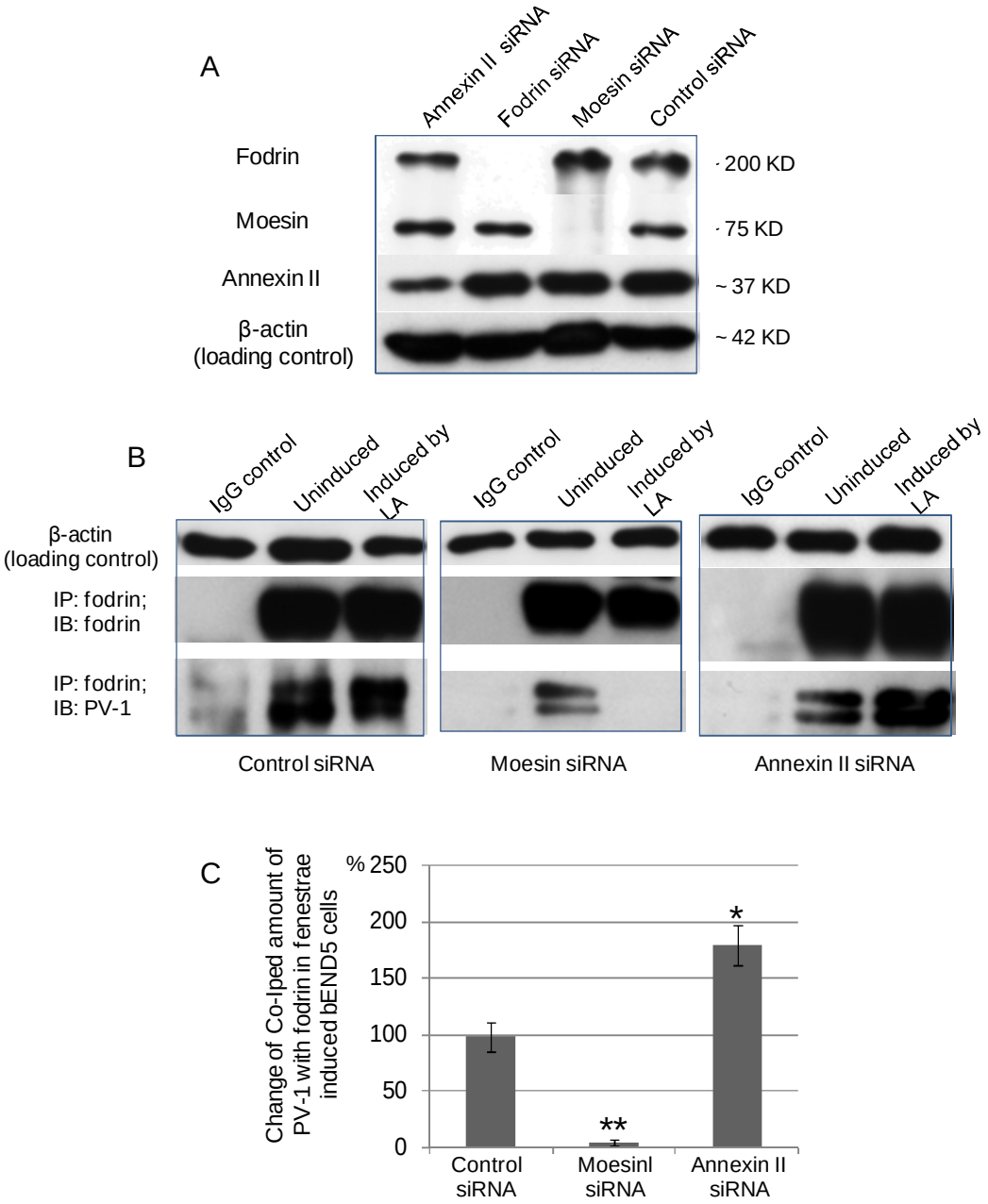

Fig. 5-10 The interaction between fodrin and fenestral PV-1requires moesin.

A. Protein expressions was not affected by siRNA transfection
B. PV-1 coimmunoprecipitated with fodrin in uninduced bEND5 cells, however, PV-1 failed to coimmunoprecipitate with fodrin in moesin depleted and LA (latrunculin A) treated bEND5 cells.
C. Densitometry analysis showed, in bEND5 cells that were treated by LA for fenestra induction, there was almost no Co-IPed PV-1 with fodrin in moesin depleted bEND5 cells, but the Co-IPed PV-1 with fodrin increased in annexin II reduced bEND5 cells. N = 3, error bars denote ±SEM, * $P < 0.001$; ** $P < 0.0001$

5.5.3 The dynamic partnership between fodrin and actin during fenestra formation

To further appreciate the dynamic reorganisation of the membrane skeleton during fenestra formation, we dissected the interaction between fodrin and β-actin by coimmunoprecipitation following a fenestra induction time course, since β-actin was reported as the building block of the actin protofilaments in the fodrin-based membrane skeleton (Pinder, 1978). Cells were treated with 1.25 μM latrunculin A to induce fenestra formation, and the induction was interrupted at different time points. In the uninduced bEND5 cells, the intact membrane skeleton was indicated by the strong β-actin band that was pulled down together with fodrin. After 10 minutes of latrunculin A addition, the amount of β-actin coimmunoprecipitated with fodrin dramatically decreased, presumably due to the rapid disassembly of actin filaments and the associated cytoskeleton. At later time points, increased actin coimmunoprecipitation with fodrin was observed, suggesting a newly established association between fodrin and β-actin (Fig. 5-11). A the end of incubation, a 30-minute washing with PBS restored the coimmunoprecipitated β-actin with fodrin to the base level before latrunculin A addition.The dynamic change of β-actin associated with fodrin, together with the interaction among fodrin, PV-1 and moesin, strongly suggest that a fodrin-, actin- and moesin-based membrane skeleton formed in fenestral sieve plates and associates with the diaphragm protein PV-1.

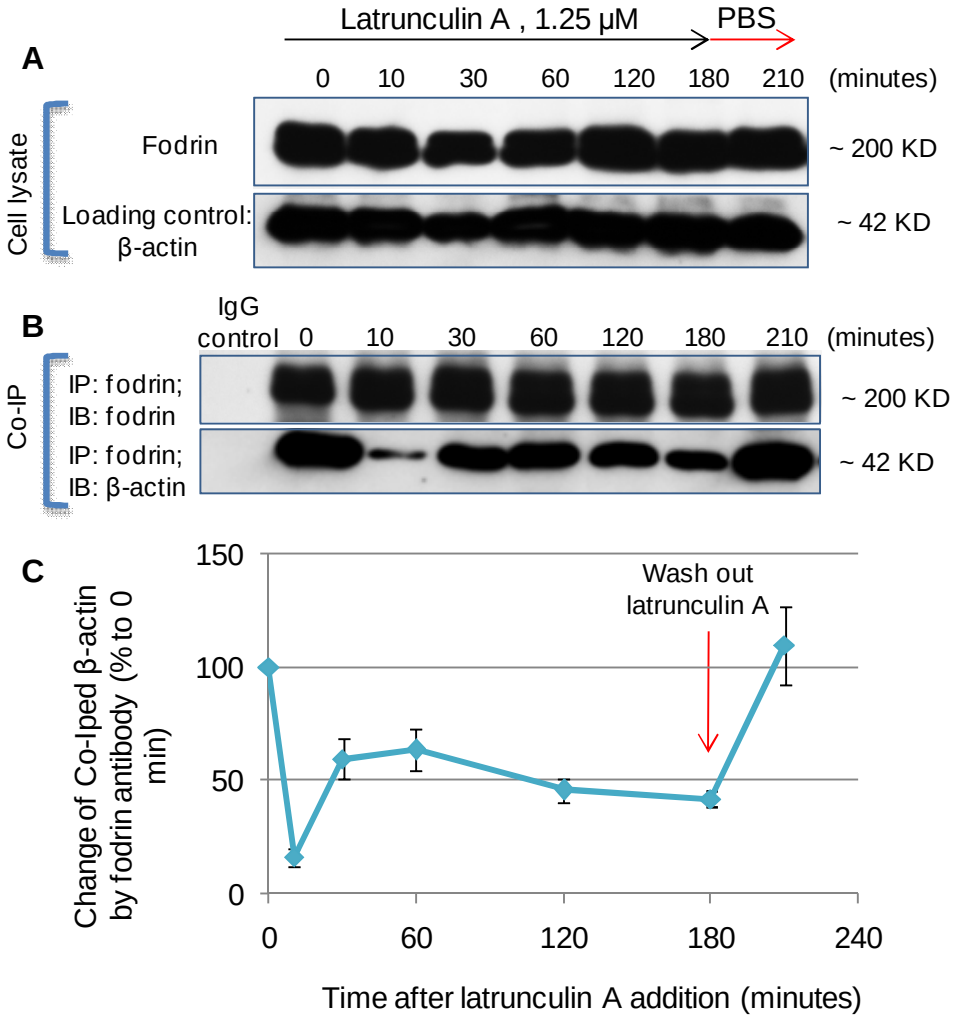

Fig. 5-11 Dymanic interaction between fodrin and β-actin during fenestra formation.

A. There was no change of fodrin and β-actin expression during the time course of fenestrae induction triggered by latrunculin A at 1.25 μM.

B. The amount of β-actin Co-IPed (coimmunicipitated) with fodrin went to a dynamic change during the time course of fenestrae induction. After 10 minutes of latrunculin A addition, the amount of β-actin Co-IPed with fodrin dramatically decreased, but then increased at later time points. At the end of incubation, a 30-minute washing with PBS restored the Co-IPed β-actin to the base level before latrunculin A addition. IP, immunoprecipitation; IB, immunoblot.

C. Densitometry change of CO-IPed β-actin with fodrin during the time course of fenestra induction. The result of every time point is the average of 3 independent experiments. Error bars denote ± SEM.

5.6 Discovery of Na,K-ATPase in fenestral sieve plates

Having identified the role of fodrin and moesin in fenestral sieve plates formation, I next sought to identify additional components that may interact with the cytoskeleton. Since ERM proteins appear to provide a link between the membrane and the cytoskeleton, my next step was to identify the membrane proteins involved. A number of proteins that bind to ERM family members have been identified, including CD44, CD43, ICAM-1, ICAM-2, ICAM-3, and ERM-binding phosphoprotein 50 kDA (EBP50) (Tsukita, 1994; Yonemura, 1998; Heiska, 1998; Reczek, 1998). However, immunofluorescence analysis showed that none of these reported candidates were present in fenestral sieve plates (data not shown).

Studies in Madin-Darby canine kidney (MDCK) cells have shown that fodrin, ankyrin and Na,K-ATPase are in the same protein complex, and that the subcellular distribution of fodrin during development of a continuous monolayer of cells coincides temporally and spatially with the polarized distribution of Na,K-ATPase (Nelson, 1986 and 1989). Alper *et al.* demonstrated that the fodrin membrane skeleton preferentially colocalises with apical Na,K-ATPase rather than with the basolateral anion exchanger AE2 in the choroid plexus (1994). This implies that the interaction between the fodrin membrane skeleton and Na,K-ATPase may play an important role in establishing and maintaining special membrane domains in differentiated cells. Therefore we investigated if Na,K-ATPase was in the protein complex with fodrin in fenestral sieve plates.

5.6.1 Localisation of Na,K-ATPase in fenestral sieve plates

Na,K-ATPase, or the sodium pump, is an energy-transducing ion pump first described by Skou (1957). It is a highly-conserved integral membrane protein that is expressed in virtually all cells of higher organisms and belongs to the P-type ATPase superfamily. Na,K-ATPase is responsible for pumping Na^+ and K^+ ions across the plasma membrane, and as such is critical for maintaining cell volume and membrane potential. Na,K-

ATPase is composed of two non-covalently linked subunits – a catalytic α-subunit and an auxiliary β-subunit (Kaplan, 2002; Sweadner, 1989; Blanco, 1998). The α-subunit, Na,K-α, is composed of approximately 1000 amino acid residues with 10 transmembrane segments; and the β-subunit, Na,K-β, is a type II membrane protein with a single membrane crossing, and is composed of about 370 amino acids (Kaplan, 2002) (Fig. 5-12). Although it is often viewed solely as a sodium pump, Na,K-ATPase has been shown to have numerous ion transport-independent roles in the last decade, including roles in cell junction formation, cell migration and signal transduction (Tian, 2006; Krupinski, 2009). The general consensus is that the Na,K-ATPase carries out these non-pump roles acting primarily as a plasma membrane scaffold regulating the availability of several important signalling molecules, such as Src (Haas, 2002), PI3K (Barwe, 2005), IP3 receptor (Yuan, 2005), adaptor protein2 (Done, 2002) and PLC-γ (Li and Xie, 2009).

Immunofluorescence analysis revealed that the Na,K-ATPase was distributed ubiquitously throughout the cell membrane in untreated bEND5 cells. When cells were treated with latrunculin A for 3 hours to induce fenestra formation, Na,K-ATPase reorganised into a distinct PV-1 colocalising pattern in the well-formed fenestral sieve plates, though its expression was not limited to the sieve plates (Fig. 5-13). Within the sieve plates, immunogold labelling revealed that Na,K-ATPase was located on the rim of the fenestral pore (Fig. 5-14).

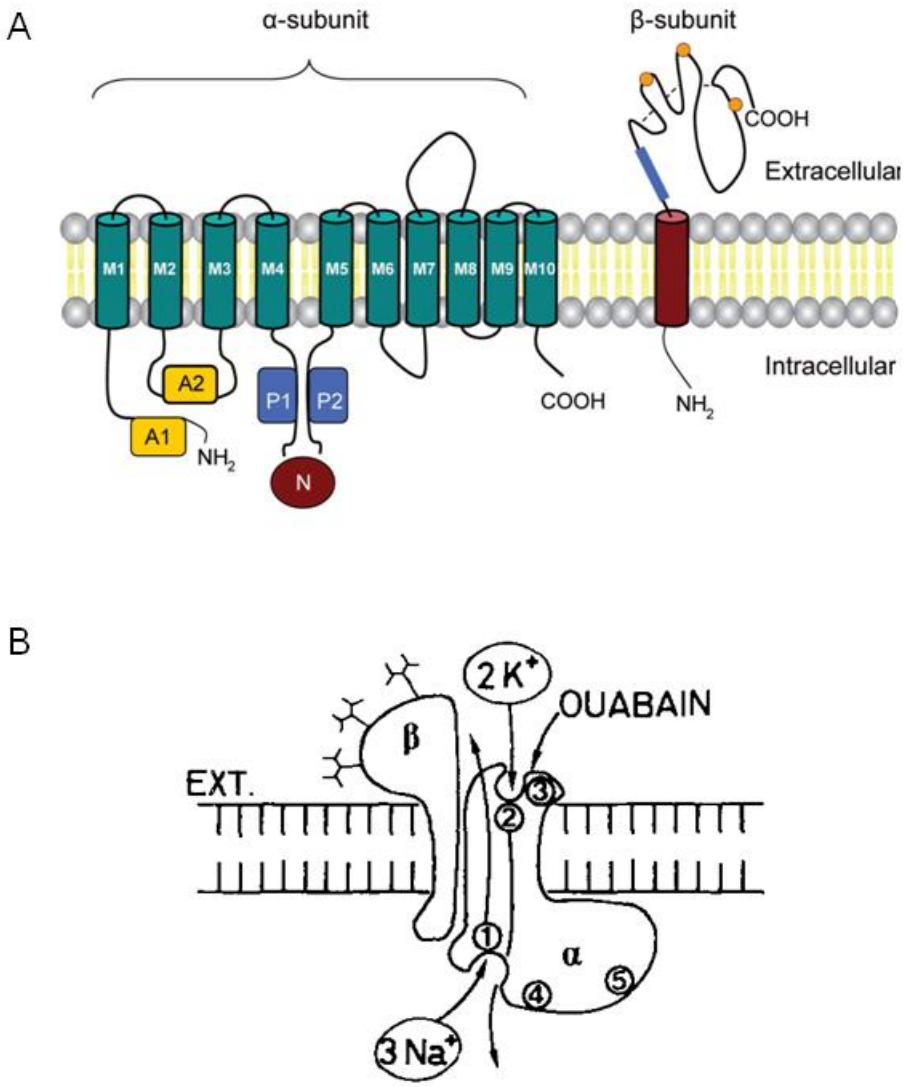

Fig. 5-12 Structure and primary function of Na,K-ATPase.

A. Na,K-ATPase is a heterodimeric integral membrane protein. The α-subunit is responsible for the catalytic activity of the enzyme. N-nucleotide-binding, P-phosphrylation, A-Axtuator domains are for ATP binding and hydrolysis. (Adapted from Benarroch, 2011.)
B. General model for Na.K-ATPase showed binding sites forr (1) Na^+ , (2) K^+, (3) ouabain, (4) phosphorylation and (5) ATP binding. (Adapted from Horisberger, 1991).

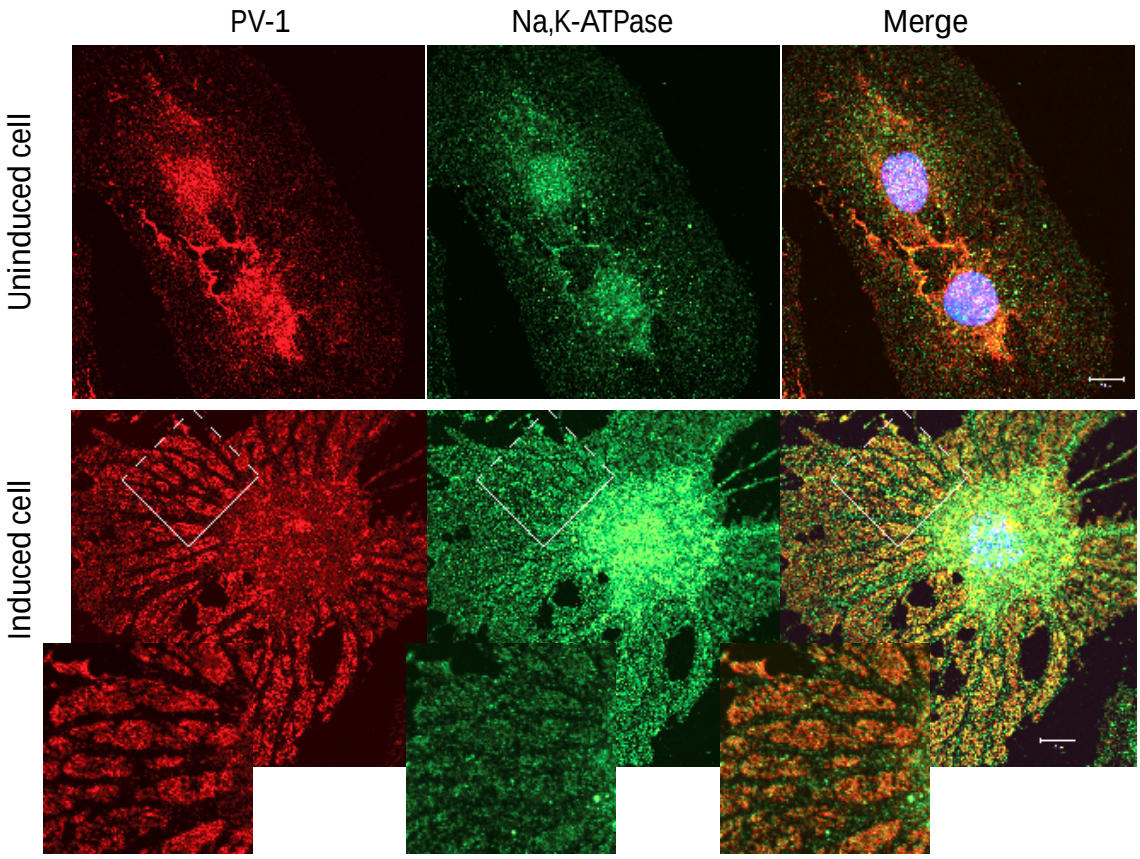

Fig. 5-13 Na,K-ATPase was present in fenestral sieve plates.
Na,K-ATPase was reorganised to colocalise with PV-1 in fenestral sieve plates in latrunculin A treated bEND5 cells.
Scale bar, 10 μm.

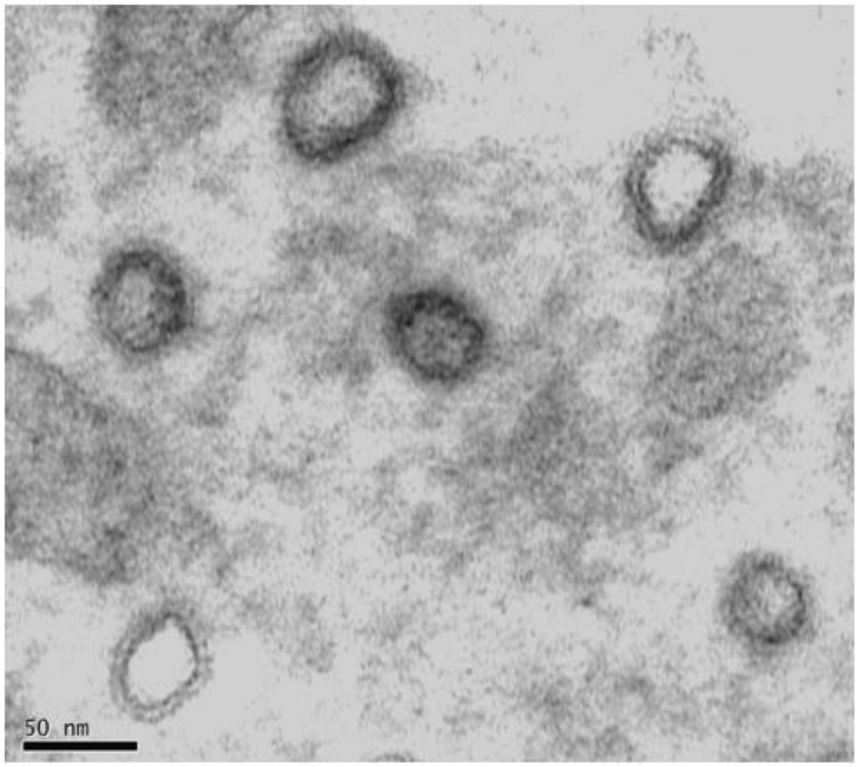

Fig. 5-14 Na,K-ATPase was located on the rim of fenestra. Immunogold labelling of Na,K-ATPase in fenestral sieve plates. Scale bar, 50 nm.

5.6.2 Interactions between Na,K-ATPase and other sieve plate components

The protein expression levels of Na,K-ATPase and PV-1 didn't change after fenestra induction (Fig. 5-15A), but PV-1 coimmunoprecipitated with Na,K-ATPase in the induced bEND5 cells only(Fig. 5-15B), implying a newly formed interaction between the Na,K-ATPase and PV-1 in fenestral sieve plates. The Na,K-ATPase has been reported to form a protein complex with caveolin-1 in caveolae (Xie, 2003), though it failed to pull down any caveolar PV-1 in untreated bEND5 cells (Fig. 5-15B). Thus the interaction between Na,K-ATPase and PV-1 is specifically related to the formation of fenestrae.

In a similar pattern, Na,K-ATPase was not pulled down by anti-fodrin antibody in untreated bEND5 cells, however, it coimmunoprecipitated with fodrin when fenestrae were induced by latrunculin A (Fig. 5-15B). Thus the interaction between Na,K-ATPase and fodirn, and PV-1, only occurred in bEND5 cells that were fenestrated, which strongly suggest these interactions play a crucial role in fenestra formation.

More interestingly, Na,K-ATPase protein level was affected by moesin and annexin II expression. Moesin knockdown significantly decreased Na,K-ATPase expression, whilst annexin II depletion almost doubled Na,K-ATPase protein level in bEND5 cells (Fig. 5-16). Given the role of moesin and annexin II in regulation of fenestra formation, the expression level of Na,K-ATPase appeared positively correlated to fenestral induction potency in bEND5 cells.

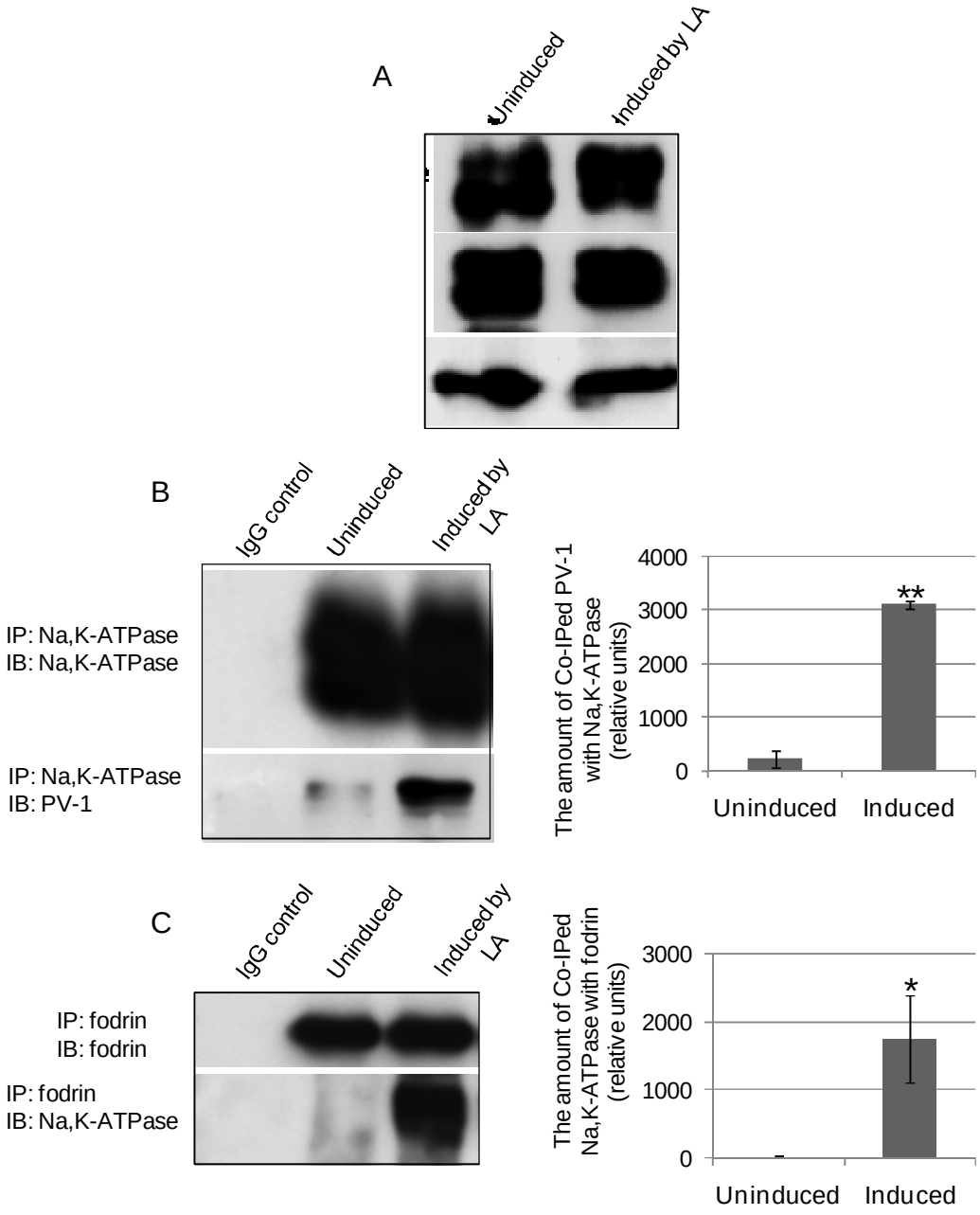

Fig. 5-15 Na,K-ATPase , PV-1 and fodrin formed a protein complex in fenestral sieve plates.

A. Na,K-ATPase and PV-1 protein levels were not affected by fenestrae induction by latrunculin A in bEND5 cells.
B. The amount of PV-1 co-IPed with Na,K-ATPase significantly increased in bEND5 cells that were induced with fenestrae. N= 3; error bars denote ± SEM, ** $P < 0.001$.
C. Na,K-ATPase co-IPed with fodrin exclusively in bEND5 cells that were induced with fenestrae. N= 3; error bars denote ± SEM, * $P < 0.01$.

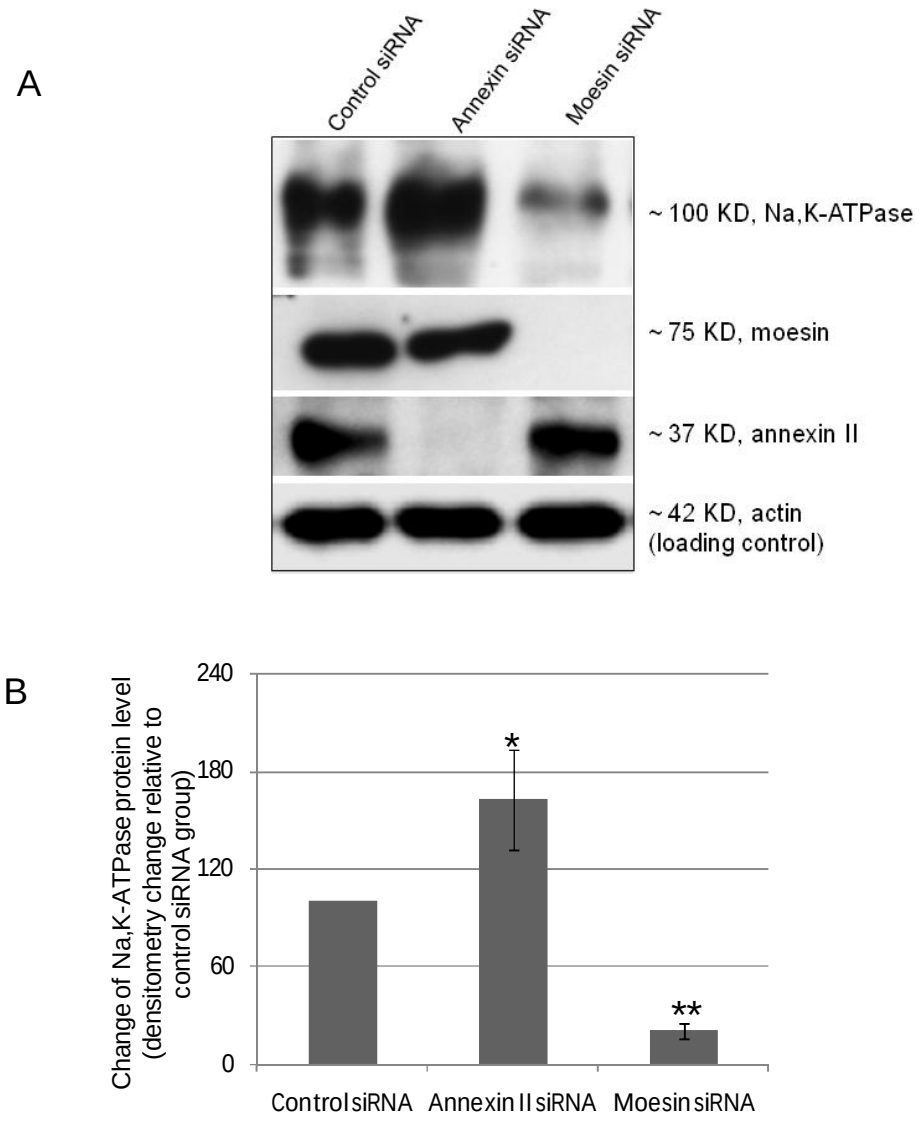

Fig. 5-16 Na,K-ATPase protein level was affected by moesin and annexin II.

A. Moesin knockdown decreased Na,K-ATPase expression while annexin II knockdown upregulated Na,K-ATPse protein level in bEND5 cells.
B. Densitometry quantification of Na,K-ATPase protein change in annexin II or moesin depleted bEND5 cells. N = 3, error bars denotes ± SEM. * $P < 0.01$; ** $P < 0.001$.

5.7 Na,K-ATPase regulates fenestra formation

5.7.1 Ouabain induced fenestra formation in bEND5 cells

Ouabain is a potent Na,K-ATPase inhibitor, and has binding sites on the extracellular portion of Na,K-α (Fig. 5-12B). We probed the effect of ouabain on fenestra formation compared to VEGF, which is a weak but reproducible inducer of fenestrae in bEND5 cells (Esser, 1998; Ioannidou, PhD Thesis, 2005). Short treatment for 3 hours with ouabain at different concentrations didn't reveal any perceivable difference in bEND5 cells (data not shown), but longer incubation for 24 hours with ouabain induced fenestra formation, characterised by distinct sieve plates delineated by microtubules as shown with immunofluorescence staining (Fig. 5-17).

The extent of PV-1 marked sieve plates formation and local actin disruption all showed a dose-dependence to ouabain concentration. The induction of fenestrae was further confirmed using TEM (Fig. 5-18). At a concentration of 200 µM, ouabain was able to induce fenestra formation to a similar extent to that caused by VEGF (75 ng/ml) incubation for 24 hours.

5.7.2 Ouabain induced vessel fenestration *in vivo*

The involvement of Na,K-ATPase in fenestra induction in bEND5 cells suggests this plasma membrane protein may be a critical regulator of the fenestra biogenesis pathway. We sought confirmation of these findings in a more relevant setting *in vivo*.

Roberts and Palade demonstrated that intradermal or topical application of VEGF could induce vessel fenestration within ten minutes *in vivo* (1995 and 1997). These findings suggest that VEGF is able to trigger a reorganisation of existing endothelial cell machinery sufficient to drive large scale fenestral pore formation. We hypothesized that the Na,K-ATPase may be a regulator downstream of VEGF signalling and tested this concept in the rodent skin and cremaster muscle settings, as described by Roberts and Palade (1995 and 1997).

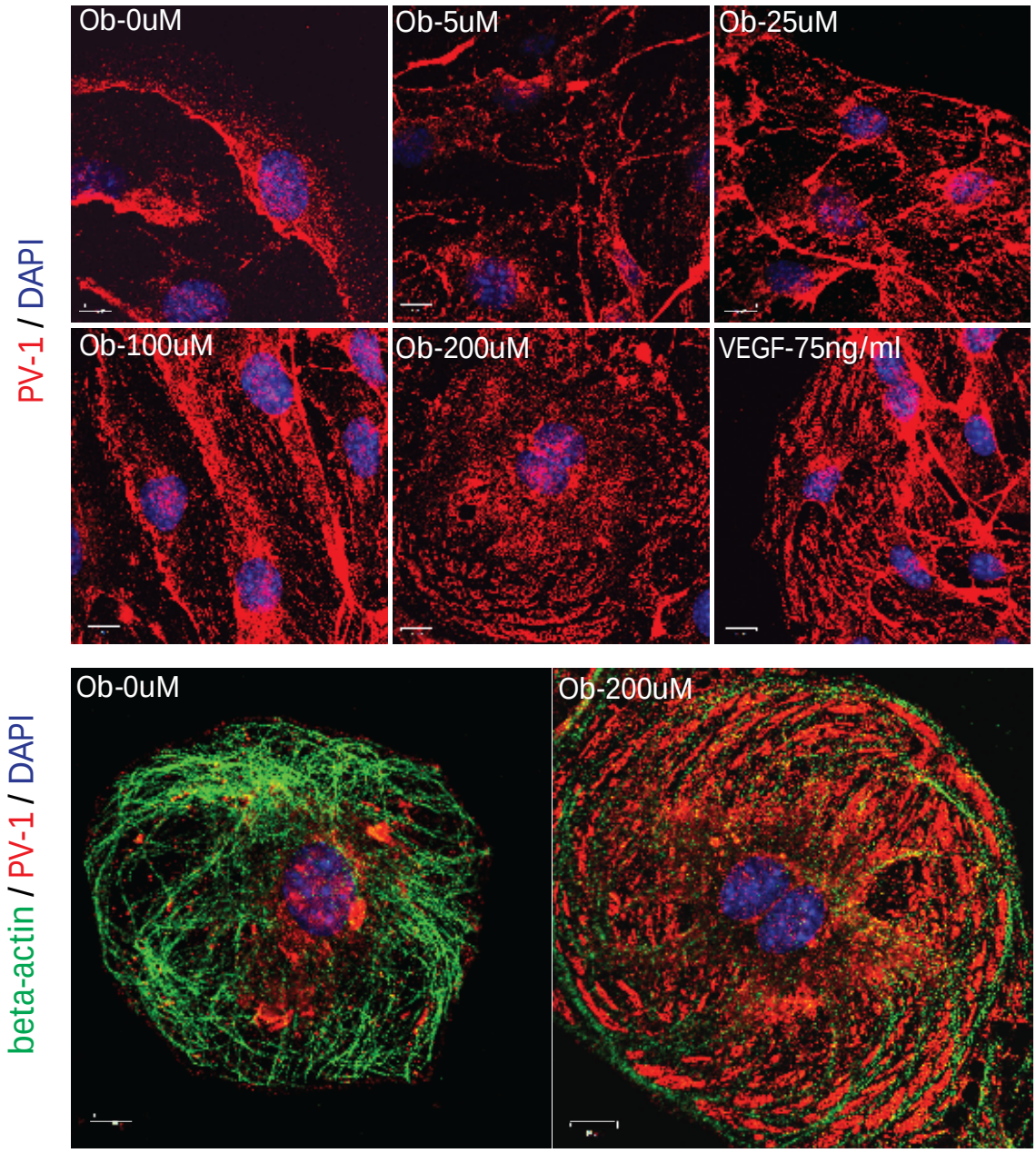

Fig. 5-17 Ouabain induced fenestra formation in bEND5 cells. Ouabain or VEGF was incubated with bEND5 cells for 24 hours. Ob, ouabain; scale bar, 10 μm.

A. The reorganisation of PV-1 into distinct pattern of sieve plates showed dose dependence to ouabain incubation, and the effect induced by Ouabain at 200 μM displayed similar level to that was induced by VEGF at 75 ng/ml, which was used as a positive control in the assay.

B. PV-1 marked fenestral sieve plates induced by ouabain at 200 μM were delineated by microtubules.

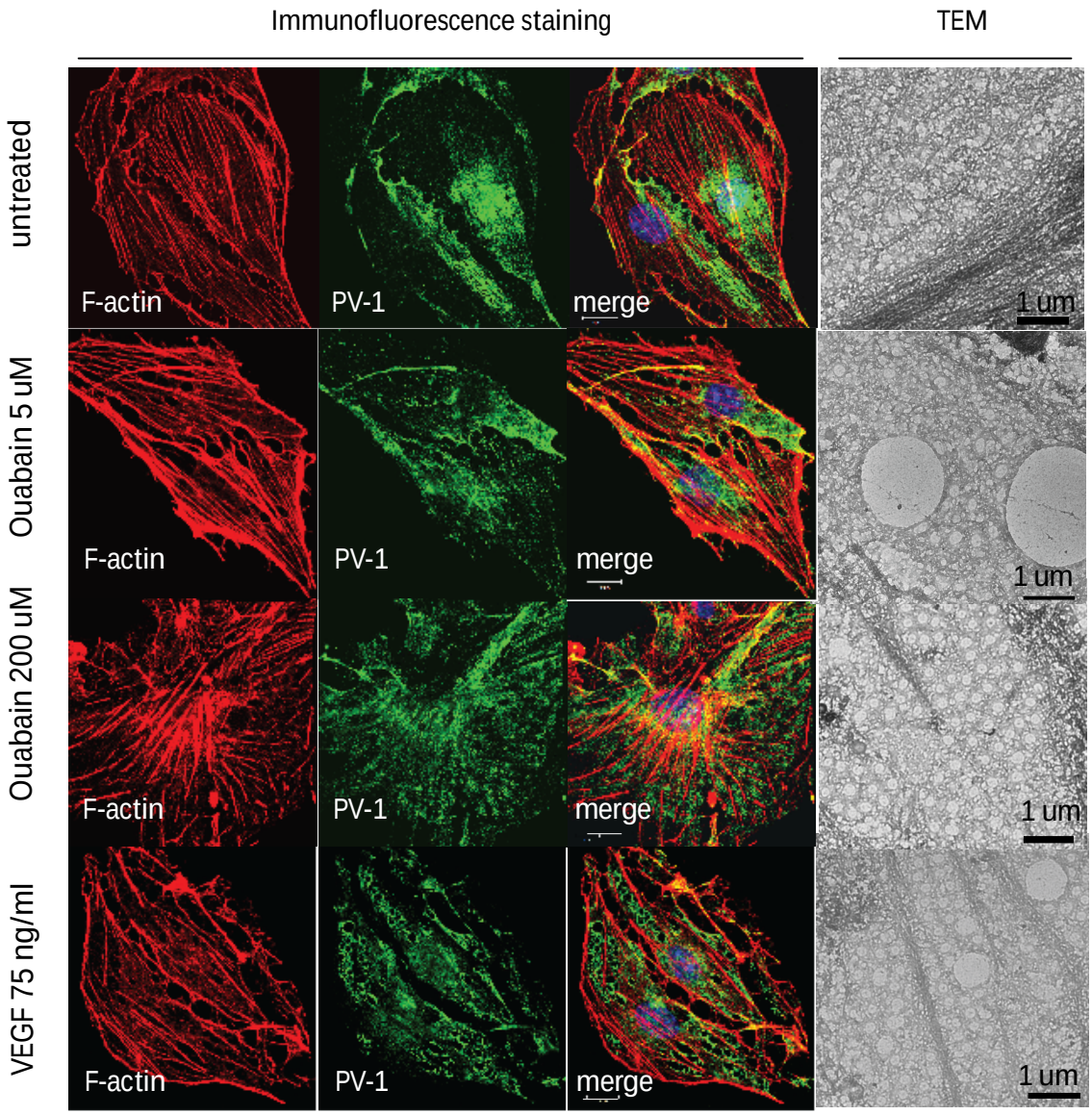

Fig. 5-18 Local actin disruption occured with ouabain-induced fenestra formation. Local actin disruption and PV-1 marked fenestral sieve plates induced by ouabain were dose dependent. The induction of fenestral pores was further confirmed by wholemount TEM. Scale bar in LM, 10 μm; scale bar in TEM, 1 μm.

5.7.2.1 Ouabain increased fluorescence leakage both in a mouse skin model and in a rat cremaster model

We first examined a mouse skin model to test whether ouabain could induce changes in vascular permeability. Although fenestrae display a diameter of around 60 nm (Bennett, 1959), the radial fibrils of the diaphragm further divide the fenestra into small pores with an arc length of about 5 nm (Bearer, 1985). Therefore we used a 3kDa fixable FITC-dextran with a mean diameter of 2.4 nm to determine if oubain induced vascular permeability, a potential indicator of fenestra formation (Tripathi, 1977). Under epifluoresence microscopy, there was a slight fluorescence increase in PBS-injected skin samples compared to samples without injection - most likely due to the injection procedure itself. Significant fluorescence leakage was observed in samples treated for 10 minutes with VEGF (20 ng in 30 µl) (Roberts, 1995), or ouabain at concentrations of 200 µM and 1 mM (Fig. 5-19). To be consistent with the concentration used with bEND5 cells, we chose the concentration of ouabain at 200 µM for subsequent experiments (Fig. 5-19). However, due to the sparse capillaries in skin tissue and the interference of follicles, it was difficult to locate the affected capillaries by fluorescence or EM. We therefore turned to the rat cremaster model described in Roberts' publications (1995 and 1997) for further investigation.

As seen with epifluoresence microscopy, topical application of ouabain or VEGF resulted in increased fluorescence leakage in the cremaster muscle sample (Fig. 5-19), especially in areas rich in capillaries, which were identified based on their small size and parallel pattern relative to muscle fibers. We further studied the cause of fluorescence leakage using ultrastructual analysis.

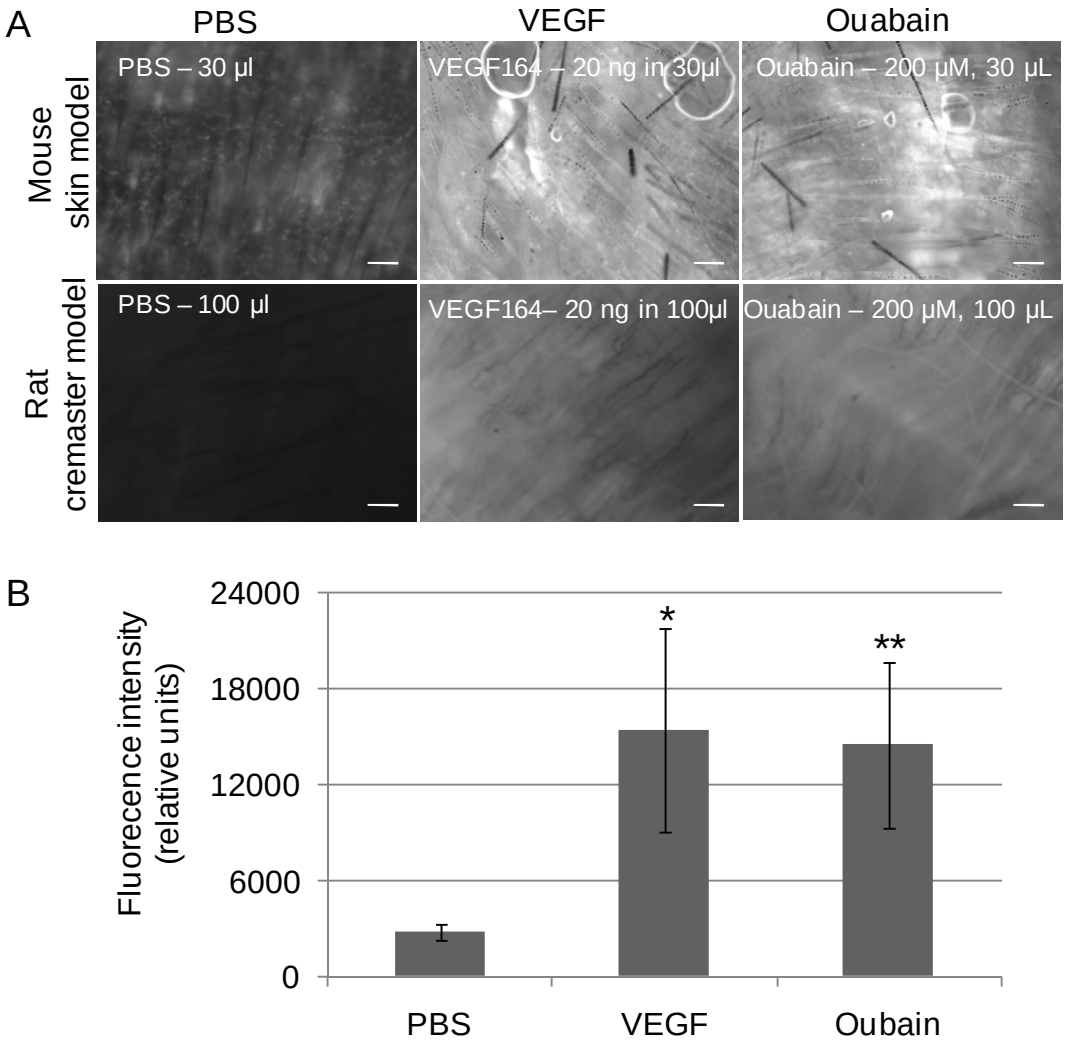

Fig. 5-19 Ouabain induced fluorescence leakage *in vivo*.

A. For the mouse skin model, 30 µl oPBS, VEGF164 (20 ng in 30 µl) or ouabain (30 µl at 200 µM) was injected subcutaneously into the mouse abdomen. For the rat cremaster model, 100 µl of PBS, VEGF164 (75 ng in 100 µl) or ouabain (100 µl at 200 µM) was applied topically onto the surgically exposed rat cremaster muscle. Animals were sacrificed 10 minutes later. Fixable FITC-Dextran (3 kDa) was used to track vessel leakage. Scale bar, 20 µm.
B. Quantification of vascular leakage indicated by fluorescence intensisty. $N \geq 3$ for each group.Error bars denote ±SEM.* $P < 0.05$; ** $P < 0.01$

5.7.2.2 Ouabain induced endothelial fenestrae in the rat cremaster muscle vasculature

Guided by the FITC-dextran tracer, the region with the strongest fluorescence leakage was cut out and processed, then super-thin sections were cut and stained for TEM imaging. Electron microscopy revealed that the microvasculature in the cremaster muscle contained a continuous endothelium that rarely, if ever, was fenestrated (Fig. 5-20). An initial striking effect of just 10 minutes of ouabain or VEGF exposure was the resulting attenuation of the capillary vessel walls (Fig. 5-20). Consistent with the studies by Roberts (1995), topical application of VEGF caused endothelium fenestration after ten minutes (Fig. 5-21A) and breakdown of intercellular junctions, as indicated by a platelet trapped by the basement membrane (Fig. 5-21B). Remarkably, topical application of ouabain for 10 minutes also induced fenestra biogenesis in muscle capillaries (Fig. 5-22, A and B). These newly formed fenestrae were around 60 nm in diameter and typically had a diaphragm. In appropriate sections, the characteristic central knob of the diaphragm was readily distinguishable (Fig. 5-22, arrows). Occasionally, transendothelial channels with diaphragms on the luminal and abluminal sides of the endothelium was also found (Fig. 5-22B, asterisk). We also observed opening of intercellular junctions in ouabain-treated samples (Fig. 5-22C, long arrow). Similar findings were also observed with another cardiac glycoside, digoxin, which is also used to inhibit the Na,K-ATPase in cardiovascular disease patients, strongly supporting the role of this ion transporter in fenestra biogenesis (data not shown).

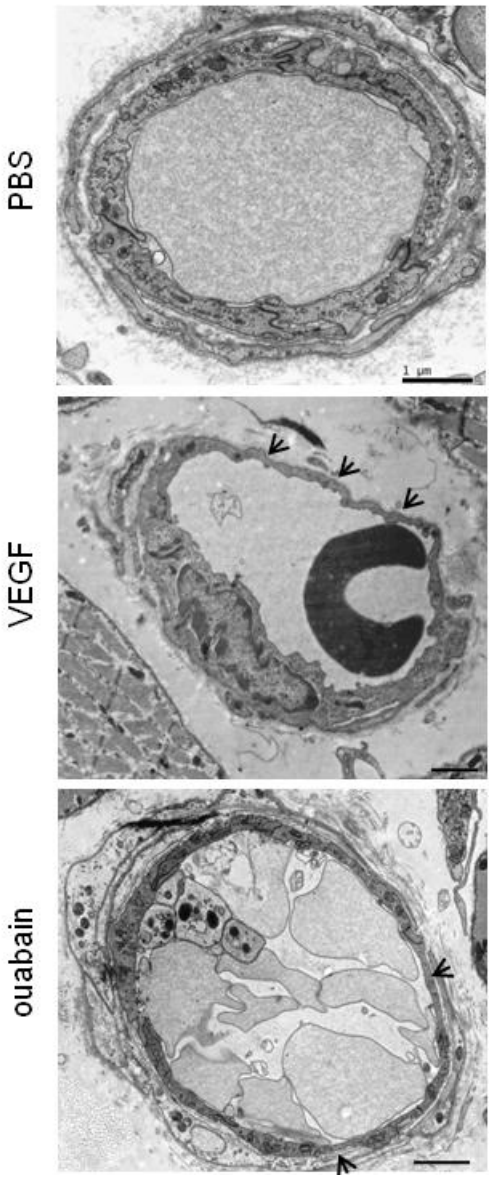

Fig. 5-20 Ouabain and VEGF caused attenuation of the vessel wall.
Section TEM images of vessels in cremaster samples treated with PBS (100 µl), VEGF (75 ng in 100 µl) or ouabain (100 µl at 200 µM) for 10 minutes. Attenuated vessel was was observed in VEGF or ouabain treated samples (short arrows).
Scale bar, 1 µm

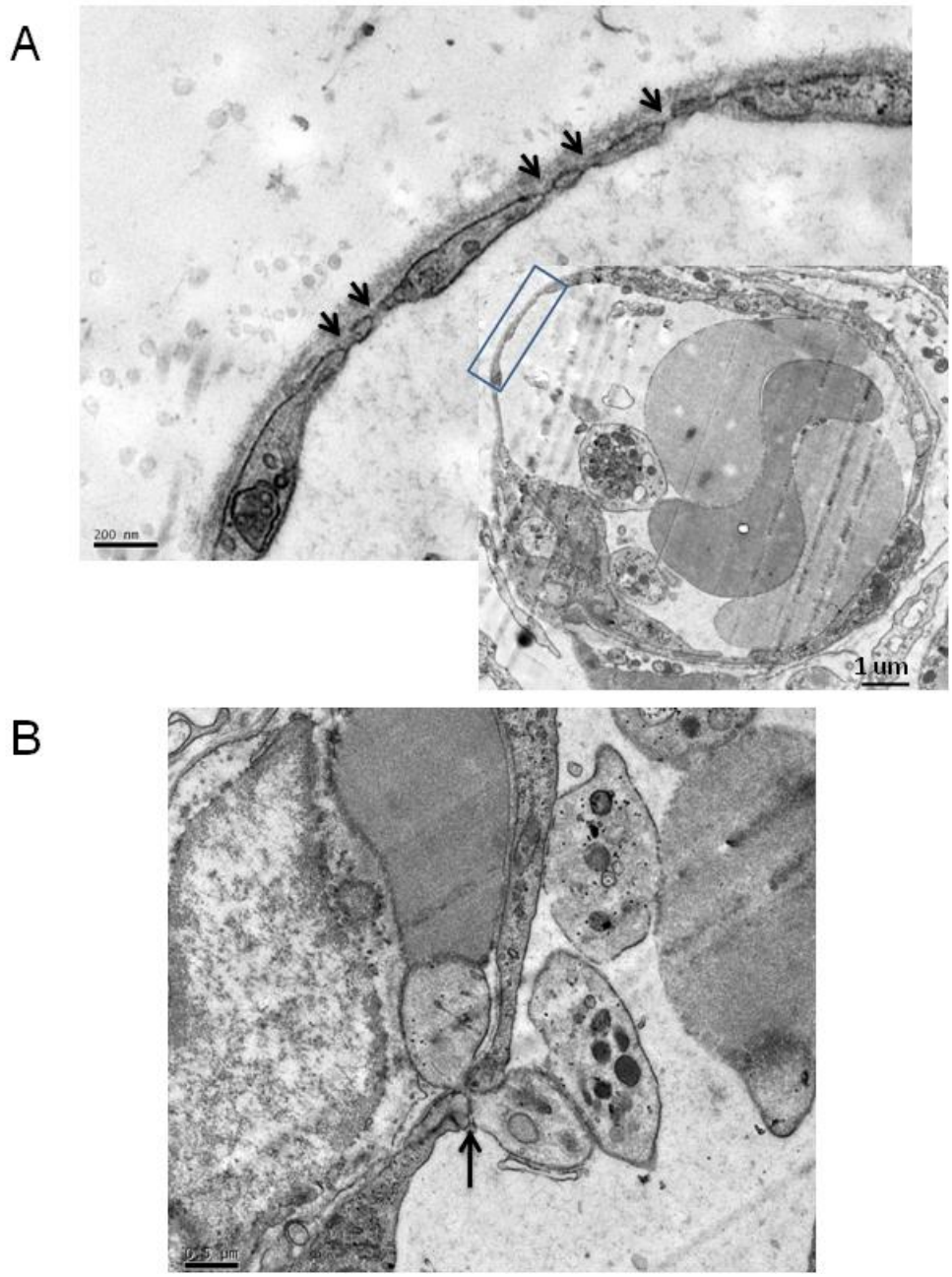

Fig. 5-21 Validation of VEGF inducing vessel fenestration *in vivo.*

VEGF (75 ng in 100 µl) was topically applied to rat cremaster tissue for 10 minutes.

A. A fenestrated endothelium. Arrows, fenestrae.
B. An endothelial cell with a platelet going through an intercellular junction opening, long arrow.

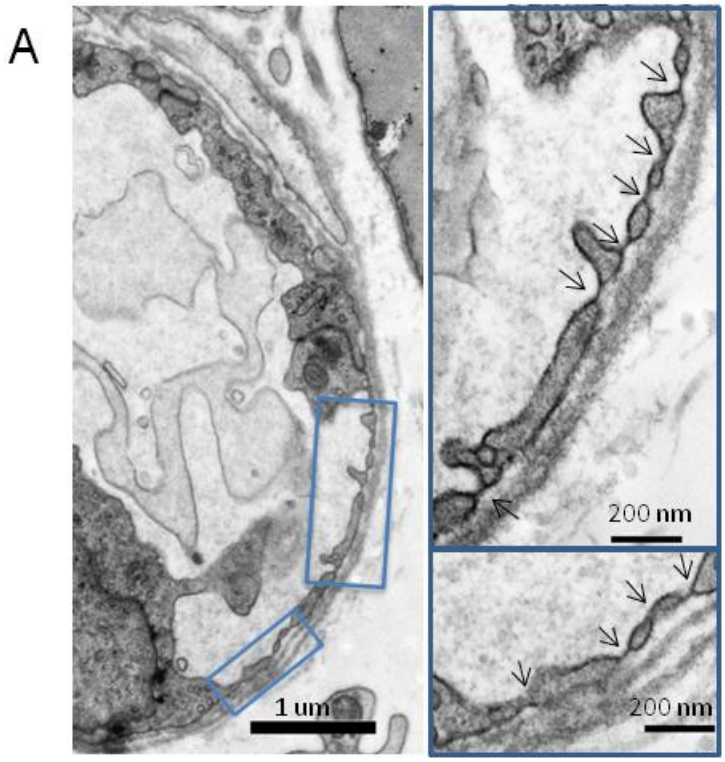
A
1 um
200 nm
200 nm

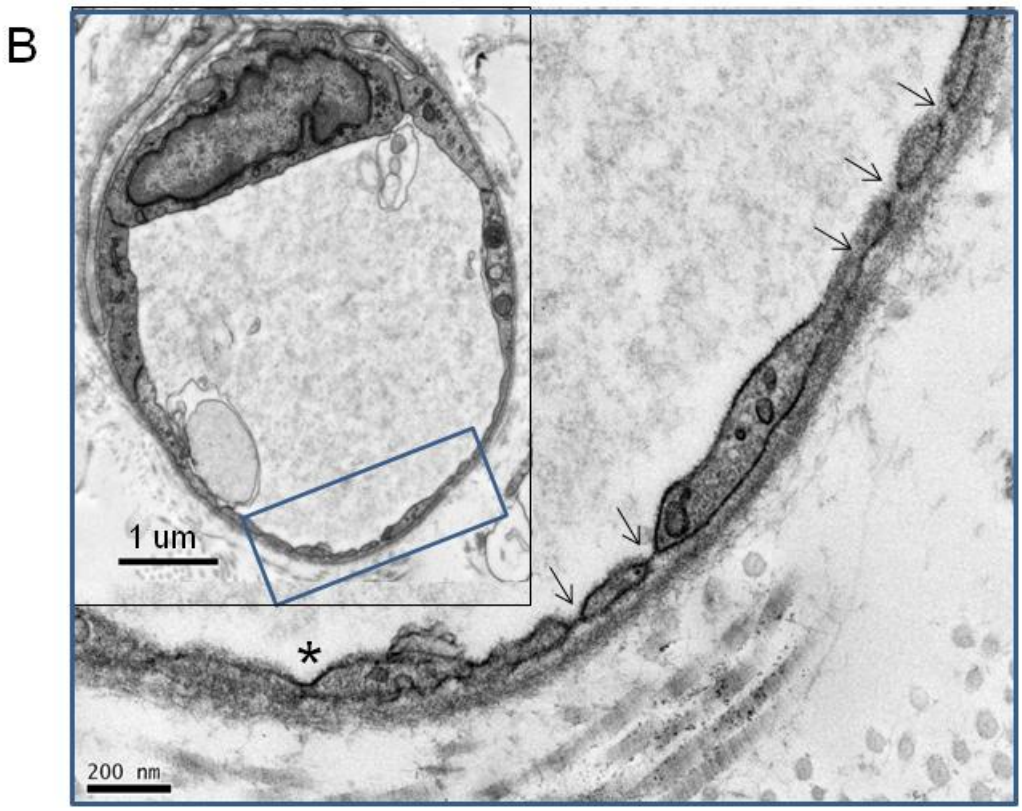
B
1 um
*
200 nm

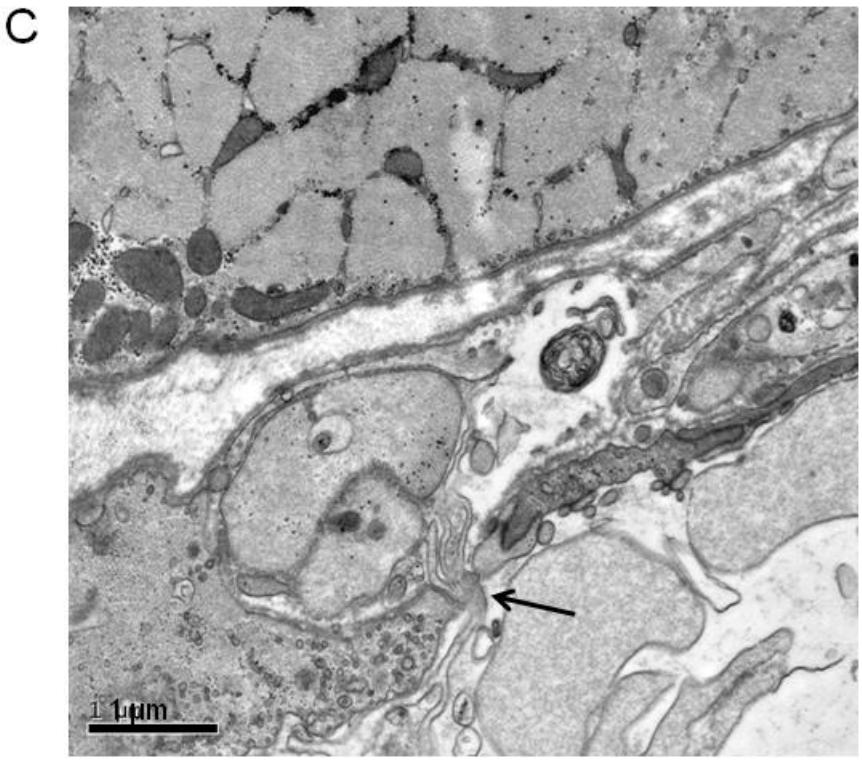

Fig. 5-22 Ouabain induced vessel fenestration *in vivo.*
100 µl of ouabain at 200 µM were topically applied to rat cremaster tissue for 10 minutes.

A. An endothelial cell with extensive fenestration. Arrows, fenestrae.
B. Another endothelial cell with fenestrae (arrows) and a transendothelial channel (asterisk).
C. An endothelial cell with an intercellular junction opening (long arrow).

5.7.2.3 Quantification of ouabain-induced fenestra formation in the rat cremaster muscle

To further detail the potency of ouabain-induced endothelial fenestration, we quantified ouabain-induced fenestration frequency and extent in comparison with VEGF-induced fenestration. After 10 minutes exposure, it was observed that almost all vessel changes occurred in the most superficial layer of the cremaster tissue, which received the maximum exposure from the topical administration. Therefore, I quantified the vessels in that layer of cremaster tissue, as indicated in Fig. 5-23. In both VEGF- and ouabain treated samples, most of the vessels in the superficial layer appeared attenuated, though ouabain treatment caused significantly more vessels to display endothelial fenestration (Fig. 5-24A). The extent of endothelial fenestration, either counted as the fenestra number per fenestrated vasculature (Fig. 5-24B) or measured by percentage of fenestrated vessel length (Fig. 5-24C), was similar between ouabain and VEGF treatment.

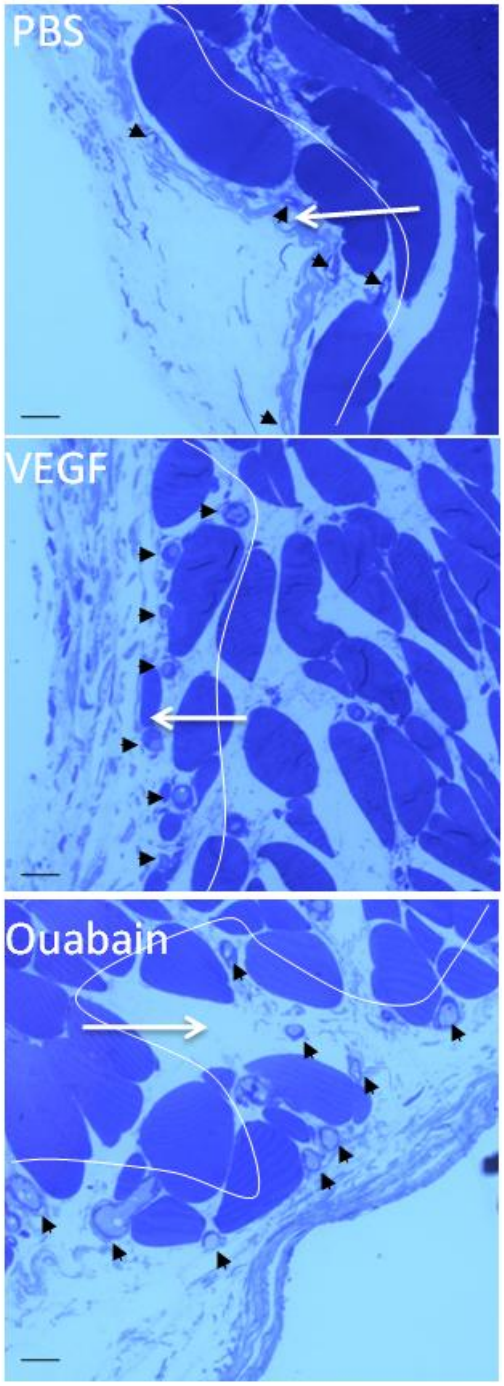

Fig. 5-23 Localisation of attenuated vessels in cremaster tissue.
Semi-thin sections were stained with a 1% toluidine blue/borax mixture at 60˚C. Attenuated vessels were mostly located in the superficial layer of cremaster tissue. The superfacial layer was indicated by the white curving line in the direction of the white arrow, and vessels in the most superficial area were indicated by black arrow heads. Scale bar, 10 μm.

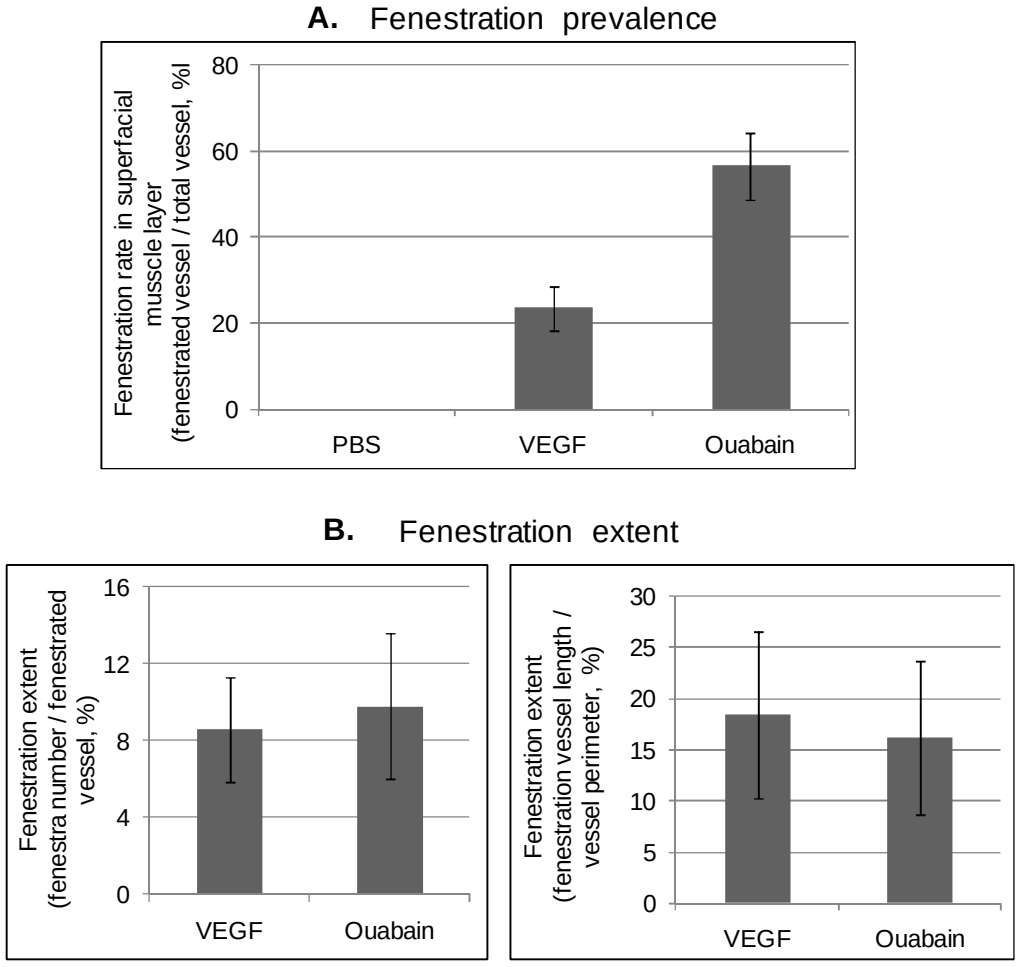

Fig. 5-24 Quantification of vessel fenestration in rat cremaster tissue.

A. The prevalence of vessel fenestration was measured by the percentage of fenestrated vessel in the superfacial layer of cremaster tissue. Ouabain caused more vessels being fenestrated than VEGF did, whilst there was no fenestrated vessel in PBS treated samples.
B. Fenestration extent was indicated by fenestra number per vessel (B left), or by percentage of fenestrated vessel length (B right). Ouabain and VEGF caused similar degree of fenestration.

The result is the representative of 3 independent experiments. $N \geq 20$ (about 20 to 30 of vessels were quantified for each treatment.), error bars denote ±SEM.

5.8 PI3K signalling is an important pathway involved in fenestra formation

Oubain inhibition can recruit, assemble and activate the lipid kinase phosphatidylinositol 3-kinase (PI3K) (Liu, 2007; Zhou, 2001). PI3K catalyzes the production of phosphatidylinositol (PtdIns), including PtdIns(3,4)P2, PtdIns(3,5)P2, and PtdIns(3,4,5)P3, which are linked to an extraordinarily diverse group of cellular functions, including cell survival pathways, intracellular trafficking, and cytoskeletal rearrangements (Cantley, 2002). Blocking PI3K activity with wortmannin at 1 μM or LY294002 at 10 μM completely inhibited latrunculun A- or ouabain-induced fenestra formation (Fig.5-25). On the contrary, another pharmacological inhibitor of Rho family small GTPases, Rho, Rac, and Cdc42 (ROCK), which control the assembly and disassembly of the actin cytoskeleton in response to extracellular signals(Kaibuchi, 1999; Jaffe and Hall, 2005), did not compromise fenestra formation triggered by latrunculin A or ouabain. (Fig. 5-25).

5.8.1 Dynamic change of PI3Ks during fenestra induction

The PI3K isoforms are divided into three classes, PI3K I, II and III. In cardiac myocytes, ouabain activates class IA PI3K but not IB (Liu, 2007). IA PI3K was also reported to associate with Na,K-ATPase to regulate cell motility in MDCK cells (Barwe, 2005). Class IA PI3K is composed of a p110 regulatory subunit and a p85 catalytic subunit (Carpenter, 1990). Western analysis indicated that p110α was the major catalytic subunit in bEND5 PI3K, and the phosphorylation level of the regulatory subunit, p85, changed greatly before and after fenestra formation (Fig. 5-26A). A more-detailed study on the time course of fenestra induction showed that p85 underwent a dramatic change in phosphorylation status upon latrunculin A addition. P85 was greatly phosphorylated at the beginning of the induction course, followed by a dramatic dephosphorylation from 30 minutes of induction, presumably during the reorganisation process for fenestra formation. The phosphorylation level of p85 increased slightly toward the end of the induction, when the fenestral structure was stabilised. A 30-minutes washout with PBS at the end of the incubatin restored the phosphorylation level

of p85 to the base level before the addition of latrunculin A (Fig. 5-26B). The dynamic change in p85 phosphorylation during the fenestra induction implied the active participation of PI3K signalling in fenestra formation.

5.8.2 Na,K-α associates with the p85 regulatory subunit of PI3K

It has been reported that Na,K-ATPase activates PI3K through the association between Na,K-α and p85 (Barwe, 2005), which in return regulates the trafficking of Na,K-ATPase (Yudowski, 2000). Immunoprecipitation analysis revealed that Na,K-α coimmunoprecipitated with p85 in bEND5 cells. However, there was a significant increase in the p85 levels associated with Na,K-α in bEND5 cells that are fenestrated by either latrunculin A or ouabain (Fig. 5-27). These results suggest the close association between PI3K p85 and Na,K-ATPase may play an important role in the process of fenestra formation.

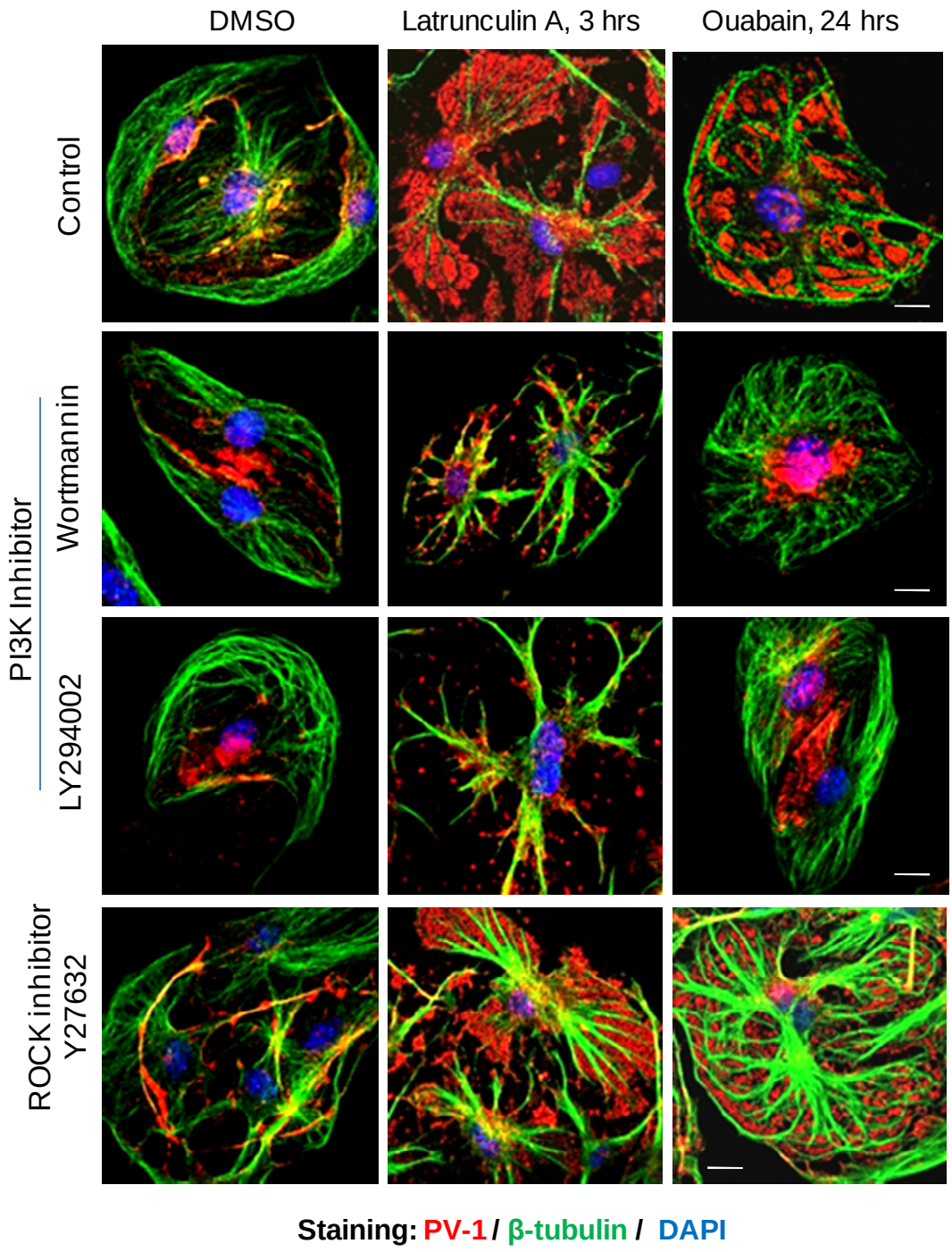

Fig. 5-25 Exploration of signalling pathways involved in fenestra formation. Microtubule delineated, PV-1 marked fenestral sieve plates were induced in bEND5 cells by latrunculin A (1.25 μM) for 3 hours, or by ouabain (200 μM) for 24 hours (top panel). Co-treatment with PI3K inhibitor, wortmannin (1 μM) or LY294002 (10 μM) inhibited fenestra formation induced by latrunculin A or ouabain (middle panels). Co-treatment with ROCK inhibitor, Y27632 (10 μM) didn't compromise fenestra formation induced by latrunculin A or ouabain. Scale bar, 10 μm.

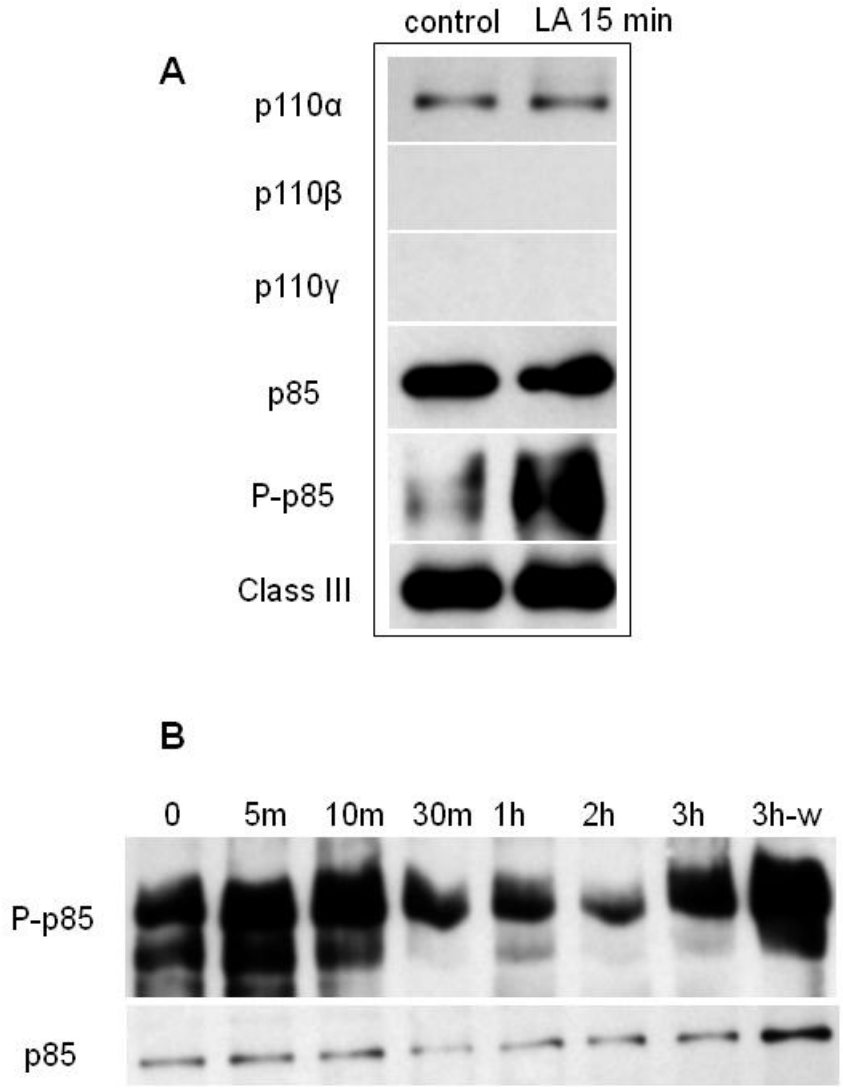

Fig. 5-26 The PI3K subunit p85 changed phosphorylation status during fenestra formation.

Latrunculin A (LA) induced dramatic changes in p85 phosphorylation in bEND5 cells.

A. Phosphorylated p85, but not other components of PI3Ks, increased greatly when latrunculin A was added to bEND5 cells.
B. Time course of p85 phosphorylation during fenestra induction triggered by latrunculin A at 1.25 μM.

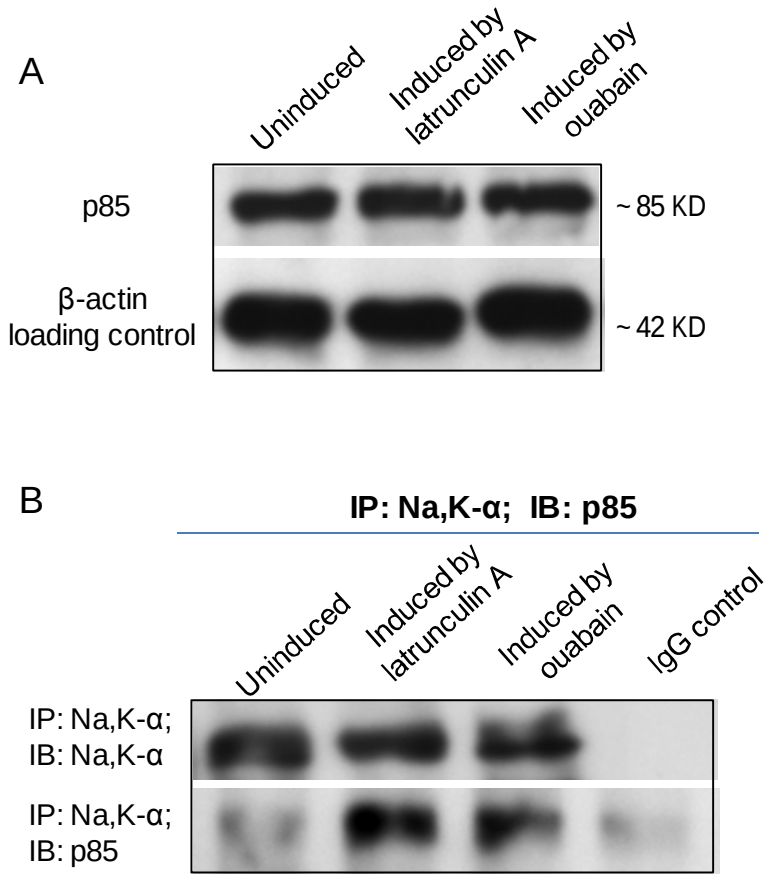

Fig. 5-27 PI3K subunit p85 was associated with Na,K-α in fenestral sieve plates. Protein level of PI3K subunit p85 didn't change before and after fenestra induction triggered by latrunculin A (1.25 μM) for 3 hours or by ouabain (200 μM) fo24 hours (A). However, p85 only Co-IPed with Na,K-α in bEND5 cells that were treated by latrunculin A or ouabain for fenestra induction (B).
IP, immunoprecipitation; IB, immunoblot.

5.9 Discussion

Although an underlying cytoskeleton responsible for subcellular organisation of fenestrae has long been speculated to exist, the tools have not existed to probe the nature of this cyto-architecture. What started as the development of an *in vitro* fenestra biogenesis model and proteomic analysis, has now evolved to the identification of molecular interactions linking moesin, short actin filaments (presumably protofilaments), fodrin and plasma membrane proteins PV-1 and the Na,K-ATPase to the fenestra and sieve plate. Interference with these interactions using chemical inhibitors or siRNA strongly supports the importance of these interactions in fenestra formation and provides a conceptual framework for future studies.

In erythrocytes, a spectrin-based membrane skeleton supports cell shape, maintains cell membrane integrity, and facilitates mechanical properties of a cell membrane that encounters much stress within the blood stream (Delaunay, 2006; Perrotta, 2008). Mutations in spectrins or protein 4.1 lead to hereditary elliptocytosis, characterised by abnormal shape, increased membrane fragility and reduced deformability of erythrocytes (Liu, 1990; Whitfield, 1991). Similarly, in non-erythroid cells the fodrin-based submembrane skeleton is involved in cell architecture, morphology, and plasma membrane stability (Goodman, 1981; Wu, 2001). For example, in epithelial cells, depletion of β2-spectrin by siRNA results in a failure to form a new lateral membrane in interphase and in mitotic cells (Kizhatil, 2007).

The identification of the fodrin membrane cytoskeleton as a major feature of fenestra sieve plate formation and architecture, in retrospect, should come as no surprise. Fenestrated endothelial cells have highly attenuated regions of the cell between the microtubule, intermediate filament and organelles “struts”. These sieve plate regions are thin and presumably fragile, being perforataed with hundreds of pores. The presence of a submembrane cytoskeleton would provide both structural stability to the

plasma membrane, and an underlying architecture to enable the remarkable organisation of pores both in terms of inter-pore distances and their alignment in linear arrays.

The Na,K-ATPase is best appreciated for its role in the regulation of ion homeostasis in mammalian cells, though it has long been reported to be involved in signalling linked to reorganisation of specialized cell membrane domains. During the development of polarity in MDCK cells, the cellular change in fodrin expression coincides temporally and spatially with the development of the polarized distribution of the Na,K-ATPase (Nelson, 1986). Nelson *et al* further showed that the fodrin membrane skeleton and Na,K-ATPase are in the same protein complex in polarized MDCK cells (1987). Our results showed that the interaction between Na,K-ATPase and the fodrin membrane skeleton is specific to bEND5 cells that are fenestrated, but not in normal bEND5 cells. The ability of ouabain to induce breakdown of tight junctions has been well documented in epithelial cells (Rajasekaran, 2005). In human RPE cells, Na,K-ATPase inhibition by ouabain results in decreased tight junction membrane contact points and increased tight junction permeability (Rajasekaran, 2003). We occasionally observed intercellular junction openings in ouabain-treated rat cremaster tissue, though the increased vessel permeability was largely due to the significant induction of fenestrae in vascular endothelium. Our study is the first to report the regulatory function of Na,K-ATPase in vascular fenestration.

Though still preliminary, our results do suggest that it is the regulation of PI3K signalling that may be the critical role played by the Na,K-ATPase. Dopamine-mediated endocytosis and inhibition of Na,K-ATPase involve activation of PI3K by Na,K-ATPase binding to p85 (Yudowski, 2000). In Moloney sarcoma virustransformed MDCK cells, the association of Na,K-α with p85 was involved in the activation of PI3K (Barwe, 2005). We also observed increased association between Na,K-α and p85 in fenestrated bEND5 cells. Independent of the precise mechanistic role played by the ion transporter, the results with the cardiac glycoside ouabain lend the strongest support to a novel, central regulatory role for the Na,K-ATPase in fenestra biogenesis.

Chapter 6

Moesin-, annexin II- and Na,K-ATPase-regulated cytoskeleton remodelling plays a central role in fenestra formation

-general discussion and future perspectives

Abbreviations

ABPs	actin binding proteins
AMD	age-related macular degeneration
BSA	bovine serum albumin
DMEM	Dulbecco's modified Eagle medium
ER	endoplasmic reticulum
ERGIC	ER-Golgi intermediate compartment
ERM	ezrin, radixin, and moesin
FAK	focal adhesion-associated kinase
FACR	fenestrae-associated cytoskeleton ring
GEnC	glomerular endothelial cell
GFP	green fluorescent protein
GFR	glomerular filtration rate
HA	hemagglutinin
HSPG	heparan sulfate proteoglycans
HuVEC	human umbilical vein endothelial cells
LM-EM	light microscopy-electron microscopy
LSEC	liver sinusoidal endothelial cells
MβCD	methyl-β-cyclodextrin
MDCK	Madin-Darby canine kidney
MT	middle T antigen
NPC	nuclear pore complex
PBS	phosphate-buffered saline
PDK1	phosphoinositide-dependent protein kinase-1
PFA	paraformaldehyde
PI3K	phosphatidylinositol 3-kinase
PIP2	phosphatidylinositol 4,5 biphosphate
PMA	phorbol myristate acetate

PtdIns	phosphatidylinositol
PV-1	plasmalemmal vesicle–associated protein–1
RA	retinoic acid
RPE	retinal pigment epithelium
SNARE	soluble N-ethylmaleimide sensitive fusion protein attachment protein receptor
TGF-β	transforming growth factor β
VEGF	vascular endothelial growth factor
VVOs	vesiculo-vacuolar organelles

Chapter 6 Moesin-, annexin II- and Na,K-ATPase-regulated cytoskeleton remodelling plays a central role in fenestra formation -general discussion and future perspectives

The formation of fenestrated endothelium is accompanied by extensive changes in the structure and properties of the plasma membrane. The most striking changes are the cellular reorganization leading to an extremely attenuated cell periphery and the rapid and orderly formation of numerous transcellular pores. The processes by which these changes occur have remained largely undefined.

Our efforts to better understand the mechanisms of fenestra formation led us to the actin cytoskeleton. Actin reorganization is essential in many dynamic cellular processes, including the formation of filopodia and lamellipodia in cell movement (Theriot, 1991), membrane trafficking (Kakosonen, 2000, Smythe, 2006; Egea, 2006), cell adhesion (Reddig, 2005; Gates, 2005; Delon, 2007), and neurite extension (Govind, 2001; Ledesma, 2003). Given the widespread role of actin in cellular dynamics, it would seem plausible that it would be an important part of cell shape changes, sub-cellular reorganisation and membrane fusion during fenestra formation. However, the fact that fenestra formation in our model system is triggered by disruption of the actin cytoskeleton with disrupting agents such as latrunculin A initially led us away from proposing an active role for actin.

Actin-disrupting agents have been used extensively in studies examining the potential involvement of actin cytoskeleton organization or actin dynamics in various biological functions. Although the severity of the alterations in actin cytoskeleton and cell morphology caused by these agents depends on the cell type, the most common change is cell edge retraction accompanied by the formation of radial tubular protrusions

(Lázaro-Diéguez, 2007). This phenomenon, termed arborisation in cell shape, is a natural change due to the elastic energetics of shape change when adhesion points and the actin cytoskeleton are disrupted (Bar-ziv, 1999) (Fig. 6-1A).

In our *in vitro* fenestra biogenesis model, bEND5 cells displayed the reported changes in cell shape, namely periphery retraction and arborisation, following treatment with latrunculin A. (Fig. 6-1B). Therefore, we initially concluded that the removal of actin microfilaments led to shape changes which could support the further formation of fenestrae. Also, several studies have shown that the disassembly of the actin cytoskeleton which is essential prior to membrane fusion, is a major aspect of fenestra formation (Aunis, 1988; Muallem, 1995; Braet, 1996). Furthermore, fenestral sieve plates are extremely attenuated, at 30-40 nm cellular thickness, requiring removal of nearly all organelles and classical cytoskeletal filaments. These findings all appeared to point to the importance of removing filamentous actin to enable fenestra formation.

However, the high degree of cellular organisation that was observed in fenestrated endothelium still suggested the involvement of some type of cytoskeletal element. For example, sieve plates form between microtubular protrusions. Importantly, despite the apparent lack of cytoplasmic support elements, sieve plates are perforated with fenestrae that are aligned in highly ordered arrays (Fig. 6-2). A potential solution to this paradox following our decision is to revisit the role of the actin cytoskeleton in fenestra formation.

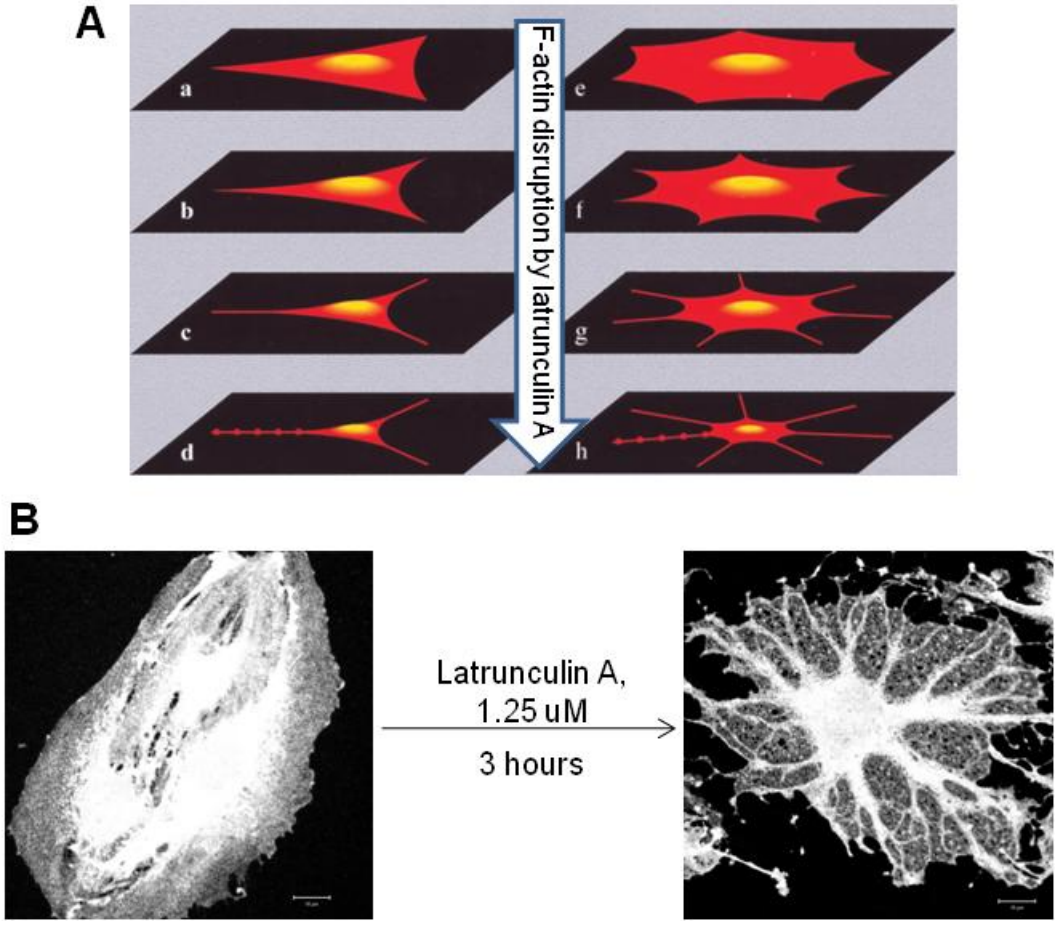

Fig. 6-1 Cell arborisation caused by collapse of cortical actin.

A. Shapes of cells calculated from the theory as a function of the changing ratio between the balanced surface tension and effective elastic line tension at their edges. Polygonal cell with n adhesion points (n=3 for a-d, n=7 for e-h) went arborisation and pearling (d, h) when cells were treated with latrinculin A. (Adapted from Bar-Ziv, 1999.)
B. CD31 staining showed a bEND5 cell changed into arborised shape with latrunculin A treatment, but maintained an extremely attenuated cell region between the thick arbors. Scale bar, 10 μm.

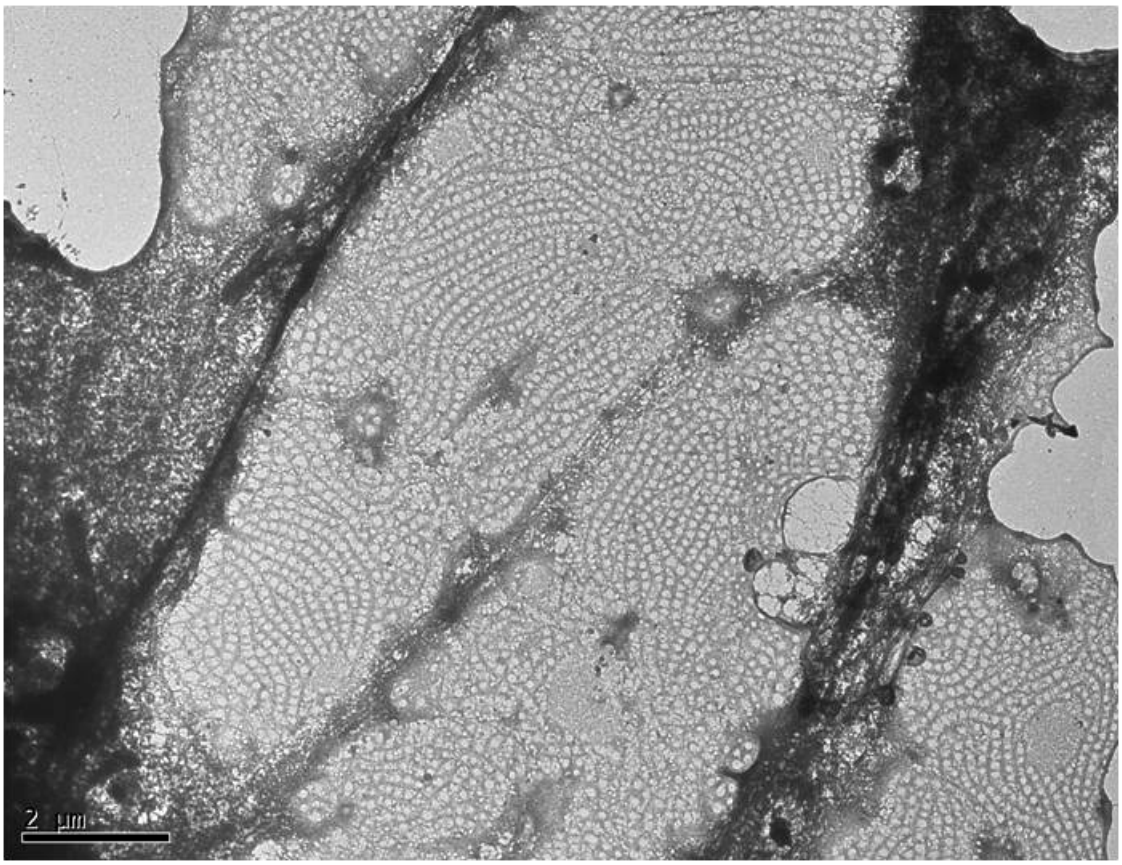

Fig. 6-2 Highly ordered organisation of fenestrae in the sieve plates.
Wholemount TEM image of a fenestrated bEND5 cell revealed the highly ordered linear array of fenestral organisation.
Scale bar, 2 µm.

6.1 Moesin is essential for fenestra formation

My thesis began with trying to resolve the observations that actin filament disassembly triggers fenestra formation, yet proteomic analysis suggested an enrichment of actin binding proteins associated with fenestrated plasma membranes. Efforts were initially focused on the cytoskeletal adapter protein, moesin. The importance of moesin in fenestra formation was clearly demonstrated in the moesin-depleted bEND5 cells, which displayed lack of fenestral pores and compromised sieve plate formation. Moesin's role in fenestra formation was also supported by results from use of the dominant-negative N-moesin-GFP. As described in chapter 4, although overexpression of the moesin lacking the F-actin binding C-terminal still led to the formation of what we have termed a pseudo-sieve-plate at the cell periphery, there're no fenestral pores in those distinct microdomains. Immunofluorescence analysis also revealed the absence of F-actin, fodrin and Na,K-ATPase in those pseudo-sieve-plates (Fig. 4-8; Fig. 6-3). These data support a role for moesin in the cytoskeleton assembly required for fenestra formation.

Its precise role is not known, though the well documented role of moesin in actin assembly may provide insights in this regard. Vaheri *et al* first proposed that, besides their commonly recognised linker protein function, ERM proteins may also play a more general role in *de novo* actin assembly on membrane surface (1997). Mackay et al showed that recombinant ERM protein, especially moesin, can reconstitute actin assembly in permeable cells in response to activation of Rho and Rac (1997). Moesin and ezrin were recruited by phagosomes from the cytoplasm to facilitate the *de novo* actin assembly on phagosomal membranes (Defacque, 2000). Recent works in epithelial cells further showed that moesin promotes actin remodelling in response to tumor necrosis factor-α (Takahashi, 2010) or transforming growth factor-β (Haynes, 2011). Moesin may as well function as an adapter to facilitate cytoskeleton reassembly required for fenestra formation. Indeed, a recent study of endocytic, clathrin-coated

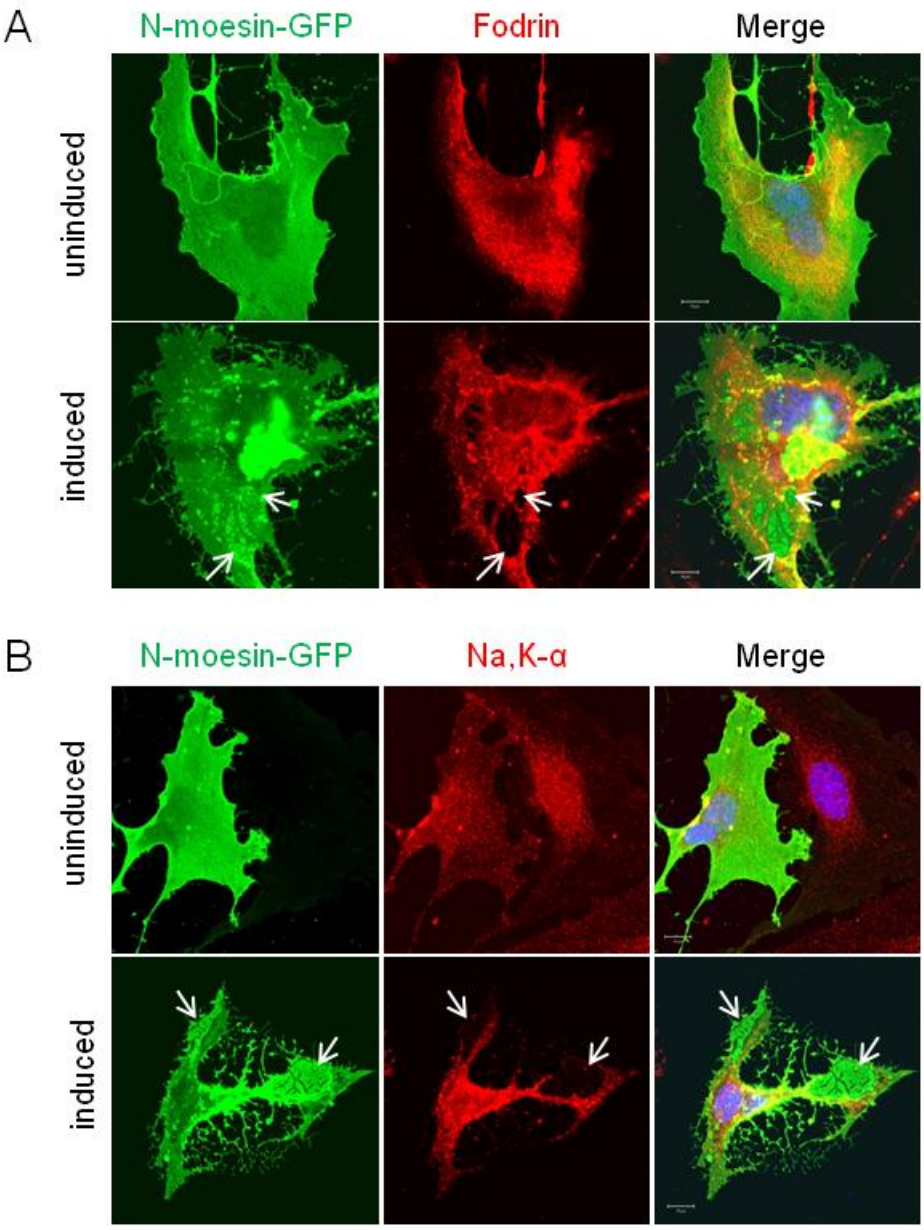

Fig. 6-3 The F-actin binding domain of moesin is essential to reassembly of membrane skeleton and Na,K-ATPase in fenestral sieve plates.

Absence of fodrin membrane skeleton (A) or Na,K-ATPase (B) in the sieve-plate-like microdomains in N-moesin-GFP transfected bEND5 cells.

Arrows, sieve-plate-like-microdomains in latrunculin A treated bEND5 cells.

Scale bar, 10 μm.

vesicles demonstrated that moesin drives membrane trafficking by binding PIP2 on nascent clathrin-coated vesicles and the actin cytoskeleton (Barroso-González, 2009).

In addition, moesin may also play a less dynamic, but more structural role in assembly of the actin-fodrin cytoskeleton. Band 4.1 protein, a moesin-related protein and member of the FERM protein superfamily, is a component of the spectrin-based membrane skeleton in erythrocytes (Liu, 1987). Although spectrin normally binds to and crosslinks F-actin (KD = 2×10^{-4} M), its affinity for F-actin increases eight orders of magnitude in the presence of protein 4.1 (KD = 10^{-12} M) (Goodman, 1988). Loss of protein 4.1 results in elliptocytic red blood cells, whose abnormal form can result in haemolytic anaemia, suggesting compromised membrane stability in red blood cells (Delaunay 2007). Similar to the role of band 4.1 in erythrocytes, moesin may be a structural component organising fenestrae in the sieve plates.

However, the findings from the dominant negative moesin also suggest that formation of the attenuated pseudo-sieve-plate microdomains may be independent of the actin-fodrin cytoskeleton network. The lack of fodrin and particularly, F-actin in this region was surprising, since F-actin is known to contribute to lammellipodia formation (Heath, 1993; Small, 1998 and 2002), and the pseudo-sieve-plate is essentially an attenuated thin, lammellipodia-like structure. The puzzling phenomenon was also observed in N-moesin-GFP overexpressed NIH3T3 cells. Amieva et al observed that, during retraction of lamellipodia, an accumulation of aboundant membraneous structures, which are enriched with the GFP-labelled domain, are devoid of actin and endogenous moesin (1999). The molecular assembly of these membraneous structure and the pseudo-sieve-plates is unclear. Nevertheless, the fact that the pseudo-sieve-plate was not observed in moesin knockdown cells suggests that the C-terminally truncated moesin may retain a functional activity that contributes to the formation of this plasma membrane microdomain. Crepaldi *et al* proposed that the tight binding of N-domain could be responsible for a global impairment of membrane protein redistribution, assembly of

cell surface and cytoskeletal structures (1997), though the exact mechanism clearly need further investigation.

6.2 The interaction between Na,K-ATPase and the fodrin membrane skeleton is essential to fenestra formation

In epithelial cells, Na,K-ATPase localises to and regulates tight junctions function (Rajasekaran, 2003). In addition to pumping Na^+ out of and K^+ into the cell, Na,K-ATPase also functions in forming signalling microdomain by interacting with other proteins. Through the third cytosolic domain of Na,K-α, Na,K-ATPase interacts with PLC-γ (Li and Xie, 2009), adaptor protein 2 (Done, 2002) and actin-regulating protein cofilin (Kim, 2002). The N-terminus of Na,K-ATPase interacts with PI3K p85 subunit, IP3 receptor and caveolin-1 (Yudowski, 2000; Cai, 2008). Protein complex of Na,K-ATPase, PI3K and annexin II at the plasma membrane regulates cell motility (Barwe, 2005). The Na,K-ATPase/Src complex functions as a signal receptor for cardiotonic steroids including ouabain (Li and Xie, 2009). Rajasekaran *et al* proposed a model for the role of Na,K-ATPase through its scaffolding partners in regulation of tight junctions in epithelial cells (Fig. 6-4) (Rajasekaran, 2009).

The close association between Na,K-ATPase and submembrane cytoskeleton has been demonstrated by several studies (Nelson and Veshnock, 1987; Devarajan, 1994; Zhang, 1998). Na,K-ATPase also binds to moesin with links to actin and modifies ankyrin binding (Kreamer, 2003). In bEND5 cells, the interaction between Na,K-ATPase and the fodrin cytoskeleton only exists bEND5 cells that are fenestrated, presumably in fenestral sieve plates, and the link is dependent on moesin expression. More interestingly, moesin knockdown significantly reduced the protein level of Na,K-ATPase in bEND5 cells, which very likely resulted from the limiting amount of moesin, just as the level of erythroid anion transporter early in development is limited by the lack of moesin (Cox, 1987). On the contrary, an increased level of Na,K-ATPase associates with elevated expression of moesin in opossum kidney cells (Silva, 2009). These observations and our data support the idea that moesin serves as a

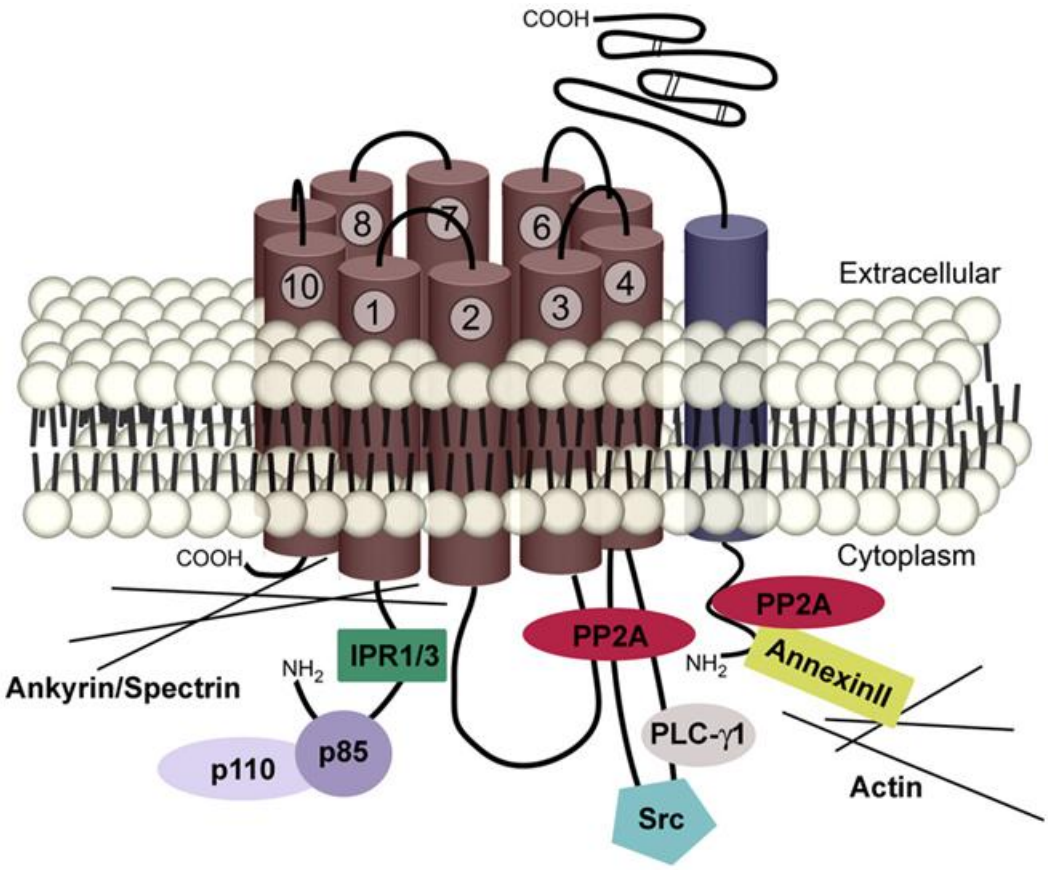

Fig. 6-4 Schematic model of Na,K-ATPase as a scaffolding signalling platform. Na,K-α interacts with IPR1/3 (IP receptor 1 and 3), PI3K p85 subunit, PP2A, Src and PLC-γ1. Na,K-β binds to annexin II and PP2A. Na,K-ATpase also directly associates with actin cytoskeleton (ankyrin, spectrin/fodrin).
(Adapted from Rajasekaran, 2009.)

molecule directly linking Na,K-ATPase to the fodrin membrane skeleton, and may modify interaction with ankyrin and the Na,K-ATPase similar to how protein 4.1 modifies the binding of ankyrin to erythrocyte anion exchanger AE1 (Cox, 1987; Akker, 2010).

6.3 Annexin II-regulated membrane-cytoskeleton remodelling negatively modulates fenestra formation

Like ERM proteins, annexin II possesses a highly conserved membrane binding module at its N-terminus and an F-actin binding site at its C-terminus (reviewed in Swairjo, 1994 and Filipenko, 2001). Annexin II is a component of F-actin-rich comet tails that propel newly formed endocytic vesicles from the plasma membrane to the cell interior (Merrifield, 1999). It is also a component of the F-actin pedestals that form at the membrane-attachment sites of enteropathogenic *Escherichia coli* (Zobiack, 2002). The role of annexin II in regulation of membrane-cytoskeleton dynamics is further emphasized by its specific association with membrane-associated actin, rather than stress fibres or cytoplasmic actin filaments, at sites of cholesterol-rich membrane domains (Babiychuk, 2000). Thus the opposing effect on fenestra formation caused by depletion of moesin and annexin II may have resulted from competition of binding to membrane-associated actin between annexin II and moesin, besides the competition for binding to PIP2-rich membrane microdomains.

Our data suggest that annexin II may also regulate fenestra formation by modulating expression of Na,K-ATPase. Increased expression of Na,K-ATPase was found in annexin II-depleted bEND5 cells. Na,K-β was reported to suppress cell motility through binding to annexin II (Barwe, 2005). In bEND5 cells, the increased expression of Na,K-α could be triggered by feedback from the diminishing interaction between Na,K-β and annexin II due to reduced annexin II, just as depletion of Na,K-β in moloney sarcoma virus-transformed MDCK cells increases Na,K-α levels (Barwe, 2005).

6.4 Membrane skeleton components colocalise with PV-1 in other fenestrated endothelium

We sought to determine if the observations in bEND5 cells might apply more broadly to fenestrated cells/tissue. First, we found that moesin and fodrin were strongly expressed and colocalised with PV-1 in highly fenestrated choriocapillaries. Other ERM members were expressed in different layers of retina. These data are consistent with a role for the fodrin cytoskeleton in fenestrated endothelium *in vivo*.

Braet *et al.* proposed a fenestra-associated cytoskeleton ring around cultured LSEC fenestra (1995). To investigate whether the membrane skeleton was also present in LSEC sieve plates, we isolated mouse LSEC and cultured them *in vitro*. LSEC rapidly lost their fenestrae in culture, but interestingly, PV-1 was up-regulated after 2-3 days of culture, and abundant PV-1-marked fenestral sieve plates could be induced by latrunculin A. The induced fenestrae were confirmed by TEM (data not shown). Immunofluorescence analysis revealed that spectrin/fodrin and ankyrin B colocalised with PV-1 in fenestral sieve plates in the cultured LSEC (Fig. 6-5). Our observations suggest that the fenestra-associated cytoskeleton ring of LSEC may be a fodrin-based membrane skeleton.

We speculate that the fodrin membrane skeleton serves not only as a supporting structure to give distensability and rigidity to fenestral sieve plates, as it does in the erythrocyte plasma membrane, but also provides the organisation of pores into ordered arrays.. The membrane cytoskeleton may also function together with the diaphragm, to define the fenestral pore size. As discussed below, besides simply structural support and architectural information, the submembrane cytoskeleton and associated plasma membrane proteins such as PV-1 and the Na-K ATPase are likely to regulate signalling important for fenestra formation and function.

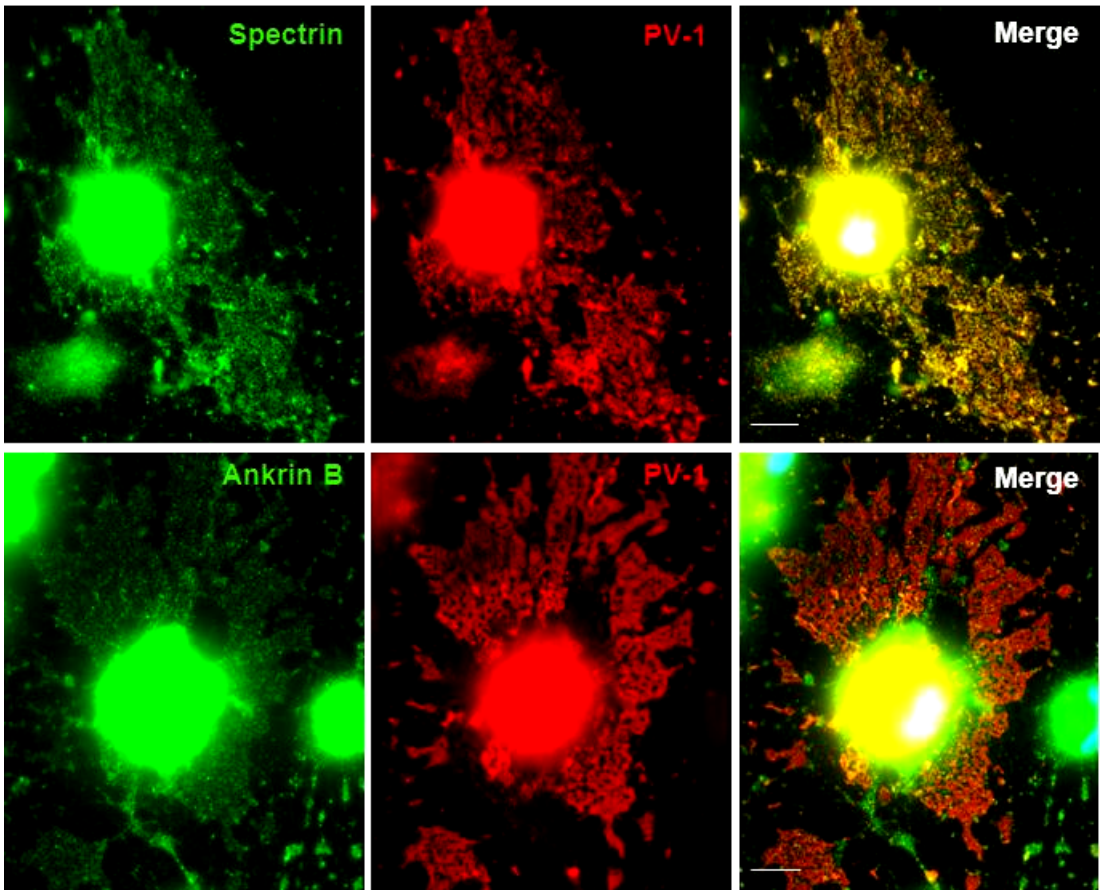

Fig. 6-5 Membrane skeleton in cultured LSEC fenestral sieve plates.
PV-1 was induced when LSEC was cultured for 7 days, and PV-1 marked fenestral sieve plates were induced by latrunculin A (1.25 uM) for 3 hours. Membrane skeleton componets, spectrin and ankrin B colocalised with PV-1 in fenestral sieve plates. Scale bar, 10 μm
(Courtesy to Dr. Victoria Coles, UCL Institute of Ophthalmology, London).)

6.5 The role of PI3K and PtdIns in fenestra formation

Our study identified PI3K as a major signalling protein involved in fenestra formation. PI3Ks are a family of enzymes that are originally defined on the basis that they could phosphorylate the 3-position hydroxyl group of the inositol ring of PtdIns (Katso, 2001). The three reactions catalysed by PI3Ks are shown in Fig. 6-6 (Hawkins, 2006). The activation of PI3K is now recognised as one of the most prevalent signal transduction events used by cell-surface receptors to control intracellular events (Stephens, 1993; Wymann, 1998; Vanhaesebroeck, 2001; Cantley, 2002;). More importantly, PI3K substrate and products PtdIns are involved widely and critically in the field of cell signalling and regulation. Inositol phospholipids have long been known to have an important regulatory role in cell physiology. These lipids, especially PIP2, function in classical cell-surface signal transduction, regulation of membrane traffic, organisation of the cytoskeleton, and ion channel activity (McLaughlin, 2002).

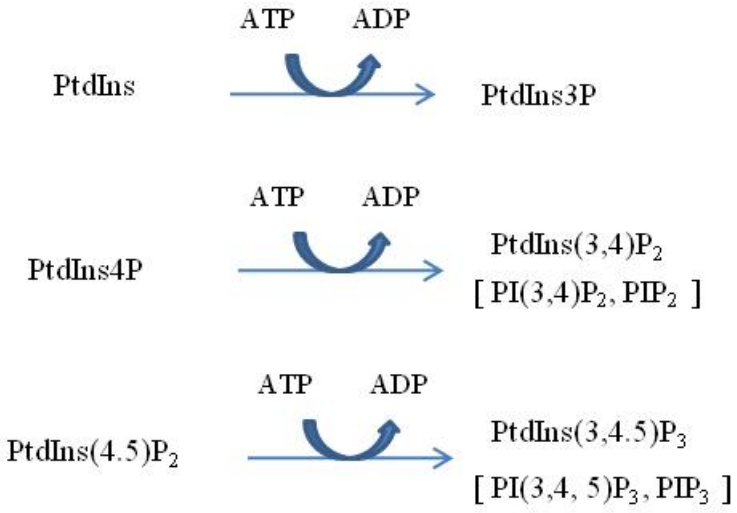

Fig. 6-6 Primary function of PI3K. The three reactions catalysed by PI3K, which phosphorylate the 3-position hydroxyl group of the inositol ring of PtdIns. (Recreated from Hawkins, 2006).

Not only is PI3K activity linked to actin filament reorganisation and membrane ruffling via the action of Rho and Rac (Chen, 1999), but also it regulates functions of proteins that involved in fenestra formation, particularly Na,K-ATPase. The interaction between the SH3 domain of PI3K p85 and the proline-rich motif in Na,K-α was reported in regulation of endocytosis of Na,K-ATPase (Yudowski, 2000). Barwe and co-workers also showed that the cell motility suppressing function of Na,K- β is dependent on PI3K activiation, especially the interaction between PI3K p85 and Na,K-α (Barwe, 2005). PI3K, along with Src, are essential parts for ouabain induced, Na,K-ATPase mediated signal cascades (Li and Xie, 2009). Furthermore, PI3K products PIP2 was also reported to stimulate Na,K-ATPase endocytosis thus inhibiting Na,K-ATPse activity (Gallicchio , 2009).

Although the PI3K activity is also reported essential for ERM proteins phosphorylation in neuronal cells, its major regulating impact to moesin and annexin II is from membrane PIP2(Jeon, 2009). Binding to PIP2 is a prerequisite for ERM protein activation (Bretscher, 1995), whilst annexin II is recruited to membrane raft structures by the specific interaction with PIP2 (Rescher, 2004).

Also, membrane PIP2 is a critical regulator of the actin cytoskeleton. In addition to facilitating actin polymerization (Sechi, 2000; Yin, 2003), PIP2 regulates the function of several actin cross-linking- and regulatory proteins that are critical for the assembly of actin filaments and membrane attachment (reviewed in Logan, 2006). Future work to identify the direct role of PIP2 in fenestra formation will provide a link between PI3K and the down-stream effectors involved in fenestra formation, and will further our understanding of membrane-cytoskeleton dynamics during fenestra biogenesis.

One interesting angle to pursue involves the polyoma middle T antigen. Among the hundreds of cell lines screened for fenestra induction, the two cell lines that displayed potent fenestra induction, bEND5 and Py4.1, are both MT-transformed cell lines (Ioannadou, 2006). Polyoma virus middle T-antigen is a 421 amino acid protein that is a highly effective oncogene, able to transform established cells to a fully transformed,

tumorigenic phenotype (Treisman, 1981). It interacts with and activates src-family tyrosine kinase, which then phosphorylates MT to provide binding sites for PI3K, PLCg-1, PP2A, etc. (reviewed in Keith, 2001). In many respects, MT can be considered to be a permanently active analogue of a growth factor receptor. MT transformation results in an increase in the amount of the PtdIns, PI(3,4)P2 and PI(3,4,5)P_3, products of PI3K activity, and the increase is abolished by removal of the PI3K binding site (Gorga, 1990; Serunian, 1990). In fact, PI3K activity was first observed in the 1980s with a tight link with MT oncoprotein (Sugimoto, 1984; Whiteman, 1985). Thus, MT transformation might prime the signalling machinery in these cells, and in some as yet unknown way drive reorganisation of the actin-fodrin cytoskeleton and formation of sieve plates following disassembly of cortical and microfilament actin networks. Future work with gain- and loss of function MT may further elucidate the role of PI3K and other signalling factors in fenestra formation.

6.6 *In vivo* implications

Fenestra formation is a rapid and reversible process, though it involves a wide range of regulating factors and biological events. The identification of fenestra components and dissection of the membrane-cytoskeleton interplay leading to fenestra formation provide a conceptual framework for further studies elucidating fenestra biogenesis. Our findings also provide new molecular targets and tools for probing fenestra structure and function *in vivo*.

We identified the membrane skeleton as the supporting cytoskeletal structure in fenestral sieve plates. Consistent with the suggested role of Na,K-ATPase and fodrin membrane skeleton in the establishment of specialised microdomains (Nelson, 1986 and 1989; Alper, 1994), our data showed that regulation of Na.K-ATPae by ouabain induced fenestra formation in bEND5 cells. These data were further extended *in vivo* by the work with ouabain and the Na,K- ATPase. With topical application as short as 10 minutes, ouabain is able to induce endothelial fenestration in vessels that normally are not fenestrated, with an efficacy even more potent than VEGF. Our data showed a new

role of the multi-functional Na,K-ATPase in modulating vascular permeability by regulating endothelial fenestration.

Na,K-ATPase serves as the highly conserved unique binding site for cardiac glycosides such as ouabain, digoxin, and digitoxin. Ouabain and digoxin are used widely in the treatment of congestive heart failure (Kaplan, 2005). The proposed mechanism is that inhibition of Na,K-ATPase results in increased cytosolic Na^+, which in turn activates the Na^+/Ca^{++} exchange pump, and Ca^{++} influx leads to increased muscle contractility (Meyer-Lehnert, 1993). However, chronic use of ouabain causes inhibition of Na^+ efflux, and this Na^+ retention may lead to unexpected side effects, especially in the renal system. Indeed, ouabain has been implicated in adrenocorticotropic hormone-induced hypertension (Dostanic-Larson, 2005). Ouabain-induced endocytosis of Na,K-ATPase was reported to play an important role in renal adaptation to volume expansion and hypertension (Kaplan, 2005).

The role of Na,K-ATPase in the eye setting is even more intriguing. Reduced Na,K-ATPase activity in RPE cells was reported in an animal model with diabetes (MacGregor, 1986). Significantly decreased retinal Na,K-ATPase activity has been shown in streptozotocin-induced diabetic rats (Ottlecz, 1996). Studies from Rajasekan's group demonstrated that Na,K-ATPase inhibition by ouabain results in decreased tight junction membrane contact points and increased tight junction premeability (Rajasekaran, 2003 and 2005). Our study is the first to demonstrate that inhibition of Na,K-ATPase also increases permeability in endothelial cells, though by inducing fenestra formation rather than solely tight junction breakdown. With reference to human disease, the ultrastructual analysis of retinal vessels from diabetic patients revealed that some of the vessels were fenestrated, but the tight junctions between endothelial cells were rarely altered (Ishibashi, 1993). In addition, defenestration of choriocapillaries or even loss of choriocapillaries has been observed in age-related macular degeneration patients (Neuhardt, 1999), though no link to Na,K-ATPase has been provided to date. These changes may contribute to pathological processes such as drusen formation and

thickening and reduced permeability of Bruch's membrane. However, the molecular mechanism for these changes is largely unknown. The findings in our study may provide novel approaches to understand the permeability changes, especially changes in choriocapillary fenestration that occurs during AMD pathogenesis.

6.7 Limitations

Fenestra formation involves a bewildering range of cellular activities, including actin reorganisation, membrane cytoskeleton reassembly, membrane remodelling, membrane protein and lipid endocytosis, vesicle trafficking, and membrane fusion. The end point of this dynamic process is the formation of numerous transcellular pores. Future work will need to dissect how the function of some of the regulatory proteins described herein, contributes to pore and sieve plate architecture.

Fusion of two lipid bilayers in an aqueous environment is a two-step process. First, the membranes are brought together into close proximity, then the boundary between the hydrophilic and hydrophobic portions of the layer is destabilised (Jahn, 2003). Thus the membrane fusion events generally require 1) molecules that tether and dock membranes and bring them into close proximity; 2) molecules that locally disturb the lipid bilayers, such as by induction of extreme membrane curvature; and 3) molecules that give spatially organise the process. The driving force for membrane fusion can come either from protein–lipid or protein-protein interactions, ultimately primed by ATP (Martens, 2008). The preliminary data in chapter 3 showed that syntaxin 4 is highly expressed in bEND5 cells and colocalised with PV-1 in fenestral sieve plates (Fig. 3-14C). Future studies using gain- and loss of function of syntaxin 4 may provide more information on its functional role in fenestra formation. Immunostaining of other fusion-related proteins, such as the Rab proteins Rab4 and Rab5 and the exocyst component Exo70, didn't give any conclusive information (data not shown). However, their involvement in fenestra formation cannot be ruled out, since they may have functioned earlier than the end stage of fenestra formation, especially since the fusion machinery tends to move away from the fusion zone (Martens, 2008). Future work with live imaging may prove valuable to

provide information about the membrane trafficking and fusion step in fenestra formation.

Another area that deserves attention is the membrane trafficking. Fenestra formation was proved a highly dynamic process in our in vitro cell model. The dynamic segregation of PV-1 from caveolin-1 and the compromised fenestra formation by microtubule disruption suggested the involvement of endocytic pathway during fenestra induction. Endocytosis inhibition by MβCD showed the essential role of clathrin- or caveolin- dependent endocytic pathway in fenestra formation. However, Treatment of dynamin inhibitor Dynasore in bEND5 cells resulted in significantly decreased detection of PV-1 – the fenestra marker in our *in vitro* cell model, which made it impossible to preclude its effecting on fenestra formation. Future work coupled with corresponding ultrastructural analysis will provide more concluding information on the role of dynamin-dependent endocytosis in fenestra formation.

Our preliminary exploration in signalling pathways showed that PI3K played an important role in fenestra biogenesis. Our data from ROCK inhibitor showed that inhibition of Rho family small GTPase didn't compromise fenestra formation induced by latrunculin A or ouabain. ROCK member RhoA has been documentd as a key regulator of the cortical actin cytoskeleton (Hamada, 2001; D'Angelo, 2007). Reducing expression of Rho strongly suppresses loss of moesin function phenotypes (Speck, 2003; Hipfner, 2004; Molnar, 2007), and overexpression of Rho in epithelial cells produces a phenotype similar that caused by lack of moesin (Carreno, 2008). Interestingly, annexin II is reported to positively regulate Rho activity in Caco-2 epithelial cells (Babbin, 2007). Annexin II co-immunoprecipitates with endogenous Rho and constitutively active RhoA, and annexin II siRNA transfection leads to Rho disassociation from the membrane and decreased Rho activity (Babbin, 2007). So we speculate that the RhoA pathway very likely has a negative effect on fenestra formation similar to that of annexin II, though future experiments with an optimal Y27632 concentration are needed to explore the precise role of Rho during fenestra formation.

Clearly there are also some interesting protein complexes that need further definition and understanding; for example, the Na,K-ATPase signalling scaffold, the fodrin submembrane cytoskeleton and potentially, the middle T antigen scaffold. Advanced ultrastructural techniques such as high pressure freezing and tomography coupled with immunolabelling techniques could yield critical insights in the future.

6.8 Summary

Through our effort to understand fenestra biogenesis, we identified that actin, the actin-binding protein moesin, the fodrin membrane skeleton, and the integral protein Na,K-ATPase all are part of the fenestral sieve plate structure. We also found that another actin-binding protein, annexin II, negatively regulates fenestra formation. PI3K activity was shown to be required for fenestra formation, whilst the negative regulation of Rho/ROCK proteins on fenestra formation cannot be ruled out.

How do these factors work together to regulate fenestra formation? Based on our results, we propose the following model to explain the mechanism of moesin-, annexin II- and Na/K-ATPase- regulated fenestra induction in bEND5 cells (Fig. 6-7). Both the binding of ouabain to Na,K-ATPase and latrunculin A activate PI3K by direct effects on F-actin depolymerisation, by massive cortical release of Ca^{++} triggered by F-actin disruption, or by an unknown mechanism (Lim, 2002). Association of Na,K-α and p85 subunit is likely the common step in both latrunculin A- and ouabain-induced PI3K activation, since coimmunoprecipitation of p85 with Na,K-α increased in both latrunculin A- and ouabain-triggered fenestra induction. Through downstream effectors or as a direct effect of the PI3K products PIP2 and PIP3, the plasma membrane remodels to form sieve-plate-like microdomains enriched for moesin. In turn, the relocalised moesin, through its F-actin-binding domain, initiates F-actin reassembly and membrane skeleton reorganisation. The newly formed membrane skeleton network functions at minimum in the following three ways: 1) it brings the targeted plasma membrane into close proximity; 2) it directs and facilitates the transport of materials required for fenestra formation, such as membrane fusion proteins, PV-1, and Na,K-ATPase, into the right

location; and 3) it directs the fusion process and restricts the location of structural proteins. The internalisation of PV-1, Na,K-ATPase and other proteins is most likely triggered by disruption of cortical actin and activation of PI3K. Another actin-binding protein, annexin II, negatively regulates fenestra formation by competing for the Na,K-β subunit, binding to PI3K products, and activating ROCK proteins.

These findings depict complex but well-coordinated membrane-cytoskeleton dynamics during fenestra formation. Our results provide a conceptual framework linking actin rearrangement to membrane remodelling during fenestra biogenesis, and identify new molecular tools for probing fenestra structure and function. However, our model now must be continually challenged as we develop additional data in the future. It is our hope that manipulation of fenestra components and/or signalling pathways may potentially lead to regulation of vascular permeability and identification of targets for novel treatments targeted to endothelial permeability-related diseases.

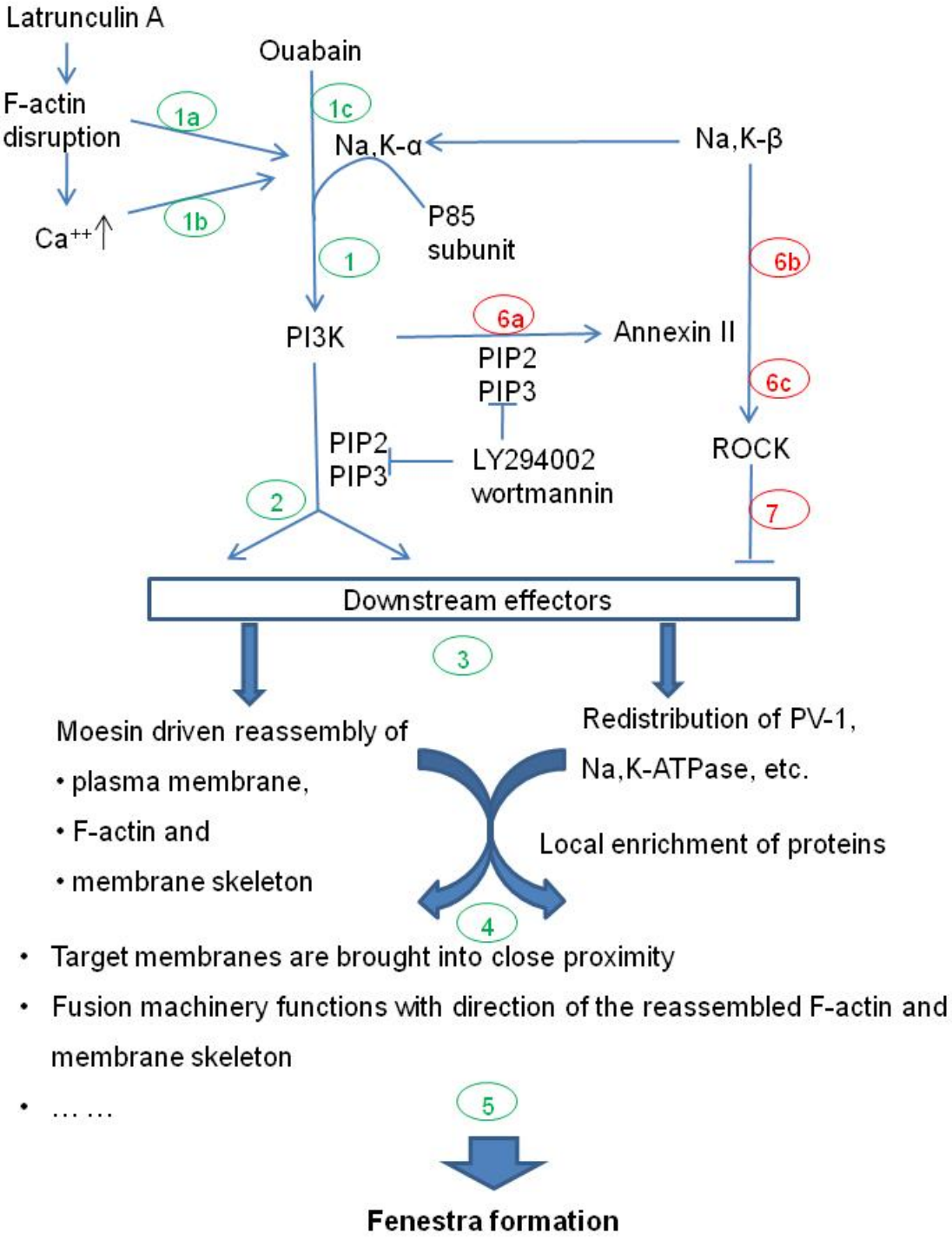

Fig. 6-7 Schematic model for a proposed mechanism of actin-, moesin- and Na,K-ATPase- regulated fenestra formation.

1. PI3K is activated by latrunculin-A triggered F-actin depolymerisation (1a) and/or the following Ca^{++} release (1b), or by the binding of ouabain (1c). Association of Na,K-α and p85 subunit is likely the common step in both latrunculin A- and ouabain-induced PI3K activation.

2. PI3K downstream effectors are activated.

3. Moesin drives F-actin and membrane skeleton reorganisation and plasma membrane remodelling; protein redistribution for space clearance may also take place in this step.

4. Target membranes are brought into close proximity, and fenestra formation required proteins, e.g. fusion proteins, PV-1, etc. are translocated into place with the direction of the reorganised F-actin microfilament and membrane skeleton.

5. Fenestral sieve plates form.

6. Annexin II negatively regulate fenestra formation by competitively binding to PI3K products (6a) and Na,K-β (6b), which in turn activates ROCK pathway (6c).

7. ROCK activation negatively regulates fenestra formation.

Supplements

Supplemental Figure-1 Negative controls used in immunofluorescence staining

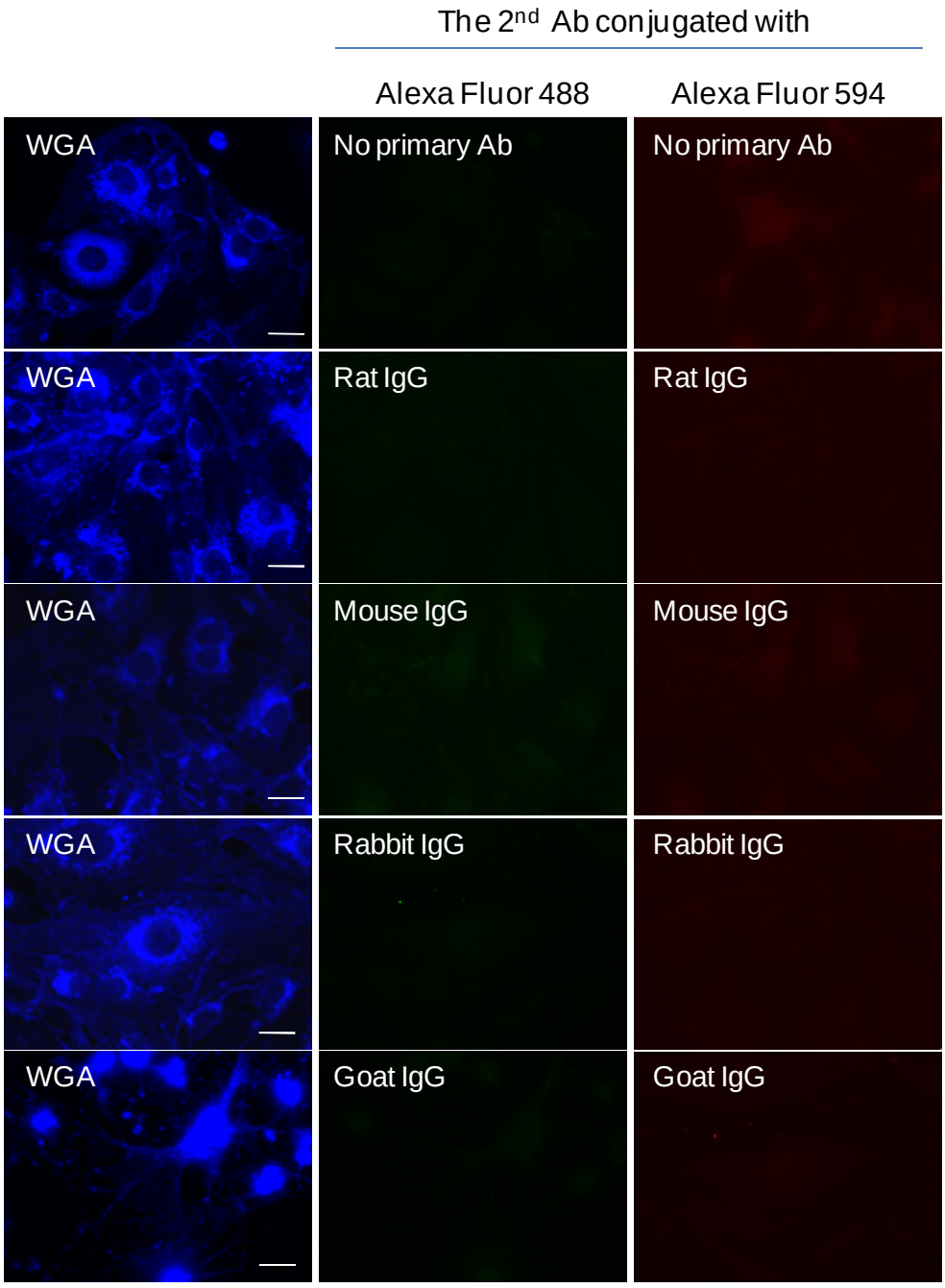

WGA, wheat germ agglutinin was used to label the cells; immunoglobulin G (IgG) from different species were used as negative controls for immunofluorescence staining. Scale bar, 10 μm.

Supplemental Table-1 Summary of candidate proteins from proteomic analysis (Ioannidou, 2005, PhD Thesis)

Function	Protein Name	Total Change	P-value	Cell Type
Cytoskeletal association	Cofilin, non-muscle isoform	Unique spot	N/A	bEND5
	Myosin light chain 2A and 2B, smooth muscle isoform	1.488	0.0012	bEND5
	Twifilin-1	1.671	0.021	bEND5
	Transgelin 2	-	unknown	bEND5
	Protein Tyrosin Kinase 9	2.258	0.0048	Py4.1
	Kinesin Light Chain (KLCt)	1.772	0.0032	Py4.1
Membrane remodeling / endocytosis	Radixin / Moesin	3.811	0.0032	Py4.1
	Nucleotide diphosphate kinase B (nm23-M2)	1.251 / 1.16	0.030 / 0.945	bEND5
	Nucleotide diphosphate kinase A (nm23-M1)			
	Nucleotide diphosphate kinase B (nm23-H2)			
	Paralemmin	1.772	0.0267	Py4.1
	Annexin II	1.193	0.3104	bEND5
Transcription / Translation	Putative RNA-binding protein 3	1.251	0.0303	bEND5
	Heterogeneous nuclear rbonucleoprotein K (hnRNP K)	1.883/1.71	0.193/0.1852	bEND5
	Eukaryotic translation inhibition factor H	-1.012	0.9481	bEND5
	Musculin (Myogenec repressor)			
Housekeeping	60 kDa heat shock protein, mitochondrial precursor	-1.176	0.3662	bEND5
	ATP synthase, H+ transporting mitochondrial F1 complex, β subunit	1.358	0.371	bEND5
	ATP synthase β chain, mitochondrial precursor			
Metabolism	A – Enolase (non-neural isoform)	1.826	0.0251	bEND5
		2.038/1.772	0.0021/o.o266	Py4.1

Supplemental Figure-2　Subtractive analysis of proteins regulated after latrunculin A treatment of bEND5 cells.

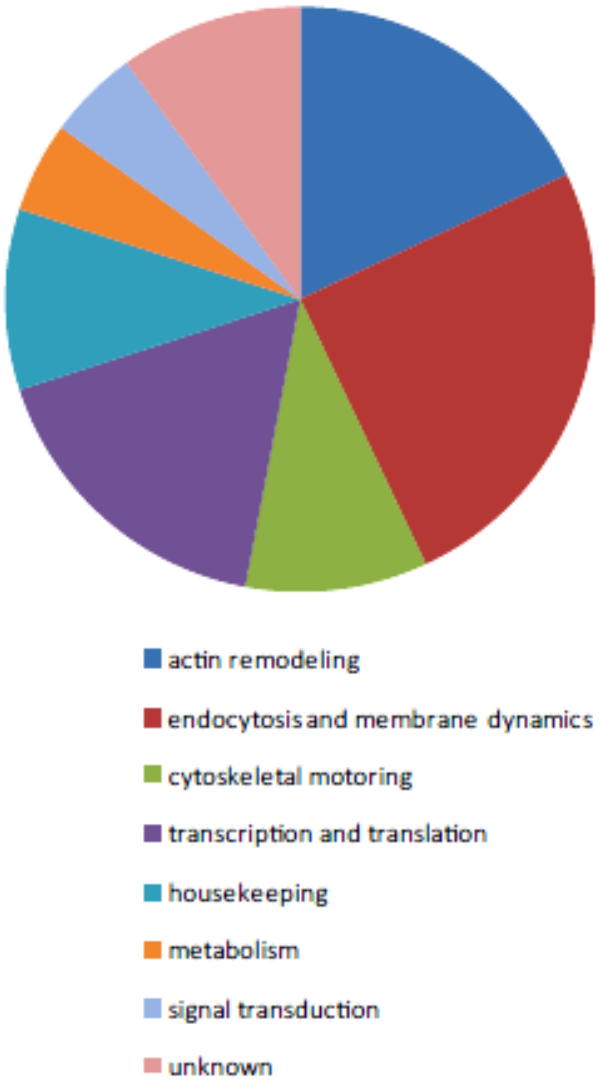

References

Adamis AP, Shima DT, Yeo KT, Yeo TK, Brown LF, Berse B, D'Amore PA, Folkman J.Synthesis and secretion of vascular permeability factor/vascular endothelial growth factor by human retinal pigment epithelial cells. Biochem Biophys Res Commun. 1993 Jun 15;193(2):631-8.

Algrain M, Turunen O, Vaheri A, Louvard D. and Arpin M. Ezrin contains cytoskeleton and membrane binding domains accounting for its proposed role as a membrane-cytoskeletal linker. J. Cell Biol. 1993, 120: 129-139.

Alper SL, Stuart-Tilley A, Simmons CF, Brown D and Drenckhahn D. The fodrin-ankyrin cytoskeleton of choroid plexus preferentially colocalizes with apical Na+K(+)-ATPase rather than with basolateral anion exchanger AE2. J Clin Invest. 1994, 93(4):1430–1438

Amieva MR, Litman P, Huang L, Ichimaru E, Furthmayr H. Disruption of dynamic cell surface architecture of NIH3T3 fibroblasts by the N-terminal domains of moesin and ezrin: in vivo imaging with GFP fusion proteins. Journal of Cell Science, 1999, 112: 111-125.

Amieva MR, Furthmayr H. Subcellular Localization of Moesin in Dynamic Filopodia, Retraction Fibers, and Other Structures Involved in Substrate Exploration, Attachment, and Cell-Cell Contacts. Experimental Cell Research. 1995, 219 (1):180-196.

Andrews PM, Investigation of cytoplasmic contractile and cytskkeletal elements in the kidney glomerulus. Kidney Int. 1981, 20(5): 549-562.

Antonin W. Nuclear Envelope: Membrane Bending for Pore Formation? Current Biology , 2009, 19 (10): 410-412.

Appenzeller-Herzog C, Hauri HP. The ER-Golgi intermediate compartment (ERGIC): in search of its identity and function. J. Cell. Sci. 2006, 119 (11): 2173–83.

Arias IM. The biology of hepatic endothelial cell fenestrae. In: Schaffer F, Popper H, editor. Progress in Liver Diseases IX. Philadelphia: WB Saunders; 1990, p11–26.

Aunis D, Bader MF. The cytoskeleton as a barrier to exocytosis in secretory cells. J Exp Biol. 1988, 139: 253-66.

Avasthi PS, Evan AP, Hay D. Glomerular endothelial cells in uranyl nitrate-induced acute renal failure in rats. J Clin Invest 1980, 65: 121–127.

Avasthi PS, Evan AP, Huser JW, Luft FC: Effect of gentamicin on glomerular ultrastructure. J Lab Clin Med 1981, 98:444-454.

Babbin BA, Parkos CA, Mandell KJ, Winfree LM, Laur O, Ivanov AI, Nusrat A. Annexin 2 regulates intestinal epithelial cell spreading and wound closure through Rho-related signalling. Am J Pathol. 2007, 170(3):951-66.

Babiychuk EB, Draeger A. Annexins in cell membrane dynamics. Ca(2+)-regulated association of lipid microdomains. J Cell Biol. 2000 Sep 4;150(5):1113-24.

Bailey, E, Bottomley MJ, Westwell S, Pringle JH, Furness PN, Feehally J, Brenchley PE and Harper SJ. Vascular endothelial growth factor mRNA expression in minimal change, membranous, and diabetic nephropathy demonstrated by non-isotopic in situ hybridisation . J Clin Pathol 1999, 52:735-738.

Bankston PW, and Milici AJ, A survey of the binding of polycationic ferritin in several fenestrated capillary beds: indication of heterogeneity in the luminal glycocalyx of fenestral diaphragms, Microvasc Res 1983, 26: 36–48.

Bankston PW, Pino RM. The development of he sinusoids of fetal rat liver: morphology of endothelial cells, Kupper cells, and transmural miagration of blood cells into sinusoids. Am J Anat, 1980, 159 (1): 1-15.

Barroso-González J, Machado JD, García-Expósito L, Valenzuela-Fernández A. Moesin regulates the trafficking of nascent clathrin-coated vesicles. J Biol Chem. 2009 Jan 23;284(4):2419-34.

Barwe SP, Anilkumar G, Moon SY, Zheng Y, Whitelegge JP, Rajasekaran SA, Rajasekaran AK. Novel role for Na,K-ATPase in phosphatidylinositol 3-kinase signalling and suppression of cell motility. Mol Biol Cell. 2005 Mar;16(3):1082-94.

Bar-Ziv R, Tlusty T, Moses E, Safran SA, Bershadsky A. Pearling in cells: a clue to understanding cell shape. Proc Natl Acad Sci U S A. 1999 Aug 31;96(18):10140-5.

Baumann O. Biogenesis of surface domains in fly photoreceptor cells: fine-structural analysis of the plasma membrane and immunolocalization of Na+, K+ ATPase and alpha-spectrin during cell differentiation. J Comp Neurol 1997, 382: 429–442.

Bearer E.L. and Orci L, Endothelial fenestral diaphragms: a quik-freeze, deep-etch study. J Cell Biol, 1985, 100(2): 418-28.

Benarroch EE,Na+, K+-ATPase Neurology January 18, 2011 vol. 76 no. 3 287-293

Bennett HS, Lutf JH, Hampto JC. Morphological classifications of vertebrate blood capillaries. Am J Physiol. 1959, 196(2):381-90.

Bennett V, Gilligan DM. The spectrin-based membrane skeleton and micron-scale organization of the plasma membrane. Annu Rev Cell Biol, 1993, 9:27– 66.

Bennett V. The membrane skeleton of human erythrocytes and its implications for more complex cells. Annu. Rev. Biochem. 1985, 54:273-304.

Bennett V., Baines AJ, and Davis JQ. Ankyrin and synapsin: spectrin-binding proteins associated with brain membranes. J. Cell. Biochem. 1985, 29:157-169.

Berryman M, Franck Z, Bretscher A. Ezrin is concentrated in the apical microvilli of a wide variety of epithelial cells whereas moesin is found primarily in endothelial cells. J Cell Sci. 1993 Aug;105 (Pt 4):1025-43.

Bershadsky AD , Vasiliev JM. Cytoskeleton. New York: Plenum Press, 1988, p298p.

Biochim. Biophys. Acta 1998, 1404: 271–281

Blanco G, Mercer RW. Isozymes of the Na-K-ATPase: heterogeneity in structure, diversity in function. Am J Physiol. 1998, 275: 633–650.

Bonilha VL, Finnemann SC, Rodriguez-Boulan E. Ezrin promotes morphogenesis of apical microvilli and basal infoldings in retinal pigment epithelium. J Cell Biol. 1999 Dec 27;147(7):1533-48.

Borisy, GG., and Svitkina TM. Actin machinery: pushing the envelope. Curr. Opin. Cell Biol. 2000, 12:104–112.

Braet F, De Zanger R, Baekeland M, Crabbe E, Van Der Smissen P, Wisse E. Structure and dynamics of the fenestrae-associated cytoskeleton of rat liver sinusoidal endothelial cells. Hepatology 1995, 21: 180–189.

Braet F, De Zanger R, Baekeland M, Crabbé E, Van Der Smissen P, Wisse E. Structure and dynamics of the fenestrae-associated cytoskeleton of rat liver sinusoidal endothelial cells. Hepatology. 1995 Jan; 21(1):180-9.

Braet F, De Zanger R, Jans D, Spector I, Wisse E. Microfilament-disrupting agent latrunculin A induces an increased number of fenestrae in rat liver sinusoidal endothelial cells: comparison with cytochalasin B. Hepatology. 1996, 24: 627–635.

Braet F, De Zanger R, Kalle W, Raap A, Tanke H, Wisse E. Comparative scanning, transmission and atomic force microscopy of the microtubular cytoskeleton in fenestrated liver endothelial cells. Scanning Microsc Suppl. 1996; 10:225-35; discussion 235-6.

Braet F, Kalle WH, De Zanger RB, De Grooth BG, Raap AK, TankeHJ, Wisse E. Comparative atomic force and scanning electron microscopy:an investigation on fenestrated endothelial cells in vitro. J Micros 1996, 181: 10–17.

Braet F, Soon LL. Diaphragmed fenestrae in the glomerular endothelium versus nondiaphragmed fenestrae in the hepatic endothelium. Kidney International, 2005, 68: 1902–1902.

Braet F, Spector I, De Zanger R, Wisse E. A novel structure involved in the formation of liver endothelial cell fenestrae revealed by using the actin inhibitor misakinolide. Proc Natl Acad Sci USA, 1998, 95(23): 13635–13640.

Braet F, Spector I, Shochet N, Crews P, Higa T, Menu E, De Zanger R, Wisse E. The new anti-actin agent dihydrohalichondramide reveals fenestrae-forming centers in hepatic endothelial cells. BMC Cell Biol. 2002, 3: 7.

Braet F, Wisse E, Probst I. The long-term culture of pig liver sinusoidal endothelial cells: the Holy Grail found. Eur J Cell Biol 2005, 84: 745–748.

Braet F, Wisse E. Structural and functional aspects of liver sinusoidalendothelial cell fenestrae: a review, 2002, Comp Hepatol 1: 1.

Bray D. Cell movements. New York: Garland, 1992, p406.

Breier G, Albrecht U, Sterrer S, Risau W. Expression of vascular endothelial growth factor during embryonic angiogenesis and endothelial cell differentiation. Development. 1992, 114(2):521-32.

Brenner SL, Korn ED. Spectrin/actin complex isolated from sheep erythrocytes accelerates actin polymerization by simple nucleation. Evidence for oligomeric actin in the erythrocyte cytoskeleton. J Biol Chem. 1980, 255:1670–1676.

Brenner SL, Korn ED. Spectrin-actin interaction. Phosphorylated and dephosphorylated spectrin tetramer cross-link F-actin. J Biol Chem. 1979, 254: 8620–8627.

Bretscher A, Edwards K, Fehon RG. ERM proteins and merlin: integrators at the cell cortex. Nature Reviews Cell and Molecular Biology. 2002, 3:586–599.

Bretscher A, Gary R, Berryman M. Soluble ezrin purified from placenta exists as stable monomers and elongated dimers with masked C-terminal ezrin-radixin-moesin association domains. Biochemistry. 1995, 34: 16830–7.

Bretscher A, Purification of an 80,000-dalton protein that is a component of the isolated microvillus cytoskeleton, and its localization in nonmuscle cells, J. Cell Biol. 1983, 97: 425–432.

Burgoyne, R. and T. Cheek, Reorganization of peripheral actin filaments as a prelude to exocytosis. Biosci. Rep., 1987. 7: 281-288.

Burns MS, Hartz MJ. The retinal pigment epithelium induces fenestration of endothelial cells in vivo. Curr Eye Res. 1992, 11(9):863-73.

Burridge K and Chrzanowska-Wodnicka M. Focal adhesions, contractility, and signalling. Annu. Rev. Cell Dev. Biol. 1996, 12:463–518.

Cai T, Wang H, Chen Y, Liu L, Gunning WT, Quintas LE, Xie ZJ.Regulation of caveolin-1 membrane trafficking by the Na/K-ATPase. J Cell Biol. 2008 Sep 22;182(6):1153-69.

Candela ME, Geraci F, Turturici G, Taverna S, Albanese I, Sconzo G. Membrane vesicles containing matrix metalloproteinase-9 and fibroblast growth factor-2 are released into the extracellular space from mouse mesoangioblast stem cells. J Cell Physiol. 2010 Jul;224(1):144-51.

Cantley LC. The phosphoinositide 3-kinase pathway. Science. 2002 May 31;296 (5573):1655-7.

Capo V, Ozzello L, Fenoglio CM, Lombardi L, Rilke F. Angiosarcomas arising in edematous extremities: immunostaining for factor VIII-related antigen and ultrastructural features. Hum Pathol. 1985, 16: 144–50.

Carley WW, AJ Milici, JA Madri. Extracellular matrix specificity for the differentiation ofcapillary endothelial cells. Exp Cell Res, 1988, 178(2): 426-34.

Carreno S, Kouranti I, Glusman ES, Fuller MT, Echard A, Payre F. Moesin and its activating kinase Slik are required for cortical stability and microtubule organization in mitotic cells. J Cell Biol. 2008 Feb 25;180(4):739-46.

Castellano E, Downward J. RAS Interaction with PI3K, More Than Just Another Effector Pathway. Genes & Cancer March 2011, 2(3): 261-274.

Chishti AH, Kim AC, Marfatia SM, Lutchman M, Hanspal M, Jindal H, Liu SC, Low PS, Rouleau GA, Mohandas N, Chasis JA, Conboy JG, Gascard P, Takakuwa Y, Huang SC, Benz EJ, Jr., Bretscher A, Fehon RG, Gusella JF, Ramesh V, Solomon F, Marchesi VT, Tsukita S, Tsukita S, Hoover KB, et al. The FERM domain: a unique module involved in the linkage of cytoplasmic proteins to the membrane. Trends Biochem Sci. 1998, 23:281–2.

Chowdhury AK. Participation of endothelial cells in the development of glomerulosclerosis: a study on murine serum sickness nephritis with mitomycin C. Pathol Int 1996, 46: 173–182.

Clark SA, Angus HB, Cook HB, Oxner RBG, Gorge PM, Fraser R: Defenestration of hepatic sinusoids as a causeof hyperlipoproteinaemia in alcoholics. Lancet 1988, 2: 1225-1227.

Clementi F, Palade GE: Intestinal capillaries. I. Permeability to peroxidase and ferritin. J Cell Biol, 1969, 41 : 33 –58.

Cooper JA, Effects of cytochalasin and phalloidin on actin. J. Cell Biol. 1987, 105 (4): 1473–8.

Cox JV, Stack JH, Lazarides E. Erythroid anion transporter assembly is mediated by a developmentally regulated recruitment onto a preassembled membrane cytoskeleton. J Cell Biol. 1987 Sep;105(3):1405-16.

Crepaldi T, Gautreau A, Comoglio PM, Louvard D. and Arpin M. Ezrin is an effector of hepatocyte growth factor-mediated migration and morphogenesis in epithelial cells. J. Cell Biol. 1997, 138: 423-434.

Crystallization and preliminary crystallographic studies of RhoGDI in complex with the radixin FERM domain. Acta Crystallogr D Biol Crystallogr. 2001 Jun;57(Pt 6):889-90.

D'Angelo R, Aresta S, Blangy A, Del Maestro L, Louvard D, Arpin M.Interaction of ezrin with the novel guanine nucleotide exchange factor PLEKHG6 promotes RhoG-dependent apical cytoskeleton rearrangements in epithelial cells. Mol Biol Cell. 2007 Dec;18(12):4780-93.

Davila-Esqueda ME, Vertiz-Hernandez AA, Martinez-Morales F. Comparative analysis of the renoprotective effects of pentoxifylline and vitamin E on streptozotocin-induced diabetes mellitus. Ren Fail 2005, 27: 115–122.

Dawson TR, Lazarus MD, Hetzer MW, Wente SRER membrane-bending proteins are necessary for de novo nuclear pore formation. J Cell Biol. 2009 Mar 9;184(5):659-75.

De Matteis MA, Morrow JS. Spectrin tethers and mesh in the biosynthetic pathway. J Cell Sci. 2000, 113 (Pt 13):2331–2343.

De Zanger R, Wisse E. The filtration effect of rat liver fenestraed sinusoidal endothelium on the passage (remnant)chylomicros to the space ofDIsse. In: Sinusoidal Liver Cells (Edited by Knook DL, Wisse E) Amsterdam, Elsevier, 1982, p69-76.

Deen WM, Lazzara MJ, Myers BD. Structural determinants of glomerular permeability. Am J Physiol Renal Physiol 2001, 281: 579–596.

Defacque H, Egeberg M, Habermann A, Diakonova M, Roy C, Mangeat P, Voelter W, Marriott G, Pfannatiel J, Faulstich H, Griffins G. The EMBO J, 2000, 19: 199-212.

Deissler H, Deissler H, Lang S, Lang GE. VEGF-induced effects on proliferation, migration and tight junctions are restored by ranibizumab (Lucentis) in microvascular retinal endothelial cells. Br J Ophthalmol. 2008, 92(6):839-43.

Dejana E, Spagnuolo R, Bazzoni G. Interendothelial junctions and their role in the control of angiogenesis, vascular permeability and leukocyte transmigration. Thromb. Haemost. 2001, 86:308–315.

Delaunay J. The molecular basis of hereditary red cell membrane disorders. Blood Rev. 2007, 21(1):1-20.

Delon J, Kaibuchi K, Germain RN, Exclusion of CD43 from the Immunological Synapse Is Mediated by Phosphorylation-Regulated Relocation of the Cytoskeletal Adaptor Moesin. Immunity, volume 15, Issue 5, November 2001, p691–701.

Devarajan P, Scaramuzzino DA, Morrow JS, Ankyrin binds to two distinct cytoplasmic domains of Na,K-ATPase alpha subunit, Proc. Natl. Acad. Sci. U. S. A. 1994, 91: 2965–2969.

Doné SC, Leibiger IB, Efendiev R, Katz AI, Leibiger B, Berggren PO, Pedemonte CH, Bertorello AM. Tyrosine 537 within the Na+,K+-ATPase alpha-subunit is essential for AP-2 binding and clathrin-dependent endocytosis. J Biol Chem. 2002 May 10;277(19):17108-11.

Dostanic-Larson I, Van Huysse JW, Lorenz JN, Lingrel JB. The highly conserved cardiac glycoside binding site of Na,K-ATPase plays a role in blood pressure regulation. Proc Natl Acad Sci U S A. 2005 Nov 1;102(44):15845-50.

Drust DS, Creutz CE.Aggregation of chromaffin granules by calpactin at micromolar levels of calcium. Nature. 1988 Jan 7;331(6151):88-91.

Dunaevsky A, Connor EA. F-Actin Is Concentrated in Nonrelease Domains at Frog Neuromuscular Junctions. The Journal of Neuroscience, 2000, 20(16):6007-6012.

Dvorak AM, Kohn S, Morgan ES, Fox P, Nagy JA, Dvorak HF. The vesiculo-vacuolar organelle (VVO): a distinct endothelial cell structure that provides a transcellular pathway for macromolecular extravasation. J Leukoc Biol 1996, 59: 100–115.

Edwards KA, Demsky M, Montague RA, Weymouth N, Kiehart DP.GFP-moesin illuminates actin cytoskeleton dynamics in living tissue and demonstrates cell shape changes during morphogenesis in Drosophila. Dev Biol. 1997 Nov 1;191(1):103-17.

Edwards SD, Keep NH. The 2.7 A crystal structure of the activated FERM domain of moesin: an analysis of structural changes on activation. Biochemistry. 2001;40:7061–8.

Egea G, Lazaro-Dieguez F, and Vilella M. Actin dynamics at the Golgi complex in mammalian cells. Curr. Opin. Cell Biol. 2006, 18: 168-178.

Eitzen G, et al. Remodeliing of organelle-bound actin is required for yeast vacuole fusion. J Cell Biol, 2002, 158 (4): 669-679.

Elvevold K, Smedsrod B, Martinez I. The liver sinusoidal endothelial cell: a cell type of controversial and confusing identity. Am J Physiol Gastrointest Liver Physiol 2008, 294: 391–400.

Emans N, Gorvel JP, Walter C, Gerke V, Kellner R, Griffiths G, Gruenberg J. Annexin II is a major component of fusogenic endosomal vesicles. J Cell Biol. 1993, 120(6):1357-69.

Engelhardt B. K. Wollburg-Buchholze, H Wolburg. Involvement of the choroid plexus in central nervous system inflammation. Microsc Res Tech, 2001, 52(1): 112-29.

Esser S, Wolburg K, Wolburg H, Breier G, Kurzchalia T, Risau W. Vascular endothelial growth factor induces endothelial fenestrations in vitro. J Cell Biol, 1998, 140: 947–959.

Evan AP, Luft FC. Effect of alloxan-induced diabetes on the glomerular filtration barrier of the rat. Ren Physiol 1980, 3: 257–264.

Feng D, Nagy JA, Ultrastructural studies, 1999.

Feng D, Nagy JA, Ultrastructural studies, 2002.

Feng D, Nagy JA, Hipp J et al. Reinterpretation of endothelial cell gaps induced by vasoactive mediators in guinea-pig, mouse and rat: many are transcellular pores. J Physiol. 1997, 504(P3):747–761.

Fievet BT, Gautreau A, Roy C, Del Maestro L, Mangeat P, Louvard D, Arpin M. Phosphoinositide binding and phosphorylation act sequentially in the activation mechanism of ezrin. J Cell Biol. 2004 Mar 1;164(5):653-9.

Fiévet BT, Louvard D, Arpin M, ERM proteins in epithelial cell organization and functions, Biochem. Biophys. Acta. 2007, 1773: 653–660.

Filipenko NR, Waisman DM The C-terminus of annexin II mediates binding to F-actin. J Biol Chem, 2001, 276:5310–5315.

Florey, HW. The endothelial cells. Brit. Med. J. 1966, 1: 487–490.

Folkman, J. and Haudenschild C, Angiogenesis in vitro. Nature, 1980, 288(5791): 551-6.

Franck Z., Gary R. and Bretscher A. Moesin, like ezrin, colocalizes with actin in the cortical cytoskeleton in cultured cells, but its expression is more variable. J. Cell Sci. 1993, 105: 219-231.

Fraser R, Bosanquet AG, Day WA. Filtration chylimicrons by the liver may influence cholesterol metabolism and atherosclerosis. Atherosclerosis, 1978, 29: 113-3.

Fraser R, Clark SA, Bowler LM, Day WA. Pantethine inhibites diet-induced hypercholeterollaemia by dilating the liver sieve. N Z Med J 1988, 101:86-87.

Fraser R, Clark SA, Bowler LM, Murray FEM, Wakasugi J, Ishihara M, Tomikawa M. The opposite effects of nicotine and pantethine on the porosity of the liver sieve and lipoprotein metabolism. In: Cells of the Hepatic Sinuisoid 2 (Edited by: Wisse E, Knook DL, Decker K) Leiden, Kupper Cell Foundation,1989, p335-338.

Fraser R, Clark SA, Day WA, Murray FEM. Nocotine decreases the porosity of the rat liver sieve: a possible mechanism for hypercholesterolaemia Br J Exp Pathol 1988, 69: 345-350.

Fraser R, Day WA, Fernando NS. Athrosclerosis and the liver sieve. In Cells of the Hepatic Sinusoid I (Edited by Kim A, Knnok DL, Wisse E) Rijiswijk, Kupper Cell Foundation, 1986, 317-322.

Fraser R, Dobbs BR, Rogers GWT. Lipoprotein and the liver sieve: the role of the fenestrated sinusoidal endothelium in lipoprotein metabolism, athrosclerosis, and cirrhosis. Hepatology, 1995, 21: 863-874.

Fraser R, Heslop VR, Murray FE, Day WA: Ultrastructural studies of the portal transport of fat in chickens. Br J Exp Pathol 1986, 67:783-791.

Furchgott RF and Zawadzki JV, The obligatory role of endothelial cells in the relaxation of arterial smooth muscle by acetylcholine, Nature, Lond. 1980, 288: 373–376.

Furchgott RF, Role of endothelium in response of vascular smooth muscle, Circulation Res. 1983, 53: 557–573.

Furuya S. Ultrastructure and formation of diaphragmed fenestrae in cultured endothelial cells of bovine adrenal medulla. Cell Tissue Res. 1990, 261:97–105.

Futter CE, and White IJ. Annexins and endocytosis. Traffic 2007, 8(8): 951–958.

Futterman, S. Metabolism and Photochemistry in the Retina, in Adler's Physiology of the Eye, 6th edition, ed. R.A. Moses. St. Louis: C.V. Mosby Company, 1975, p406-419.

Gallicchio MA, Bach LA.Advanced glycation end products inhibit Na+ K+ ATPase in proximal tubule epithelial cells: role of cytosolic phospholipase A2alpha and

phosphatidylinositol 4-phosphate 5-kinase gamma. Biochim Biophys Acta. 2010 Aug;1803(8):919-30.

Gates J and and Peifer M. Can 1000 reviews be wrong? Actin, alpha-Catenin, and adherens junctions. Cell Vol. 2005, 123: 769-772.

Gautier A, Bernhard W, Oberling C. Sur I'exsitence d'un appareli lacunaria pericpillarie du glomerule de Malpighi, revele par la microscopie electrinique. Competes rendus de la séances de la Societe de Biologie. 1950, 144: 1605-7.

Gerke V, Moss SE. Annexins: From structure to function. Physiol Rev 2002, 82:331–371.

Ghitescu LD, Crine P, Jacobson BS. Antibodies specific to the plasma membrane of rat lung microvascular endothelium. Exp Cell Res. 1997, 232: 47–55.

Glacy SD. Subcellular distribution of rhodamine–actin microinjected into living fibroblastic cells. J. Cell Biol. 1983, 97: 1207–1213

Goodman SR, et al. Identification of a spectrin-like protein in nonerythroid cells. Proc Natl Acad Sci U S A. 1981, 78:7570–7574.

Goodman SR, Krebsb KE, Whitfield CF, Riederer BM, Zagon IS. Kay MMB. Spectrin and Related Molecules. Biochemistry and Molecular Biology, 1988, 23 (2): 171 – 234.

Goodman SR. Discovery of nonerythroid spectrin to the demonstration of its key role in synaptic transmission. Brain Res Bull. 1999, 50:345–346.

Gorga FR, Riney CE, Benjamin TL.Inositol trisphosphate levels in cells expressing wild-type and mutant polyomavirus middle T antigens: evidence for activation of phospholipase C via activation of pp60c-src. J Virol. 1990, 64(1):105-12.

Govind S, Kozma R, Monfries C, Lim L, Ahmed S.Cdc42Hs facilitates cytoskeletal reorganization and neurite outgrowth by localizing the 58-kD insulin receptor substrate to filamentous actin. J Cell Biol. 2001 Feb 5;152(3):579-94.

GrandPre T, Nakamura F, Vartanian T, Strittmatter SM, Identification of the Nogo inhibitor of axon regeneration as a Reticulon protein, Nature 2000, 403: 439–444.

Grangerd N, Grangerj P, Brace RA, Parkerr E and Taylor,A AE. Analysisof the permeability characteristics of intestinal capillaries. Circ. Res. 1979, 44: 335-344.

Haas M, Wang H, Tian J, Xie Z. Src-mediated inter-receptor cross-talk between the Na^+/K^+-ATPase and the epidermal growth factor receptor relays the signal from ouabain to mitogen-activated protein kinases. J Biol Chem. 2002 May 24; 277(21):18694-702.

Hall PV, Proc. V. Ann. Conf. Nephrotic Syndrom, New York, The National Nephrosis Foundation, Inc, 1954.1.

Hamada K, Seto A, Shimizu T, Matsui T, Takai Y, Tsukita S, Tsukita S, Hakoshima T.

Hamada K, Seto A, Shimizu T, Matsui T, Takai Y, Tsukita S, Tsukita S, Hakoshima T. Han X, Wang CT, Bai J, Chapman ER, Jackson MB. Transmembrane segments of syntaxin line the fusion pore of Ca2+-triggered exocytosis. Science , 2004, 304 (5668): 289–92.

Hanks SK, M. B. Calalb MB, Harper MC, and Patel SK. Focal adhesion protein-tyrosine kinase phosphorylated in response to cell attachment to fibronectin. Proc. Natl. Acad. Sci. USA 1992, 89:8487–8491.

Hansko R, Frank PG, Ben-Jonathan N, Lisanti MP. PV-1 is negatively regulated by VEGF in the lung of caveolin-1, but not caveolin-2, null mice. Cell Cycle 2006, 5: 2012–2020.

Harder T, Kellner R, Parton RG and Gruenberg J. Specific release of membrane-bound annexin II and cortical cytoskeletal elements by sequestration of membrane cholesterol. The American Society for Cell Biology, 1997; 8(3), 533-545.

Harvey T. McMahon1 & Jennifer L. Gallop. Review Article Membrane curvature and mechanisms of dynamic cell membrane remodeling. Nature, 2005, 438: 590-596.

Harvey W. Exercitation Anatomica de Motu Cordis et Sanguintis in Animalibus. Everymans'd library, 1908: London, J.M. Dent &Co,; New York, E.P. Dutton &Co.

Hawkins PT, Anderson KE, K. Davidson K, Stephens LR. Signalling through Class I PI3Ks in mammalian cells Biochemical Society Transactions, 2006, 34 (5): 647-662.

Hayes MJ, Merrifield CJ, Shao D, Ayala-Sanmartin J, Schorey CD, Levine TP, Proust J, Curran J, Bailly M, Moss SE. Annexin 2 binding to phosphatidylinositol 4,5-bisphosphate on endocytic vesicles is regulated by the stress response pathway. J Biol Chem. 2004 Apr 2;279(14):14157-64.

Hayes MJ, Moss SE. Annexin 2 has a dual role as regulator and effector of v-Src in cell transformation. J Biol Chem. 2009, 284(15):10202-10.

Hayes MJ, Shao D, Bailly M, Moss SE. Regulation of actin dynamics by annexin 2. EMBO J. 2006 May 3;25(9):1816-26.

Haynes J, Srivastava J, Madson N, Wittmann T, Barber DL.Dynamic actin remodeling during epithelial-mesenchymal transition depends on increased moesin expression. Mol Biol Cell. 2011 Dec;22(24):4750-64.

Heath, JP and Holifield, BF. On the mechanisms of cortical actin flow and its role in cytoskeletal organization of fibroblasts. Symp. Soc. Exp. Biol. 1993, 47:35–56.

Heimann K, et al. Specific isoforms of actin-binding proteins on distinct populations of Golgi-derived vesicles. J Biol Chem. 1999, 274:10743–10750.

Heiska L, Alfthan K, Gronholm M, Vilja P, Vaheri A, Carpen O. Association of ezrin with intercellular adhesion molecule-1 and -2 (ICAM-1 and ICAM-2). Regulation by phosphatidylinositol 4, 5- bisphosphate. J Biol Chem. 1998;273:21893–900

Heltianu C, Bogdan I, Constantinescu E, Simionescu M. Endothelial cells express a spectrin-like cytoskeletal protein. Circ Res. 1986 Apr;58(4):605-10.

Heltianu C, et al. Endothelial cells express a spectrin-like cytoskeletal protein. Circ Res. 1986, 58: 605–610.

Henkind, P., Hansen, R.I., Szalay, J. Ocular Circulation, in Physiology of the Human Eye and the Visual System, ed. R.R. Records. Maryland: Harper & Row Publishers, 1979, p98-155 and p119.

Hipfner DR, Keller N, Cohen SM. Slik Sterile-20 kinase regulates Moesin activity to promote epithelial integrity during tissue growth. Genes Dev. 2004 Sep 15;18(18):2243-8.

Hoeflich KP, Tsukita S, Hicks L, Kay CM, Ikura M. Insights into a single rod-like helix in activated radixin required for membrane-cytoskeletal cross-linking. Biochemistry. 2003, 42:11634–41.

Horisberger JD, Lemas V, Kraehenbühl JP, Rossier BC. Structure-function relationship of Na,K-ATPase. Annu Rev Physiol. 1991;53:565-84.

Ichimura K, Stan RV, Kurihara H, Sakai T. Glomerular endothelial cells form diaphragms during development and pathologic conditions. J Am Soc Nephrol 2008, 19: 1463–1471.

Ichiro Shiojima, Kenneth Walsh Role of Akt Signalling in Vascular Homeostasis and Angiogenesis. Circulation Research. 2002, 90: 1243-1250

Ida H, Ishibashi K, Reiser K, Hjelmeland LM, Handa JT Ultrastructural aging of the RPE-Bruch's membrane-choriocapillaris complex in the D-galactose-treated mouse. Invest Ophthalmol Vis Sci. 2004, 45(7):2348-54.

Ioannidou S, Deinhardt K, Miotla J, Bradley J, Cheung E, Samuelsson S, Ng YS, Shima DT. An in vitro assay reveals a role for the diaphragm protein PV-1 in endothelial fenestra morphogenesis. Proc Natl Acad Sci USA, 2006, 103: 16770–16775.

Ioannidou S. Structural and functional analysis of vascular permeability. PhD Thesis at UCL, 2005.

Irie T, Fukunaga K, Pitha J. Hydroxypropylcyclodextrins in parenteral use. I: Lipid dissolution and effects on lipid transfers in vitro. J Pharm Sci. 1992 Jun;81(6):521-3.

Ishibashi T, Inomata H. Ultrastructure of retinal vessels in diabetic patients. Br J Ophthalmol. 1993 Sep;77(9):574-8.

Jaffe AB, Hall A. Rho GTPases: biochemistry and biology. Annu Rev Cell Dev Biol. 2005;21:247-69.

Jahn R, Scheller RH. SNAREs: Engines for membrane fusion. Nat Rev Mol Cell Biol 2006, 7: 631–643.

Jankovics F, Sinka R, Lukácsovich T, Erdélyi M. MOESIN crosslinks actin and cell membrane in Drosophila oocytes and is required for OSKAR anchoring. Curr Biol. 2002 Dec 10;12(23):2060-5.

Jena BP. Secretion machinery at the cell plasma membrane. Curr Opin Struct Biol 2007, 17: 437–443.

Jeon S, Park JK, Bae CD, Park J.NGF-induced moesin phosphorylation is mediated by the PI3K, Rac1 and Akt and required for neurite formation in PC12 cells. Neurochem Int. 2010, 56(6-7): 810-8.

Jo´sko J, Gwó´zd´z B, Hendryk S, Jedrzejowska-Szypu ka H, S owi-´nski J, Jochem J: Expression of vascular endothelial growth factor (VEGF) in rat brain after subarachnoid haemorrhage and endothelin receptor blockage with BQ-123. Folia Neuropathol, 2001, 39: 243-251.

Job C, Lagnado L. Calcium and protein kinase C regulate the actin cytoskeleton in the synaptic terminal of retinal bipolar cells. J Cell Biol 1998, 143:1661–1672.

Johnson, C., And Hanson, K. M. Capillary filtration in the small intestine of the dog. Circ. Res. 1966, 19: 766-773.

Johnsson N, Johnsson K, Weber K (1988). "A discontinuous epitope on p36, the major substrate of src tyrosine-protein-kinase, brings the phosphorylation site into the neighbourhood of a consensus sequence for Ca2+/lipid-binding proteins.". *FEBS Lett.* 236 (1): 201–4.

Jones SM, Howell KE, Henley JR, Cao H, McNiven MA.Role of dynamin in the formation of transport vesicles from the trans-Golgi network. Science. 1998 Jan 23; 279(5350):573-7.

Jones SM, Howell KE, Henley JR, Cao H, McNiven MA.Role of dynamin in the formation of transport vesicles from the trans-Golgi network. Science. 1998, 279(5350):573-7.

Kaibuchi K, Kuroda S, Amano M. Regulation of the cytoskeleton and cell adhesion by the Rho family GTPases in mammalian cells. Annu Rev Biochem. 1999;68:459-86.

Kamba T, Tam BY, Hashizume H, Haskell A, Sennino B, Mancuso MR, Norberg SM, O'Brien SM, Davis RB, Gowen LC, Anderson KD, Thurston G, Joho S, Springer ML, Kuo CJ, McDonald DM. VEGF-dependent plasticity of fenestrated capillaries in the normal adult microvasculature. Am J Physiol Heart Circ Physiol 2006, 290: 560–576.

Kaplan JH, Biochemistry ofNa, K-ATPase, Annu. Rev. Biochem. 71 (2002) 511–535.

Kaplan JH.The sodium pump and hypertension: a physiological role for the cardiac glycoside binding site of the Na,K-ATPase. Proc Natl Acad Sci U S A. 2005 Nov 1;102(44):15723-4.

Katso R, Okkenhaug K, Ahmadi K, White S, Timms J, Waterfield MD. (2001). Cellular function of phosphoinositide 3-kinases: implications for development, homeostasis, and cancer. Ann Rev Cell Dev Biol 17: 615–675.

Keith A. Gottlieb andLuis P. Natural Biology of Polyomavirus Middle T Antigen Microbiol. Mol. Biol. Rev. June 2001 vol. 65 no. 2 288-318.

Kim M, Jung J, Park CS, Lee K.Identification of the cofilin-binding sites in the large cytoplasmic domain of Na,K-ATPase. Biochimie. 2002 Oct;84(10):1021-9.

Kiseleva E, Morozova KN, Voeltz GK, Allen TD, Goldberg MW.Reticulon 4a/NogoA locates to regions of high membrane curvature and may have a role in nuclear envelope growth. J Struct Biol. 2007, 160(2):224-35.

Kitajiri S, Fukumoto K, Hata M, Sasaki H, Katsuno T, Nakagawa T, Ito J, Tsukita S, Tsukita S. Radixin deficiency causes deafness associated with progressive degeneration of cochlear stereocilia. J Cell Biol. 2004 Aug 16;166(4):559-70.

Kizhatil K, Yoon W, Mohler PJ, Davis LH, Hoffman JA, et al. Ankyrin-G and beta2-spectrin collaborate in biogenesis of lateral membrane of human bronchial epithelial cells. J Biol Chem. 2007;282:2029–2037.

Kobayashi M, Takaya S, Koie H, Nagai K. Glomerular endothelial changes in cyclosporine A-treated rats: scanning and transmission electron microscopic studies. Jpn J Surg 1991, 21: 210–215.

Kraemer DM, Strizek B, Meyer HE, Marcus K, Drenckhahn D.Kidney Na+,K(+)-ATPase is associated with moesin. Eur J Cell Biol. 2003 Feb;82(2):87-92.

Kremer JR, Mastronarde DN, McIntosh JR.Computer visualization of three-dimensional image data using IMOD. J Struct Biol. 1996 Jan-Feb;116(1):71-6.

Krupinski T, Beitel GJ.Unexpected roles of the Na-K-ATPase and other ion transporters in cell junctions and tubulogenesis. Physiology (Bethesda). 2009 Jun;24:192-201.

Kunda P, Pelling AE, Liu T, Baum B.Moesin controls cortical rigidity, cell rounding, and spindle morphogenesis during mitosis. Curr Biol. 2008 Jan 22;18(2):91-101.

Lambert O, Gerke V, Bader MF, Porte F, Brisson A.Structural analysis of junctions formed between lipid membranes and several annexins by cryo-electron microscopy. J Mol Biol. 1997 Sep 12;272(1):42-55.

Lankes WT, Furthmayr H, Moesin: a member of the protein 4.1-talinezrin family of proteins, Proc. Natl. Acad. Sci. U. S. A. 1991, 88: 8297–8301.

Larre I, Lazaro A, Contreras RG, Balda MS, Matter K, Flores-Maldonado C, Ponce A, Flores-Benitez D, Rincon-Heredia R, Padilla-Benavides T, Castillo A, Shoshani L, Cereijido M.Ouabain modulates epithelial cell tight junction. Proc Natl Acad Sci U S A. 2010 Jun 22;107(25):11387-92.

Lazarides E, Hubbard BD. Immunological characterization of the subunit of the 100 A filaments from muscle cells. Proc. Natl. Acad. Sci. U.S.A. 1976, 73 (12): 4344–8.

Lázaro-Diéguez F and Egea G. Comparative study of the impact of the actin cytoskeleton on cell shape and membrane surface in mammalian cells in response to actin toxins. Modern Research and Educational Topics in Microscopy, 2007, 362-369.

Ledesma MD, Dotti CG.Membrane and cytoskeleton dynamics during axonal elongation and stabilization. Int Rev Cytol. 2003;227:183-219.

Lengyel I, Tufail A, Hosaini HA, Luthert P, Bird AC, Jeffery G. Association of drusen deposition with choroidal intercapillary pillars in the aging human eye. Invest Ophthalmol Vis Sci. 2004, 45(9):2886-92.

Levick JR and Smaje LH. An Analysis of the Permeability of a Fenestra. Microvascular Research 1987, 33, 233-256.

Li Q, Nance MR, Kulikauskas R, Nyberg K, Fehon R and Karplus PA. Self-masking in an intact ERM-merlin protein: An active role for the central α-helical domain, J. Mol. Biol. 2007, 365: 1446–1459.

Li Z, Xie Z.The Na/K-ATPase/Src complex and cardiotonic steroid-activated protein kinase cascades. Pflugers Arch. 2009 Jan;457(3):635-44.

Lim D, Lange K, Santella L. Activation of oocytes by latrunculin A. FASEB J. 2002 Jul;16(9):1050-6.

Litman P, Amieva MR, Furthmayr H.Imaging of dynamic changes of the actin cytoskeleton in microextensions of live NIH3T3 cells with a GFP fusion of the F-actin binding domain of moesin. BMC Cell Biol. 2000;1:1.

Liu L, Zhao X, Pierre SV, Askari A. Association of PI3K-Akt signalling pathway with digitalis-induced hypertrophy of cardiac myocytes Am J Physiol Cell Physiol. 2007 Nov;293(5):C1489-97

Liu SC, Derick LH, Palek J. Visualization of the Hexagonal Lattice in th Erythrocyte Membrane Skeleton. The Journal of Cell Biology, Volume 104, March 1987, 527-536.

Liu SC, Zhai S, Palek J, Golan DE, Amato D, Hassan K, Nurse GT, Babona D, Coetzer T, Jarolim P, et al.Molecular defect of the band 3 protein in southeast Asian ovalocytosis. N Engl J Med. 1990 Nov 29;323(22):1530-8.

Llena JF, Cespedes G, Hirano A, Zimmerman HM, Feiring EH, Fine D. Vascular alterations in delayed radiation necrosis of the brain. An electron microscopical study. Arch Pathol Lab Med. 1976, 100(10):531-4.

Lombardi, T, et al., In vitro modulation of endothelial fenestrae: opposing effects of retinoic acid and transforming growth factor beta. J Cell Sci, 1988. 91 (Pt 2):313-8.

Lombardi, T, R. Montesano, and L. Orci, Phorbol ester induces diaphragmed fenestrae in large vessel endothelium in vitro. Eur J Cell Biol, 1987. 44(1): 86-89.

Lombardi, T. et al. Endothelial diaphragmed fenestrae: in vitro modulation by phorbol myristate acetate. J Cell Biol, 1986. 102(5):1965-70.

Lupas A. Prediction and analysis of coiled-coil structures. Methods Enzymol. 1996, 266: 513-525.

Lupulescu A, The role of Vitamine A, beta-carotene E and C in cancer cell biology. Int J Vitam Nutr Res 1994, 64: 3-14.

Lux SE. Spectrin-actin membrane skeleton of normal and abnormal red blood cells. Semin Hematol. 1979 Jan;16(1):21-51.

MacGregor LC, Matschinsky FM. (1986) Altered retinal metabolism in diabetes. II. Measurement of sodium-potassium ATPase and total sodium and potassium in individual retinal layers. J Biol Chem 261:4052–4058.

Macia E, Ehrlich M, Massol R, Boucrot E, Brunner C, Kirchhausen T. Dynasore, a cell-permeable inhibitor of dynamin. Dev Cell. 2006, 10(6):839-50.

Mackay DJ, Esch F, Furthmayr H, Hall A.Rho- and rac-dependent assembly of focal adhesion complexes and actin filaments in permeabilized fibroblasts: an essential role for ezrin/radixin/moesin proteins. J Cell Biol. 1997 Aug 25;138(4):927-38.

Majno G, Shea SM, Leventhal M. Endothelial contraction induced by histamine-type mediators: an electron microscopic study. J Cell Biol. 1969, 42:647–672.

Mann, G. E., Smaje, L. H., And Yudilevich, D. Permeability of the fenestrated capillariesin the cat submandibular gland to lipid-insoluble molecules. J. Physiol. 1979, 297: 335-354.

Marieb E and Hoehn K, Human anatomy and Physiology, the 7th edition, 2007. p601.

Martens S, McMahon HT.Mechanisms of membrane fusion: disparate players and common principles. Nat Rev Mol Cell Biol. 2008 Jul;9(7):543-56.

Mastronarde DN. Dual-axis tomography: an approach with alignment methods that preserve resolution. J Struct Biol. 1997 Dec;120(3):343-52.

Matsui T, Yonemura S, Tsukita S, Tsukita S. Activation of ERM proteins in vivo by Rho involves phosphatidyl-inositol 4-phosphate 5-kinase and not ROCK kinases. Curr Biol. 1999 Nov 4;9(21):1259-62.

Mayran N, Parton RG, Gruenberg J. Annexin II regulates multivesicular endosome biogenesis in the degradation pathway of animal cells. The EMBO Journal, 2003, 22 (13): 3242-3253.

McDonald KL & Auer M (2006) High-pressure freezing, cellular tomography and structural cell biology, Biotechniques 41: 137, 139, 141.

McLaughlin S, Wang J, Gambhir A, Murray D.PIP(2) and proteins: interactions, organization, and information flow. Annu Rev Biophys Biomol Struct. 2002;31:151-75.

Merrifield CJ, Moss SE, Ballestrem C, Imhof BA, Giese G, Wunderlich I, Almers W.Endocytic vesicles move at the tips of actin tails in cultured mast cells. Nat Cell Biol. 1999 May;1(1):72-4.

Meyer-Lehnert H, Wanning C, Michel H, Bäcker A, Kramer HJ. Cellular mechanisms of action of a ouabain-like factor in vascular smooth-muscle cells. J Cardiovasc Pharmacol. 1993;22 Suppl 2:S16-9.

Michael R. Logan and Craig A. Mandato. Regulation of the actin cytoskeleton by PIP2 in cytokinesis. Biol. Cell 2006, 98: 377–388

Milici AJ, Furie MB, and Carley WW, The formation of fenestrations and channels by capillary endothelium in vitro. Proc Natl Acad Sci U S A, 1985, 82(18): 6181-5.

Mitchison TJ and Cramer LP. Actin based cell motility and cell loco motion. Cell 1996, 84: 371-379.

Moesin and its activating kinase Slik are required for cortical stability and microtubule organization in mitotic cells. J Cell Biol. 2008 Feb 25;180(4):739-46.

Molnar C, de Celis J. Independent roles of Drosophila Moesin in imaginal disc morphogenesis and hedgehog signalling. Mech. Dev. 2006, 123: 337–351.

Moncada S,Herman AG, Higgs EA, Vane JR. Differential formation of prostacyclin (PGX or PGI2) by layers of the arterial wall. An explanation for the anti-thombotic properties of vascular endothelium. Thromb. Res. 1977c, 11: 323–344.

Morales M, Cilicos MA, Goda Y. Actin-dependent regulation of neurotransmitter release at central synapses. Neuron, 2000, 27(3): 539-550.

Muallem S. Kwiatkowska K, Xin Xu X, and Yin HL. Actin Filament Disassembly Is a Sufficient Final Trigger for Exocytosis in Nonexcitable Cells. The Journal of Cell Biology, 1995, 128 (4): 589-598.

Mundy DI, Machleidt T, Ying YS, Anderson RG, Bloom GS. Dual control of caveolar membrane traffic by microtubules and the actin cytoskeleton. J Cell Sci. 2002, 15;115(Pt 22):4327-39.

Nagai T, Yokomori H, Yoshimura K, Fujimaki K, Nomura M, Hibi T, Oda M. Actin filaments around endothelial fenestrae in rat hepatic sinusoidal endothelial cells. Med Electron Microsc. 2004 Dec;37(4):252-5.

Nagy JA, Benjamin L, Zeng H, Dvorak AM, Dvorak HF. Vascular permeability, vascular hyperpermeability and angiogenesis. Angiogenesis. 2008, 11(2):109-19.

Nagy JA, Feng D, Vasile E, Wong WH, Shih SC, Dvorak AM, Dvorak HF.Permeability properties of tumor surrogate blood vessels induced by VEGF-A. Lab Invest. 2006, 86(8):767-80.

Naito M, Wisse E. Effect of endothelial fenestrations on chylomicron transport in neonatal rat liver sinusoids. Cell Tissue Res. 1978, 190(3):371-82.

Nelson WJ, Veshnock PJ, Ankyrin binding to (Na++K+)ATPase and implications for the organization of membrane domains in polarized cells, Nature, 1987, 328: 533–536.

Neuhardt T, May CA, Wilsch C, Eichhorn M, Lütjen-Drecoll E. Morphological changes of retinal pigment epithelium and choroid in rd-mice. Exp Eye Res. 1999, 68(1):75-83.

Nielsen s, Agre P, The aquaporin family of water channels in kidney. Kidney Int 1995, 48: 1057-1068.

Niggli V, Andréoli C, Roy C, Mangeat P. Identification of a phosphatidylinositol-4,5-bisphosphate-binding domain in the N-terminal region of ezrin. FEBS Lett. 1995 Dec 4;376(3):172-6.

Niggli V, Rossy J. Ezrin/radixin/moesin: Versatile controllers of signalling molecules and of the cortical cytoskeleton. The International Journal of Biochemistry & Cell Biology 2008, 40: 344–349.

Orci L, Gabby KH, Lalaisse WJ. Pabcreatic beta-cell web: its possible role in insulin secretion. Science, 1972, 175(26): 1128-1130.

Ottlecz A, Bensaoula T.Captopril ameliorates the decreased Na+,K(+)-ATPase activity in the retina of streptozotocin-induced diabetic rats. Invest Ophthalmol Vis Sci. 1996 Jul;37(8):1633-41.

Palade GE, Simionescu M and Simionescu N, Differentiated microdomains in the vascular endothelium. In: M.L. Nossel and M.J. Vogel, Editors, Pathobiology of the Endothelial Cell, Academic Press, New York, 1982.

Palade GE. 1953. Fine Structure of Blood Capillaries. J. Appl.Phys. 1953, 24: 1424.

Palade, GE, Transport in quanta across the endothelium of blood capillaries. Anat Rec, 1960. 136: 254.

Pallon TL. Aquaporin 1, Urea Transporters, and Renal Vascular Bundles. J Am Soc Nephrol, 2007, 18: 2798–2800.

Palmer MJ, Ashton DS and Moncada S, Vascular endothelial cells synthesize nitric oxide from l-arginine, Nature, Lond. 1988, 327: 524–526.

Palmer MJ, Ferrige AG and S. Moncada S, Nitric oxide release accounts for the biological activity of endothelium-derived relaxing factor, Nature, Lond. 1987, 327: 524–526.

Pappas GP, Sagen J. Fine structural correlates of vascular permeability of chromaffin cell transplants in CNS pain modulatory regions. Exp Neurol. 1988, 102: 280–9.

Park S, Chapuis N, Tamburini J, Bardet V, CornilletLefebvre P, Willems L, Green A, Mayeux P, Lacombe C, and Bouscary D. Role of the PI3K/AKT and mTOR signalling pathways in acute myeloid leukemia. Haematologica 2010, 95: 819-828.

Pataky F, Pironkova R, Hudspeth AJ. Radixin is a constituent of stereocilia in hair cells. Proc Natl Acad Sci U S A. 2004 Feb 24;101(8):2601-6.

Pauleikhoff D, Barondes MJ, Minassian D, Chisholm IH, Bird AC. Drusen as risk factors in age-related macular disease. Am J Ophthalmol. 1990, 109:38–43.

Pearson MA, Reczek D, Bretscher A, Karplus PA. Structure of the ERM protein moesin reveals the FERM domain fold masked by an extended actin binding tail domain. Cell. 2000, 101:259–70.

Pease DC, Electron microscopy of the vascular bed of the kidney cortex. Anat Rec, 1955, 121(4): 701-21.

Perrotta S, Gallagher PG, Mohandas N. Hereditary spherocytosis. Lancet. 2008 Oct 18;372(9647):1411-26.

Pinder JC, Ungewickell E, Bray D, Gratzer WB.The spectrin-actin complex and erythrocyte shape. J Supramol Struct. 1978;8(4):439-45.

Pino RM, Essner E. Structure and permeability to ferritin of the choriocapillary endothelium of the rat eye. Cell Tissue Res. 1980, 208 (1): 21-7.

Pino RM, The cell surface of a restrictive fenestrated endothelium. I. Distribution of lectin-receptor monosaccharides on the choriocapillaris. Cell Tissue Res. 1986, 243: 145-155.

Pino RM. Binding and endocytosis of heparin-gold conjugates by the fenestrated endothelium of the rat choriocapillaris. Cell Tissue Res. 1987 Nov;250(2):257-66.

Pitha J, Irie T, Sklar PB, Nye JS. Drug solubilizers to aid pharmacologists: amorphous cyclodextrin derivatives. Life Sci. 1988;43(6):493-502.

Polesello C, Payre F. Small is beautiful: what flies tell us about ERM protein function in development. Trends Cell Biol. 2004;14:294–302.

Pradhan D, et al. alpha-Catenin binds directly to spectrin and facilitates spectrin-membrane assembly in vivo. J Biol Chem. 2001, 276:4175–4181.

Pratt BM, et al. Mechanisms of cytoskeletal regulation. Modulation of aortic endothelial cell spectrin by the extracellular matrix. Am J Pathol. 1984, 117:349–354.

Rajasekaran AK, Rajasekaran SA. Role of Na-K-ATPase in the assembly of tight junctions. Am J Physiol Renal Physiol, 2003, 285: 388–396.

Rajasekaran SA, Barwe SP, Rajasekaran AK.Multiple functions of Na,K-ATPase in epithelial cells. Semin Nephrol. 2005 Sep;25(5):328-34.

Rajasekaran SA, Rajasekaran AK. Na,K-ATPase and epithelial tight junctions. Front Biosci. 2009 Jan 1;14:2130-48.

Ramamurthi KS, Losick R. Negative membrane curvature as a cue for subcellular localization of a bacterial protein. Proc Natl Acad Sci U S A. 2009 Aug 11;106(32):13541-5.

Rand JH. Antiphospholipid antibody-mediated disruption of the annexin-V antithrombotic shield: a thrombogenic mechanism for the antiphospholipid syndrome. J Autoimmun. 2000 Sep;15(2):107-11.

Rappoport JZ, Heyman KP, Kemal S, Simon SM (2008) Dynamics of Dynamin during Clathrin Mediated Endocytosis in PC12 Cells. PLoS ONE, 2008, 3(6): e2416.

Reczek D, Bretscher A. The carboxyl-terminal region of EBP50 binds to a site in the amino- terminal domain of ezrin that is masked in the dormant molecule. J Biol Chem. 1998;273:18452–8.

Reddig PJ and Juliano RL. Clinging to life: cell matrix adhesion and cell survival. Cancer Metastasis Rev. 2005, 24: 425-439.

Reeves W, Kanwa Y and Farquhar M, Assembly of the glomerular filtration surface: Differentiation of anionic sites in glomerular capillaries of newborn rat kidney. J. Cell Biol. 1980, 85: 735–753.

Rescher, U., Ruhe, D., Ludwig, C., Zobiack, N. & Gerke, V. Annexin 2 is a phosphatidylinositol (4,5)-bisphosphate binding protein recruited to actin assembly sites at cellular membranes. J. Cell Sci. 117, 3473–3480 (2004).

Rhodin JA, The diaphragm of capillary endothelial fenestrations. J Ultrastruct Res. 1962, 6: 171-85.

Risau W. Differentiation of endothelium. FASEB J. 1995, 9(10):926-33.

Risau W. Induction of blood-brain barrier endothelial cell differentiation. Ann N Y Acad Sci. 1991;633:405-19.

Risau, W, Flame I: Vasculogenesis. Annu Rev Cell Dev Biol 1995, 11: 73–91.

Roberts WG, Palade GE. Endothelial fenestrae and fenestral diaphragms. In: Morphogenesis of Endothelium, edited by Risau W and Rubanyi GM. Amsterdam, The Netherlands: Harwood Academic, 2000, p23–41.

Roberts WG, Palade GE. Increased microvascular permeability and endothelial fenestration induced by vascular endothelial growth factor. J Cell Sci. 1995, 108 (Pt 6):2369-79.

Roberts WG, Palade GE. Neovasculature induced by vascular endothelial growth factor is fenestrated. Cancer Res 1997, 57: 765–772.

Rodal SK, Skretting G, Garred O, Vilhardt F, van Deurs B, Sandvig K. Extraction of cholesterol with methyl-beta-cyclodextrin perturbs formation of clathrin-coated endocytic vesicles. Mol Biol Cell. 1999 Apr;10(4):961-74.

Rogers GWT, Dobbs BR, Fraser R. Decreased hepatic uptake of cholesterol and retinol in the dimethylnitrosamine rat model of cirrhosis. Liver, 1992, 12: 326-329.

Rostgaard J, and Qvortrup K, Electron microscopic demonstrations of filamentous molecular sieve plugs in capillary fenestrae. Microvasc. Res. 1997, 53: 1-13.

Rubin LL, Hall DE, Porter S, Barbu K, Cannon C, Horner HC, Janatpour M, Liaw CW, Manning K, Morales J, et al A cell culture model of the blood-brain barrier. J Cell Biol. 1991, 115(6):1725-35.

Ruhrberg C. Growing and shaping the vascular tree: multiple roles for VEGF. Bioessays, 2003, 25 (11): 1052-60.

Ryan US et al. Fenestrated endothelium of the adrenal gland: freeze-fracture studies. Tissue Cell, 1975, 7(1): 181-90.

Satchell SC and Braet F. Glomerular endothelial cell fenestrations: an integral component of the glomerular filtration barrier. Am J Physiol Renal Physiol. 2009, 296(5): 947–956.

Schmidt-Erfurth U, Rudolf M, Funk M, Hofmann-Rummelt C, Franz-Haas NS, Aherrahrou Z, Schlötzer-Schrehardt U. Ultrastructural changes in a murine model of graded Bruch membrane lipoidal degeneration and corresponding VEGF164 detection. Invest Ophthalmol Vis Sci. 2008, 49(1):390-8.

Schnitzer JE, Liu J, Oh P. Endothelial caveolae have the molecular transport machinery for vesicle budding, docking, and fusion including VAMP, NSF, SNAP, annexins, and GTPases. J Biol Chem 1995;270:14399–14404.

Sechi AS, and Wehland J. The actin cytoskeleton and plasma membrane connection: PtdIns(4,5)P(2) influences cytoskeletal protein activity at the plasma membrane. J. Cell Sci. 2000, 113, 3685–3695.

Seemann J, Jokitalo EJ, Warren G. The role of the tethering proteins p115 and GM130 in transport through the Golgi apparatus in vivo. Mol Biol Cell. 2000;11(2):635-45.

Senger DR, Galli SJ, Dvorak AM, Perruzzi CA, Harvey VS, Dvorak HF. Tumour cells secrete a vascular permeability factor that promotes accumulation of ascites fluid. Science. 1983, 219:983–5.

Serunian LA, Auger KR, Roberts TM, Cantley LC.Production of novel polyphosphoinositides in vivo is linked to cell transformation by polyomavirus middle T antigen. J Virol. 1990 Oct;64(10):4718-25.

Shibata S, Fukushima M, Mori K. Ultrastructure of capillary permeability in human brain tumours. 2: Mechanisms of contrast enhancement in gliomas. No Shinkei Geka. 1986;14:311–6.

Silva E, Soares-da-Silva P. Protein cytoskeleton and overexpression of Na(+),K(+)-ATPase in opossum kidney cells. J Cell Physiol. 2009, 221(2):318-24.

Simionescu M, Simionescu N, and Palade GE. Preferential distribution of anionic sites on the basement membrane and the abluminal aspect of the endothelium in fenestrated capillaries. J Cell Biol 1982, 95:425–434.

Simionescu M, Simionescu N, Palade GE: Morphometric data on the endothelium of blood capillaries. J Cell Biol 1974, 60 : 128 –152.

Simionescu N, Lupu F, Simionescu M. Ring of membrane sterols surround the openings of vesicles and fenestrae, in capillary endothelium. JCB, 1983, 97: 1592-1600.

Simionescu N. Cellular aspects of transcapillary exchange. Physiol Rev . 1983, 63: 1536–79.

Singer SJ, Nicolson GL. The fluid mosaic model of the structure of cell membranes. Science, 1972, 175: 720-731.

Skou JC. The influence of some cations on an adenosine triphosphatase from peripheral nerves.Biochim.Biophys.Acta (1957) 23 394–401.

Small JV, Rottner K, Kaverina I and Anderson KI. Assembling an actin cytoskeleton for cell attachment and movement. Biochimica et Biophysica Acta, 1998, 1404: 271-281.

Small JV, Stradal T, Vignal E and Rottner K. The lamellipodium:where motility begins. TRENDS in Cell Biology, 2002, 12(3):112-9.

Small JV, Tottner K, Kaverina I. Function design in the actin cytoskeleton. Curr Opin Cell Biol 1999, 11: 54-60.

Smythe E, Ayscough KR. Actin regulation in endocytosis. J. Cell Sci. 2006, 119: 4589-4598.

Sorensson J, Fierlbeck W, Heider T, Schwarz K, Park DS, Mundel P, Lisanti M, Ballermann BJ. Glomerular endothelial fenestrae in vivo are not formed from caveolae. J Am Soc Nephrol 2002, 13: 2639–2647.

Speck O, Hughes SC, Noren NK, Kulikauskas RM, Fehon RG.Moesin functions antagonistically to the Rho pathway to maintain epithelial integrity. Nature. 2003 Jan 2;421(6918):83-7.

Spector I, Braet F, SChchet N, Bubb Mivhael. New anti-actin drugs in the study of the organization and function of the actin cytoskeleton. Microscopy Research and Technique 1999, 47: 18-37.

Spector I, Braet F, Shochet NR, Bubb MR.New anti-actin drugs in the study of the organization and function of the actin cytoskeleton. Microsc Res Tech. 1999 Oct 1;47(1):18-37.

Stan RV, Ghitescu L, Jacobson BS, Palade GE.Isolation, cloning, and localization of rat PV-1, a novel endothelial caveolar protein. J Cell Biol. 1999, 145(6):1189-98.

Stan RV, Kubitza M, Palade GE. PV-1 is a componentof the fenestral and stomatal diaphragms in fenestratedendothelia. Proc Natl Acad Sci USA. 1999, 96: 13203–7.

Stan RV, Roberts WG, Predescu D, Ihida K,Saucan L, Ghitescu L, Palade GE. Immunoisolation and partial characterization of endothelial plasmalemmal vesicles (caveolae). Mol Biol Cell. 1997, 8(4):595-605.

Stan RV, Tkachenko E, Niesman IR. PV1 is a key structural component for the formation of the stomatal and fenestral diaphragms. Mol Biol Cell 2004, 15: 3615–3630.

Steffan AM, Gendrault JL, and Kirn A, Increase in the number of fenestrae in mouse endothelial liver cells by altering the cytoskeleton with cytochalasin B. Hepatology, 1987, 7(6):1230-1238.

Steffan, AM et al., Mouse hepatitis virus type 3 infection provokes a decrease in the number of sinusoidal endothelial cell fenestrae both in vivo and in vitro. Hepatology, 1995, 22(2): 395-401.

Stephens L, Smrcka A, Cooke FT, Jackson TR, Sternweis PC, Hawkins PT. A novel phosphoinositide 3 kinase activity in myeloid-derived cells is activated by G protein beta gamma subunits. Cell. 1994 Apr 8;77(1):83-93.

Stossel TP. The machinery of cell crawing. Sci Am 1994, 271: 54-63.

Strickland LA, Jubb AM, Hongo JA, Zhong F, Burwick J, Fu L, Frantz GD, Koeppen H. Plasmalemmal vesicle-associated protein (PLVAP) is expressed by tumour endothelium and is upregulated by vascular endothelial growth factor-A (VEGF). J Pathol, 2005, 206: 466–475.

Sugimoto H, Hamano Y, Charytan D, Cosgrove D, Kieran M, et al: Neutralization of circulating vascular endothelial growth factor (VEGF) by anti-VEGF antibodies and soluble VEGF receptor 1 (sFlt-1) induces proteinuria. J Biol Chem 2003, 278: 12605–12608.

Swairjo MA, Seaton BA.Annexin structure and membrane interactions: a molecular perspective. Annu Rev Biophys Biomol Struct. 1994;23:193-213.

Sweadner KJ. Isozymes of the Na+/K+-ATPase. Biochim Biophys Acta. 1989;988:185–220.

Takahashi E, Nagano O, Ishimoto T, Yae T, Suzuki Y, Shinoda T, Nakamura S, Niwa S, Ikeda S, Koga H, Tanihara H, Saya H.Tumor necrosis factor-alpha regulates transforming growth factor-beta-dependent epithelial-mesenchymal transition by promoting hyaluronan-CD44-moesin interaction. J Biol Chem. 2010 Feb 5;285(6):4060-73.

Theriot JA, Mitchison TJ. Actin microfilament dynamics in locomoting cells. Nature. 1991 Jul 11;352(6331):126-31.

Theriot JA. Actin filament dynamics in cell motility. Adv Exp Med Biol 1994, 358: 133-145.

Thomas A. Marino, Langman's Medical Embryology, 1998, chapter 12 . Development of the cardiovascular system.

Tian J, Cai T, Yuan Z, Wang H, Liu L, Haas M, Maksimova E, Huang XY, Xie ZJ. Binding of Src to Na+/K+-ATPase forms a functional signalling complex. Mol Biol Cell. 2006 Jan;17(1):317-26.

Tian J, Xie ZJ. The Na-K-ATPase and calcium-signalling microdomains. Physiology (Bethesda), 2008, 23:205–211.

Toyoda M, Najafian B, Kim Y, Caramori ML, Mauer M. Podocyte detachment and reduced glomerular capillary endothelial fenestration in human type 1 diabetic nephropathy. Diabetes 2007, 56: 2155–2160.

Treisman R, Novak U, Favaloro J, Kamen R.Transformation of rat cells by an altered polyoma virus genome expressing only the middle-T protein. Nature. 1981 Aug 13;292(5824):595-600.

Trier, J.S. The fine structure of the parathyroid gland. J Biophys Biochem Cytol, 1958, 4(1): 13-22.

Tripathi RC, Tripathi BJ. A new method for light and electron microscopic localization of fluorescein-labelled dextran in ocular tissue using epoxy-resin embedding. Exp Eye Res. 1977 Sep;25(3):259-64.

Tsukita S, Oishi K, Sato N, Sagara J, Kawai A, Tsukita S. ERM family members as molecular linkers between the cell surface glycoprotein CD44 and actin-based cytoskeletons. J Cell Biol. 1994;126:391–401

Turunen O, Wahlstrom T, Vaheri A. Ezrin has a COOH-terminal actin-binding site that is conserved in the ezrin protein family. J Cell Biol. 1994, 126:1445–53.

Uittenbogaard A, Everson WV, Matveev SV, Smart EJ. Cholesteryl ester is transported from caveolae to internal membranes as part of a caveolin-annexin II lipid-protein complex. J Biol Chem 2002;277: 4925–4931.

Ungewickell E, Bennett PM, Calvert R, Ohanian V, Gratzer WB.In vitro formation of a complex between cytoskeletal proteins of the human erythrocyte. Nature. 1979 Aug 30;280(5725):811-4.

Vaheri A. Carpen O. Heiska L. Helender TS. Juha Jääskeläinen J. Majander-Nordenswan P. Sainio M. Timonen T. Turumen O. The ezrin protein family: membrane-cytoskeleton interactions and disease associations. Current Opinion in Cell Biology 1997, 9:659-666.

Van den Akker E, Satchwell TJ, Williamson RC, Toye AM. Band 3 multiprotein complexes in the red cell membrane; of mice and men. Blood Cells Mol Dis. 2010 Jun 15;45(1):1-8.

Van Driel D, Provis JM, Billson FA. Morphology of intraretinal new vessels in the PETH rat. Graefes Arch Clin Exp Ophthalmol. 1988;226(6):576-82.

Vanhaesebroeck B, Leevers SJ, Ahmadi K, Timms J, Katso R, Driscoll PC, Woscholski R, Parker PJ, Waterfield MD.Synthesis and function of 3-phosphorylated inositol lipids. Annu Rev Biochem. 2001;70:535-602.

Voeltz GK,Prinz WA, Shibata Y, Rist JM, Rapoport TA. A Class of Membrane Proteins Shapingthe Tubular Endoplasmic Reticulum. Cell, 2006, 124: 573–586.

Wallow IH, Geldner PS. Endothelial fenestrae in proliferative diabetic retinopathy. Invest Ophthalmol Vis Sci. 1980, 19: 1176–83.

Wang H, et al. Ouabain assembles signalling cascades through the caveolar Na+/K+-ATPase. J Biol Chem. 2004, 279:17250–17259.

Wehland J, Osborn M, Weber K. Phalloidin-induced actin polymerization in the cytoplasm of cultured cells interferes with cell locomotion and growth. Proc. Natl. Acad. Sci. U.S.A. 1977, 74 (12): 5613–7.

Welch MD, Mallavarapu A, Rosenblatt J, Mitchison TJ. Actin dynamics in vivo. Curr Opin Cell Biol 1997, 9:54-61.

Whikehart DR, Biochemistry of the Eye. Boston: Butterworth-Heinemann, 1994, p73.

Whitfield CF, Follweiler JB, Lopresti-Morrow L and Miller BA. Deficiency of a-Spectrin Synthesis in Burst-Forming Units-Erythroid . Blood, 1991, 78: 3043-3051.

Whitman M, Kaplan DR, Schaffhausen B, Cantley L, Roberts TM. Association of phosphatidylinositol kinase activity with polyoma middle-T competent for transformation. Nature. 1985;315:239–42.

Wisse E, De Zanger R, Jacobs R, Lobular gradients in endothelial fenestrae and sinusoidal diameter favour centrolobular exchange processes: a scanning EM study. In: Sinusoidal Liver Cells (Edited by: Knook DL, Wisse E). Amsterdam, Elsevier 1982, p61-67.

Wisse E. An ultrastructural characterization of the endothelial cell in therat liver sinusoid under normal and various experimental conditions, as acontribution to the distinction between endothelial and Kupffer cells. JUltrastruct Res 1972, 38: 528–562.

Wisse E., An electron microscopic study of the fenestrated endothelial lining of rat liver sinusoids. J Ultrastruct Res. 1970, 31(1):125-50.

Wisse W, De Zanger RB, Charels K, Van Der Smissen P and McCuskey RS, The liver sieve: considerations concerning the structure and function of endothelial fenestrae, the sinusoidal wall and the space of Disse, Hepatology 5 1985, 683–692.

Wolfgang H. Goldmann, Robert M. Ezzelli, Eileen D. Adamson, Verena Nigg, Gerhard Isenberg. Vinculin, Tanlin and Focal adhesions. Journal of Muscle Research and Cell Motility 1996, 17: l-5.

Wright PL, Smith KF, Day WA, Fraser R. Small liver fenestrae may explain the susceptibity of rabbits to atherosclerosis. Arteriosclerosis, 1983, 3: 344-348.

Wu S, Sangerman J, Li M, Brough GH, Goodman SR, Stevens T. Essential control of an endothelial cell ISOC by the spectrin membrane skeleton. J Cell Biol. 2001 Sep 17;154(6):1225-33.

Wymann MP, Pirola L.Structure and function of phosphoinositide 3-kinases. Biochim Biophys Acta. 1998 Dec 8;1436(1-2):127-50.

Xie Z.Molecular mechanisms of Na/K-ATPase-mediated signal transduction. Ann N Y Acad Sci. 2003, 986:497–503.

Xu H, Shi BM, Lu XF, Liang F, Jin X, Wu TH, Xu J. Vascular endothelial growth factor attenuates hepatic sinusoidal capillarization in thioacetamide-induced cirrhotic rats. World J Gastroenterol 2008, 14: 2349– 2357.

Yamada E., The fine structure of the renal glomerulus of the mouse.J Biophys Biochem Cytol. 1955, 25;1(6):551-66.

Yamamoto I, Horita S, Takahashi T, Tanabe K, Fuchinoue S, Teraoka S, Hattori M, Yamaguchi Y. Glomerular expression of plasmalemmal vesicle-associated protein-1 in patients with transplant glomerulopathy. Am J Transplant, 2007, 7: 1954–1960.

Yin HL, Janmey PA.Phosphoinositide regulation of the actin cytoskeleton. Annu Rev Physiol. 2003;65:761-89.

Yokomori H, Oda M, Yoshimura K, Nagai T, Ogi M, Nomura M, Ishii H. Vascular endothelial growth factor increases fenestral permeability in hepatic sinusoidal endothelial cells. Liver Int., 2003, 23: 467–475.

Yokomori H. New insights into the dynamics of sinusoidal endothelial fenestrae in liver sinusoidal endothelial cells. Med Mol Morphol. 2008 Mar; 41(1):1-4.

Yonemura S, Hirao M, Doi Y, Takahashi N, Kondo T, Tsukita S, Tsukita S. Ezrin/radixin/moesin (ERM) proteins bind to a positively charged amino acid cluster in the juxta-membrane cytoplasmic domain of CD44, CD43, and ICAM-2. J Cell Biol. 1998; 140:885–95

Yu LY, Korhonen L, Martinez R, Jokitalo E, Chen Y, Arumäe U, Lindholm D.Regulation of sympathetic neuron and neuroblastoma cell death by XIAP and its

association with proteasomes in neural cells. Mol Cell Neurosci. 2003 Mar;22(3):308-18.

Yuan Z, Cai T, Tian J, Ivanov AV, Giovannucci DR, Xie Z. Na/KATPase tethers phospholipase C and IP3 receptor into a calcium-regulatory complex, Mol. Biol. Cell 16 (2005) 4034–4045.

Yudowski GA, Efendiev R, Pedemonte CH, Katz AI, Berggren PO, Bertorello AM. Phosphoinositide-3 kinase binds to a proline-rich motif in the Na+, K+-ATPase alpha subunit and regulates its trafficking. Proc Natl Acad Sci U S A. 2000 Jun 6;97(12):6556-61.

Zhang S, Malmersjö S, Li J, Ando H, Aizman O, Uhlén P, Mikoshiba K, Aperia A. Distinct role of the N-terminal tail of the Na,K-ATPase catalytic subunit as a signal transducer. J Biol Chem. 2006 Aug 4;281(31):21954-62.

Zhang, HR. Scanning electron-microscopic study of corrosion casts on retinal and choroidal angioarchitecture in man and animals. Prog. Ret. Eye Res. 1994, (13): 243-270.

Zhou X, Jiang G, Zhao A, Bondeva T, Hirszel P, Balla T. Inhibition of Na,K-ATPase activates PI3 kinase and inhibits apoptosis in LLC-PK1 cells. Biochem Biophys Res Commun 2001, 285: 46–51.

Zobiack N, Rescher U, Laarmann S, Michgehl S, Schmidt MA, Gerke V.Cell-surface attachment of pedestal-forming enteropathogenic E. coli induces a clustering of raft components and a recruitment of annexin 2. J Cell Sci. 2002 Jan 1;115(Pt 1):91-8.